Hungarian Academy of Sciences
Centre for Energy Research

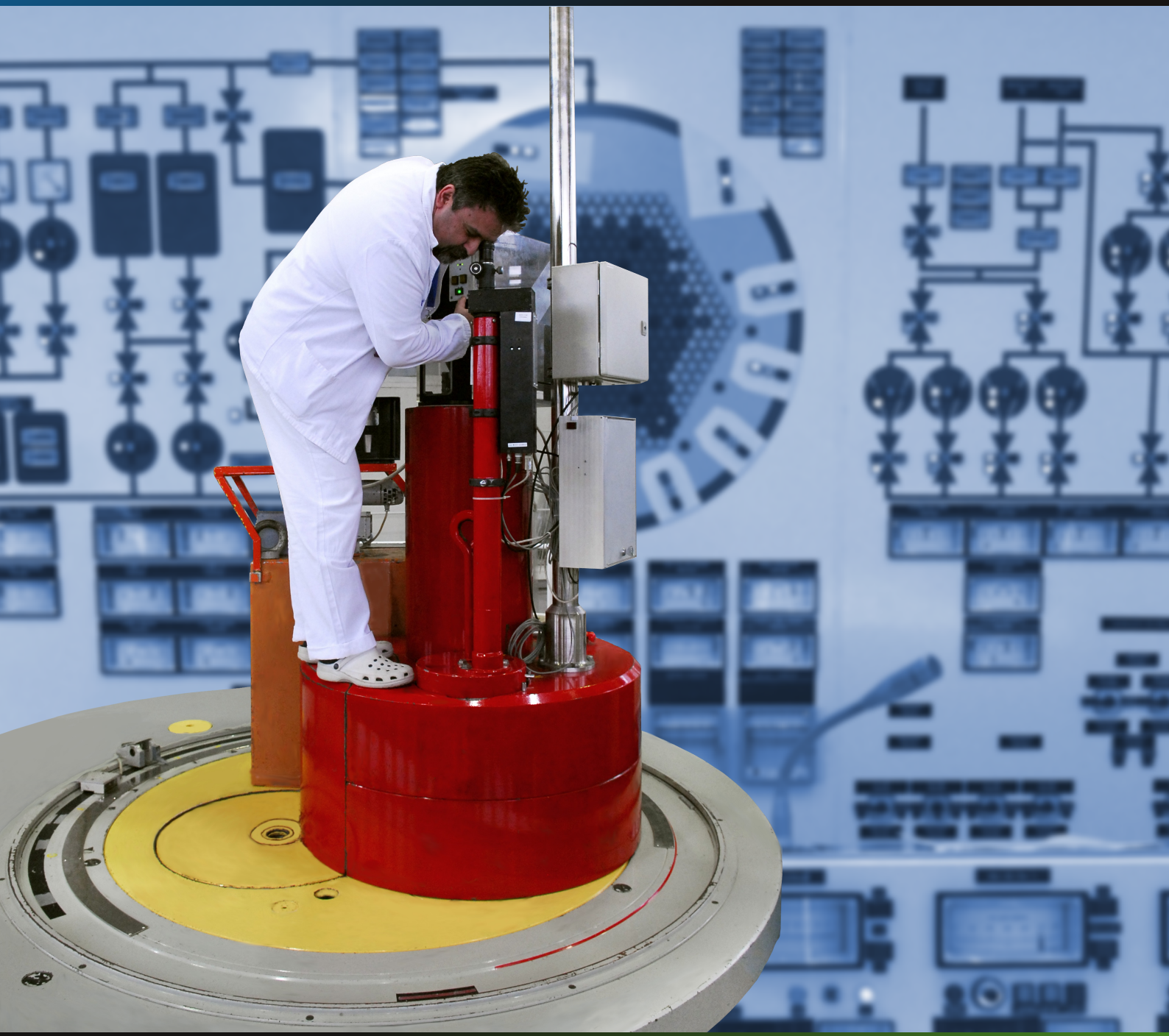

Progress report on Research Activities

2017

HUNGARIAN ACADEMY OF SCIENCES
CENTRE FOR ENERGY RESEARCH

29-33 KONKOLY-THEGE MIKLÓS ÚT

1121 BUDAPEST, HUNGARY

PROGRESS REPORT
ON RESEARCH ACTIVITIES
IN 2017

DEAR READER,

Welcome to the 2017 yearbook published by the MTA Centre for Energy Research (MTA EK), summarizes the scientific results of its three institutions and highlights the many new projects started in 2017. This booklet provides a summary of works performed by individual research personnel and by research groups in the Centre.

The year 2017 was very successful in terms of awarded grants and new opportunities. A collaborative project has been launched investigating the nuclear fuel cladding thermo-mechanical properties in various conditions, awarded by the National Research, Development and Innovation Office (NKFIH).

Research in nuclear safety within the framework of the Hungarian Sustainable Nuclear Technology Platform continued. The project reached a milestone this year and a comprehensive assessment of future nuclear energy research needs and the related human resources and potential financial allocations have been performed. The results of this analysis were published in a vision report, which was submitted to Hungarian funding bodies and decision makers.

A new "Lendület" (Momentum) research group of MTA EK MFA was awarded a grant to study topological insulators which have the potential of being major components in quantum computers.

Another new research project in the field of renewable energy was supported by the Ministry of National Economy, which uses synergies between our Centre and the MTA Wigner Physical Research Centre, also on this site. The title of the project is "Strategic Workshop on the Technological Challenges of Renewable Energy Systems". I Its objectives fully fit into the MTA EK's research strategy.

Using synergies and increasing collaborations between EK's three institutions enhances the gradual development in all the fields of alternative energy research, which should lead to a deceleration of the rate of the climatic changes and to more sustainable energy production schemes and to a healthier environment.

Ákos Horváth
Director General
foigazgato@energia.mta.hu

CONTENTS

MISSION STATEMENT OF MTA CENTRE FOR ENERGY RESEARCH

- Research and development in the field of nuclear science and technology for facilitating the adoption and the safe use of nuclear technology in Hungary.
- To participate in international research effort aiming at the establishing a new generation of nuclear power plants and closing the fuel cycle.
- Maintaining and improving competence in nuclear science and technology, especially in the field of nuclear safety, security, health physics, nuclear and isotope chemistry.
- To guarantee the safe operation of Budapest Research Reactor (BRR), and to ensure the accessibility of the research facilities around the reactor.
- Research activities to improve nuclear analytical and imaging methods and their applications for energy and materials science.
- Perform studies in the field of environmental physics related to energy generation, renewable energies, energy storage and their impact on public health, and on environmental safety.
- Research and development in the field of low carbon energy technologies and of energy saving in industrial technologies.
- Interdisciplinary research on complex functional materials and nanometer-scale structures, exploration of physical, chemical, and biological principles, their exploitation in integrated micro- and nanosystems, and in the development of characterization techniques.
- Dissemination of the results in international programs, education and industrial research.

SCIENTIFIC ADVISORY BOARD OF THE MTA CENTRE FOR ENERGY RESEARCH

The Board consists of five Hungarian and two foreign leading scientists. The last meeting of the board took place in Budapest, 11 April 2018. The management of EK presents usually an overview of the R & D activities in the previous year as well as figures about financial data and analyses of human resources. The R&D plans for the coming year and for the near future are also presented. The Board members usually comment the presentations and ask questions.

Members of the Board:

- Prof. Dr. László Keviczky (Chair), MTA Institute for Computer Techniques and Automation
- Dr. Hervé Bernard, Deputy Chairman, Centre French Alternative Energies and Atomic Energy Commission (CEA)
- Dr. Maximilian Fleischer, Head of Department of Corporate Technology, Siemens AG
- Prof. Dr. Ádám Kiss, Eötvös Loránd University
- Dr. Zoltán Homonnay, Head of Laboratory of Nuclear Chemistry, Eötvös Loránd University
- Mr. István Hamvas, Director General, Paks Nuclear Power Plant
- Dr. József Rónaky, Scientific Advisor, Hungarian Atomic Energy Authority

ORGANIZATION STRUCTURE OF THE MTA CENTRE FOR ENERGY RESEARCH

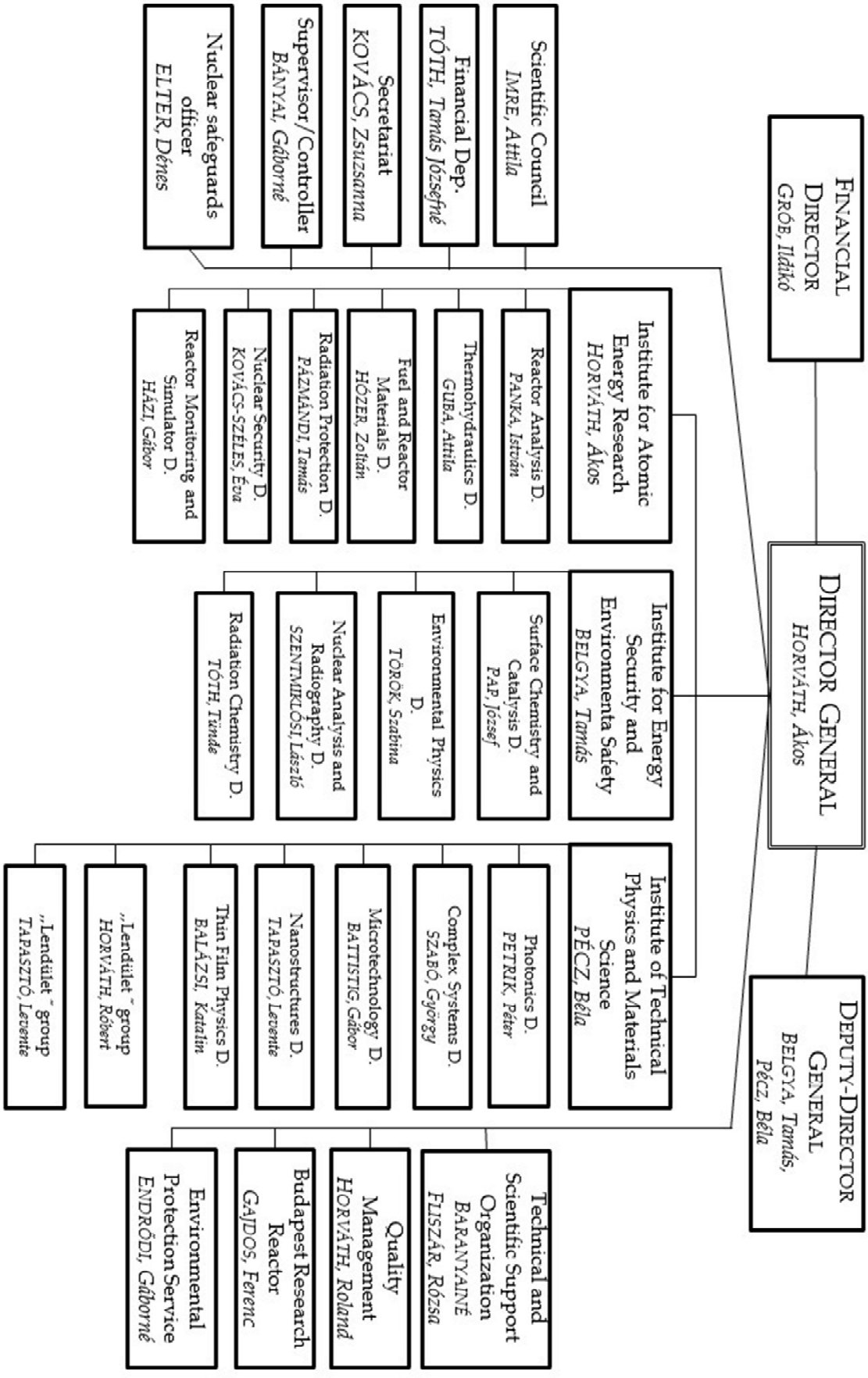

QUALITY MANAGEMENT

In order to achieve the highest quality of research, development, design, condition monitoring and valuation, engineering, contracting and managing in design, production, implementation and inspection, the Research Centre's quality management system has been continuously upgraded by the recommendations of ISO 9001 standard since 1994. Reviewing our QM system by integral audits and management reviews, evaluating improvement opportunities, maintaining project documentation, infrastructure, supporting communication, ensuring the competence of workers the management improves the Centre's QM system. For the new organization structure our Quality Policy has been renewed. Many new employees induced a need to upgrade our QM tuition practice. We organised the work and fire safety educations. Our QM system has been certified by Hungarian Standards Institution, IQNet, and MVM Paks NPP.

MAGYAR SZABVÁNYÜGYI TESTÜLET
HUNGARIAN STANDARDS INSTITUTION
H-1082 Budapest, Horváth Mihály tér 1.

TANÚSÍTÁSI OKIRAT
CERTIFICATE

Tanúsítjuk, hogy a
We certify that the Quality Management System of
Magyar Tudományos Akadémia
Energiatudományi Kutatóközpont
(kivéve az MFA és a Reaktorüzem)
H-1121 Budapest, Konkoly Thege út 29-33.

minőségirányítási rendszere megfelel a szabvány követelmény pontjainak a következő alkalmazási területen:
kutatás, fejlesztés, tervezés, állapotértékelés és szakértvényzés, mérnökszolgálat, kivált alkotási tevékenység tervezési, gyártási, kivitelezési és vizsgálati munkák irányítására, atomenergia alkalmazása körében eljáró független műszaki szakértői tevékenység
meets the requirements of the standard for the following activities:
research, development, design, condition monitoring and valuation, engineering, contracting and managing in design, production, implementation and inspection, independent technological expert activity in the field of application of nuclear energy

MSZ EN ISO 9001:2015 (ISO 9001:2015)

A tanúsítási okirat érvényes / This certificate is valid: **2017. 06. 26. – 2020. 06. 25.**
Ez a tanúsítvány az MSZT által évente kiadott fennartási határozattal együtt érvényes.
This certificate is valid together with the maintenance decision annually issued by MSZT.
A tanúsítási okirat száma / Reg. number: **503/0309(6)**
Budapest, 2017. június 26.
Az első tanúsítás dátuma / Date of the first certification: **1999. 06. 22.**

Pónyai György
ügyvezető igazgató

THE INTERNATIONAL CERTIFICATION NETWORK

CERTIFICATE

MSZT as an IQNet Partner hereby states that the organization:

HUNGARIAN ACADEMY OF SCIENCES CENTRE FOR ENERGY RESEARCH
except Institute of Technical Physics and Materials Science (MFA) and Reactor Department (Reaktorüzem)
H-1121 Budapest, Konkoly Thege út 29-33.

for the following scope
research, development, design, condition monitoring and valuation, engineering, contracting and managing in design, production, implementation and inspection, independent technological expert activity in the field of application of nuclear energy

(EA scope: 33, 34, (11))

has implemented and maintains a
Quality Management System
which fulfils the requirements of the following standard:

ISO 9001:2015

Issued on: 26-06-2017
First issued on: 22-06-1999

The validity date is the same as the original certificate issued by MSZT.*
Registration Number: **HU-MSZT-503/0309(6)-97(6)**

Michael Drechsel
President of IQNet

György Pónyai
General Director of MSZT

AZ MVM PAKSI ATOMERŐMŰ ZRT. IGAZOLJA, HOGY
KÖVETELMÉNYEINEK AZ

MTA ENERGIATUDOMÁNYI KUTATÓKÖZPONT

MINŐSÉGIRÁNYÍTÁSI RENDSZERE

MEGFELEL.

MINŐSÍTETT TERÜLET:

ABOS 1, 2, 3 biztonsági osztályokba sorolt technológiai rendszerek és rendszerelemek átalakításával, javításával, karbantartásával és üzemeltetésével összefüggően főkonzulensi, tervezői, szakértői, valamint független műszaki szakértői tevékenységek végzése.

A MINŐSÍTÉS ÉRVÉNYESSÉGI IDEJE: 2020.07.31.

A MINŐSÍTÉS SZÁMA: KM 70/2017

EZEN MINŐSÍTŐ LAP A MELLÉKLETTEL EGYÜTT ÉRVÉNYES.

Paks, **2017. augusztus 14.**

BÁDSZ JÓZSEF
főosztályvezető

HORVÁTH GYÖRGY
osztályvezető

atom erőmű
mvm

Certifications by Hungarian Standards Institution, IQNet, and MVM Paks NPP

BUDAPEST RESEARCH REACTOR

One of the most important strategic large scale research facilities in Hungary is the Budapest Research Reactor (BRR). It serves the needs of an extensive and diverse scientific community by supporting R&D opportunities, helping innovation and providing a strong environment for training and education.

Bird's eye view of the Budapest Research Reactor

The BRR is a VVR-type reactor that uses light water as moderator and cooling fluid. The power of the reactor is 10 MW provided from low enrichment uranium fuel, and its main purposes – as established during the feasibility/functionality study - are: radioisotope production, production of thermal and cold neutron beams for research and applications in all areas, development of new functional materials and neutron activation analysis.
The core is designed to have about 10-11 reactor cycles per year, each having a time-span of 10 days. We are committed to long-term safety and responsible operations, taking care of the wastes from the spent fuel coming from the reactor. Besides the temporary spent fuel storage pool, we also operate a long term spent fuel storage building for the physical and environmental separation between the reactor and the spent fuel storage.

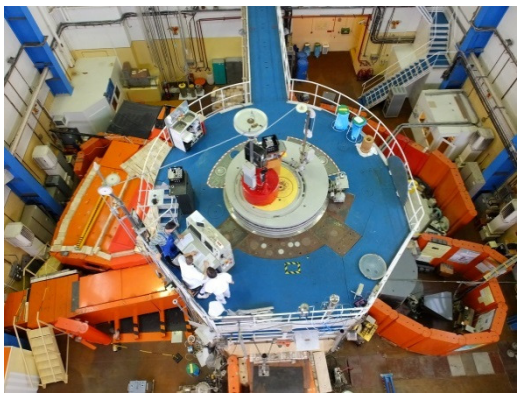

Top view of the research reactor

Layout of the BRR's facilities

The reactor hosts three kind of activities: the research activities utilizing neutron beams, the production of radioisotopes for medical, industrial and research purposes, and the provision of national and international training courses. We are proud of our innovative flagship research topics, which are carried out with a network of neutron beam stations, including beam-lines of thermal neutrons, experiments on powder and residual stress diffractometry, radiography, biological irradiations and beam-lines of cold neutrons for experiments on small angle neutron scattering, reflectometry, prompt gamma activation analysis and nuclear data measurements. In accordance with recent worldwide trends, we are open to establishing new industrial relations, and supporting innovation. The BRR's experimental facilities are open for science based on excellence for researchers from all over the world. We aim to increase our competence on special topics, to implement new technologies, to develop new materials, and to promote and exploit our R&D capacity at the national and regional/international level. During the past years the BRR hosted several international schools on various technical and research topics, special trainings in the field of reactor physics, reactor operation, nuclear measurement techniques, and safety and environmental issues.

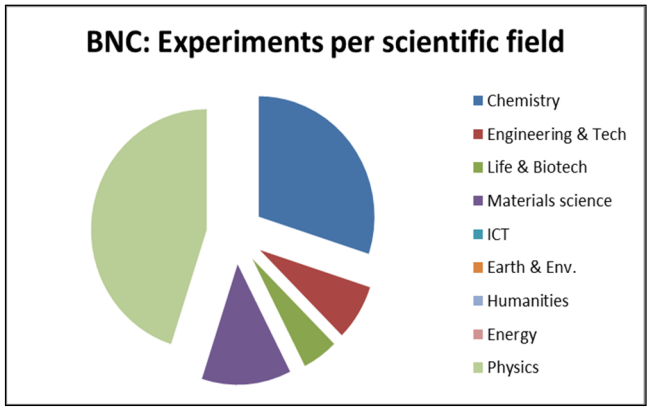

The BRR is used by groups from different scientific communities including the medical, environmental, material, archaeological, nuclear sciences and industry, as well as several Hungarian Universities. Neutron beams are uniquely suited to study the structure and dynamics of materials at the atomic level. The Budapest Neutron Centre (BNC) coordinates the scientific utilization of the research reactor. Some of main research topics currently are:

- neutron scattering, used to examine changes of sample properties under different physical conditions such as variations in vacuum or pressure, high and low temperature, and magnetic field, modelling real-world conditions.
- using prompt and delayed neutron activation analysis, it is possible to measure the concentration of elements in ppm and ppb levels even for small samples. Atoms of a sample become radioactive by exposure to neutrons from the reactor. They decay by gamma-rays characteristic for each element that can be detected by suitable detectors
- neutron activation is also used to produce different radioisotopes, widely used in industry and medicine. For example, Y-90 microspheres to treat liver cancer are produced by bombarding Y-89 with neutrons, which are captured.
- testing reactor materials; materials are subjected to intense neutron irradiation which causes radiation damage of their crystalline structure. For instance, some steels become brittle. Thus, the so called high-entropy alloys which resist embrittlement are to be used in nuclear reactors.
- production of radioisotopes for different applications such as medicine, sterilization and industrial use.
- applied research using neutron beams to produce images. Examples are dynamic neutron radiography of the cooling system of a refrigerator or visualization of fuel burning in the engine system of a car, and tomography of different materials and items.

The BNC provides researchers with 15 neutron instruments; 13 instruments are installed directly on the horizontal beam ports of the reactor or at the thermal and cold neutron guides, while the other 2 are placed at the vertical irradiation channels. The instruments are supported by a variety of sample environments and data analysis and visualization capabilities.

The BNC provides facility access to the international neutron user community through a peer-review system. Local scientists assist researchers and industrial users to find the appropriate neutron techniques that meet their research needs. The various neutron scattering instruments in BNC cater to a large number of users from Europe and has grown in strength and stature over the years.

BNC is a member of the European network of neutron centres and CERIC-ERIC, and a partner in recent EU Framework Programme projects (NMI3-II, CHANDA, IPERION, SINE2020, ESS-BrigthnESS).

BNC is strongly committed to the training of future professionals from Hungary and all over the world in co-operation with the International Atomic Energy Agency. We cooperate with Hungarian universities (Budapest University of Technology and Economics, Eötvös Loránd University (ELTE), Pannon University, …), and BNC accommodates students for laboratory practice for studying nuclear-based techniques. A specialized course was developed for geology students of the ELTE to introduce nuclear analytical techniques into their education. BNC organizes the Central European Training School on Neutron Scattering annually, to train young scientists in neutron physics and to attract new users. The school provides insight into neutron scattering, element analysis and imaging techniques and their applications to study the structure and dynamics of condensed matter.
The Budapest Research Reactor is open to the public. Members of the local communities and high school and university students are invited to visit regularly and learn more about the amazing nuclear science possibilities available at BRR.

Research staff of the Budapest Research Reactor facilities in the operator's room.

ENVIRONMENTAL PROTECTION SERVICE

In the last years the Environmental Protection Service (EPS) operated in compliance with the pertinent laws and orders. EPS is a functional unit of MTA Centre for Energy Research (MTA EK). In accordance with our main tasks, EPS took and measured environmental samples, which were collected over the whole territory of the KFKI Campus.

Measurements of different types and sensitivities are performed by EPS for the detection and analysis of radioactive materials, including gamma-ray spectroscopy, selective alpha and beta counting and liquid scintillation spectrometry.

In the year of 2017 we made several improvements in our laboratory equipment. We renewed the on-line gamma radiation monitoring network at the Campus and upgraded our Environmental Protection Regulation. We expanded our lab-instrumentation (handheld nuclide-identifier spectrometer and other portable radiation detectors). We improved the measurement features of our in-vivo whole body counter (Figure 1.).

We purchased additional radioactive sources and performed calibration procedures in order to make our detectors more sensitive to environmental control measurements.

The routine monitoring programme was reconsidered on the basis of the regulatory requirements. The ideal frequency of the sampling was also determined properly and declared in the new instruction of the measurements. Dose rate meters were installed at 17 critical points of the site. The locations of the measurement points were determined to ensure the detection of the near ground releases from the major nuclear facilities (Figure 2.). In addition, the control of the safe transportation and storage of radioactive materials can be monitored. These active gamma-dose-rate measurements were supplemented with 9 TL dosimeters, which are located at the major measurement points and provide monthly integrated gamma-dose data.

The laboratory of the Environmental Protection Service participated in several interlaboratory comparison exercises and proficiency tests in 2017. Processes and critical elements could be identified with the help of the comparisons of results to improve the adequate analysis of the environmental samples. As part of the validation of the methodology, accurate data processing methods were developed and put into practice for the estimation of the detection limits and the quantification of the measurement uncertainties.

EPS took part in the education of groups of trainees of international education courses supported by the International Atomic Energy Agency (IAEA). They studied the operation of nuclear research centres and research reactors including the tasks of the environmental protection service.

Furthermore, we host MSc students from universities of sciences from Hungary for their diploma thesis work.

Figure 1: In-vivo whole body counter

Figure 2: Gamma detector with sound and light alarm

Gáborné, Endrődi
Head of Department
endrodi.gaborne@energia.mta.hu

I. EU OR NKFIH SUPPORTED RESEARCH ACTIVITIES

HUNGARIAN NUCLEAR RESEARCH PROGRAM

Árpád Farkas

Objective

The Hungarian Nuclear Research Program (2014-2018) is a research and development project funded by the National Research, Development and Innovation Office (NKFIH, project identifier: VKSZ_14-1-2015-0021; homepage: vksz14.kfki.hu). The participants of the consortium project are: Centre for Energy Research, Hungarian Academy of Sciences (MTA EK, as coordinator), Budapest University of Technology and Economics (BME), Hungarian Academy of Sciences Institute for Nuclear Research (MTA ATOMKI), National Public Health Institute (OKI) and Nuclear Safety Research Institute Ltd (NUBIKI). The main goals of the project are to conduct high level research on the technologies supporting the long-term and safe use of atomic energy and to maintain and extend the Hungarian nuclear professional knowledge. One of the main efforts of the project is oriented towards providing technical and scientific background for the safe operation of the existing blocks of the Paks NPP and preparing for the installation of the new reactors. State-of-the-art research on the safe disposal of spent fuel and development of novel approaches to study different aspects of new generation reactors are also organic parts of the project. Elaboration of the mid-term strategic plans of the Hungarian nuclear research infrastructure is also in focus within this complex research program.

Figure 1: Central building of the EK

Results

In 2017 significant progress has been achieved in each of the three main taskgroups, namely: (i) experimental nuclear physics; (ii) simulation of reactor processes; and (iii) nuclear waste management and research on new generation nuclear power plants. Among the most important research results of the project in 2017, it is worth noting the advances in the field of characterization of new reactor materials, development of new structural integrity analysis methods and simulation of thermomechanical behavior of metallic structural materials. Important model development and validation has been carried out in the area of reactor core design and safety analysis of the new Paks reactors. In addition, significant effort has been spent to integrate the VVER-440 and VVER-1200 compact simulator models. In addition, a new model of fluvial radioisotope transport has been developed and applied. Numerical methods were developed to quantify the internal burden of the inhaled radionuclides and to simulate their interaction with the human cells [2]. Important results were achieved also concerning the planning, modelling and safety analysis of the ALLEGRO fourth generation gas cooled demonstration reactor [1]. These results are in focus also because of their importance in relation to the key objectives of the V4G4 excellence center. In 2017 a comprehensive assessment of future nuclear energy research needs and the related human resources and potential financial allocations has been performed. The results of this analysis were published in a vision report, which was submitted to Hungarian funding bodies and decision makers [3].

Figure 2: Graphical User Interface for development of VVER440 compact simulator

Remaining work

The remaining tasks of the ongoing project will be completed until the end of 2018.

Related publications

[1] B. Batki, A. Keresztúri and I. Panka: *Calculation of core safety parameters and uncertainty analyses during unprotected transients for the ALLEGRO and a sodium-cooled fast reactor*, Annals of Nuclear Energy **118**, 260-271 (2017)

[2] B. G. Madas, E. J. Drozsdik: *Effects of mucus thickness and goblet cell hyperplasia on microdosimetric quantities characterizing the bronchial epithelium upon radon exposure*, International Journal of Radiation Biology. doi: 10.1080/09553002.2018.1511931 (2017)

[3] *Visions report of the Sustainable Nuclear Energy Technology Platform for 2019-2022*, in Hungarian. Edited by János Gadó. Available at: http://faetp.energia.mta.hu/dl/Vision_Report_2017_v4.pdf

THE ALLEGRO PROJECT

János Gadó, Ákos Horváth, Zoltán Hózer

Objective

Corresponding to the European initiative on launching research in the field of Generation IV nuclear reactors, the nuclear research institutes of the Visegrad 4 countries and the French CEA started a co-operation on the development of the Gas Cooled Fast Reactor demonstration reactor ALLEGRO in 2010. The final objective of the co-operation is to build and operate this reactor but the construction has to be preceded by a long period of research and development related to various technological issues and the design of the reactor has to be prepared in several steps. ALLEGRO can start operation not earlier than in 2030.

Methods

The ALLEGRO Project Preparatory Phase was launched by the consortium of the nuclear research institutes of the Visegrad 4 countries (V4G4) in 2015. In the preparatory phase of the ALLEGRO Project (2015-2025), the conceptual design will be elaborated and the necessary research-development-qualification tasks will be executed. During the design of ALLEGRO the usual design methods will be applied. By 2018, a pre-conceptual design will be elaborated using the existing CEA 2009 Design with the necessary additions and modifications. Design additions and modifications are motivated by the safety concerns related to the CEA 2009 Design. After 2018 the conceptual design will be elaborated (by 2025) which will be the basis of submitting the construction license application. Elaboration of the detailed design, construction, commissioning and operation will be a task of a new consortium.

A literature review was carried out for the identification of the most suitable candidates for the fuel of refractory ALLEGRO core.

SiC_f/SiC type duplex and triplex type claddings were produced in KAERI (Korea Atomic Energy Research Institute) for the nuclear fuel. This cladding type is a candidate material for the refractory core of the ALLEGRO reactor. High temperature testing in a He atmosphere with different impurities and detailed scanning electron microscope analyses of the cladding samples was carried out at MTA EK

Results

In the framework of the ALLEGRO project several basic documents have been created and they are gradually being followed (Design and Safety Roadmap, ALLEGRO Design Specifications, ALLEGRO Safety Requirements, ALLEGRO V4G4 Concept Database). They show the directions of the design works. The EURATOM FP7 project ESNII+ and the Horizon 2020 project VINCO contributed to the ALLEGRO project by benchmarking reactor physical and thermo-hydraulic computational models. The safety of the reactor is of primary importance and several solutions have been elaborated to solve the most difficult issues.

The execution of the various tasks was started in the framework of national programs, like the Hungarian National Nuclear Research Program NNKP. Several reports were issued by the Hungarian partners MTA EK, NUBIKI and BME NTI which are referenced in connection with NNKP related projects.

A summary paper was prepared [1] for the significant IAEA conference on fast reactors.

Taking into account the irradiation experience, fabrication capabilities and reprocessing options it is proposed to consider carbide fuel in the design of the refractory ALLEGRO core. The availability of more data on irradiated fuel and the larger fabrication experience supports this decision. The fuel for the refractory core of the ALLEGRO reactor could be composed of UC or (U,Pu)C pellets in SiCf/SiC cladding. During the design of the fuel geometry a relatively large gas gap must be considered to avoid pellet-cladding interactions. The design of the fuel element must be supported with detailed fuel behaviour calculations.

The experimental results showed that the mass changes observed during the high temperature (1000 °C) treatment of SiC_f/SiC with a high content of nitrogen and hydrogen in helium were very similar to the results of testing the same materials in pure helium. In the case of methane impurities in helium the decomposition of methane and the formation of carbon deposits led to a mass gain of the SiC samples.

Remaining work

The finalization of safety relevant solutions requires further studies.

Related publications

[1] L. Bělovský, J. Gadó, B. Hatala, A. Vasile and G. Wrochna: *The ALLEGRO Experimental Gas Cooled Fast Reactor Project*, Proc. of the Intn'l Conf. on Fast Reactors and Related Fuel Cycles, 26-29 June 2017, Yekaterinburg, Russia

[2] Z. Hózer, T. Novotny, E. Perez-Feró, Á. Horváth, A. Pintér Csordás, L. Illés, Daejong Kim Weon-Ju Kim: *Testing of SiC_f/SiC claddings for ALLEGRO gas cooled fast reactor conditions*, MTA EK-FRL-2017-219-1-1-M0

[3] E. Slonszki, Z. Hózer: On the selection of fuel for the second core of ALLEGRO gas cooled fast reactor, MTA EK-FRL-2017-218-1-1-M0

BUDAPEST NEUTRON CENTRE AND SINE2020 PROJECT

Rózsa Baranyai

The Budapest Research Reactor (BRR) is one of the leading scientific infrastructures in Hungary and Central-Europe. It's basic scientific activity is the use of neutrons and neutron beams for basis physics research and for material investigations. 13 neutron instruments are installed directly at the beam ports of the reactor or on the neutron guides originating from the cold neutron source. The Budapest Neutron Centre (BNC) coordinates the scientific utilization of the BRR and makes available its facilities to the international neutron user community through the peer-review process.

The Transnational Access (TNA) to the European neutron facilities is financed through the EU supported NMI3 project. The project finished in 2016, but it is still considered as a successful collaboration for science. Within the TNA part of the program the neutron facilities provided 5000 beam days to the European neutron science community. This generated over 210 publications in peer-reviewed journals. BNC was part of the success story.

SINE2020, the world-class Science and Innovation with Neutrons in Europe in 2020, is a consortium of 18 partner institutions from 12 countries. The European Union funds it through the H2020 program. BNC is involved in the Industry Consultancy workpackage (WP4) and the Training in neutron scattering; from proposal to publication; e-learning and schools workpackage (WP3).

Coordination in Schools focuses on two types of activities: i) training in the basics of neutron related science and techniques, and ii) advanced studies of basic and applied research with neutrons, including instrumentation. The basic "introductory" neutron schools are intended for young scientists and PhD students as well as for other new comers to the field, while the "advanced schools" focus on more advanced users. The requests are higher, on average, for the introductory schools than for the advanced schools.

The Industry Consultancy workpackage demonstrates the potential of neutron methods to companies not familiar with neutron analytical techniques. It encourages the industrial users to exploit the unique feature of neutron techniques in R&D. SINE2020 can arrange test measurements and feasibility studies. BNC participated in two test measurements in 2017. One was a density measurement for the Sandvik Company, and the other was a nanoscale structure investigation of cellulose fibers for the Novozymes Company. The results of the density measurement were presented in a SINERGI2018 conference in Amsterdam; one of the keynote speakers was Hjalmar Staf from Sandvik AB, Sweden. The title of his talk was "Improving cutting tools with insights from neutron tomography".

BNC is open to form new industrial relationships, and the automotive sector is one of the areas where we have the capacity to provide unique solutions with our neutron beam trials. BNC offers a high-level and stable infrastructure with an internationally trained scientific staff to solve specific issues, providing inspection activities to enhance top-level, innovative solutions and offering competitiveness to potential user companies through the application of the unique properties of neutrons. BNC took part in the Automotive Exhibition (of 2017 in Hungary) as an exhibitor. We presented information on an ensemble of non-destructive analytical and imaging techniques, which provide information - from the atomic to the macroscopic level - on the elemental composition and structural features of materials and components relevant for the automotive industry. We placed a one-page advertisement about BNC and neutron methods offered to the automotive industry in the Great Book of Hungarian Automotive Industry IV.

Figure 1: BNC stand at Automotive Exhibition 2017

BNC is strongly committed to the training of future professionals. In cooperation with Hungarian universities, BNC accommodates students for laboratory practice for studying nuclear-based techniques. BNC also organizes the Central European Training School on Neutron Scattering on a regular basis to train young scientists and attract new users.

TRANSNATIONAL ACCESS WITHIN THE EC H2020 IPERION CH PROJECT

Zsolt Kasztovszky[1], László Szentmiklósi[1], Zoltán Kis[1], Ildikó Harsányi[1], Adél Len[1,2], Katalin Bajnok[2], György Káli[2], Imre Kovács[2], Zoltán Szőkefalvi-Nagy[2], László Rosta[2], Veronika Szilágyi[1]

[1]Centre for Energy Research, [2]Wigner Research Centre for Physics

Objective

Within the IPERION CH European H2020 project, transnational access is offered to European experts of Heritage science, to perform experiments at the instruments of the Budapest Neutron Centre. In most of the short term experimental projects, compositional and structural data are obtained using mostly non-destructive methods, from which information regarding provenance, condition, and genuineness of the objects are concluded

Methods

In the frame of the transnational access, Prompt Gamma Activation Analysis (PGAA), Instrumental Neutron Activation Analysis (NAA), Neutron Radiography (RAD), Time of Flight Neutron Diffraction (TOF-ND), Small Angle Neutron Scattering (SANS) and complementary PIXE can be used.

Results

In 2017, six experimental proposals have been successfully completed. Two experiments aimed to determine the alloying components of Celtic, Greek and Medieval silver coins using PGAA, in order to identify the supposed minting techniques and workshops. In another experiment, Ottoman coloured glass fragments excavated in the region of Dobroudja, Romania have been measured by PGAA and PIXE. We aimed to determine the colorants and other major components in order to identify the supposed workshops. Furthermore, Neolithic polished stone axes, blades and beads have been analysed by PGAA and PIXE, as well as marble fragments from a gothic cloister which have been analysed by PGAA and SANS in order to determine the provenance of their raw materials.

Highlight: Characterization of excavated Napoleonic artefacts from the Berezina battlefield in Belarus using PGAA

A set of lead balls excavated from the battlefields of the Napoleonic war have been analyzed by PGAA and in-beam NAA at the BNC. The objects had already undergone PGAA at NPI (Nuclear Physics Institute, The Academy of Science of the Czech Republic, Rez Prague) and those results showed that there was a compositional difference between Waterloo and Berezina balls, thus provoking the question: was this difference due to actual chemical properties of the original artefacts (thus possibly due to ores used and/or fabrication methods) or were they the results of surface contamination and inherent in the bulk PGAA method used? We wished to carry out tests at BNC on cleaned and uncleaned balls from Waterloo to understand the previous results/hypotheses.

Our results confirmed that surface contamination was indeed an important part of the chemical makeup of the uncleaned balls. It is postulated that Si and Al are environmental contaminating elements. Cl is also likely to be due to contamination, forming $PbCl_2$. The same is also true for S, forming lead sulfide (PbS) and lead sulphate (PbSO4), and for iron, where ferric hydroxide ($Fe(OH)_3$) can be found in mineralized goethite and hematite. If we therefore discount these elements, we found significant Sn and As content in the Berezina balls and a much higher Cu content in the Waterloo balls as well as Ag and Sb at levels not present in the Berezina balls.

Figure 1: Photo of the uncleaned gun balls

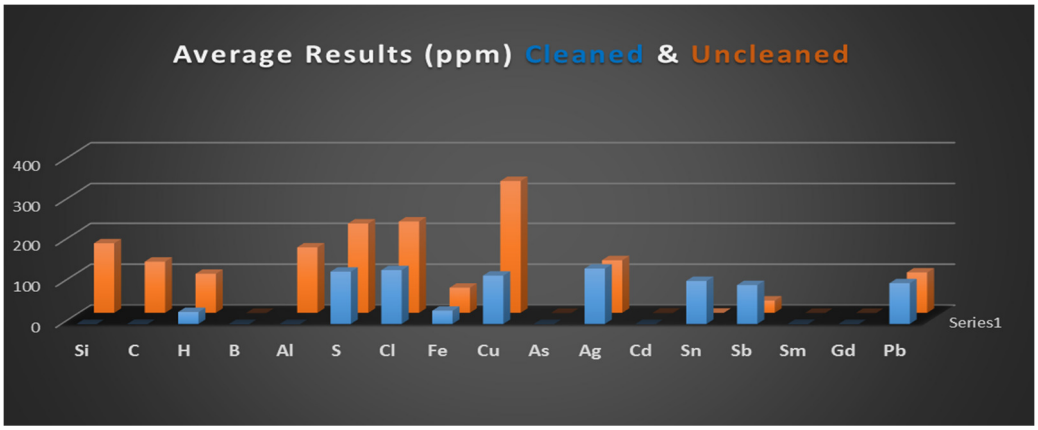

Fig. 2: Difference in the composition of cleaned and uncleaned balls, measured by PGAA

Remaining work

Until the end of the IPERION CH project in Sept. 2019, two more calls for proposals will be announced, and further new experimental proposals are expected in the field of Heritage Science.

Related publication

[1] M. I. Dias, Zs. Kasztovszky, M.I. Prudêncio, A.C. Valera, B. Maróti, I. Harsányi, I. Kovács and Z. Szőkefalvi-Nagy: *X-ray and neutron-based non-invasive analysis of prehistoric stone artefacts: a contribution to understand mobility and interaction networks*, Archaeological and Anthropological Sciences **9,** 1-15 (2017)

[2] B. Constantinescu, D. Cristea-Stan, Z. Szőkefalvi-Nagy, I. Kovács, I. Harsányi and Zs. Kasztovszky: *PIXE and PGAA – Complementary methods for studies on ancient glass artefacts (from Byzantine, late medieval to modern Murano glass)*, Nuclear Instruments and Methods in Physics Research B **417,** 105–109 (2018)

[3] L. Szentmiklósi, B. Maróti, Z. Kis and Zs. Kasztovszky: *Integration of neutron-based elemental analysis and imaging methods and applications to cultural heritage research*, Journal of Archaeological Science: Reports **20,** 476–482 (2018)

[4] M. I. Dias, Zs. Kasztovszky, M.I. Prudêncio, I. Harsányi, I. Kovács, Z. Szőkefalvi-Nagy, J. Mihály, Gy. Káli, A. C. Valera and A. L. Rodrigues: *Investigating beads from Chalcolithic funerary cremation contexts of Perdigões, Portugal*, Journal of Archaeological Science: Reports **20,** 434–442 (2018)

[5] D. Atkins, J. Beaucour, T. Pirling, U. Koester, N. Kardjilov, F. Ott, E. Ando', A.Tangettini, I. Tomandl, I. Groutso, C. Montet-Beaucour, I. Matuschevskaya, V. Danilovitch, S. Dernovitch, V. Kochman and V. Lakiza: *Neutron and laboratory x-ray characterization of excavated Napoleonic artefacts from the Berezina Battlefield in Belarus* (oral presentation), NINMACH 2017, 11-13 Oct 2017, Budapest, Hungary

"NPI (Nuclear Physics Institute, The Academy of Science of the Czech Republic, Rez Prague)"

COLLABORATION WITH THE EUROPEAN SPALLATION SOURCE

Margit Fábián, Eszter Dian, Katalin Gméling, Dávid Hajdú, Milán Klausz, Péter Zagyvai

Objective

The European Spallation Source (ESS) aspires to be the brightest neutron source of the world, which requires a joint and organised effort of the neutronics community, as well as research and development in fields like shielding and neutron detection.

For this purpose, the key objective of the 6th Work Package (WP) of the BrightnESS* Grant - Collaboration, communication and dissemination - is to strengthen the community building between members of the supply chain and stakeholders. The goal is to gain future users' trust from science and industry by means of expanding the ESS community and network. Regarding the communication, the objective is to raise awareness about ESS as the role model for managing large-scale in-kind contributions to research infrastructures. By raising awareness about ESS, the member states will be supported in their decision making process for joining other international projects which will be built in partnerships. In addition, these communication measures will support the exchange of best practice among research infrastructures, which are built with a significant amount of in-kind contributions.
For the effective and reasonable utilization of the available funds, several simulations and measurements have to be performed as a contribution to the decision making process e.g. for the selection of the appropriate detector technologies or shielding design.
As an example, different detectors and detector setups are considered for the small angle neutrons scattering instruments (SANS) of the ESS, which will be challenged by the expected high count rate provided by the unique neutron yield of the ESS. On the other hand, in terms of shielding, a new PE-B4C-concrete (polyethylene plus boron-carbide) has been developed as part of the SINE2020 project, to improve the neutron absorption effect of concrete below 10 MeV, where iron has resonances in the cross section. It's essential to know the activation of the shielding material, like concrete and its metal components, both considering short-term effects on personnel during the operation phase and long-term effects on the decommissioning of the ESS facility.

Scientific and public outreach

The main objective of this task is to achieve a broad dissemination of the information and communication materials and to develop target-group specific prospectuses. The following activities are envisaged for the respective target groups:

Shareholders and stakeholders: they will receive the regular newsletter about the project and will be invited to project related events.

Future users: i) producing materials for use in scientific journals, ii) promotion and encouragement of publishing articles related to the achievements of the project, iii) promoting and co-branding BrightnESS at related events, workshops and conferences, iv) employing social media, v) liaising with university networks to disseminate informational material about the possibilities offered by the project for students.

Industry: industry outreach will occur through the hosting, collaboration and co-branding of events targeted at industry.

Methods for experimentation and simulations

Potential off-the-shelf detectors, like the ^{3}He-tubes or the BCS (boron coated straw) detectors were tested with realistic Monte Carlo simulations using Geant4. The detectors were compared in terms of count rate capability under realistic ESS operational conditions.

For the shielding activation study, typical shielding materials, like metal (Al, Cu and stainless steel) and concrete samples were irradiated in the fast and the rotating vertical irradiation channels of the Budapest Research Reactor for neutron activation analysis (NAA). The samples were measured with a High-purity Germanium (HPGe) detector, from which their activity and composition was determined. The composition of the samples was also determined with prompt gamma activation analysis (PGAA).

Results

Communication and collaboration:

Budapest Neutron Centre (BNC) a partner in ESS instrumentation and the BrightnESS, BNC is involved to prepare a video pilot project, with name **BNC-BrightnESS partner video;** https://www.youtube.com/watch?v=dNi_dTaBh6c&t=14s

11th Central European Training School (CETS); More than 30 students from all over Europe participated at the annual CETS at BNC in Budapest and got a unique insight into the ESS project; https://brightness.esss.se/news-and-press/11th-central-european-training-school-neutron-techniques

The *15th Conference & Exhibition of the European Ceramic Society* (ECerS2017) took place in Budapest, Hungary, from the 9th to the 13th of July, 2017. The MTA Centre for Energy Research/BNC hosted the Ceramic and Composites in Harsh Nuclear Environment event. The BrightnESS project was invited to present the European Spallation Neutron Source, give an overview

about the ESS and the future scientific and user possibilities. The dialogue's main part focused on two questions; how neutrons can be used to meet the industrial challenges and what are the access possibilities to the ESS; https://brightness.esss.se/news-and-press/ceramics-and-composites-in-harsh-nuclear-environment-meeting

The 2nd *Neutron Imaging and Neutron Methods in Archaeology and Cultural Heritage* (NINMACH2017) was held in Budapest from 11–13 October 2017. The conference was a significant event, bringing together 103 participants from 24 countries. Besides the keynote lectures and the invited talks, the conference hosted a diverse range of talks connected to five main topics: 1. Imaging, 2. Multi-technique approach and complementary methods, 3. PGAA & NAA, 4. Neutron scattering, and 5. Facilities, techniques and data processing. The organizers of the NINMACH conference aimed to give continuity to the discussions started in this conference and to encourage cooperation exp. in frame of different projects, like BNC, IperionCH proposals, or in the near future using the ESS infrastructure.; https://brightness.esss.se/news-and-press/budapest-neutron-centre-hosts-ninmach2017

*Academic-Industrial workshop: o*n the 1 December 2017, the Roland Eötvös Physical Society with the Hungarian Academy of Sciences supported by the BrightnESS held a successful meeting on the subject on enhancing collaboration between the academic sector and the industry. The forum also discussed the role of large-scale European research facilities (exp. ESS, ESRF) in industrial use. The industrial sector also expressed their wish that their needs should be incorporated in the curriculum of physics education.

Experiments and simulations:

The activation experiment confirmed that the newly developed PE-B4C-concrete is not activated as much as the initial reference concrete, but the study also revealed the importance of trace elements in terms of activation.

The first results of the detector simulation project raised the awareness of the neutronics community on the expected challenging count rates in the ESS.

Remaining work

In terms of the BrightnESS tasks, this will be the second year of a three-year project; in 2019 the work will continue according to the well-prepared WP6 schedule.

In the last year of the SINE2020 related shielding study, the impact of the trace elements will be examined by Monte Carlo simulations. ***The detector count rate study is a three-year project, several additional detectors and instrument setups are going to be compared in the upcoming two years.***

Related publications

[1] *Novel Technology Advances as Budapest Neutron Centre Leads Optimisation of ESS Moderator*; https://europeanspallationsource.se/article/novel-technology-advances-budapest-neutron-centre-leads-optimisation-ess-moderator

[2] E. Dian et al: *Preparation for activation measurements of concrete and PE-B4C-concrete to be applied for shielding at the European Spallation Source,* J. Phys.: Conf. Ser. **1021,** 012050 (2018)

* Building a Research Infrastructure and Synergies for Highest Scientific Impact on ESS - BrightnESS

THE CHANDA TRANSNATIONAL ACCESS

Tamás Belgya[1], Celal Asici[2], Lerendegui-Marco[3], Boglárka Maróti[1] and Ildikó Harsányi[1]

[1]MTA EK, [2]Eskisehir Osmangazi University (Turkey), [3]Universidad de Sevilla (Spain)

Objective

The objective is to provide Transnational Access (TNA) to certain experimental facilities for use by researchers from the European Union (EU) and associated countries in the field of nuclear data measurements for the nuclear power industry and other applications.

Methods

The Solving Challenges in Nuclear Data for the Safety of European Nuclear Facilities (CHANDA) is an EU founded project aiming to provide high quality nuclear data for modelling innovative GEN-IV reactors and for performing model calculations to find the best construction to make fission based energy production sustainable and to improve safety including the closure of nuclear fuel cycle.

The CHANDA project applied the user access schemes that were worked out in the preceding supported periods of the nuclear data measurement projects such as FP7 ERINDA and FP6 EFNUDAT. The MTA EK joined to the CHANDA project in 2014 with its Prompt Gamma Activation Analysis (PGAA) facility. We accept proposals that use our sample chamber environment and data acquisition systems, as well as arbitrary setups with user-brought acquisition systems. In the case of using our regular setup, we help to analyse the data, while in the case of use of external acquisition systems the users are expected to analyse the data.

Results

In 2017 we performed two experiments which were accepted by the Program Advisory Committee of CHANDA. 1./ In July an experiment entitled "Investigation of the gamma-strength function of ^{232}Th nucleus from thermal neutron capture" proposed by a Turkish PhD student and his advisor. In this case, our own Th sample was used.

2./ In October an experiment entitled "Thermal neutron capture cross section of ^{242}Pu at the Budapest Research Reactor via PGAA" proposed by a Spanish ERC group leader and his PhD student. The samples for this experiment came from the CERN n-TOF facility.

High quality radiative neutron capture and associated background spectra were measured on ^{232}Th metal powder-sample. After careful subtraction of the background and the gadolinium spectrum (a difficult to separate component of Th ore with a very large capture cross section) and unfolding with the response functions of the PGAA detector, a pure, full energy spectrum of ^{233}Th was extracted. This spectrum can be simulated with a homemade statistical simulation program to find out the best gamma-ray strength functions that satisfactorily models the decay patterns of the gamma rays in the ^{233}Th decay scheme. The PhD student continues the time consuming job of the data reduction.

Two highly enriched ^{242}Pu samples electroplated on Al backings and covered by a thin Ti layer were used as targets for a series of measurement to determine the ^{242}Pu cross section in the ^{242}Pu(n,γ)^{243}Pu reaction. Supplementary experiments were also performed to measure the Al, Ti, H and background contributions to subtract from the 243Pu spectrum. Beside these experiments, ^{242}Pu samples were also irradiated with a gold monitor to determine the size of the radiative capture cross section of ^{242}Pu using our comparator method. The data reduction of this latter work has been evaluated. The full energy spectrum, which was also calculated by the unfolding method, can be seen in Fig. 1.

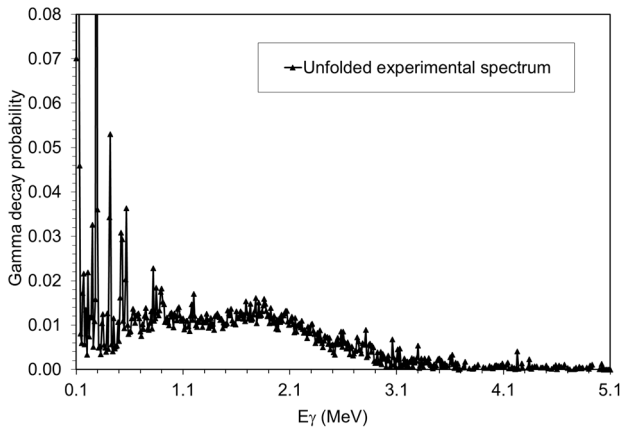

Figure 1: Unfolded ^{243}Pu gamma-ray spectrum from neutron radiative capture reaction.

Remaining work

A manuscript for the ^{242}Pu cross section experiments is ready for submission to Phys Rev. C. Modelling of the strength functions are under development.

IN VESSEL MELT RETENTION EXPERIMENTS ON THE CERES FACILITY

Attila Guba, Gábor Baranyi, György Ézsöl, Valér Gottlasz, Attila Nagy, István Trosztel

Objective

The Fukushima accident in Japan highlighted that both the in-depth understanding of Severe Accident phenomenology and the development or improvement of adequate severe accident management measures are essential in order to further increase the safety of the nuclear power plants operated in Europe. As a result of the Fukushima accident, the European Council requested that a comprehensive risk and safety assessments ("Stress Tests"1,) be performed on all European nuclear power plants.

Among the findings and recommendations to be taken into account, one directly targets molten corium stabilization and the needs for analysis and selection of feasible strategies and implementation of provisions against containment degradation by molten corium. The compilation report highlights also the need for further studies regarding Severe Accident timing including core melt, Reactor Pressure Vessel (RPV) failure, etc… to improve Severe Accident Management Guidelines (SAMG) strategies for European NPPs. In case of severe accidents when the core is melting the falling debris is gathering in the bottom of the vessel. In the molten material, density separation is taking place. On the bottom, the high density material forms a crust layer on the vessel wall which insulates the heat flow. Most of the still rather high decay heat attacks the reactor vessel at the light metal layer, which is called a "focusing event". If the cooling is inadequate, the high heat flux can melt the vessel material causing vessel failure. For the new generation power plants, a so called "core catcher" is installed under the reactor vessel to maintain the molten material in the case of loss of vessel integrity. For the existing older power plants, the installation of the core catcher may not be feasible or too expensive.

One of the new Severe Accident Management strategies which is attracting more and more interest is the In Vessel Melt Retention (IVMR) strategy for Light Water Reactors (PWR, BWR, VVER). Ensuring that the corium could stay in the RPV (as happened during the TMI-2 accident) during a Severe Accident would reduce significantly the loads on the last barrier (the containment) and therefore reduce the risk of release of Fission Products to the environment for most of the Severe Accident Scenarios.

This type of Severe Accident Management strategy has already been incorporated in the SAMGs of several operating small size Light Water Reactors (reactors below 500 MWe (like VVER440)) and is part of the SAMG strategies for some Gen III+ PWRs like the AP1000. The main objective of the project is to evaluate if the In Vessel Melt Retention (IVMR) Severe Accident Management strategy could be applicable to other Light Water Reactors (PWR, VVER, BWR).

Methods

As a severe accident management measure, the in-vessel corium retention by external cooling of the reactor pressure vessel has been selected for the Paks Nuclear Power Plant of VVER-440/213 type. To support the implementation in the Paks plant, a research and development program has been going on at the MTA EK, Budapest, Hungary. The research program is primarily based on the experimental research practice gained in the PMK-2 projects, the first integral type experimental and computer code modelling program for the VVER-440/213 plants, with participation of 29 countries from European and overseas countries. Due to the very high safety significance of the possible accident processes leading to core meltdown, the design and construction of an integral type model of the cooling loop to be implemented in the Paks plant was initiated. The model, named CERES (Cooling Effectiveness on Reactor External Surface), was put into operation in the hall of the PMK-2 facility, using the power units, water treatment and data acquisition system of PMK-2. The CERES is a scaled down model of the cooling system intended to apply to the Paks NPP, having a 1:40 slice of the vessel, while the scaling of 1:1 for the elevations was maintained to provide the same gravitational driving forces for circulation. The heating system representing the molten material is flexible to be able to adjust to the necessary profile. The design represents the power plant sump level, which leads to having the level in the cavity. Therefore, no circulation is possible; the flow channel is a U-tube like configuration.

The CERES facility is an integral type model of the cooling loop as it is in the plant for external cooling of the reactor vessel. The cooling channel in the vessel model, has different gap sizes between the vessel and cavity walls, having a "critical" narrow gap size. It is critical from the viewpoint of the heat extraction, because, to some extent, it can block the steam in the narrow gap. The length of the narrow gap coolant channel section is 900 mm. The critical gap size can be varied across the experiment series. Heaters provide heat load caused by the corium with values and distribution as calculated by the ASTEC code. The operating pressure of CERES is atmospheric.

Results

For the IVMR project, an elevated sump water level is used since in other VVERs the sump level may be much higher than the level used for Paks Nuclear Power Plant experiments. To achieve the increased water level a new tank is installed at the top elevation. With this layout the water level is high enough to close the loop on the top, which results in the possibility of natural circulation. Since the presence of the continuous circulation, the heat removal at the focusing effect is much better compared to that with the lower level non-circulating configuration. The heating power used in the transient was increased to a very high value and the heat removal was still successful.

The results of the experiment may be used for validation purposes.

PARTICIPATION IN THE EU SAFEST PROJECT

Imre Nagy, Róbert Farkas, Nóra Vér, Péter Szabó, Zoltán Hózer

Objective

In the framework of the EU SAFEST project, experimental facilities are used for the simulation of reactor accident scenarios. The main objective in 2017 was the rebuilding of the CODEX test facility for the execution of a new air ingress test.

Methods

The CODEX facility was extended with several new features in order to meet the requirements of the forthcoming test. Part of the new elements was purchased from different companies, and significant work (welding, construction, making electrical and gas supply connections, etc.) was performed in the mechanical workshop of the laboratory.

Results

The reconstruction of the CODEX-AIT-3 test facility included the following main tasks:

- Fuel rods with zirconia pellets and double internal heaters were fabricated and a bundle of seven fuel rods was constructed.
- External heating and top cooling was applied on the test section in order to provide the necessary boundary temperature conditions.
- A new mass spectrometer was connected to monitor the outlet gas composition.
- Special flow controllers and a pump were built into the facility to establish steam and oxygen starvation conditions in the high temperature phase of the test.
- A new DC power supply system was installed to reach the target temperature (1600 °C) in the bundle.
- The steam valves were replaced by new ones with robust design to avoid steam leakage observed in an earlier test.
- A gas system was connected to the central fuel rod in such a way that pressurization up to bursting could be performed during the oxidation phase of the experiment.

Figure 1: new elements of the CODEX facility (left-to-right) scheme of the heated fuel rod, view of the bundle with thermal insulation, cooler of the test section and mass spectrometer

A single rod heating test was performed to check the new electrical heating system with zirconia pellets. A temperature of 1000 C was reached and the test lasted for more than one hour in an argon atmosphere. Degradation was observed in the lower part of the rod, probably due to eutectic interactions between the non-oxidized cladding surface and the K type thermocouple. The test provided useful information for the finalization of the bundle design and at the same time it proved the applicability of the two heater wires design inside of the fuel rod.

Remaining work

The CODEX-AIT-3 experiment will be carried out and the post-test examination of the degraded bundle will be performed. The database of measured data will be collected.

Related publication

[1] Z. Hózer, I. Nagy: Status of CODEX Air Ingress Test CODEX-AIT-3, presentation at the SAFEST Project Progress Meeting April 23, 2018, Sol Costa Atlantis, Spain

ZIRCONIUM MATERIALS SCIENCE STUDIES

Zoltán Hózer, Ildikó Szenthe, Márta Horváth, Ferenc Gillemot, Gábor Uri, Erzsébet Perez-Feró, Tamás Novotny, Zsolt Kerner, Nóra Vér, Áron Horváth, Zoltán Kis, Márton Király, Richárd Nagy, Attila Nagy, Ádám Almási

Objective

The primary aim of this three-year project is the extension of our knowledge on the behaviour of Zr cladding tubes in both normal and extreme reactor conditions. The experimental data can be used for model development. New examination techniques are being introduced to characterize the structural changes in the investigated alloys.

Methods

Several different experimental and numerical tools were used in the first year of the project:

- The irradiation of Zr samples is being carried out in the Budapest Research Reactor. Special sample holders were developed and a dedicated channel is being used in the reactor core for this purpose.
- The normal operational corrosion was simulated in autoclaves at 300 °C temperature and 86 bars pressure. The water compositions used corresponded to different phases of reactor operation.
- A high temperature vacuum system was used for charging Zr samples with hydrogen. A careful calibration was performed and the amount of absorbed hydrogen was determined with several methods. The homogeneity of the H distribution was examined using neutron radiography.

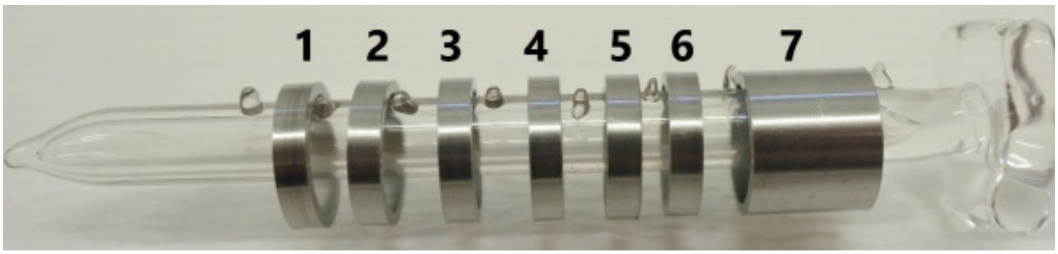

Figure 1: View of Zr rings and sample holder used in the hydrogen charging procedure

- A high temperature furnace was used for the oxidation of Zr in a steam atmosphere and for treatment in an inert gas. Some of the samples were quickly moved into cold water after the oxidation in order to simulate a water quench. Other samples were cooled down slowly in argon. The oxidation tests were carried out in the temperature range of 600–1200 °C.
- An optical system with high speed cameras was used to monitor the high temperature ballooning of cladding tubes in a high temperature furnace.
- The mechanical interaction of a pellet and it's cladding was simulated with a segmented mandrel tool in a tensile test machine. The samples could be heated up 300 °C in the facility. Finite element simulation was used for the numerical modelling of cladding tube mandrel tests.

Results

The irradiation of 186 ring and axial samples has been started in the Budapest Research Reactor. Most of the samples were pre-treated in an inert gas or hydrogen atmosphere. The first period of irradiation has been successfully completed.

The mass gain was measured during 28 days of treatment in autoclaves and the corrosion kinetics was determined for both E110 and E110G alloys in different water chemistry conditions. These samples are available for further testing and examinations.

More than 600 Zr samples were charged with hydrogen for further examinations. The kinetics of H uptake was determined. It was observed that in the phase transition range $\beta Zr \Rightarrow \beta+\delta Zr$ the uptake accelerated significantly, probably due to the microstructural changes.

The database of oxidation kinetics of E110 and E110G alloys was extended with more than one-hundred new data points. Samples with slow and fast cool-down were produced for mechanical testing. Samples treated in an inert gas at high temperature are available for the evaluation of the effects of oxidation and thermal treatment.

Video recording of cladding deformation at high temperatures was successfully performed for several samples. A numerical evaluation was introduced to characterise the time dependent variation of the cladding geometry. The burst pressures of E110 type samples tested at 700 °C, 800 °C and 900 °C temperature with 0.03 bar/s, 0.3 bar/s, 1.5 bar/s, 3 bar/s and 6 bar/s pressurization rates were determined to support code development.

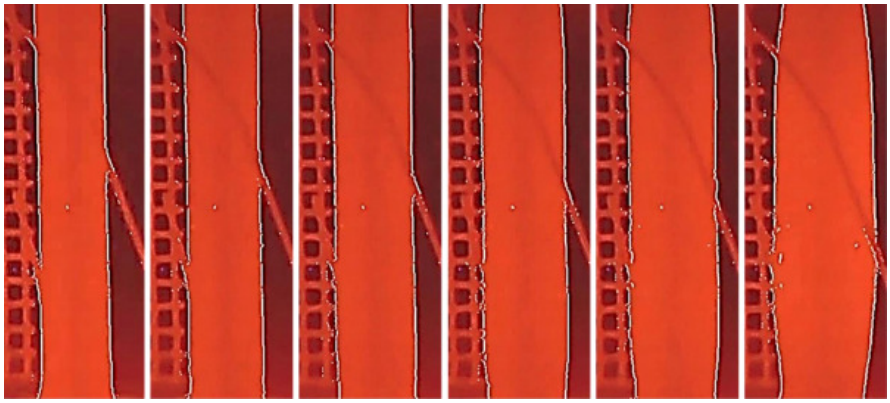

Figure 2: Contour of cladding samples during ballooning at 800 °C with 0,4 bar/s pressurization rate, the time difference between the pictures is 3 s (left-to-right)

The mandrel tests were carried out with as received and with heat treated cladding rings. The force-displacement curves were recorded for each test. The first experience with the segmented tool showed that short rings suffered relatively large deformations and the long rings could be considered more representative for the fuel rod cladding. The numerical analyses pointed out the importance of friction forces in the segmented tool and provided valuable information for further tests.

Figure 3: View of 2 mm and 8 mm long ductile cladding rings after mandrel tests (left) and finite element model of the segmented tool

Remaining work

The irradiation of Zr samples will be continued to reach higher neutron fluence values. The mechanical testing of irradiated samples will be carried out after a several year storage in hot cells.

Mechanical testing of hydrogen charged, thermally treated and oxidised samples will be performed. Examination of cladding microstructure will be carried out for selected samples.

Mandrel testing will be performed with new lubricant materials and with chemically pre-treated samples.

Related publications

[1] I. Szenthe, M. Horváth, F. Gillemot, G. Uri: *Irradiaton of Zr alloys in the Budapest Research Reactor*, MTA EK-FRL-2017-229-1-1-M0, in Hungarian (2017)

[2] E. Perez-Feró, T. Novotny, Zs. Kerner: *Corrosion of Zr claddings*, MTA EK-FRL-2017-230-2-1-M0, in Hungarian (2017)

[3] N. Vér, T. Novotny, Á. Horváth, Z. Kis, E. Perez-Feró: *Charging of Zr cladding with hydrogen*, MTA EK-FRL-2017-230-1-1-M0, in Hungarian (2017)

[4] E. Perez-Feró, T. Novotny: *Oxidation of Zr cladding in steam at atmospheric pressure*, MTA EK-FRL-2017-232-2-1-M0, in Hungarian (2017)

[5] E. Perez-Feró, T. Novotny: *Thermal treatment of Zr samples in inert gas atmosphere*, MTA EK-FRL-2017-232-1-1-M0, in Hungarian (2017)

[6] M. Király, R. Nagy, A. Nagy, Á. Almási: *Investigation of high temperature ballooning of cladding tubes*, MTA EK-FRL-2017-234-1-3-M0, in Hungarian (2017)

[7] R. Nagy, M. Király: *Finite element simulation of cladding tube mandrel tests*, MTA EK-FRL-2017-236-1-1-M0, in Hungarian (2017)

NONDESTRUCTIVE EVALUATION (NDE) SYSTEM FOR THE INSPECTION OF OPERATION-INDUCED MATERIAL DEGRADATION IN NUCLEAR POWER PLANTS – NOMAD

Ildiko Szenthe, Ferenc Gillemot, Antal Gasparics, Gábor Vertesy

Objective

NOMAD (European Research Project) focuses on the non-destructive investigations of RPV (Reactor Pressure Vessel) steels to better assess their integrity for lifetime management. The primary goals of NOMAD are:

- Development and calibration of an NDE tool for the in-situ inspection of cladded RPV material which may have microstructure heterogeneities.
- Validation of the surveillance programs with respect to an actual vessel under LTO (long term operation) conditions.

In order to reach these goals, multiple NDE methods will be used on samples at many scales under neutron irradiated conditions: e. g. micromagnetic, electrical, ultrasound and acoustic emission methods. The results will be compared and combined in order to define a hybrid approach and finally demonstrate it in a modular way.

Methods

Non-irradiated material with different microstructures will be used for sensor optimization without any radiation hazard. Non-destructive evaluations will be performed in hot cells for the irradiated samples.

MTA-EK apply magnetic adaptive testing (MAT) based on a systematic measurement and evaluation of minor magnetic hysteresis loops. This technique is a way towards optimization of hysteresis testing. Special emphasis has been taken to optimize the measurement conditions, considering the optimal design of the magnetizing head and optimization of the measurement parameters, such as the slope of magnetizing current, sampling frequency, and step of magnetizing current between minor loops.

Results

MTA EK has participated in the selection of the materials, ensured the as-received samples and blocks from 15kH2NMFA and JRQ type RPV material. The team performed heat treatment studies on A508Cl.2, 15kH2NMFA and JRQ materials and evaluated them. The Measurement Team has performed an initial NDT (Non-destructive Evaluation Test) experiment in order to investigate the material homogeneity. If measurements are performed with different magnetizing yokes, the shape of the permeability loops are rather different. Based on the results we have chosen the yoke to be used in the future.

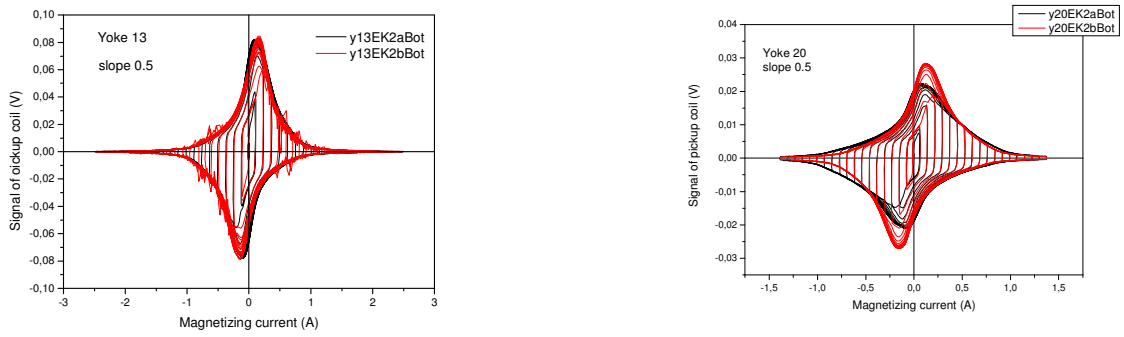

Figure 1: Permeability loops measured on different 15kH2NMFA samples, using different size magnetizing yokes

Remaining work

During the future measurements, the hysteresis loops of the differently degraded samples will be compared and evaluation of loops will result in a large number of parameters, some of them characterizing the material degradation. This gives us a good chance to provide reliable data about material degradation.

EK PROGRESS IN THE ATLAS+ PROJECT

Levente Tatár

Objective

The main objective of the ATLAS+ (Advanced Structural Integrity Assessment Tools for Safe Long Term Operation) project is to develop advanced structural assessment tools to better address the safe long-term operation of nuclear reactor coolant pressure boundary systems. In such sense, the ATLAS+ is a direct continuation of the STYLE (EU FP7) project. One of the most important work packages of the ATLAS+ project is WP1: "Design and execution of simulation oriented experiments to validate models at different scales". On a small scale, MTA EK is involved in material characterization experiments. On the medium scale, MTA EK, in close cooperation with BZN (Bay Zoltán Nonprofit Ltd. for Applied Research), will carry out a medium size experiment. It consists of welding an extension arm to the MU (Mock-up) produced in the STYLE project, preparing a notch in it, developing a crack by fatigue and studying the crack extension under loading. Figure 1. shows the conceptual setup and parts of the MU. Preparatory work for this experiment is shared between MTA EK and BZN; the experiment itself will be carried out by BZN on their Instron 8850 testing machine.

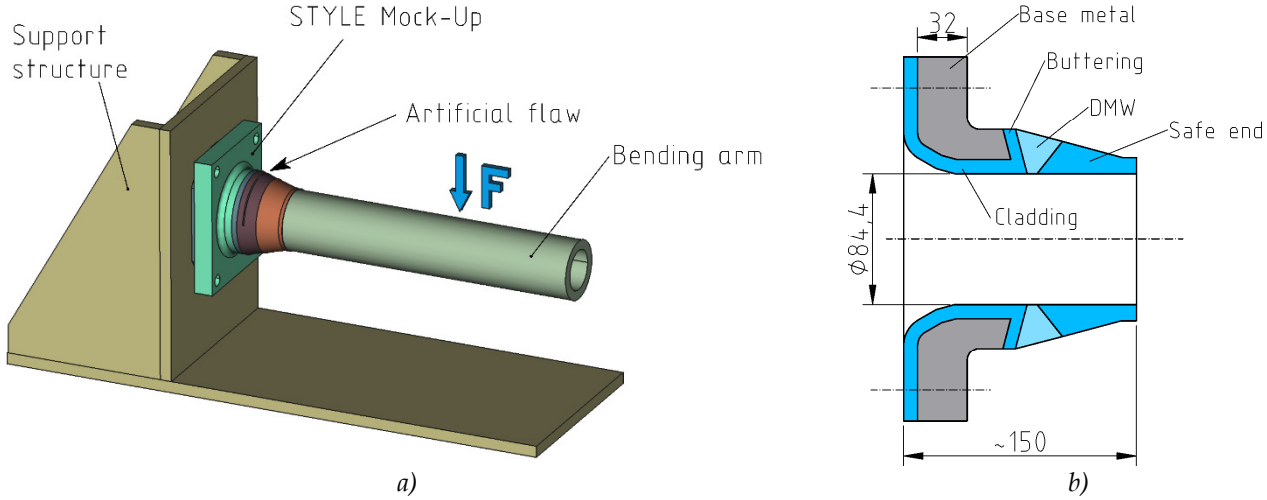

Figure 1: a) Concept of experimental set-up, b) Parts of the MU. (DMW=Dissimilar Metal Weld)

Methods

To assure that the experiment can be carried out successfully, a number of subtasks have to be carried out.

- To assure that the force and displacement of the Instron testing machine are enough to develop a crack from the notch by fatigue and to obtain a noticeable crack propagation during the final loading
- To assure that the support structure or its bolts (not shown in figure) will not fail during the preparatory fatigue precracking or the final test.
- To assure that no clashing occurs during the experiment between different parts of the object being tested or the object and the testing machine and that the testing machine will not be damaged.

To reach our goal basic analytical computations, FE (finite element) computations on simplified models and fracture mechanics computations based on results from FE computations have been involved.

Results

Preliminary results show that the fracture toughness of the base metal is too high to achieve crack propagation using the testing machine at BZN, even with a crack with a 180° opening. This means, that the crack has to be placed in the DMW or in the buttering layer. Based on the results of the MULTIMETAL (EU FP7) project we can presume that the buttering layer has considerably lower fracture toughness than the DMW. However, due to its shape, the crack edge has to be tilted, which complicates the manufacturing process and it is inconvenient from a simulation point of view too. Another important result of these preliminary computations is that a tubular bending arm with inside and outside diameters corresponding to the diameters of the safe end can't carry enough moment to break even a halfway cut DMW or buttering layer.

Remaining work

As the materials used in the MULTIMETAL project are similar, but not the same as materials used in the MU, we intend to cut a piece from the MU and use for material characterization. As the material obtained in such a way is very limited, a careful planning is needed for the experiments on specimens. Based on these data, the exact location of the notch can be determined. When all pre-test calculations will be finished, the physical preparations for the experiment will begin.

Related publication

[1] L. Tatár, Sz. Szávai: *D1.1.3. WWER dissimilar weld: fracture mechanics analysis on MU.* ATLAS+ Report. 2018.

STRENGTHENING NUCLEAR SECURITY BY PARTICIPATING IN HORIZON-2020 PROJECTS

András Kovács, Péter Völgyesi

Objective

In order to strengthen nuclear security in Hungary and worldwide, the Nuclear Security Department got involved in three different Horizon-2020 EU projects. The aim of the ***C-BORD*** („effective Container inspection at BORDer control points") project (2015-2018) is to develop, improve and test new comprehensive and cost-effective detection methods for higher efficiency Non-Intrusive Inspection (NII) of freight containers to be used both at sea ports and at land border crossing points. The ***INSIDER*** ("Improved Nuclear Site Characterization for Waste Minimization in Decommissioning under Constrained Environment") project (2017-2021) prepares us for the necessary tasks concerning the decommissioning and dismantling (D&D) of nuclear facilities (power reactors, fuel cycle plants, research facilities) until their remediation and clearance, which is a global international industrial challenge for the XXI-st century. Thus, the project aims at developing and validating an improved integrated methodology of characterisation based on different new methods of statistical processing and modelling, coupled with present (and adapted) analytical and measurement methods, with respect to sustainability and economic objectives. The aim of the third project, the ***ITRAP+10 Phase II*** **(„**Illicit Trafficking Radiation Assessment Program") (2017-2018) is to monitor l the technical conditions and scientific capabilities of 5 European test laboratories dedicated to testing various portable, relocatable and mobile radiation detector systems, i.e. spectroscopic radiation portal monitors (SRPM), handheld radioactive isotope identification devices (RIID) and personal radiation detectors (PRD) according to the relevant international standards.

Methods

1. In the ***C-BORD*** project an advanced X-ray scanning system (developed by Smiths Detection), a set of relocatable and mobile radiation portal monitors (RPM, developed by Symetrica Ltd. and CEA) and a new design of gas phase detectors (developed at the University of Manchester and Bonn-Sieg-Rhein University) are planned to be tested at the Röszke land border crossing point in 2018. The next generation of cargo ***X-ray scanning system*** has been designed to improve both the accuracy and the material classification capabilities (high energy material discrimination of the X-ray images). The new HCVM-T X-ray scanner is capable of operating both in portal and in mobile modes (Figure 1). The complete X-ray system is included in the trailer. These X-ray screening systems are designed to optimize security checks at ports, airports and border crossings. These systems are used to inspect entire trucks (cabin included), containers, and smaller vehicles, even for threats such as explosives, narcotics, weapons of mass destruction (WMDs), contraband, as well as for manifest verification, reducing the need for manual inspection. When equipped with the automatic radioactive material detection (ARDTM) (optional), the HCVM-T simultaneously carries out both the X-ray inspection and an analysis to detect the presence of radioactive gamma- and/or neutron-emitting materials within the container or vehicle. The trailer is equipped with an electrical motor that allows independent forward and backward motion. The HCVM-T series systems use a range of electron accelerators from 4 MeV to 6 MeV, allowing steel penetration ranging from 280 mm to 320 mm, while providing a high throughput of up to 25 trucks per hour in scan mode and up to 150 trucks per hour in pass through mode, with up to 4 system operators in the cabin.

Figure 1: The HCVM-T X-ray scanning system with the pass through mode deployed.

The ***current version of RPMs*** is a new generation of passive neutron and gamma detection systems used both in mobile and relocatable arrangements, designed to detect radioactive and nuclear materials. The main aim of the passive technology development is to achieve better sensitivity and improved isotope identification. The new design is capable of determining the category of the radioactive material and its position in the cargo. These relocatable and mobile detector units were tested both in the test laboratory and in the mobile laboratory (VW Transporter) of MTA EK (Figure 2). During the tests only low activity sealed radioactive sources and NORM materials (e.g. fertilizers, zircon sand) were used in the test laboratory. Besides this RPM system, similar gamma and neutron detectors were located in the mobile laboratory of MTA EK (Figure 2 right) and were tested on the campus of MTA EK, as well as in various regions of Hungary.

Figure 2: Relocatable and mobile radiation detector modules of Symetrica under test in the test laboratory (left) and in the mobile laboratory (right) of MTA EK

2. The ***INSIDER*** project was started during the last quarter of 2017, and therefore only evaluation of the available literature data, but no experimental work has been carried out so far, with special emphasis on the performance of the planned experimental techniques under constrained environmental conditions (high temperature and humidity, dose rate, etc.).

3. Concerning the ***ITRAP+10 Phase II*** project, experimental work, i.e. testing of the radiation detectors, e.g. an SRPM, a RIID and a PRD, has not started yet. In order to be ready for the required detector tests, preparatory work to assure and control the required technical conditions at the test laboratory was performed.

Results

1. In the ***C-BORD*** project, the current relocatable and mobile version of radiation portal monitors (gamma and neutron detectors) of Symetrica Co. Ltd. were tested by using various radioactive and NORM materials (e.g. fertilizers, zircon sand) in the test laboratory and also in the mobile laboratory of MTA EK (Figure 2). The aim of these tests was the control and potential improvement of these detectors for the field validation test exercises to be held in 2018 at the Röszke land border crossing place. The tests were carried out according to the requirements of the ANSI 4243-2006 international standard and the detectors identified the different radioactive and neutron sources close to 100% of the time, demonstrating the required technical capabilities and the applicability of the detectors for the field validation exercises.

2. The first results of the ***INSIDER*** project involved the collection of information about instruments and methodologies currently in use for radiological characterization of contaminated sites and structures in constrained environments. The other completed task involved the identification of European companies which specify methodologies for radiological characterization of nuclear installations undergoing decommissioning.

3. Concerning the ***ITRAP+10 Phase II*** project, all necessary technical capabilities of the test laboratory (Figure 2, left) of MTA EK were checked and improved and the required gamma and neutron radiation sources were collected, controlled and tested.

Remaining work

Next steps of the work include the testing of the ***C-BORD*** technologies at the Röszke land border crossing place, the ***INSIDER*** in-field gamma spectrometry measurements at two research reactors undergoing decommissioning and the test measurements of the three different types of radiation detectors in the ***ITRAP+10 Phase II*** project.

Related publications

[1] ***A. Price, P. Völgyesi,*** A. Kovács, L. Morales-Rueda, I. Cullen, M. Foster and G. Dermody: *A Mobile Modular Radiation Detection System Offering Low-Cost Isotope ID and Neutron Source Triage,* International Conference on Advancements in Nuclear Instrumentation Measurements Methods and their Applications, Liege, Belgium, 22. June, 2017.

PARTICIPATION IN THE ACTIVITIES OF THE MULTIDISCIPLINARY EUROPEAN LOW DOSE INITIATIVE

Balázs Madas

Objective

MELODI (Multidisciplinary European Low Dose Initiative) is a European radiation protection research platform with a focus on research on health risks after exposure to low-dose ionising radiation. MTA EK is one of its members since 2013. A major activity of MELODI is the establishment and updating of a long term (>20 years) Strategic Research Agenda (SRA) for research on low dose risk for radiation protection in Europe. The SRA is intended to guide the priorities for national and European research programmes and the preparation of competitive calls at the European level [1]. In 2017, a joint roadmap for radiation protection research had to be prepared also, as a deliverable of the CONCERT project (European Joint Programme for the Integration of Radiation Protection Research) with strong involvement of MELODI.

Methods

A dedicated working group (WG) for the development of the SRA has been formed in 2014 with one member from MTA EK. Since then the WG yearly updates the SRA based on new findings and newly identified research needs. The WG meets once or twice a year. Before 2016, annual MELODI Workshops, and since then the European Radiation Protection Week series provide input and an open forum for discussions on the MELODI SRA. The first joint roadmap has been prepared together with other members of the European radiation protection research community [2].

Results

The MELODI Strategic Research Agenda 2017 has been approved and published in October 2017. The First joint roadmap draft has been submitted in November 2017 [2]. Besides these documents, an article with the strategic research agenda has been also published in Radiation and Environmental Biophysics [1].

There are six key areas of research identified in the MELODI SRA and roadmap: (1) To explore the shape of the dose-response relationship for radiation-induced health effects; (2) To understand the potential impact of individual susceptibility on radiation-induced health effects; (3) To identify, develop and validate biomarkers for exposure, early and late effects for cancer or/and non-cancer diseases; (4) To explore and define the role of epigenetic modifications in radiation-induced health effects; (5) To explore the roles of specific target cells for radiation-induced late developing health effects; (6) To understand the health effects of inhomogeneous dose distributions, radiation quality and internal emitters.

MELODI also encourages education and training in disciplines to maintain, develop and improve skills amongst the low dose health risk research community. In this regard it is important to encourage training by those in the relevant more fundamental sciences. The skills amongst the MELODI community in data management, data mining and bioinformatics are judged to be suitable for further development. In terms of infrastructures for research, MELODI encourages, where appropriate, (1) the use of archived biological materials from prior research, (2) the integration of experienced laboratory networks improving the robustness of results via intercomparisons, (3) the integration of expertise from outside the conventional fields of radiation research, (4) the use of the wider EU scientific infrastructures for, amongst other things genomics, microscopy, structural biology, computing where relevant, (5) the provision of access to the wider community of researchers, where new infrastructures are proposed or developed.

The First joint roadmap draft promotes long-term research to assess the effects of ionising radiation on humans and the environment, and to provide knowledge, methods and tools to improve practical radiation protection. The joint roadmap encourages basic and applied research, highlights the need to continuously update the state of the art of related research fields, and promotes the assessment on human health and ecological effects of ionising radiation in combination with other stressors. The joint roadmap presents a table plotting the exposure scenarios of humans and the environment against different anthropogenic and natural exposure contexts. The exposure contexts are categorised in such a way as to ease stakeholder mapping and consultation. This table will serve to inventory and prioritise the missing knowledge or operational tools to be tackled by the radiation protection research community in the next decades. The joint roadmap also addresses the needs with regard to research infrastructure and education and training.

Remaining work

The SRA has to be updated on a yearly basis. In 2018, a gap analysis and a statement on research priorities has to be also prepared in view of the EURATOM (European Atomic Energy Community) Calls (NFRP-2018-8 and NFRP-2018-9). Stakeholder consultations are planned to assess whether the proposed draft joint and individual roadmaps match the research needs perceived and identified by stakeholders. A second version of the joint roadmap will be published in 2019.

Related publications

[1] M. Kreuzer, A. Auvinen, E. Cardis, M. Durante, M. Harms-Ringdahl, J. R. Jourdain, et al.: *Multidisciplinary European Low Dose Initiative (MELODI): strategic research agenda for low dose radiation risk research*, Radiation and Environmental Biophysics **57**, 5–15 (2018)

[2] N. Impens, J. Repussard, M. Kreuzer, S. Bouffler, H. Vandenhove, J. Garnier-Laplace, et al.: *First joint roadmap draft*, CONCERT deliverable D3.4. (2017)

II. RESEARCH AND DEVELOPMENT RELATED TO NUCLEAR POWER PLANTS

UNCERTAINTY ANALYSIS OF CRITICAL HEAT FLUX MEASUREMENTS CARRIED OUT AT MTA EK

Attila Guba, Imre Nagy, Gusztáv Mayer

Objective

This work is an extension of our previous Critical Heat Flux (CHF) study published in Nuclear Engineering and Design (http://dx.doi.org/10.1016/j.nucengdes.2016.10.026), where the CHF measurements were carried out in an internally heated vertical annulus. A total of 111 CHF data points were measured in the low pressure and low mass flux range. The results were compared to five selected well-known CHF correlations. We pointed out that several published CHF correlations had significant error when they were compared to our measurements in the low flow, low pressure range. In that previous work the effect of the measurement uncertainties has not been evaluated in the comparison. For this reason, we analysed these uncertainties in detail.

Methods

For the uncertainty analysis we used the standard Monte Carlo sampling method. In order to assess these effects, as a first step in this study, we selected one CHF data point (among the 111) which represents our earlier data the best. Secondly, we determined and evaluated the possible sources of uncertainties in our previous measurements. Based on these data a Monte Carlo calculation was carried out in order to assess the effect of the measurement uncertainties during the comparison process we presented earlier.

Results

The results showed that the uncertainties do not influence our previous conclusions significantly, i.e. the relatively high error of the correlations cannot be explained by the measurement uncertainties (Figure 1). This indicates the need for further CHF studies in the low flow and low pressure range.

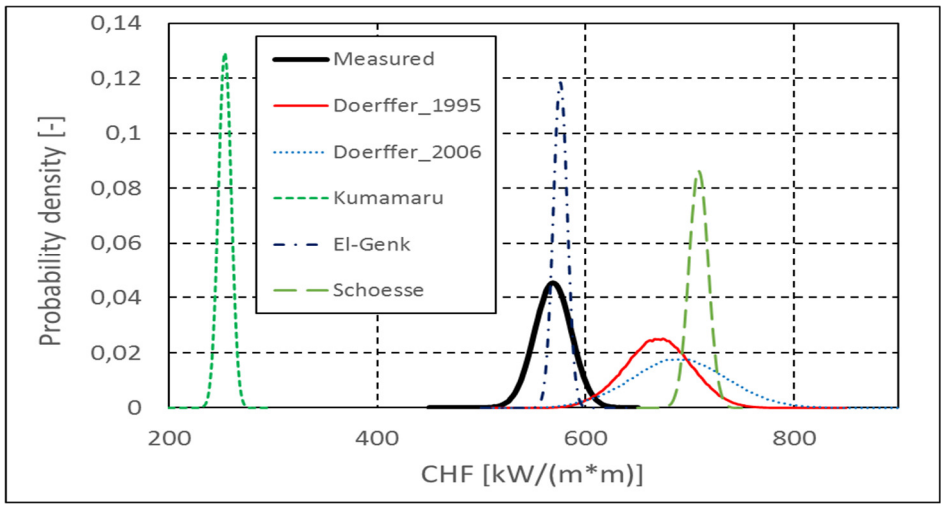

Figure 1: Probability density functions of the calculated critical heat flux correlations

Related publication

[1] G. Mayer, I. Nagy and A. Guba: *Uncertainty Analysis of Critical Heat Flux Measurements Carried Out for Internally Heated Vertical Annulus*, NURETH-17, International Topical Meeting on Nuclear Reactor Thermal Hydraulics, Xi'an, Shaanxi, China, Sept. 3-8, 2017

ADVANCED METHODOLOGIES AND MODELS FOR FUTURE STRUCTURAL INTEGRITY CALCULATIONS

Tamás Fekete, Dániel Antók, Levente Tatár

Background

Structural Integrity (SI) refers to a branch of engineering science that deals with '*the safe operation of engineering components, structures and materials, and addresses the science and technology that is used to assess the margin between safe operation and failure*' –as specified by the European Structural Integrity Society (ESIS).

In case of an actual engineering system that is specifically designated to perform certain technological functions, SI is the technical term that describes both the load-carrying characteristics as well as the stability conditions of the load-bearing solid structure. In other words, SI is the capability of the solid structure to keep all technological aspects together that serve the objectives of the design, assuring that the construction will be safe, up to the technically allowable service lifetime of the system, during normal operation, and also in accidental situations that have a probability to occur at or above a certain level, taking into account the ageing of structural materials and their defective character.

In the scientific domain, SI denotes a relatively young field of engineering science, which deals with the evaluation of engineering solid structures from the safety point of view; that is, how, and for how long they are able to operate under various conditions without catastrophic damage (e.g. brittle fracture, tearing or collapsing), taking into consideration the ageing processes occurring in the structural materials and their stability-reducing effects.

The Reactor Pressure Vessels (RPVs) are the critical components of a nuclear power plant (NPP), as they limit the lifespan of power plants the most. RPVs have very large dimensions (e.g. VVER-440 V213: 149 mm wall thickness with 3800 mm diameter); they work at elevated temperatures (≈270 – 290 °C) and high pressure(s) (≈12.2 MPa). The most important function of the RPV is maintaining constant pressure and temperature conditions that are necessary for controlled power generation during operation. It is also responsible for stable thermodynamic conditions while heating up and cooling down the reactor and, in case of an emergency, for safe cooling down the core and preventing the release of radioactive materials into the containment. The most relevant ageing mechanisms in the structural materials of an RPV are: (1) neutron irradiation assisted ageing, (2) fatigue and (3) thermal ageing. The evaluation of the SI of long term operating RPVs requires adequate knowledge of thermo-mechanical constitutive behaviour (i.e. stress-strain characteristics) and the fracture mechanics properties of their structural materials in various aged states.

The SI of fuel rod cladding tubes is another very important branch of the nuclear reactor technology. Their fast fracture could cause unacceptable release of radioactive products into the coolant liquid of the primary circuit, so these cladding tubes are also safety relevant parts of the system.

Today, there is a growing demand for a simulation model whose predictive capabilities are better than the currently generally used standard engineering models. This requires the application of more physically based, more complex, nonlinear models for future SI analyses of safety-critical NPP components. All physical systems in the real world are inherently nonlinear. One of the most difficult tasks of an analyst is to decide whether a nonlinear analysis is really needed, and if so, exactly where, and to what degree.

During SI analyses, the ultimate – strongly nonlinear – behaviour of a component can be considered as a result of synergistic effects of five nonlinear 'basic' mechanisms: 1) change in the geometry of the component (large deformations occurring at least locally); 2) change in the temperature of the component 3) elastic-plastic or elastic-viscous-plastic material behaviour; 4) change of relevant material parameters along the temperature-path; 5) change of the material behaviour during operation. Because of the inherent nonlinear character of each problem, the effects of the basic mechanisms cannot in general be entirely separated from each other, so the interactions between these 'basic' mechanisms make the development of a methodology for nonlinear SI problems a challenging research topic.

Objective

The final objective of the research program is to develop a unified, coherent analysis methodology and advanced models for future nonlinear SI calculations of various safety relevant systems of NPP units.

The main research directions of the program are formulated as follows:

- Large deformation models for analyses of engineering structures;
- Complex material models for future engineering SI problems;
- Advanced assessment methods for evaluations of material tests;
- Long-time ageing of RPV structural materials.

The treatment of kinematics taking into account geometric nonlinearity is considered applicable here, as – from the physical point of view – the nonlinear theory permits the consideration of increased generality and deeper insight afforded by the finite deformation theory. Complex constitutive models are needed to describe connected material phenomena more precisely wherein strains can be inevitably large. A new modelling framework needs also more advanced methods for the evaluation of material tests.

Methods

In the theoretical part of the project, a material model development – based on a systematic theoretical study– is being conducted in order to elaborate a state-of-the art theoretical and simulation method that seems promising for applications in future industrial SI projects. In the modelling part, numerical models are being developed for special research problems first. These models will be further developed for industrial applications.

Results

The main goal during the theoretical part of the project is the elaboration of a complex material model that is able to describe plasticity and damage in a coupled fashion. Large deformation plasticity theory is used to model the effects of geometrical nonlinearities. Plastic-damage material behaviour is modelled by the Gurson–Tvergaard–Needleman (GTN) material model. The GTN model is based on the hypothesis that the impairment caused by void nucleation and growth in a metal may be macroscopically described by extending the von Mises plasticity theory using a damage variable. The central part of the GTN model, the plastic potential is of the form:

$$\Phi(T,\sigma_m,d^*,f)=\frac{\sigma_v^2(T)}{\sigma_m^2}+2d^*q_1\,cosh\left(q_2\frac{tr(T)}{2\sigma_m}\right)-(1+(q_1d^*)^2)=0$$

where T represents the Cauchy stress tensor, and σ_v designates the local von Mises stress. The yield stress of the matrix material is designated by σ_m, d^* denotes the effective damage variable and f represents the void volume fraction in the matrix material. The parameters q_1 and q_2 were introduced originally by Tvergaard to improve the behaviour of the model for larger values of f. The effective damage variable d^* –which accounts for the effect of the coalescence of neighbouring voids on the yield behaviour– is defined according to following rules:

$$d^*=\begin{cases}d & d<d_c\\ d_c+k(d-d_c) & d\geq d_c\end{cases}\qquad k=\frac{(d_u^*-d_c)}{(d_f-d_c)},\qquad d_u^*=\frac{1}{q_1}$$

where d denotes the damage variable, d_c is critical value of the damage variable at which coalescence occur, and d_f is the ultimate value, at which loss of the load carrying capacity of the material is expected. The evolution equation for the damage variable d is formulated according to the theory of weakly nonlocal – diffusive – internal variables in the internal variable approach of irreversible thermodynamics, as follows:

$$\dot{d}+c\cdot\nabla^2 d=\dot{f}$$

The source of the damage evolution is the evolution of the local void volume fraction ($\dot{f}$), which is composed of the sum of the local void growth $\dot{f}_{growth}$ and the local void nucleation $\dot{f}_{nucleation}$:

$$\dot{f}=\dot{f}_{growth}+\dot{f}_{nucleation}=\overbrace{(1-f)\cdot tr(\varepsilon_p)}^{growth\ part}+\overbrace{A(\varepsilon_m)\cdot\dot{\varepsilon}_m}^{nucleation\ part}$$

where ε_p designates the plastic strain tensor, and ε_m denotes the equivalent plastic strain as follows:

$$\dot{\varepsilon}_m=\sqrt{\frac{2}{3}\varepsilon_p:\varepsilon_p},\varepsilon_m=\int_0^t\dot{\varepsilon}_m\,d\tau$$

Using these symbols, $A(\varepsilon_m)$ is defined as follows:

$$A(\varepsilon_m)=\frac{f_n}{\sqrt{2\pi s_n^2}}\cdot exp\left(\frac{-(\varepsilon_m-\varepsilon_n)^2}{2s_n^2}\right)$$

where ε_n denotes the critical value of ε_m at the maximum of void nucleation, s_n means the standard deviation of ε_m around ε_n, and f_n designates the influence of the process on the damage evolution. The material model will be implemented into user defined subroutines in the MSC Marc FEM system.

In the modelling part of the project, a calculation methodology that simulates the ballooning tests of fuel cladding tubes (Fig. 1. a) has been developed based on a geometrically and materially nonlinear formulation of the problem. Large deformation plasticity theory was used to model the effects of geometrical and material nonlinearities that are present in the system during calculations. The plastic flow curves of structural materials are being developed from tensile test results. Numerical calculations were performed using the MSC Marc FEM code. During the process, a parametric study was conducted to assess the influence of geometrical imperfections and material inhomogeneities on the test results, because – based on theoretical considerations – it was expected that even small geometrical imperfections or material inhomogeneities can have strong effects on the final state, more specifically on the geometry and on the stress-strain state of the test piece.

The 3D finite element models of the ballooning specimens have been tested. The simulations have been performed on a geometrically perfect tube model, with an assumed ring-like material inhomogeneity (Fig. 1. b). The calculation results are presented in Fig 1. (c). It can easily be seen that the final shape and the (plastic) strain field evolves into a 3D structure. Comparing the calculated shape with the experimental result depicted in Fig. 1. a, it can be concluded that the tested ballooning specimen most likely had some initial – ring-like – material inhomogeneity. In the case of another model, the material inhomogeneities were postulated randomly along the tube wall (Fig. 2. a). Results of the simulations are presented in Fig. 2. b. It can easily be recognised that the final shape and the plastic strain field evolves also in this case into a real 3D structure.

Based on the improved theoretical and numerical results, it can be stated that more complex models provide a deeper understanding of the events occurring during material tests as well as contribute to the development of more advanced models for future SI calculations.

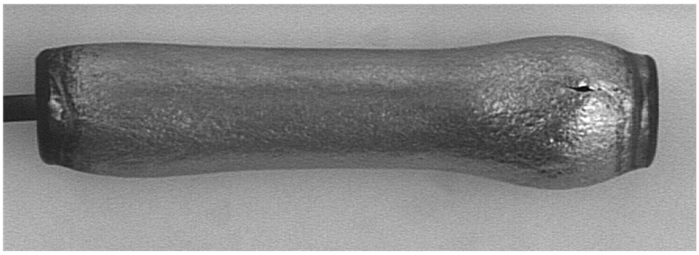

(a)

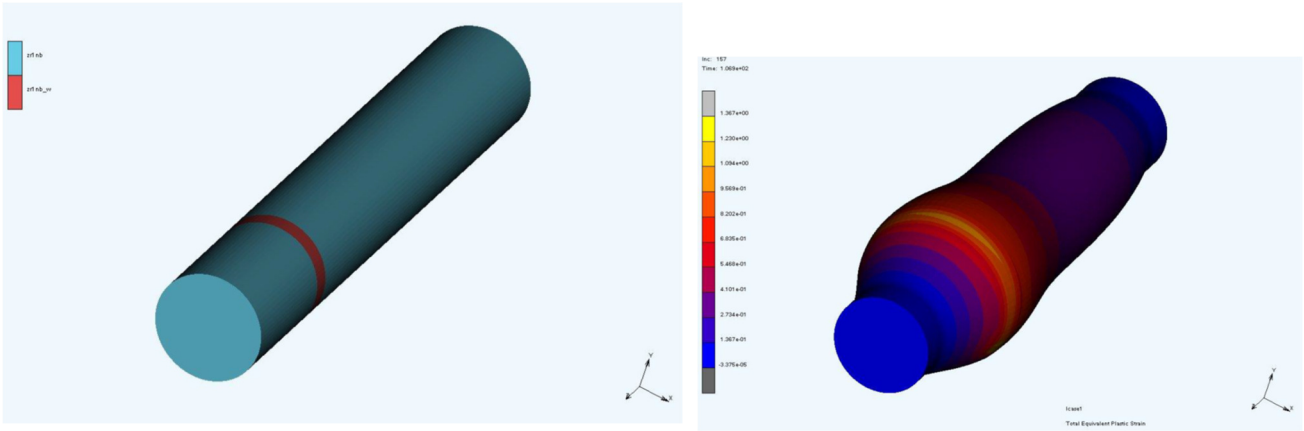

(b) *(c)*

Figure 1: A fuel cladding tube piece after the ballooning test (a), FEM model of the tube with a ring shaped initial material inhomogeneity (b), results of the simulation (c)

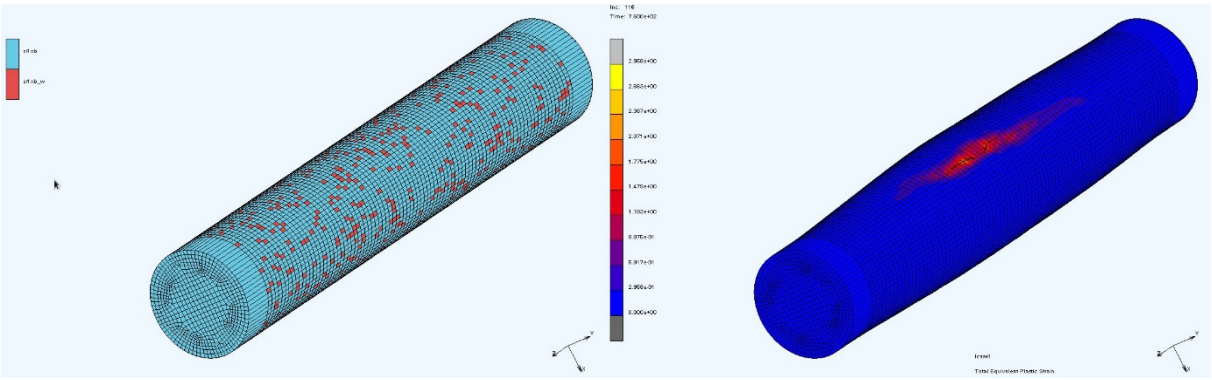

Figure 2: FEM model of a tube piece with randomly distributed initial material inhomogeneities (a), final results of the ballooning simulation (b)

The parameters of a given material model are determined by adequate measurement procedures. A measurement procedure consists of the necessary observations and their evaluation using the very same material model. During SI calculations, the behaviour of the structure will be examined on its more complex geometrical model that is dependent on the material model of the relevant phenomena occurring in the structure during its operation. The key point for reliable calculation results is that the same material model needs to be applied to the structure model as well as to the material model used to evaluate the material tests, to meet the requirement that '*the theory and the experiments need to be harmonized*'. Nowadays, very simple material models are used in standard measurement evaluation procedures that cannot be used to determine the parameters of complex material models. Advanced assessment methods for the evaluations of material tests are being developed therefore, in order to ensure that the appropriate theoretical framework is used when estimating the parameters of a material model. 3D numerical models have been developed for the evaluation of tensile tests (Fig. 3. a.) and of three-point bend fracture tests (Fig. 3. b.), using the MSC Marc FEM system.

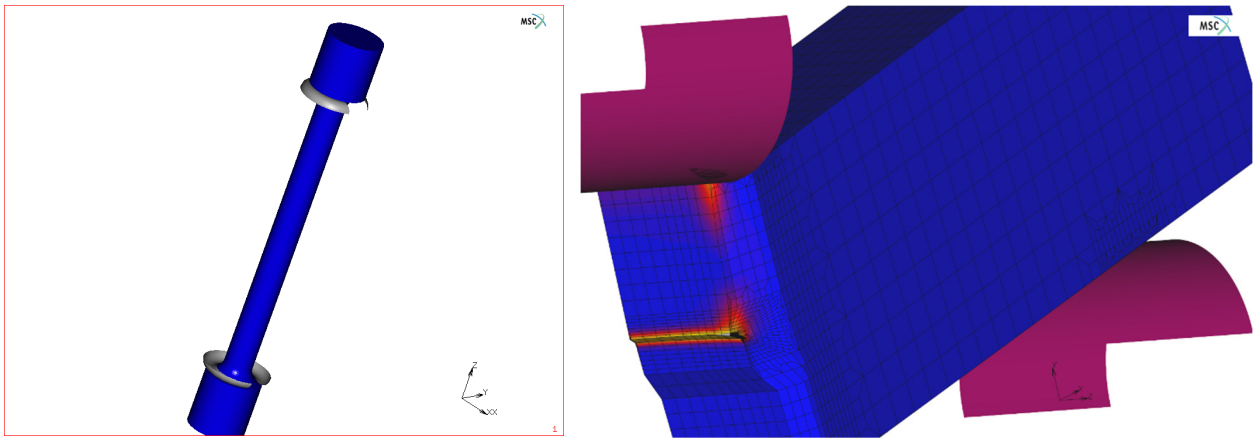

Figure 3: 3D FEM model of a tensile test specimen (a) and a three-point bend fracture mechanics specimen (b)

Remaining work

Further models in the frame of the above depicted research directions are in a research phase.

SIMULATION OF SPENT FUEL POOL LOSS OF COOLANT ACCIDENTS IN THE CORE DEGRADATION EXPERIMENT FACILITY

Imre Nagy, Nóra Vér, Róbert Farkas, Márta Horváth, Mihály Kunstár, Zoltán Hózer,

Objective

The investigation of fuel behaviour related phenomena during loss of coolant (LOCA) accidents in the spent fuel pool was addressed in the experiments. The identification of failure mechanisms due to pressurization and oxidation was the focus of the study.

Methods

VVER cladding materials were tested in the CODEX (COre Degradation EXperiment) facility. The bundles of seven rods were heated by internal electric heaters placed into alumina pellets. Both traditional and sponge based E110 claddings were used in the same bundles. The rods were pressurised and a different initial pressure was set for each of the rods. The simulated scenario was based on the results of the safety analysis performed for a LOCA event in the spent fuel pool of the Paks VVER-440 nuclear power plant.

Results

The CODEX-LOCA-SFP1 and the CODEX-LOCA-SFP2 simulated about 3 hours dry conditions in a spent fuel pool. At the beginning of the experiments the test sections were filled up with water. The tests started with boiling off the coolant and after that a slow heat-up rate was applied.

The maximum temperatures were 924 °C in the first and 896 °C in the second test. The first test was carried out with steam starving conditions in order to simulate limited steam access to the zirconium surfaces.

Due to different internal pressures the fuel rods suffered different degrees of deformation and some of the high pressure rods burst open.

The Zr cladding did not reach a brittle state, and all fuel rods survived the water quench at the end of the tests. The maximum oxide scale observed in the second test reached 10 µm.

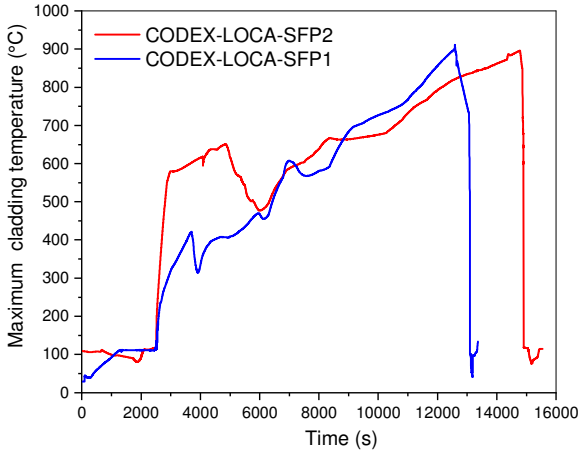

Figure 1: Maximum cladding temperatures in the CODEX-LOCA-SFP1 and CODEX-LOCA-SFP2 tests (left) and cross section of CODEX-LOCA-SFP2 bundle at 480 mm elevation (right)

Remaining work

Detailed post-test examination of CODEX-LOCA-SFP2 cross sections will be carried out

Related publications

[1] I. Nagy, N. Vér, R. Farkas, M. Horváth, M. Kunstár, Z. Hózer: *Experimental Simulation of Spent Fuel Pool LOCA Accidents in the CODEX Facility*, MTA EK-FRL-2017-701-1-1-M0, in Hungarian (2017)

[2] Z. Hózer, I. Nagy, N. Vér, R. Farkas: *Simulation of Loss-of-Coolant Accidents in the CODEX integral test facility*, EHPG, Lillehammer, Norway, 25-28. September, 2017, EHPG_F2.7

MTA EK PARTICIPATION IN THE OECD NEA BENCHMARK ON PELLET-CLADDING MECHANICAL INTERACTION

Katalin Kulacsy

Objective

In its efforts to facilitate co-operation between member countries and to seek excellence in nuclear safety, technology and science, the OECD Nuclear Energy Agency (NEA) organizes benchmarks, which are well defined modelling or experimental exercises aimed at comparing and assessing codes or experimental procedures. One of them was the pellet-cladding mechanical interaction (PCMI) benchmark whose purpose was to improve understanding and modelling of PCMI by simulating fast power increases called ramps. A number of ramp cases were defined, starting from a short hypothetical fresh fuel rodlet, through a complete fresh fuel rod, through a beginning-of-life real ramp test, to an end-of-life real ramp test. The PCMI predictions of different fuel performance codes were then compared, first to each other, and in the real ramp test cases to measurements, and the different modelling approaches were assessed.

The benchmark started in June 2015 and ended in December 2017, followed by a thorough review and assessment of the results, which is still in progress. The work was supported by Paks NPP.

Methods

MTA EK participated in the benchmark with the steady-state fuel behaviour code FUROM-2.1.1 developed in house. The input of the code consists of manufacturing parameters, power history and model parameters, the latter making it possible to try different models built into the code.

Well tested and recommended models as well as fresh models under testing (e.g. friction between the pellets and the cladding instead of rigid sticking) were applied to the first hypothetical case. The clear simplicity of the exercise made it possible to notice strange model behaviour and improve models, and to choose the best models for the following exercises. Then all the cases were simulated using the chosen set of models.

Results

As an example, the results for the hypothetical short rodlet are shown in Fig. 1. The names of the codes are not to be disclosed until the NEA publication on the benchmark is issued, they are therefore replaced by numbers except for FUROM.

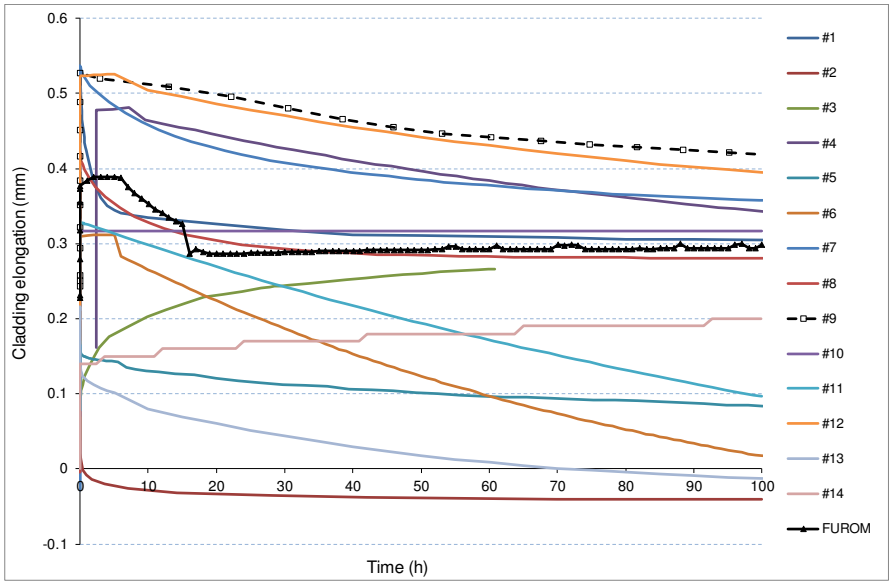

Figure 1: Results of the participating codes for the hypothetical fresh fuel rodlet.

The code FUROM proved to be capable of simulating all the cases and gave results similar to the majority of the participating codes in terms of both numerical values and comparability with the measurements. The benchmark was found to be very well structured and useful for code validation and model testing, as well as code-to-code comparison purposes.

Remaining work

The work has been completed.

Related publication

[1] K. Kulacsy: *Validation of a nuclear fuel behaviour code by modelling transient processes*, MTA EK FRL-2017-704-01-01-M0, in Hungarian (2017)

MTA EK CONTRIBUTION TO THE PERIODIC SAFETY ASSESSMENT OF PAKS NPP

János Gadó, Attila Guba, Zoltán Hózer, János Sebestyén Jánosy, Zoltán Karsa, András Keresztúri, Gábor Lajtha, Katalin Kulacsy, István Panka, Tamás Pázmándi, Péter Szántó, Iván Tóth, István Trosztel

Objective

MTA EK, together with NUBIKI (Nuclear Safety Research Institute), has been the main consultant of Paks Nuclear Power Plant (NPP) for over a decade. The main consultant supports the NPP in solving safety-related technical issues and helping with strategic planning, including

- consultancy in safety-related technical questions,
- participation in the preparation of key strategic technical decision-making,
- acting as expert reviewer concerning results of external engineering services,
- drawing up concept plans and basic technical solutions,
- working out independent proposals to solve important technical and safety-related issues.

The work is done by the most experienced and highly qualified experts.

In 2017 Paks NPP had to undergo its periodic safety assessment, due every ten years. The scope of the MTA EK contribution was the assessment of deterministic safety analyses covering Design Basis Conditions I-IV and Design Extension Condition events. The work had been prepared in 2016, the main tasks had been outlined, and certain topics had been worked out. Following these preparations, the assessment was performed and documented in 2017.

Methods

In addition to the general assessment [1] of the deterministic safety analyses included in the Final Safety Review of the NPP, MTA EK undertook the following specific investigations:

- assessment of the effects of flooding during a loss-of-coolant accident (LOCA) and verification of whether the single failures taken into account in the analyses are not direct consequences of flooding [2];
- assessment of the acceptance criteria used for deterministic safety analyses [3];
- review of the classification of accidents based on their frequencies of incidence [4];
- preparation of a detailed work plan to re-evaluate the dose map of the NPP [5].

The work was done in close collaboration with experts of NUBIKI, who were responsible for probabilistic safety analyses, severe accident analyses and the analysis of internal and external hazards.

Results

The assessment did not find any major deficiencies neither in the safety of the NPP, nor in the documentation thereof. Minor deficiencies included e.g. missing variants of certain analyses or necessary corrections to the Final Safety Review. A few improvements were also suggested, mainly in the area of environmental dose calculations.

Remaining work

The work has been completed. Certain tasks have arisen as a result of the assessment, to be performed later according to the schedule specified in the Periodic Safety Review of the NPP.

Related publications

[1] A. Guba, Z. Hózer, J. S. Jánosy, Z. Karsa, A. Keresztúri, G. Lajtha, K. Kulacsy, I. Panka, T. Pázmándi, I. Tóth, I. Trosztel: *Assessment of the Deterministic Safety Analyses Related to Design Basis and Design Extension Processes*, MTA EK TFO-2017-751-01-03-M0, in Hungarian (2017)

[2] A. Guba, I. Tóth: *Assessment of Flooding as a Failure Involved by LOCA*, MTA EK TFO-2017-751-02-01-M0, in Hungarian (2017)

[3] J. Gadó, Z. Hózer: *Acceptance Criteria of Deterministic Safety Analyses*, MTA EK TFO-2017-751-03-01-M1, in Hungarian (2017)

[4] A. Guba, I. Tóth, A. Keresztúri: *Review of the Classification of Accidents Based on their Frequencies of Incidence*, MTA EK TFO-2017-751-04-01-M0, in Hungarian (2017)

[5] T. Pázmándi, P. Szántó: P*reparation of a Detailed Work Plan to Re-Evaluate the Dose Map*, MTA EK TFO-2017-751-05-01-M0, in Hungarian (2017)

ANALYSIS OF DISSOLVED AND PARTICULATE CORROSION PRODUCTS FOUND IN THE PRIMARY COOLANT CIRCUIT OF PAKS NPP

Zsolt Kerner, Éva Kovács-Széles

Objective

Between the MTA Centre for Energy Research and the PAKS Nuclear Power Plant (NPP) there is a research contract which calls for the analysis of corrosion particles and dissolved corrosion products found in the primary and secondary cooling systems of the reactors to detect the origin or source of corrosion and to describe the transfer of corrosion products. Two series of water samples were analysed in 2017, collected during the shutdown period of block No. 3 and 4.

Methods

Water samples were filtered on a 0.4 μm pore size membrane. Particles were characterized by scanning electron microscopy (SEM). The concentrations of corrosion products (Fe, Co, Ni, Cr, Zr, Ag) in the dissolved and in the particulate fraction were measured by inductively coupled plasma mass spectrometry (ICP-MS). For the silver measurement, chemical enrichment was applied using ion-exchange chromatography. The activity of most of the corrosion products was determined by gamma-spectrometry, but the ^{63}Ni and ^{55}Fe content by liquid scintillation technique after radiochemical separation. Specific activity and the residence time of the particles in the reactor zone was calculated.

Results

Most characterised particles can be classified into one of the following types:

- iron rich particles: These often contains Cr and Ni, sometimes Zr, Mo and Ag, and the typical size is a few micrometres.
- chromium and iron rich particles: Typical size is 10-120 μm.
- zirconium rich particles, mostly in ZrO_2: Typical size is 1-10 μm.

During the shutdown period the ^{59}Fe, ^{51}Cr, ^{55}Fe and ^{95}Zr have the highest activity in the particle fraction, and ^{54}Mn, ^{58}Co and ^{60}Co in the dissolved fraction. Concentrations in the particulate fraction decrease in the Fe>Cr>Ni order, and in Ni>Mn>Fe order in the dissolved fraction. ^{63}Ni is mainly dissolved during the shutdown, but it is equally present in dissolved and particle forms during the start-up. The total activity of the dissolved fraction is higher during the shutdown and lower during the start-up compared with the particulate fraction. Co and Ag can be found in both fractions. The dissolved ^{110m}Ag activity is usually high while the primary circuit is open.

All corrosion products show concentration and activity peaks during the shutdown and restart periods, but the time and the extent is different. Collecting this data can be useful for understanding the chemical changes and transfer properties of corrosion products during transient states.

The effective residence time of the corrosion products in the reactor zone can be calculated from the specific activity. Determined residence times calculated from the specific activity of long-lived isotopes can be longer then a reactor campaign of the long-lived ^{63}Ni isotope (half-life: 100 years). The calculated values of residence time in case of ^{63}Ni isotope (half-life: 100 years) is between 48-455 days for the block No. 3 and 36-134 days for the block No. 4. The difference between the two blocks occurs in all investigated isotope cases.

Remaining work

This work was a part of an ongoing research project for PAKS Nuclear Power Plant which will be running until 2020.

Related publications

[1] É. Kovács-Széles, Zs. Kerner and N. Vajda: *Analysis of corrosion particles originated from primary circuit of block No. 4 of NPP,* Research report for MVM PAKS NPP, EK-SBL-2017-766-01-01, in Hungarian (2017)

[2] É. Kovács-Széles, Zs. Kerner and N. Vajda: *Analysis of corrosion particles originated from primary circuit of block No. 3 of NPP*, Research report for MVM PAKS NPP, EK-SBL-2017-766-02-01, in Hungarian (2017)

DEVELOPMENT OF INTERACTION TECHNIQUES FOR A VIRTUAL CONTROL ROOM

B. Katalin Szabó

Objective

The objective for 2017 was to try out the Oculus Rift head-mounted display (HMD), which is capable of providing a stereo picture, and to integrate it with the existing 3D model of the control room.

Figure 1: The Oculus Rift HMD

Methods

Since the 3D model of the virtual control room had been created with the free and open-source Blender program, the "A" plan was to integrate the Oculus with the Blender Game Engine. (The "B" plan would have been to use the more widespread Unity program which is not open-source and requires a monthly license fee, and thus is not ideal for our long-range goal of developing an inexpensive toolset.)

The Blender Game Engine has a Python script interface, so any function call handling the HMD should be initiated from a Python script. The minimally necessary functions are the displaying of a stereo picture in the HMD and handling input data from the HMD (at least the head rotation i.e. the information as to how the user turns his/her head).

The OpenHMD library (www.openhmd.net) was used for the project. An open-source Python binding has already been published for it (github.com/lubosz/python-rift). However, this binding is for the Linux operating system, and in our case a solution for Windows is more advantageous (since our previously developed interface for the Leap Motion hand tracker device and also the data communication module for the connection with the simulator exists in Windows). Thus the Windows version of the above mentioned Python binding had to be created, involving the replacement of the Linux-specific parts of the code with Windows-specific equivalents and then building a special DLL library (with the .pyd extension) which defines a Python class through which the functions of the OpenHMD library can be called.

After creating the above mentioned .pyd library, a Python code had to be written to call the OpenHMD functions through this library's Python object and process the input data of the head rotation. Then, Blender's display options had to be tuned for providing a stereo picture of appropriate size and qualities.

Results

Since the "A" plan was brought to success, it was not necessary to execute the "B" plan, although some initial steps have been taken in that direction as well.

The goal of integrating the Oculus Rift HMD with the virtual control room has been met. A demo program has been created in which it is possible to "look around" in the control room using the HMD. The advantage of this solution is that it can also be used for other HMD-s supported by the OpenHMD package. (A likely candidate is the HTC Vive HMD.)

There has also been progress in the programming interface for the Leap Motion hand tracking device. The code handling the device now uses Leap Motion's new "Orion" programming interface which provides more accurate tracking results, making the interaction more realistic.

Remaining work

Develop the interaction further (handling collisions etc.) to create a demo presentable to potential customers.

INCREASING THE RESISTANCE OF THE RADIATION AND ENVIRONMENTAL PROTECTION SYSTEM OF PAKS NPP TO EARTHQUAKES AND STATION BLACKOUT

Gábor Házi, Gergely Makai, Csaba Horváth, Attila Nagy

Objective

The major function of the radiation and environmental protection system of the Paks NPP is to detect radiation emitted by the plant and to predict its expected propagation during any incidents. The vital detection elements of this protective system are the measurement stations installed around the plant in circle with a radius of 3 km. Nine, so-called A type stations are responsible to take samples from the air with a flow-rate of 40 m^3/h and to measure the gamma dose-rate and iodine activity concentrations continuously. Samples of air are evaluated once per week in the laboratory and the continuous measurements are sent to the dosimetry control room of the plant by wire and UHF connections with a period of ten minutes. Eleven G type stations are installed between the A type stations without having any wired connections with plant. Solar panels provide their required electricity and they measure only gamma dose-rates, which are sent to the centre by radio.

One of the conclusions of the stress-test performed after the events of Fukushima was that the resistance of these stations to earthquakes and station blackout needs to be improved. In 2015 we had investigated the system with the focus on these features and we drew the conclusion that the stations should be reinforced and their accumulator capacity should be increased in order to satisfy recent requirements (e.g. 72 hours' operation without any external power supply).

After publishing our study, a decision was made by the management of the plant that a prototype of an A type station should be built and a comprehensive study of its earthquake resistance should be performed by a vibrating platform and spectrum analysis.

Methods

After we had made the design of the new station in 2016, the prototype was built in 2017 [1]. The investigations were performed at the end of 2017. The measurement elements of the station were installed in a reinforced container and detailed factory acceptance tests have been performed in our Institute. One of these tests focused on the resistance of the station against station blackout. This test was started with fully-charged battery packs, which is the normal operational state of the station, and the external power was interrupted for 72 hours. After testing, we have checked the recorded states of the battery packs. Two UPS' (Uninterrupted Power Supply) are installed in the station, one for AC loads and one for DC devices. Figure 1 shows the states of the two sets of battery packs and some other measurements during station blackout. It can be seen that iodine measurements (including aerosol form) is stopped automatically after 24 hours of the station blackout in accordance with our design, but the gamma dose-rate, which is a critical measurement in our system is measured continuously without any interruption. You can also see that battery packs can still be monitored after 72 hours, so after this test the system was able to refill them without any problem.

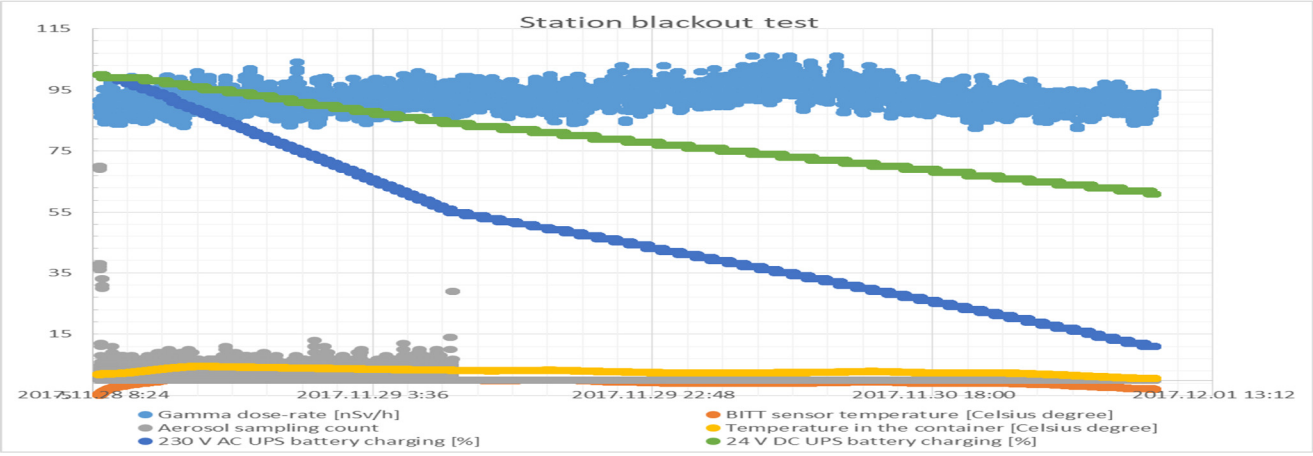

Figure 1: State of the battery packs during station blackout

After the successful factory acceptance tests, the container was transported to the Budapest University of Technology and Economics, where earthquake resistance tests were performed by TLab Ltd [2].

For these tests the container was installed on a vibrating platform and two cameras were installed inside the containers (see Fig. 2) to monitor the behaviour of the measurement elements. All devices were in operation during the vibration tests (except the air conditioner) and data were recorded outside by a notebook computer, which was in wired and UHF connection with the container's data acquisition system. Both horizontal and vertical vibrations tests have been performed based on theoretical design based earthquake spectra.

Figure 2: One of the camera views inside the container during earthquake resistance test

Results

All tests of the prototype station have been performed, successfully validating the desired resistance and operability of the full-scale prototype reconstruction of the stations.

Remaining work

The overall reconstruction of the system will be started in 2018 and it includes the replacement of each A type station with a new one corresponding to the prototype station. Furthermore, similar prototypes will be built for other types of stations (e.g. G type station) and in case of successful prototype trial, the replacement of these stations will be carried out in 2019.

Related publications

[1] A. Nagy, G. Makai, P. Káposztás: *Reconstruction of Radiation and Environment Protection System – System Description,* Technical Report 000000I02590, (2017)

[2] L. Turi: Seismic qualification of a prototype A station of SER-KK system, Technical Report, (2017)

XENON CONCENTRATION DETERMINATION WITH A POINT KINETIC MODEL

Áron Vécsi

Objective

A point kinetic model was developed to investigate the changes of the xenon concentration in a nuclear reactor.

Methods

The reactor was modelled with point kinetics equations which calculate six delayed neutron groups, the temperature of the fuel and the coolant, and take into consideration the feedback of the fuel and coolant temperatures and the calculated xenon concentration. A program was developed for numerical calculation, using the first terms of the Taylor series of the functions.

Results

Several simulation runs with different reactor events were made with the program. The constants used are valid for the Pakistan Research Reactor and the initial values were equal to the equilibrium values. The calculation makes the approximation that the inlet temperature is constant.

Fig. 1. and Fig. 2. show the calculation results for the dependence of neutron density, reactivity, iodine and xenon concentration on time when the external reactivity was ρ_{ex}=0.001 in the time interval between 100 and 200 sec, and before and after that period, ρ_{ex}=0.

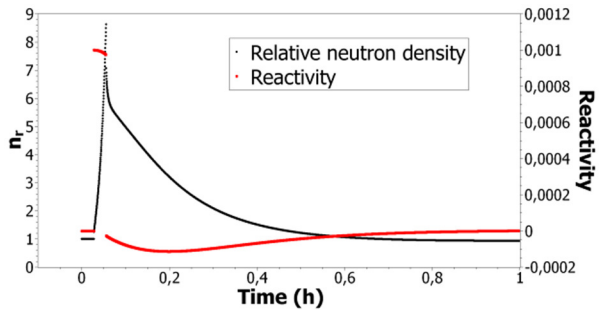

Figure 1: Neutron density and reactivity with ρ_{ex}=0.001 when t [100 s; 200 s] and h=0.0001 s time step

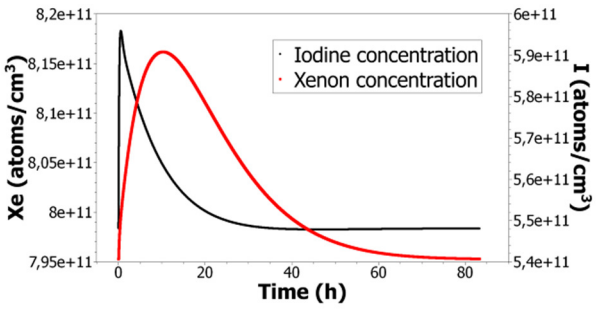

Figure 2: Xenon and iodine concentration with ρ_{ex}=0.001 when t [100 s; 200 s] and h=0.0001 s time step

The numerical solution based on Taylor-series expansions for solving the point kinetics equations coupled with thermohydraulics is suitable for the task. The results characterize the whole reactor.

This model was presented as a poster at two conferences (ENYGF - European Nuclear Young Generation Forum and NENE - International Conference Nuclear Energy for New Europe) this year.

Remaining work

This model was the first step of the PhD work. The goal is to develop an on-line monitoring system which can track the xenon concentration, and later to write a control model for the load-following reactors.

The present model needs to be extended with the dependence of the calculation on unsteady inlet water temperature. The next step of this work is to connect the written point kinetic model to the RETINA (REactor Thermohydraulics INterActive simulator) thermohydraulics model which was developed by the Hungarian Academy of Sciences Centre for Energy Research to get more realistic coolant and fuel temperatures.

Multi-point neutron kinetics equations need to be applied to investigate the axial density of the xenon concentration.

Using the signals of in-core neutron detectors and thermocouples, the measured neutron density, inlet- and outlet water temperature will be used as inputs for the model in the future.

DEVELOPMENTS IN CORE MONITORING OF THE PAKS NUCLEAR POWER PLANT

Gábor Házi, Csaba Horváth, Gergely Makai, József Páles, Sándor Kiss, Sándor Lipcsei, Zoltán Dezső

Objective

In nuclear power plants so-called core monitoring and surveillance systems are used to extract as much information as possible about the state of the reactor core based on measurements. Although only a limited number of detectors can be installed in and around a nuclear reactor core, using advanced numerical calculations the relevant physical quantities can be obtained with very high spatial resolution. The core monitoring systems, namely the reactivity, the neutron flux during refuelling and the in-core monitoring systems had become aged in Paks NPP, so their refurbishment became necessary. Since our institute developed both the reactivity monitoring system and the in-core monitoring and surveillance system, the need of our participation in the reconstruction projects of these systems was obvious. The reconstruction work of the VERONA in-core monitoring system was started in 2014 and it was finished in 2016. In the same period, we also started the introduction of an integrated reactivity and refuelling neutron-flux monitoring system in the plant using a new type of neutron flux detector.

Methods

Considering the reconstruction of the VERONA in-core monitoring system, the most relevant new features and applied methods can be summarized as follows (more details can be found in [1]):

- use of a new generation of proven hardware devices (high performance servers, thin clients for monitoring purposes, new local area network devices, network attached storage)
- use of a new generation of proven software platform (Windows Server 2012 R2),
- use of a new generation of software development tools (Visual Studio 2014, Embarcadero XE7, Visual Fortran Composer XE 2013),
- use of VMware virtualization technology,
- extension and acceleration of the reactor physics calculations using Graphics Processing Units (GPU),
- replacement of the Intellution's iFIX based process monitoring system by our homemade VisualEngine, which is a member of our SIMTONIA (SIMulation TOols for Nuclear Industrial Applications) platform.

Considering the refurbishment of the reactivity monitoring and the refuelling neutron-flux monitoring systems, first a fundamental decision was made based on our earlier results: the same detectors and measurement instrumentation should serve both systems. This approach is in contrast with the earlier practice, which utilizes different detectors (with different neutron flux ranges) during start-up and refuelling. Furthermore, these detectors have to be removed after start-up in order to avoid their damage caused by the high radiation at nominal power. So, in order to simplify the maintenance and to provide reliable neutron flux data during refuelling, start-up and at full power, a full-range ex-core neutron flux monitoring system was required, i.e. the detectors and the associated instrumentation should cover the full range of neutron flux measurements from 0% to 100% of reactor power. Additionally, the new system was required to operate continuously, to obtain a measurement archive, and to provide data for the Process Computer and the VERONA core monitoring system.

Results

The new version of VERONA was installed first in the training centre of the NPP, coupling it with the full-scope simulator of the plant. After having positive experience with the new system and finishing the training of the operation personnel, the so-called "test" system of VERONA was put in place and operated for a while. The test system is a special version of VERONA, which can receive measurement data from any of the PAKS units and therefore, it can be used to test in a preliminary way any modification in the system without influencing the operation of the real systems at the units. After a successful testing period, we installed the new system in each unit and its testing period was started. In 2017 the overall testing period was closed successfully without any problem. Fig. 1 shows the main display of VERONA's new user's interface.

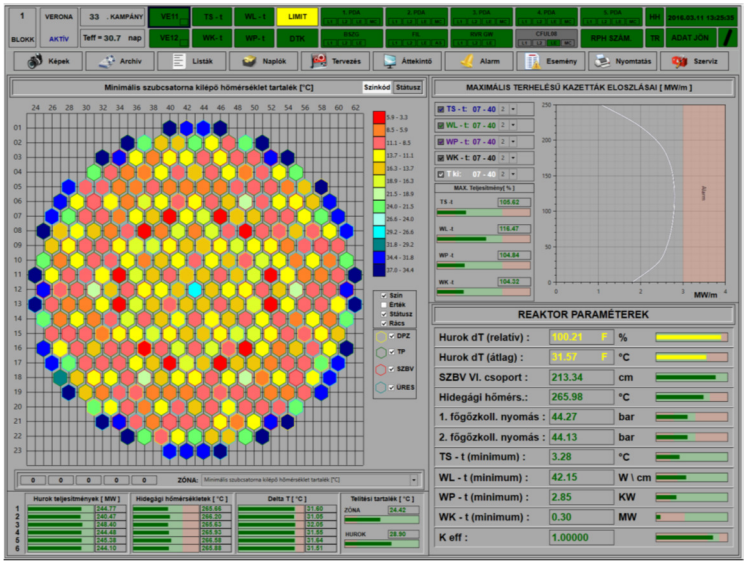

Figure 1: User's interface of VERONA core monitoring system

The development of the new reactivity and refuelling neutron-flux monitoring system was started by working out a pilot measurement system. Utilizing PHOTONIS CFUL08 type fission chambers we demonstrated the capability of our new system by a series of measurements performed first at the training reactor of Budapest University of Technology and Economics and then at the 2nd unit of Paks NPP during some reactor start-ups and shutdowns. Based on these results a new, more complex system structure was developed named ANEREM and its factory acceptance tests were performed in our institute.

Figure 2: Thin clients, two remote displays and a spare display of ANEREM during the Factory Acceptance Tests (FAT)

Remaining work

The ANEREM system will be installed in the 1st unit at the beginning of 2019 during refuelling. After a successful testing period the system will be introduced in each unit during the refuelling periods of the units.

Related publications

[1] G. Házi, J. Páles, I. Pós, Z. Kálya, T. Parkó, Cs. Horváth, G. Makai, Á. Vécsi, M. Ignits and T. Fejes: *GPU accelerated nuclear reactor core monitoring system in virtual machines*, International Journal of Computers. **2,** 255 (2017)

[2] S. Kiss, S. Lipcsei, G. Házi, Z. Dezső, T. Parkó, I. Pós, M. Ignits and L. Hományi: *Renewing the refueling neutron monitoring and reactivity measurement systems at Paks NPP*, 28th Atomic Energy Research Symposium, Munich, Germany, October 17-20, Global Research for Safety, (2017)

TESTING METHODS FOR THE CHARACTERISATION OF THE CORROSION STATE OF A STEAM GENERATOR'S HEAT TRANSFER TUBES

Zsolt Kerner, István Almási, Lászlóné Horváth, Zsolt, Horváth, Levente Illés, András Kocsonya, Boglárka Maróti, Péter Petrik

Objective

The corrosion rate of the heat transfer tubes of a reactors' steam generators depends on the chemical composition, structure and thickness of the oxide layer. Maintainance of a low corrosion rate, low corrosion release and mitigation of stress corrosion cracking are fundamental requirements for a nuclear power plant's steam generators. This can be achieved by proper chemical control and periodic examination. In the 1990's Paks NPP performed an intensive heat transfer tube investigating program in collaboration with Pannon University. Based on its results a new, detailed monitoring program was worked out. Its purpose was to detect any structural change or contamination in the oxide layer before it could have an impact on the corrosion rate. Possible experimental methods have now been discussed and tested on archival transfer tube samples. Finally, a protocol has been assembled for handling, cutting and characterizing the inner (primary water side) and the outer (secondary water side) surfaces of the radioactive cut-out samples.

Methods

The areas of the tubes to be examined was selected based on inspection by optical microscope. Rings and cylindrical shells were cut by a special band-saw in a glove box. Some cross-sectional polished samples were prepared using an epoxy mounting system and a conducting filler. The structure and elemental composition of the oxide layer were investigated by scanning electron microscopy (SEM) and energy dispersive X-ray analysis (EDS). X-ray diffraction (XRD) has been used for identification and quantification of crystalline phases. The main iron-containing compounds were characterized by conversion electron Mössbauer spectroscopy (CEMS). X-ray fluorescence spectroscopy (XRF) and particle-induced X-ray emission (PIXE) was used to detect pollutant elements. XRF mapping gave information about the elemental distribution and also the thickness variation. The thickness was calculated based on the weakening of the nickel and chromium Kα lines deriving from the base metal. Radioactive contaminants were measured by gamma spectroscopy. The corrosion rate was determined by a potentiodynamic polarization measurement carried out in a special cylindrical electrochemical cell. The applicability of methods of porosimetry and ellipsometry also were tested. XRF measurements were also carried out in-situ on the outer surface of the heat transfer tubes.

Results

A program has been worked out for the detailed characterization of the oxide layer on the inner and outer surfaces of the heat transfer tubes.

Three archival samples investigated according to the recommended protocol show the following properties: The inner and outer surfaces were covered with a hydrothermally grown oxide layer in accordance with the previous examinations. The outer surface of the tube is covered with crystalline magnetite. The thickness is basically determined by the operating position (and hence by the temperature) in the steam generator (Fig.1).

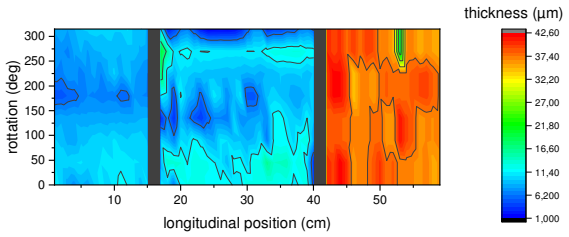

Figure 1: Maps of the outside oxide layer thickness on three tube sections taken from different steam generators based on XRF measurements shown in the figure next to each other

The oxide layer on the inner surface shows a double structure: a compact, chrome rich spinel inner layer and a magnetite outer layer. The thickness and structure differ according to the antecedents of the tube. On the inner surface of tubes from a previously decontaminated steam generator the oxide layer is thicker and the chrome content is higher, compared to a non-decontaminated tubes. On the non-decontaminated sample, the inner layer is very thin (<20 nm), the outer layer is almost pure magnetite (Fig.2). In contrast, on the decontaminated sample the inner layer is thick (1.5 µm), the outer layer contains nickel and chromium (Fig.3). The structure of the outer layer on the decontaminated tube can be crystalline or amorphous. CEMS detects amorphous $Fe(OH)_3$ in the top 300 nm layer. Its origin is unclear. The corrosion rate in boric acid solution at room temperature of all samples are low (<2 µm/year).

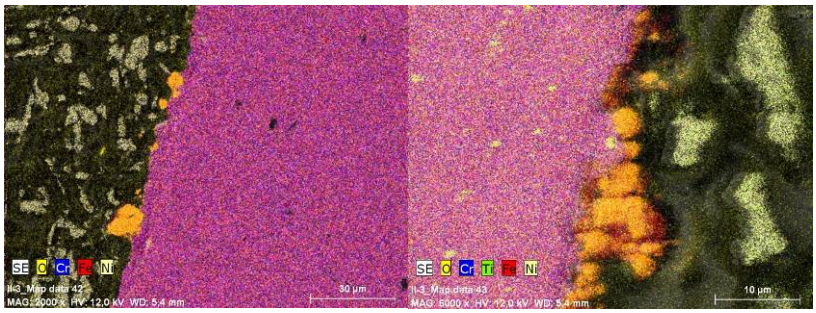

Figure 2: Oxide layer composition on the inner (left) and outer (right) surface of a non-decontaminated heat transfer tube (composite X-ray map)

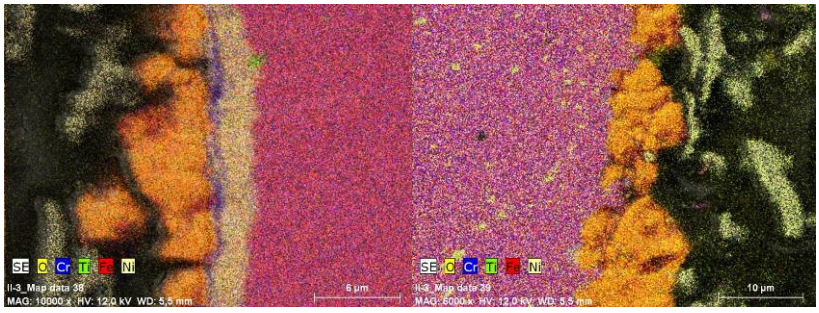

Figure 3: Oxide layer composition on the inner (left) and outer (right) surface of a decontaminated heat transfer tube

Some copper, zinc, calcium and lead contamination were found on the outer surface of the tube. The last of these is caused by the lead shielding used previously during the transport and storage of the tube. Cu and Zn are concentrated locally.

In-situ XRF measurements using a portable analyser is suitable for detecting contamination (for example Cu, Zn, Pb) on the outer surface of heat transfer tubes and determining the oxide thickness without cutting the tube.

Remaining work

Ellipsometry is a promising quick and non-destructive optical method for mapping the oxide layer thickness and porosity on the tube surface. It requires model development and a determination of material properties based on measurements on an experimentally produced series of samples.

Related publications

[1] Zs. Kerner, L. Illés, É. Kovács-Széles, G. Dósa, B. Maróti and N. Vajda: Characterization of the heat transfer tubes of block No. 2. of Paks NPP, research report for MVM PAKS NPP, MTA EK-FKKL-2016-712-01-01-M0 (2016) and MTA EK-FKKL-2016-712-01-02-M0, in Hungarian (2017)

[2] Zs. Kerner, I. Almási, L. Horváth, Zs. Horváth, L. Illés, A. Kocsonya, B. Maróti and P. Petrik: Methodes for investigatin of steam generator's heat transfer tube, research report for MVM PAKS NPP, MTA EK-FKKL-2017-708-01-M0 and MTA EK-FKKL-2017-708-02-M0, in Hungarian (2017)

SUPER-VVER REACTOR RESEARCH

György Hegyi, Csaba Maráczy, András Szabó

Objective

Super-VVER reactor is a term for two reactor concepts, which are developments of the VVER-1000 reactors and which, with revolutionary design changes, can achieve better fuel utilization and higher thermodynamic efficiency. The single circuit, supercritical pressure GEN-IV VVER (VVER-SCP) enables the coupling of a higher efficiency thermodynamic cycle, and is promising from the aspects of its closed fuel cycle and that it allows final disposal of the weapon grade plutonium stockpile. The analysis and further development of VVER-SCP were intended in this year of research.

Methods

The MULTICELL deterministic neutron transport code was used to generate few group cross sections for the supercritical MOX fuel assemblies. These few group cross sections are effective nuclear cross sections averaged over space and energy. We have applied the KARATE code system to calculate the VVER-SCP core behaviour. As there was no detailed information available in the literature on the flow paths of water in the reactor vessel, we have used the conclusions of the European High Performance Light Water Reactor (HPLWR) project on the flow scheme. The hot spots in this proposal can be potentially eliminated by multiple flows of coolant through the active core with mixing after each passing. First, the ascending coolant is heated in the central evaporator region of the core passing through the pseudocritical point, then after mixing in the upper mixing chamber flows downwards in the first superheater region. After leaving the lower mixing chamber, the coolant flows again upwards in the second superheater region located at the core periphery.

Results

The few group cross sections were generated over a wide range of plutonium content to make possible axial and radial zoning of fuel to tune the power distribution and cycle length. The supercritical thermohydraulics code package of KARATE was upgraded to treat the hexagonal geometry and the code system was used to optimize the flow regions and power distributions. Figure 1 illustrates the shaping of flow regions and the result of power distribution optimization in a 60-degree symmetry sector of the core. The power peaking values in Figure 1 are relative power distributions normalized to one.

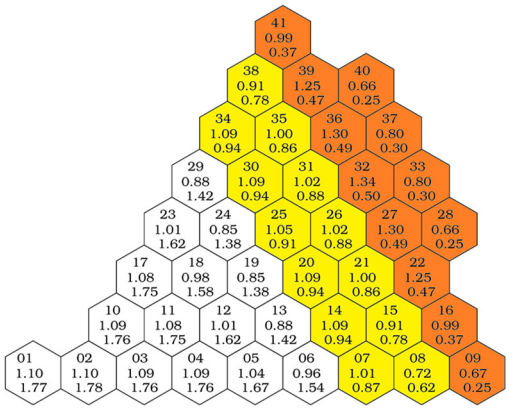

Figure 1: Beginning of cycle (BOC) relative power distributions of the three pass core VVER-SCP proposal. 1st row numbers: Fuel assembly numbering, 2nd row: Flow region radial power peaking, 3rd row: Core radial power peaking. White: evaporator, yellow: first superheater, orange: second superheater.

Remaining work

The project will last several more years. The development of tools for VVER-SCP analysis and their application will be continued.

Related publication

[1] Gy. Hegyi, Cs. Maráczy and A. Szabó: *Equilibrium Cycle Calculation of the VVER-SCP Supercritical Reactor*, 16th Nuclear Technology Symposium, Budapest, 23-24 November 2017, in Hungarian (2017)

DEVELOPMENT AND TESTING THE DETERMINISTIC NEUTRONICS MODEL OF THE NEW PAKS UNITS

Áron Brolly, György Hegyi, Gábor Hordósy, Csaba Maráczy, Emese Temesvári

Objective

The general objective of the project is the development of the elements of a code system for the alternative solution of core design and safety analysis of the new Paks units. This year, the specific aim was testing the elements of the developed KARATE-1200 code system by defining and solving a series of specific benchmark problems.

Methods

In the possible load-following mode of the new units, the cluster type control rods may move periodically over a certain axial range causing strong spectral perturbations in the fuel rods. To check the reliability of the MULTICELL neutronic transport code and the few group cross section generation method of the KARATE-1200 code system we performed verification calculations with the MCNP Monte Carlo code to model this periodic burnup process.

To verify the KARATE-1200 program package, we have defined a two dimensional test. Since the reference solution is derived from the MCNP calculation, only a 60-degree section of the zone was calculated to save time by providing reflective boundary conditions on the edges. A fictitious loading of the VVER-1200 has been selected, which contains unburnt fuel assemblies. Detailed radial reflector treatment was applied.

Results

During the load-following mode test calculations it was proven by the MCNP reference results that the production of group constants with the MULTICELL code is also appropriate in this case. Figure 1 illustrates the multiplication factor change during the periodic insertion of absorber. The MULTICELL transport code value and PARACELL value using the parameterised diffusion group constants agrees well with the MCNP result.

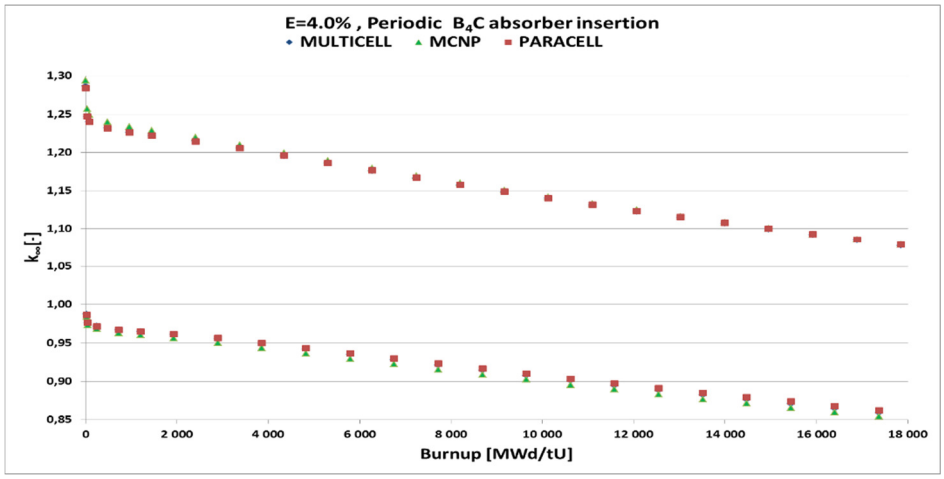

Figure 1: Multiplication factor change in a 4 % enriched assembly during the periodic insertion of absorber. Lower dots: absorber in. Upper dots: absorber out. (MULTICELL and PARACELL results are practically identical.)

By solving the two dimensional VVER-1200 tests we found the results of both the assembly and pin power distributions to be satisfactory.

Remaining work

No work remained on this particular test calculation, but the whole project lasts 3 years for development and testing of further elements of the code system.

Related publication

[1] E. Temesvári, Á. Brolly, Gy. Hegyi, G. Hordósy, Cs. Maráczy and A. Keresztúri: *Preliminary comparison of KARATE-1200 and MCNP fine mesh calculations*, 27th Symposium of AER, Munich, Germany, October 17-20, 2017 ISBN 978-963-7351-28-0, pp. 395-412

HOT CHANNEL CALCULATION METHODOLOGIES FOR THE NEW PAKS UNITS

István Panka, György Hegyi, András Keresztúri, Csaba Maráczy, Emese Temesvári

Objective

The hot channel calculation is the important final phase of the safety analysis because the fulfillment of the acceptance criteria is investigated here. In 2017, our goal was to develop a hot channel calculation methodology to be applied for the investigation of the RIA (Reactivity Initiated Accident) and ATWS (Anticipated Transient Without Scram) events of the new VVER-1200 type units at Paks. Our focus was on the calculation methodology of the coolant mixing from and to the sub-channels in the vicinity of the hot rod. This phenomenon is important because it significantly affects the heat transfer from the hot pin via the coolant thermal hydraulic state. Some few years back, a detailed methodology was elaborated, especially for the VVER-440 assemblies, but this methodology has to be improved due to the complex geometrical structure of the assemblies of the new units. The conservatism of the closed channel approximation, neglecting the hydraulic mixing effect between the sub-channels, also has to be analyzed. A special goal was to select an appropriate enveloping safety related 'frame parameter' for the limitation of the coolant thermal hydraulic conditions (i.e. sub-channel heat up).

Methods

The pin power distributions were calculated by the KARATE-1200 code system. The coolant mixing effects were investigated by using the COBRA multi-channel thermal hydraulic code, while the single closed channel calculations were carried out using the TRABCO hot channel code.

Results

Using different pin power distributions and power levels, it was found that the maximum pin power is an appropriate frame parameter for the limitation of the heating up of the coolant in VVER-1200 reactors. It was also concluded that the flat power distribution (Kk=1) inside the fuel assembly is a conservative approach (see Fig.1), and in this case the minimum DNBR (Departure from Nucleate Boiling Ratio) is located next to the instrumentation tube.

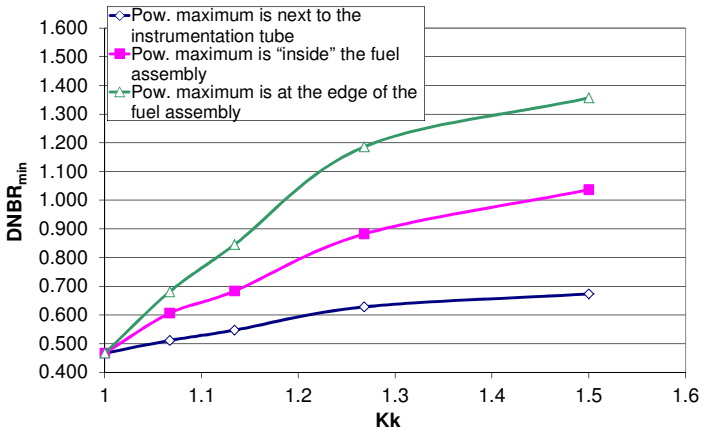

Figure 1: Minimum DNBR ($DNBR_{min}$) values for different Kk (radial pin power peaking factor) values; initial limiting power is multiplied by 1.5. (NOTE: The vertical scale parameter cannot be read, since it is cut off by the frame for the Figure. From the text, I infer that the parameter is DNBR. Correct?)

Concerning the closed channel approximation, a robust model was developed by using the TRABCO code and by decreasing the sub-channel cross flow area next to the instrumentation tube. This model was verified against COBRA multi-channel calculations at different power levels. It was stated that the elaborated single closed sub channel approach gives reasonable conservative results.

Remaining work

This project has been completed.

Related publications

[1] I. Panka, Gy. Hegyi, A. Keresztúri, Cs. Maráczy, E. Temesvári: *Hot channel calculation methodologies in case of VVER-1000/1200 reactors*, Munich, Germany, October 17-20, 2017 ISBN 978-963-7351-28-0, pp. 37-66

[2] I. Panka, Gy. Hegyi, A. Keresztúri, Cs. Maráczy and E. Temesvári: *Hot channel calculation methodologies in case of VVER-1000/1200 reactors*, Kerntechnik **83**, 4, pp. 365-375, (2018)

THERMOHYDRAULICS RESEARCHES

Attila Guba, Gábor Baranyi, György Ézsöl, Valér Gottlasz, Áron Hegedüs, Attila Nagy, Antal Takács, István Trosztel

PKL-4

The PKL-4 test programme is investigating safety issues relevant for current pressurised water reactor (PWR) plants as well as for new PWR design concepts and will focus on complex heat transfer mechanisms under two-phase flow, boron dilution and precipitation and on cool-down procedures. These issues are being investigated by means of thermal-hydraulic experiments that will be conducted at the primary coolant loop test facility PKL. This facility is owned and operated by AREVA NP and is situated in Erlangen, Germany. In the programme, in addition to tests to be run in the PKL facility, additional tests will be run in the PMK facility in Budapest, Hungary. Safety organisations, research laboratories and industry from the 14 countries are supporting the PKL project.

The tests address subjects related to current safety issues that suffer either from the lack of a dedicated database for analysis and validation of computer codes or from uncertainties in the safety evaluation stemming from open issues or questions. The extension to already existing databases related to these subjects is the foremost goal.

The PKL Phase 4 project started on 1 July 2016 and will end on 30 June 2020. It will focus on parametric studies of thermal-hydraulic procedures for model development and validation of thermal-hydraulic system codes, and on experimental verification of cool-down procedures and operation modes for different incidents and accidents. The PMK experiments are different medium size Loss Of Coolant Accidents (LOCAs). Pre-test analyses have been performed and introduced to the PKL-4 community to choose the most relevant experimental configuration. The experiments will be conducted in the spring of 2019. A set of post-test calculations will complement the project. The results are used for the validation of the computer codes and set up a best nodalisation strategy for the medium size LOCAs.

PSA-DSA

The Strategic Research Program (SRP) of the Sustainable Atomic Energy Technological Platform (SAE TP) among the research areas potentially usable for supporting the activity of the Hungarian Atomic Energy Authority contains a survey, analysis and evaluation of common topics of both the deterministic and the probabilistic safety analyses in order to improve their joint, wider scope of application.

To perform this task of the SAE TP, a four year research project has been initiated within the framework of the technical support activities for regulatory oversight carried out by the Hungarian Atomic Energy Authority (OAH) in relation to the peaceful use of atomic energy in Hungary. The research project is mainly aimed at the improvement of methods used within the deterministic and probabilistic safety analyses, as well as at the development of procedures to support the integrated application of the two analysis types.

MTA EK, together with NUBIKI (Nuclear Safety Research Institute) during the four years of the research project first a collection of the previous analyses has been performed than comparative study and evaluation example of a methodology covered by the scope of deterministic and probabilistic safety analyses have been carried out. The report gave a good example of applying the methodology while revealing the existing difficulties in joining the deterministic and probabilistic safety analyses.

Thermohydraulic Safety Analysis

Hungary is planning to build a new nuclear power plant; the Paks-II project is already going on. It is essential for the domestic research community to understand the design and the features of the new built power plant and to gain knowledge of the transient behaviour of the VVER-1200 design. To investigate this behaviour, a selection of initiating events has been chosen that represents the basic processes, including both design basis and beyond design basis accidents. Overall six initiating events have been selected. Thermohydraulic system code input decks are being prepared and tested based on a collection of the available data for a similar reference power plant. Due to lack of data on the particular Paks-II design, general components were defined and used for input. Further investigations are needed when final, correct data is available. With these shortcomings a first attempt study will be performed for the selected transients. By doing sensitivity calculations, the behaviour of the new power plant will be studied in transient conditions. During this process, the nodalisation strategy will also be investigated to reach a good representation of the plant for these transients. In the next phase the input has to be corrected and finalized with the real data. After completing the six calculations, the results will have to be compared to the relevant Russian safety analysis.

.

FINITE ELEMENT MODEL FOR STRUCTURAL INTEGRITY CALCULATIONS OF A VVER-1200 REACTOR PRESSURE VESSEL

Tamás Fekete, Dániel Antók, Levente Tatár

Objective

The Reactor Pressure Vessel (RPV) of a nuclear power plant (NPP) unit is the most critical component from the safety point of view. Therefore, it limits the allowable service time of an NPP unit the most. The most important function of the RPV is maintaining the pressure and temperature conditions that are necessary for controlled power generation during operation. It is also responsible for heating up and cooling down the reactor and, in case of an emergency, for cooling down the core and preventing the release of radioactive materials into the containment. The most relevant ageing mechanisms in the structural materials of an RPV are: (1) neutron irradiation assisted ageing, (2) fatigue and (3) thermal ageing. An RPV has large physical dimensions (in case of a VVER-1200: between ≈206- and ≈295-mm wall thickness with ≈4600 mm outer diameter); it works at elevated temperatures (≈300 – 330 °C) and high pressure(s) (≈16 MPa). The objective of the research was the development of a Finite Element model of a VVER-1200 RPV that will serve as a basis for Design Safety Calculations and later on for Structural Integrity calculations of the RPV currently under design.

Results

During the project, a full 3D model of a VVER-1200 RPV has been elaborated and implemented in the MSC Marc FEM code system. Two views of the RPV geometrical model are presented in Fig. 1.

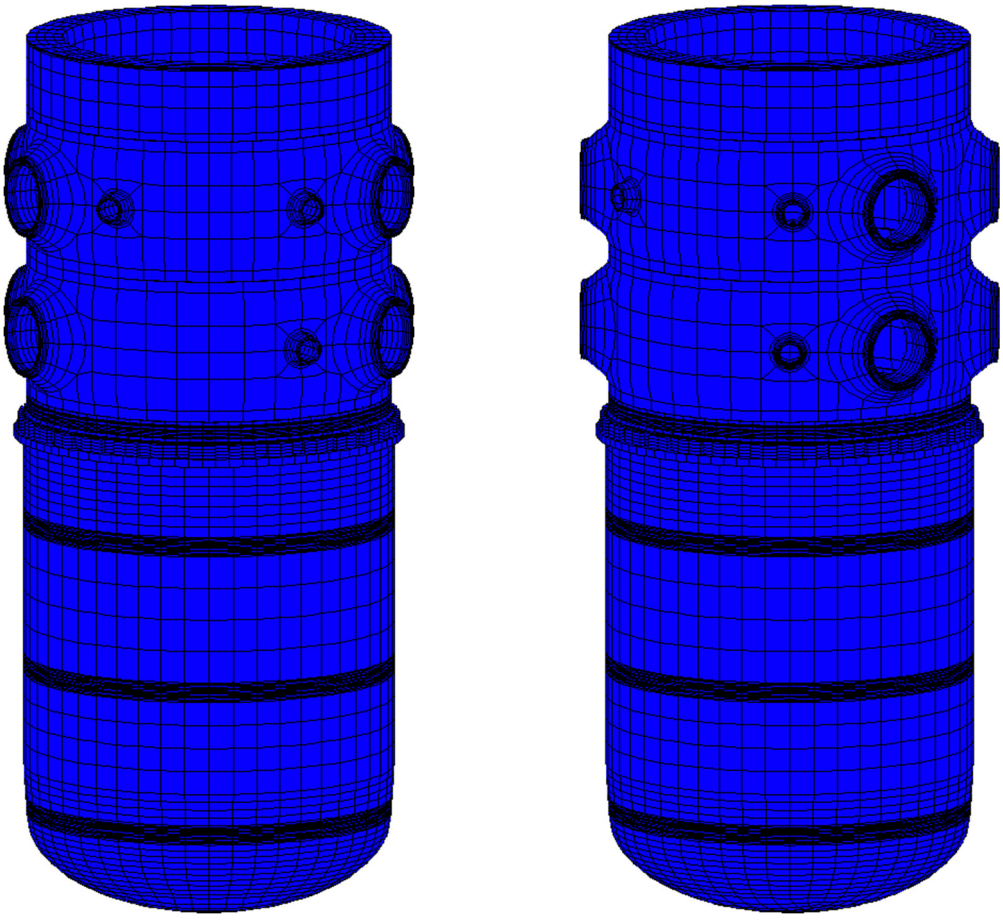

Figure 1: Two views of the 3D FEM model of a VVER-1200 RPV

Remaining work

Elaboration of more refined RPV models in the frame of the above depicted research direction is planned.

SIMTONIA BASED NEW COMPACT SIMULATOR OF PAKS NUCLEAR POWER PLANT (NPP)

József Páles, Csaba Horváth, Tamás Fogd, Gábor Házi

Objective

A new compact simulator has been built based on the model system of the present real-time full-scale simulator of the current Paks NPP using our recently developed new simulation framework called SIMTONIA (SIMulation TOols for Nuclear Industrial Applications). The major objective of this project was to prove and demonstrate the efficiency of our new framework, and to clear the ground for some foreseeable further projects like the refurbishment of the turbine and cascade control systems of the present power plant.

Methods

The development of SIMTONIA was started a few years ago and now, it provides a modern, comfortable, graphics environment for simulator developers. Using this framework there is no need of programming skills for model development, but developers having a solid knowledge of the technology can develop the simulator models. The user interface of SIMTONIA is unified, which means that independently from the technology we wish to model a unified man-machine interface to produce models of instruments and control systems, electrical, single phase fluid and two-phase flow networks. The different technological networks can be coupled with each other using the same graphics environment and they can be driven by a virtual control room environment, which also can be developed using SIMTONIA. SIMTONIA's executive and instructor systems provide real-time scheduling of the models, usual simulator operations (snapshot reading and writing, backtracking, run, step, freeze functions, etc.) in line with the well-known ISO standards.

Results

The models of the present real-time full-scope simulator of Paks NPP were moved to the platform of SIMTONIA. Part of this work was done in an automatic manner using some converter programs, but another significant part, which is implemented in Fortran language in the present simulator (e.g. the turbine controller), was redeveloped by SIMTONIA's element and model editors.

The touch-screen based user interface of the new simulator can be seen in Fig. 1.

Fig. 1: Touch-screen based control room of the compact simulator

Using these new models, a compact simulator has been assembled. The simulator includes the following models:

- RSIM – for neutron kinetics,

- RETINA - for a two-phase-fluid flow model for the reactor vessel, primary loops, steam generators, and main steam lines,
- PRIMARY - for single-phase flow and two-phase vessel models for primary loop auxiliary systems (including makeup, safety and other cooling water systems, oil systems, etc.),
- SECONDARY – for single-phase flow and two-phase vessel models for the secondary circuit (including feedwater and reheater systems, turbine, condenser, moisture separator, etc.),
- TURBLGC, VALVELGC, PUMPLGC, SWITCHLGC – for turbine, valve, pump and switch control systems,
- CRODLGC – for control rod and reactor power control system,
- RPSLGC – for reactor protection system including reactor power limiter etc.,
- ELEC – for electrical systems,
- CROOM – for modelling control room devices in touch-screens.

Remaining work

Intensive testing of the new simulator is in progress and needs to be continued, including the simulation of "heavy" transients (e.g. large break LOCA). The development of new models for Paks II NPP should be started in 2019, too.

CLASSIFICATION OF GRAVEL AND SAND COMPONENTS OF CONCRETE STRUCTURES USED FOR RADIATION PROTECTION

Katalin Gméling, Veronika Szinger-Szilágyi, Ildikó Harsányi, Boglárka Maróti, Dénes Párkányi, László Szentmiklósi, Tamás Fekete

Objective

During the construction of the new nuclear power plant units at Paks II, the concrete structures will preferably be made from domestic raw materials. For this reason, we have to be prepared with a suitable recipe for radiation-resistant, durable concrete with low neutron activation susceptibility. The key to achieve that goal is the careful selection of the raw materials (gravel and sand) based upon the compositional data obtained by analytical and petrological methods. Analysis of the chemical composition of the concrete structures surrounding the reactor vessel is important, because they are exposed to high flux neutron and gamma radiation, so their constituents might be substantially activated. Due to the neutron irradiation, the high-neutron-capture-cross-section nuclides with both short and long half-lives become highly radioactive during the reactor operation time, while isotopes with long half-lives can remain radioactive for years after the reactor shutdown.

Methods

To achieve the research objectives, we sampled systematically at the Hungarian gravel and sand mines. The gravel and the sand are debris sediments, which were transported and deposited by rivers. Thus the composition of sediments is determined by the site of origin, the distance of transport, and the depositional environment. From four different geographical regions, sixteen mines were sampled. From every selected mine four sorted (particle size: 0-4, 4-8, 8-16, 16-32 mm) and washed samples were collected. Also some cement and rock samples were analysed, in total 100 samples. The sampling was made with care, and after homogenisation, the representative portions were taken from the whole with the halving method.

The elemental compositions of the samples were determined by a combination of complementary analytical techniques (e.g.: INAA, PGAA, and XRF). Prompt gamma analysis and neutron activation analysis were performed at the MTA Centre for Energy Research. The results of these two nuclear analytical methods are comparable, and also complement each other. XRF measurements were done in SZIKKTI Labor Ltd. The following elements will have significant activities even a year after the concrete is exposed to neutron radiation: Ce, Co, Cs, Eu, Fe, Hf, Sb, Sc, Ta, Tb, Cr, Pa, Sm, Sr, Zn, Th and U. All these trace elements are enriched in so called heavy minerals (e.g. olivine, magnetite, amphibole, rutile, topaz, zircon) which are accessory constituents (<5%, but usually <0.1-0.01%) of the rocks and which have a density that is greater than 2.9 g/cm^3.

Macroscopic-, microscopic- and heavy-mineral studies were also made on the gravels. From 12 samples, the 2-4 mm fraction were selected for fine-grained pebble examinations (FPE). In addition, traditional macroscopic gravel petrography was done on the 8-16 mm and 16-32 mm fractions. Focussing on the potential source rocks of heavy minerals (i.e. heavy mineral holder rock types, HM holders), sediments containing low-quartz-content metamorphic rocks (i.e. metamorphic rocks except for quartzite), igneous (plutonic and volcanic) rocks or siliciclastic rocks (mostly sandstones) are the most promising ones for such studies.

Results

Based on the analytical and petrological results, we concluded that there are some samples with a remarkably lower, and also some with a remarkably higher "impurity profile", originating from different mines. All sand and gravel samples have SiO_2 content above 90 wt%. The major elements besides Si and O, are Al, Fe, K and Na. The Ca content is high in the Mid- and NW Hungarian gravels, while NE and SW samples have very low Ca content. Elemental analysis of the samples rated by particle size revealed that all the trace element concentrations decrease with increasing particle size, except for Cr, which has a higher concentration in gravels than in sands. Grinding the samples with a wolfram carbide mortar increases the W, La, Nd and also Co concentration of the samples. NE Hungarian gravel mines have the lowest trace element content, while those from NW Hungary Babót, from Mid-Hungary Bugyi IX and Taksony, and from SW Hungary Murakeresztúr II also have low trace element content.

Macro- and micro-scale pebble petrography of the samples showed diagnostic differences among the three major analysed regions. All of the sediments sampled are dominated by metamorphic (and especially quartzite) rock originated clasts. Low-quartz-content metamorphics (l-q m), igneous (i) and siliciclastic sedimentary (s) rock fragments (i.e. the HM holders) are dominated by the quartzite content. In the NE Hungarian region the HM holders average 48-54% of the total rock (l-q m: 35-39%, i: 6-12%, s: 4-5%). In the Mid-Hungarian region the HM holder amount is 35-41% (l-q m: 16-24%, i: 16-19%, s: 3-10%). In the NW Hungarian region it is 16-27% (l-q m: 9-16%, i: 3-11%, s: 1-9%). Furthermore, pebbles of the Mid-Hungarian region contain the highest ratio of volcanic rocks, while the pebbles of the NE Hungarian region – in addition to the quartzite – rather consist of metamorphic rocks. Gravels of the NW Hungarian region represent the most mature sediments in the investigated sample set with a >50% quartzite content.

Petrological and geochemical studies revealed that the gravel and sand from the NW Hungarian region has the lowest activation susceptibility, and thus they are the most suitable to produce concrete to be used in a high-radiation environment.

Remaining work

Samples from the SW Hungarian region need to be investigated from the petrological point of view. The gravel and concrete investigation project will be carried on in a framework of the V4-Korea Joint Research program between 2018 and 2022.

BEST ESTIMATE PLUS UNCERTAINTY ANALYSES OF GEN IV FAST REACTORS

Bálint Batki, András Keresztúri, István Panka

Objective

In this year, we focused on two types of fast reactors, an SFR and the ALLEGRO reactor. The calculations of the essential core safety parameters in fast spectrum reactors are loaded with large uncertainties due to the particularly large uncertainty of nuclear data, modelling uncertainties and possible mistakes by users. These core safety parameters such as coefficients of reactivity, power peaking factors and point-kinetics parameters play an important role during unprotected transients. The contributions to the uncertainties of the target parameters (e.g. peak cladding temperature) from the core safety parameters can be determined by uncertainty and sensitivity analyses.

Methods

Thermal hydraulics analyses of unprotected transients were performed using the ATHLET system code. The best estimate plus uncertainty analyses were based on the probabilistic GRS method. The essence of the GRS methodology is the simultaneous random sampling of the input parameters according to their probability distribution functions. In order to identify and measure the effect of the input parameters on the selected output parameters, sensitivity indices were also calculated. In this study, the neutronics was taken into account in a point kinetics approach.

Results

Best estimate values and uncertainty margins for the peak cladding temperature were calculated in the case of two types of transients (see Fig. 1). From the result of the sensitivity analyses, it was found that during unprotected overpower transients (UTOP) the most important uncertain parameters are the Doppler coefficient and the fuel thermal expansion coefficient of reactivity. The large uncertainty of the positive coolant and cladding temperature coefficients of reactivity have a significant influence on the uncertainty of the calculated peak cladding temperature, especially in the case of unprotected loss of flow (ULOF) transients. The results imply that the uncertainty of some core safety parameters should be reduced. The results adumbrate that additional safety shutdown systems need to be applied to mitigate the consequences of unprotected transients.

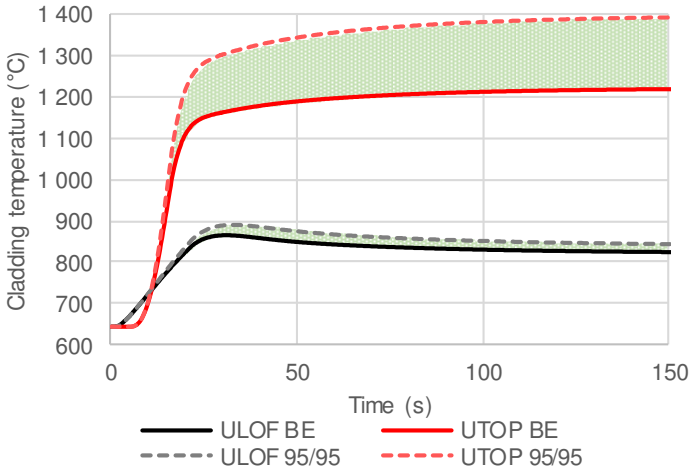

Figure 1: The best estimate of the maximum cladding temperature and the 95%/95% one-sided upper tolerance interval during the unprotected transients in the case of the ALLEGRO.

Remaining work

In the future, in order to take into account spatial effects, the point kinetics should be replaced by a 3D nodal method.

Related publications

[1] B. Batki, A. Keresztúri, I. Panka: *Calculation of core safety parameters and uncertainty analyses during unprotected transients for the ALLEGRO and a sodium-cooled fast reactor*, Annals of Nuclear Energy **118**, Pages 260-271 (2018)

[2] B. Batki, A. Keresztúri, I. Panka: *Uncertainty Analyses of Unprotected Transients in Fast Reactors from Reactor Physics Point of View*, 26th International Conference Nuclear Energy for New Europe (NENE), Bled, Slovenia, 11-14, September 2017

INVESTIGATION OF HOT DUCT BREAK SCENARIO IN ALLEGRO REACTOR USING A COMPUTATIONAL FLUID DYNAMICS TECHNIQUE

Attila Guba, István Farkas, Tatiana Farkas, Gusztáv Mayer

Objective

ALLEGRO is a demonstration reactor of the GEN IV GFR2400 gas fast reactor concept, which is currently in the pre-conceptual design phase. A recent CATHARE study (doi:10.1115/ICONE22-31094) carried out for the CEA 2009 ALLEGRO design pointed out that the required 850 °C criterion for PCT (Peak Cladding Temperature) fails in the case of a 200% hot duct break scenario when the initiating event is aggravated by a single failure of the intact loop. In those calculations the pressure loss coefficient between the hot and the cold duct was chosen to be 0.549. This value plays a pivotal role in the simulations and it influences the PCT results to a large extent.

Methods

In order to assess the conservativism of the previously chosen pressure loss coefficient we carried out a CFD (computational fluid dynamics) study for the hot duct break of ALLEGRO. Since the CFD modelling of the whole primary circuit of ALLEGRO reactor is too complex and unnecessary, we simplified the geometry by focusing solely on the hot duct break. For this reason, only the hot duct is modelled by inlet velocity and outlet pressure boundary conditions (Figure 1a). The reactor is replaced by a porous medium and its parameters were iterated from CATHARE calculations. The calculation domain with the guillotine type break can be seen in Figure 1a.

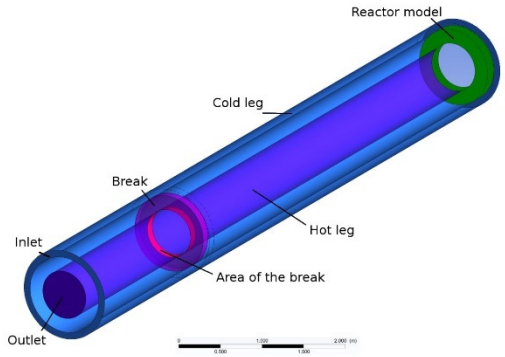

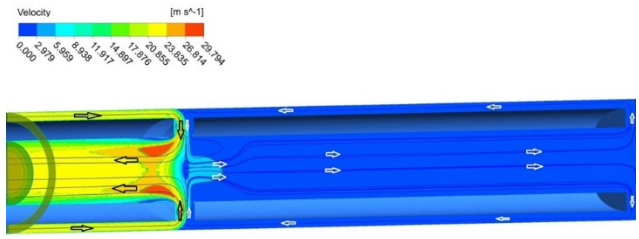

Figure 1a: Computational domain. *1b: CFD result for the 200% guillotine break. There is flow reversal in the core.*

Results

The gap between the two broken hot duct parts defines the size of the break which is usually given by an (circular cross section) equivalent diameter. In this study we varied the gap size between 3.75 cm and 30 cm, which corresponds to the equivalent break sizes of 25%-200%. (100% is the cross section of the hot duct). The results showed that the pressure loss coefficient is around 1.0 so the 0.549 value used in the previous CATHARE transient analyses had a sufficient safety margin compared to the CFD results. In the case of a 200% break, a new phenomenon was found (Figure 1b). There is a flow reversal in the core to the right of the break.

Remaining work

The next necessary step is the validation of the results for this special geometry. For this reason, specific measurements are proposed, which could be carried out at one of the V4G4 helium loops in the near future.

SENSITIVITY STUDY OF A HOT DUCT BREAK PRESSURE LOSS IN THE ALLEGRO REACTOR

Attila Guba, Gusztáv Mayer

Objective

Preliminary thermohydraulic calculations carried out for the ALLEGRO 75 MW CEA 2009 design (doi:10.1115/ICONE22-31094) pointed out that the peak cladding temperature exceeded the required temperature limit in the case of a hot duct break scenario, when the aggravation event of the stop of the second blower was taken into account. The value of the pressure loss coefficient used in the hot duct break modelling plays a pivotal role in the calculation of the corresponding peak cladding temperature (PCT). In this study we investigate how this pressure loss value influences the peak cladding temperature in the ALLEGRO reactor.

Methods

We selected the French CATHARE thermohydraulic code as a simulation tool to describe the hot duct break transient and to determine the PCT values. We carried out several transient calculations by varying the pressure loss coefficient and the results confirmed its importance.

Results

It was found that if the pressure loss coefficient is less than 1.4, the PCT limit exceeds the limit of 850 °C. (Fig.1).

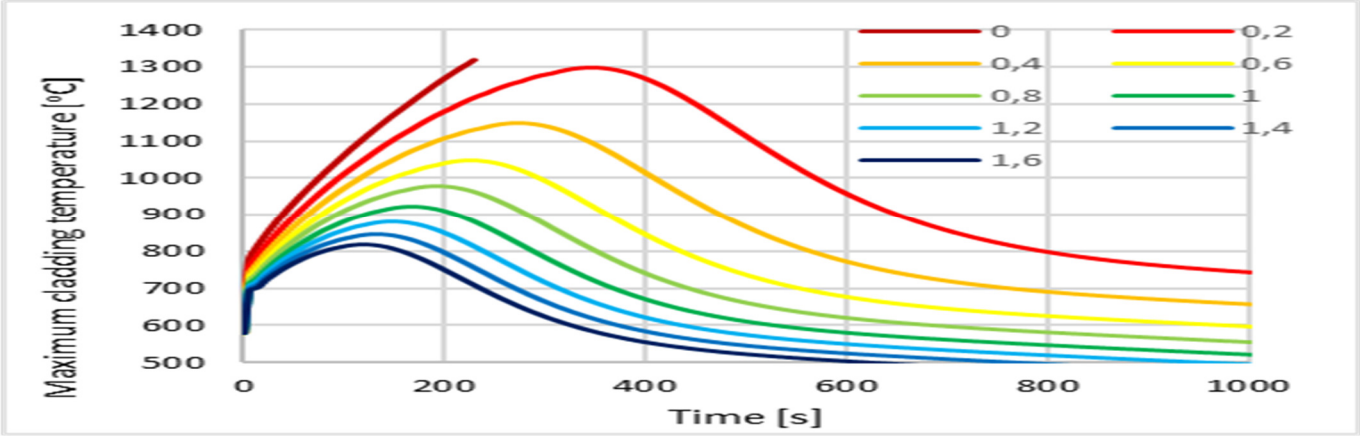

Figure 1: Time evolution of maximum cladding temperature for different pressure loss coefficient values.

Remaining work

Due to the high relevance of bypass transients in the ALLEGRO design, further calculations are necessary. These calculations have to be supported by a strong measurement program carried out in the S-ALLEGRO (Czech Republic) or STU (Slovakia) helium loops. Additional small scale measurements are proposed using air coolant.

Related publication

[1] G. Mayer and A. Guba: *Investigation of pressure loss coefficient in a hot duct break scenario in ALLEGRO reactor using the CATHARE thermohydraulic code*, Proceedings of SESDE2018, 17-19. September 2019, Budapest, Hungary

SELECTION OF FUEL FOR THE REFRACTORY CORE OF ALLEGRO GAS COOLED FAST REACTOR

Emese Slonszki, Zoltán Hózer, Tamás Novotny, Erzsébet Perez-Feró, Áron Horváth, Anna Pintér Csordás, Levente Illés

Objective

The main objective of this work was the selection of optimal materials for the refractory fuel of the ALLEGRO gas cooled fast reactor, and the start of testing those materials in a high temperature helium atmosphere.

Methods

A literature review was carried out taking into account materials found in the open literature and those provided by V4G4 partners. The selection of optimal cladding and pellet materials was based on the comparison of several criteria including in-pile fuel behaviour phenomena, fabrication, operational experience and available experimental support.

Samples of duplex and triplex type SiC_f/SiC cladding with 9.9 mm length provided by the Korea Atomic Energy Research Institute (KAERI) laboratories were tested at 1000 °C for 7 h in a helium atmosphere with and without various gas impurities. Considering the available experimental results, the effect of hydrogen, nitrogen and methane impurities was investigated in the present test series. Scanning electron microscopy and optical microscopy were used to characterize the as-received samples at MTA EK.

Results

The literature review pointed out that the most suitable candidates for the second ALLEGRO core are the carbide and nitride fuel pellets. Both materials have a high melting point and good thermal conductivity. The main disadvantages of nitride and carbide pellets is the high volumetric swelling rate. Taking into account the irradiation experience, fabrication capabilities and reprocessing options it is proposed to consider carbide fuel in the design of the second ALLEGRO core. The availability of more data on irradiated fuel and the larger fabrication experience supports this decision. The fuel for the second core of the ALLEGRO reactor could be composed of UC or (U,Pu)C pellets in SiC_f/SiC cladding.

The high temperature experiments with SiC_f/SiC tubes showed that:

- For a pure helium atmosphere and also with hydrogen or nitrogen impurities only a small mass reduction was observed.
- For a helium atmosphere with a methane impurity the decomposition of methane and the formation of carbon deposits led to a mass gain of the SiC samples.

The SEM studies of duplex samples showed that the thickness of the outer dense SiC material was not homogeneous and there are cavities among the fibres.

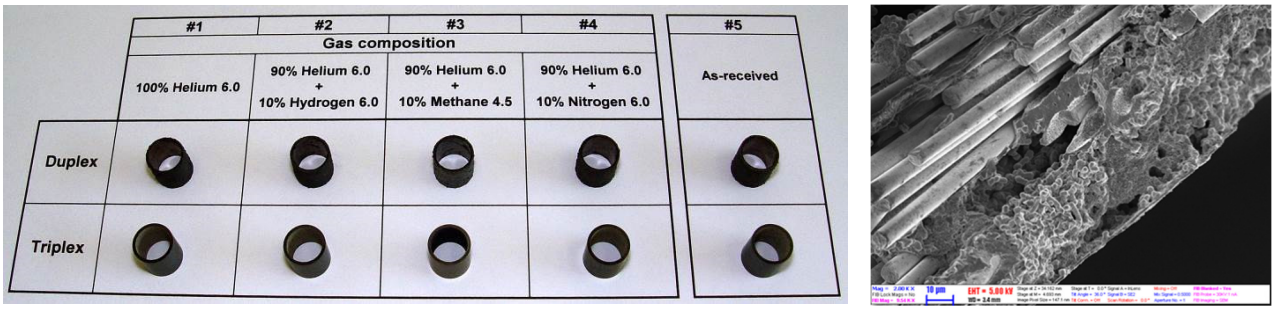

Fig. 1: View of the SiC samples after the high temperature treatment (left) and SEM image of the duplex sample (right)

Remaining work

The SiC_f/SiC samples will be further tested with scanning electron microscopy, and mechanical tests are also planned to investigate the change of mechanical load bearing capabilities.

Related publications

[1] Z. Hózer, T. Novotny, E. Perez-Feró, Á. Horváth, A. Pintér Csordás, L. Illés, Daejong Kim, Weon-Ju Kim: *Testing of SiCf/SiC claddings for ALLEGRO gas cooled fast reactor conditions,* MTA EK-FRL-2017-219-1-1-M0, in Hungarian (2017)

[2] E. Slonszki, Z. Hózer: *On the selection of fuel for the second core of ALLEGRO gas cooled fast reactor*, MTA EK-FRL-2017-218-1-1-M0, in Hungarian (2017)

COMPLEMENTARY INVESTIGATION ON IRRADIATED 316LN TYPE STEEL

Levente Tatár

Objective

Generation IV. fast breeder reactors and experimental fusion devices will want to use better structural materials for the different operating conditions. Development of these innovative reactor systems thus should be supported by material characterization programmes. The European FP7 MATTER project is one of the most recent aimed at investigating P91 and 316LN type steel candidates. The objective of our work in 2017 was to complement the work done in MATTER for 316LN type steel.

Methods

From our partners we have received a 316LN plate containing a weld for material characterization. After chemical analysis, Charpy V type specimens were manufactured from both base metal and weld, irradiated for 3 cycles in the Bagira3 irradiation rig at the BRR (Budapest Research Reactor). Vickers hardness and Charpy impact tests (widely used in industry) were performed on these specimens. The preparation of specimens and the tests complied with the EN 10 045-1 standard. Results obtained during our previous work are presented in [1]. In the framework of the MATTER project there were no experiments carried out on unirradiated specimens, so we complemented this in the current work. To investigate the effect of long term exposure to high temperatures, thermal ageing of the material has been performed. We manufactured 12 Charpy type specimens of which 6 were kept in as-received state while the other 6 were thermally aged at 550 °C for 50 hours. Hardness tests were performed along a line on the end surfaces of the specimens with a distance between individual measurements of 0.5 mm. Complementary measurements on the weld could not be carried out due to lack of material.

Results

The average values of hardness of the material are presented in Table 1. Figure 1 shows individual measurements for as received; figure 2 for the thermally aged case.

Table 1: Average measured hardness values

Material	Before irradiation (MATTER meas.)	Before irradiation (Compl. meas.)	Thermally aged	High temp. irradiated
316LN	300 HV	298.743 HV	309.042 HV	256 HV
Weld	343 HV	-	-	522 HV

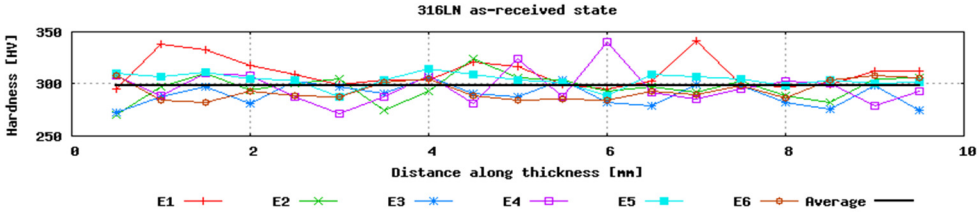

Figure 1: Measurements for specimens in as-received state

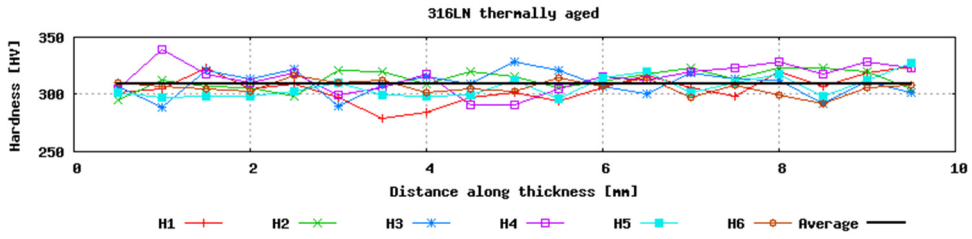

Figure 2: Measurements for thermally aged specimens

We can conclude, that the 316LN material is not prone to thermal ageing at the temperature of 550 °C.

Remaining work

Instrumented Charpy tests will be done on original and thermally aged specimens. Irradiated broken half specimens can serve as a base for new experiments, e.g. tensile tests which can complement these measurements, however, due to their still high activity the test itself can't be carried out due to limits of personal exposure, so this work has to be postponed for years.

Related publication

[1] A. Kovács, L. Tatár, F. Gillemot: *Experimental Results on Irradiated Samples in the Framework of MATTER Project*, EK Progress Report 2014

FUNCTIONAL MATERIAL PROPERTY DATABASE AND HANDBOOK FOR THE DESIGNERS OF THE DEMO FUSION REACTOR

Ferenc Gillemot, Ildikó Szenthe, Márta Horváth

Objective

The design of the first fusion reactor providing electrical energy is going on in the frame of the Eurofusion. The name of the planned device is DEMO (fusion demonstration reactor). The fusion device includes optical windows for checking the plasma state, and to deliver different heating beams to the vacuum vessel. These windows are subject to high heat and radiation, and they should maintain their optical and mechanical properties during use. Similarly, the cables used for the plasma-holding magnetic fields should resist heat, radiation and large mechanical loads. Optical and dielectrical materials are not primary-safety- related parts of the fusion device, but their reliability is highly important for its continuous operation. Research on development of these optical and dielectric materials are going on. The objective of the MTA EK task is the development and operation of a database for collecting and storing the available data, and to prepare a Functional Materials (FM) Material Property Handbook (MPH).

Methods

Earlier, the list of the data to be collected had been elaborated and discussed with the scientists and designers participating in the project. A simple Excel based database and data collection sheets had also been set up. Optical, physical, dielectrical and mechanical properties are included. The database and data collection sheets are also unified with respect to the units used and terminology. Data were collected from manufacturers' catalogues and from project reports. The format of the handbook followed the format of the Eurofer and Titanium alloys volumes which had been prepared earlier, also by the MTA EK.

Results

The first version of the FM MPH is ready. The types of the discussed material properties are summarised in table 1.

Table 1: Material properties included into the FM MPH

Material property group	Properties
Optical	Absortion, Transparency, Refractive index,
Dielectrical	Relative permittivity, Loss of tangent, Dielectric strength, Electrical resistivity
Physical	Specific heat, Thermal conductivity, diffusitivity, expansion; schock resistance, Melting point, Density, Grain size
Mechanical	Compressive and flexural strength, Young's, shear, bulk modulus; Fracture toughness, Hardness, Poisson ratio
Chemical	Chemical composition

Most of the properties are shown in figures, since they are given mostly as a function of one or more parameters (e.g. beam frequency, temperature, etc.). Properties are also given for an aged (irradiated, thermal treated etc.) condition if they are available.

The handbook also includes some other general material information and references for the data sources. A few examples from the handbook can be seen in figures 1 and 2. Presently the handbook consists of 118 pages and 14 different functional materials.

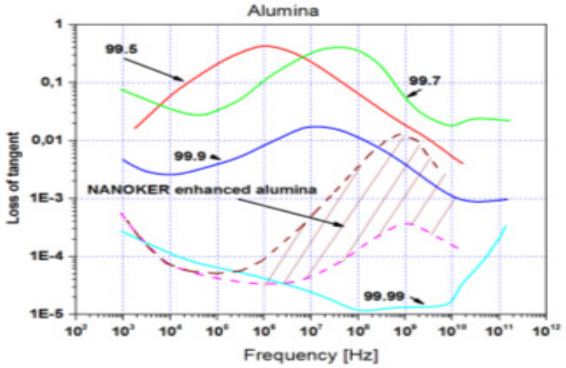

Figure 1. Loss of tangent of alumina

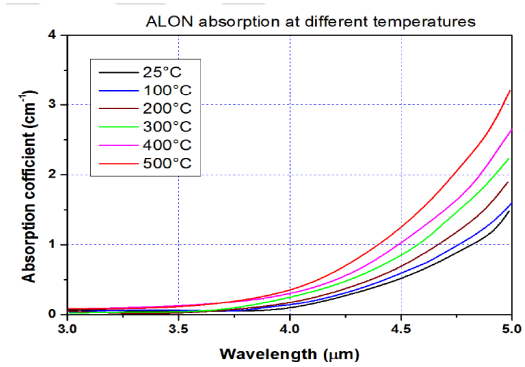

Figure 2. ALON (Aluminum oxynitride spinel) absorption at different temperatures

Remaining work

Further extension of the FM MPH, mainly with aged (irradiated etc.) properties as the new data will become available.

III. NUCLEAR SECURITY AND DOSIMETRY

DOSE MONITORING IN THE EUROPEAN MODULE OF THE INTERNATIONAL SPACE STATION (DOSIS-3D)

Andrea Strádi, Julianna Szabó, Attila Hirn, Tamás Pázmándi, Balázs Zábori, József Pálfalvi

Objective

Our work is aimed at providing dose distribution information at several locations with different shielding distributions inside the Columbus module of the International Space Station (ISS), using passive detectors. The Dosis-3D experiment (led by the German Aerospace Centre, DLR) was launched in 2012 and since then 10 measurement cycles were completed in half-year sessions, yielding dosimetric data which constitute essential information for radiation protection in space.

Methods

Two types of passive detectors are used in this experiment. LiF thermoluminescent dosimeters (TLDs) are sensitive mainly to particles with Linear Energy Transfer (LET) under 10 keV/µm in water, while nuclear track detectors (SSNTDs) measure in the high LET (10 - 1000 keV/µm in water) region, both resulting in mission integrated dose. In case of the track detectors a two-step etching process is used to reveal the latent tracks induced by short range – high LET and the lower LET particles, as well.

Results

During the last three missions (Dosis-3D/8 – 10, between the end of 2015 and the middle of 2017) the altitude of the ISS was almost constant, while the solar activity was decreasing causing gradual increase in dose contribution from Galactic Cosmic Rays due to reduced deflection by the interplanetary magnetic field. These parameters, together with the local shielding conditions are the most important variables that affect the dose inside the module. Dose rates obtained by TLDs during the last three missions varied between 206 µGy/day and 359 µGy/day as can be seen in Fig. 1. It is important to note that the values are strongly dependent on the location, and show the same tendency in all sessions. The highest dose in this predominant LET range is regularly measured at location No. 2 near the end cone of the module on the aft side, and the lowest at the location No. 9, which is on the forward side close to the hatch leading to the Harmony module, thus shielded by the bulk of the Station. Due to reduced deflection by the interplanetary magnetic field, decreasing solar activity causes increasing dose contribution from galactic cosmic rays and neutrons resulting in dose increment during the consecutive sessions.

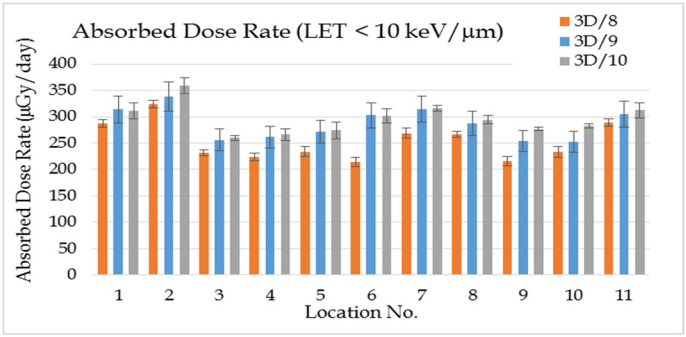

Fig. 1. Absorbed dose rates obtained by TLDs

Table 1. Track detector results for Dosis-3D/8

Location	D (µGy/d)	H (µSv/d)	Q
1	35	451	13
2	37	504	14
3	45	465	10
4	36	428	12
5	39	443	11
6	36	415	11
7	40	479	12
8	39	489	12
9	35	394	11
10	34	407	12
11	37	393	11

Table 1 summarizes the absorbed dose rates (D), the dose equivalent rates (H) and the quality factors (Q) measured by track detectors in the 8th session. In this LET range (over 10 keV/µm) the tendency of absorbed dose rates obtained at different locations is roughly similar, but the absolute values are much lower than in the subsequent missions, as expected. In summary it can be stated that the local shielding conditions can alter the dose rate near the walls inside the Columbus module by almost 20% in the LET range measurable by TLDs and SSNTDs, which must be taken into account e. g. in case of choosing the optimal location for storing, or performing radiation susceptible experiments in this module.

Remaining work

The evaluation of track detectors from the 9th and 10th session is still in progress. The DOSIS-3D project will be continued in the coming years providing measured dose data covering the whole 24th solar cycle.

Related publications

[1] T. Berger et al., DOSIS & DOSIS 3D: Long term dose monitoring on-board the Columbus Laboratory of the International Space Station (ISS) – Current status and work in progress. (oral presentation) 22nd Workshop on Radiation Monitoring for the International Space Station, 5 – 7 September 2017, Thales Alenia Space, Torino, Italy.

[2] T. Berger, S. Burmeister, D. Matthiä, B. Przybyla, G. Reitz, P. Bilski, M. Hajek, L. Sihver, J. Szabó, I. Ambrozova, F. Vanhavere, R. Gaza, E. Semones, E. G. Yukihara, E. R. Benton, Y. Uchihori, S. Kodaira, H. Kitamura, and M. Boehme: *DOSIS & DOSIS 3D: Radiation measurements with the DOSTEL instruments onboard the Columbus Laboratory of the ISS in the years 2009 – 2016.* J. Space Weather Space Clim. **7**, A8 (2017)

UNCERTAINTY ESTIMATION OF THYROID ACTIVITY MEASUREMENTS AND ITS CONSEQUENCES ON DOSE ASSESSMENT

Tamás Pázmándi, Annamária Pántya, Andor Andrási, Dorottya Jakab, Péter Zagyvai

Objective

For the great majority of incorporated radionuclides, the internal dose is estimated in two steps. In the first step the actual activity present in the body is determined by direct or indirect monitoring methods. By direct gamma spectrometric measurements activity in the whole or part of the human body can be determined (in vivo), while by the indirect methods the radioactivity of physical and biological (in vitro) samples are assessed. In the second step the intake value and the associated committed dose can be estimated on the basis of measured data considering necessary assumptions on exposure conditions (time and route of intake, chemical form etc.). In 2016 two new intelligent scintillation detectors were installed for the thyroid measurements. One of them is able to measure the ^{131}I isotope, and the other is used for the detection of ^{125}I isotope. To ensure the appropriate usability, the new equipments require adequate energy and efficiency calibration, which were performed within the framework of the study. In the executed series of measurements, the available thyroid phantoms were tested with different iodine isotopes.

Methods

Thyroid activity was measured by lead shielded NaI(Tl) scintillation detectors standing on a vertically adjustable stand for lead shielding, which allows the optimal installation of the equipment. The detector connects to the computer via USB cable, where the spectrum recording is performed by the MultiACT complex nuclear spectrometry software package. To perform the efficiency calibration, we used a plastic phantom, which imitates a human neck, within which the radioactive material is placed in a cuvette. The efficiency calibration measurements were carried out in 3 different measuring positions with 4 calibration sources with different activities. Measurements were supplemented with Monte Carlo simulations, in order to extend the study by applying a wider range of variable parameters. We also participated in the international ICIDOSE internal dose intercomparison exercise. Four case studies having different degree of complexity, have been proposed to the 84 potential participants. The second of these cases was related to routine monitoring for ^{125}I by using 6 repeated thyroid measurements on a female subject.

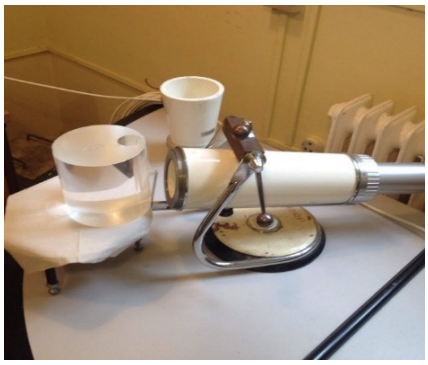

Figure 1: Thyroid measurement: detector, shielding and neck phantom

Results

It has been found that the adequate thyroid measurement results are influenced by various parameters e.g. the shape of thyroid, position of the thyroid inside the human body, the detector distance from the body surface and the distribution of the radioactivity within the organ. The experiences also demonstrated that the determination of the uncertainty of dose estimation is a complex process. The influence of the uncertainties of assumptions such as the date and route of intake, the physical and chemical form were also investigated in terms of the accuracy of the final internal dose assessment. The results of the uncertainty assessments were involved in dose estimation calculations with MONDAL 3 code. By varying the parameters, it was found that the uncertainty of the dose estimation is about 20-30%.

Remaining work

This project has been completed.

Related publications

[1] A. Pántya, A. Andrási, T. Pázmándi, P. Zagyvai, *Dose assessment of thyroid in accidental situation,* Radiation Protection online **Vol. X.**, No. 1., (2017) (in Hungarian).

[2] A. Pántya, A. Andrási, D. Jakab, T. Pázmándi, P. Zagyvai, *Uncertainty estimation of thyroid activity measurements and its consequences in dose assessment*, 5th European IRPA Congress (2018).

RAPID SEPARATION OF ACTINIDES FROM HUMAN URINE BY EXTRACTION CHROMATOGRAPHY

Márton Zagyvai, Nóra Vajda (Radanal Ltd.), László Szentmiklósi

Methods

Diglycol amide (DGA)® is a commercially available resin that contains N,N,N′,N′-tetra-n-octyldiglycolamine on an inert support. Am, U, Pu and Th are separated by extraction chromatography based on DGA resin. A previously applied method [1] was simplified by omitting the digestion and preconcentration steps before the DGA resin separation. 100 mL of water and urine samples acidified with HCl to 4M were loaded on to a 0.5 g DGA column. α-sources of various actinides were prepared by co-precipitation with NdF_3. Measurements were performed with a Si α-detector. We are further developing this method for samples taken from a nuclear reactor as well as for those from the environment, e.g. for soil and sediment samples.

Results

This year we investigated further the effect of urea (Table 1.) [2] and other constituents of human urine (Table 2.). We made model experiments with distilled water.

Table 1: Recoveries of actinides in the presence of urea.

Experiment	Recovery % *)				Comment
	Th-230	U-233	Pu-239	Am-241	
Pi36	47	65	78	65	2 g urea in 150 ml solution
Pi37	91	82	90	100	10 g urea in 150 ml solution
Pi38	93	92	88	83	10 g urea in 150 ml solution
Pi39	116	103	114	117	10 g urea in 150 ml solution
Pi40	102	95	123	95	10 g urea in 150 ml solution
Pi41	29	101	51	97	10 g urea in 150 ml solution
Pi42	63	93	102	91	10 g urea in 150 ml solution

Table 2: Recoveries of actinides in the presence of hippuric acid.

Experiment	Recovery % *)				Comment
	Th-230	U-233	Pu-239	Am-241	
Pi34	86	87	92	88	Only distilled water
Pi35	92	92	95	101	Hippuric acid

*) The estimated recovery uncertainty is about 15%.

Remaining work

1. Rapid digestion methods (fusion, microwave digestion) will be developed for different matrices of soil and sediment samples.
2. Separation of actinides will be examined for soil and sediment samples by extraction chromatography based on DGA resin. The high selectivity of DGA will probably make the preconcentration step unnecessary.
3. Feasibility of different α -source preparation procedures (electroplating, micro co-precipitation) will be examined for processing suitable actinides into multiple or single-element sources.
4. Different spectrum processing software programs (Hypermet, Genie2000) will be used for the evaluation of the measured spectra.

Related publications

[1] J. Groska, N. Vajda, Zs. Molnár, E. Bokori, P. Szeredy, M. Zagyvai: *Determination of actinides in radioactive waste after separation on a single DGA resin column*, J. Radioanal Nucl Chem **309,** 1145–1158 (2016)

[2] M. Zagyvai, N. Vajda, J. Groska, Zs. Molnár, E. Bokori, P. Szeredy: *Assay of actinides in human urine by rapid method*, J. Radioanal Nucl Chem **314,** 49–58 (2017)

NUMERICAL MODELLING OF THE INHOMOGENEITY OF A LOW DOSE INTERNAL RADIATION BURDEN

Árpád Farkas, Imre Balásházy, Ágnes Jókay, Péter Füri

Objective

The main objective of this work was to develop a dynamic biophysical, mathematical and numerical model for the quantification of the inhomogeneity of the low dose radiation burden within the large bronchial airways. As requirements, the model should consider both the phenomena of radio-aerosol deposition and clearance within the airways and should provide a more exact dosimetric and microdosimetric description of the internal burden.

Methods

Three dimensional digital airway and mucus models of an airway bifurcation corresponding to the 4th and 5th airway generations have been reconstructed based on morphometrical data derived from the published literature. A stochastic whole respiratory tract deposition model has been used to quantify the regional and airway-generation-number specific deposition fractions of the inhaled radon progenies. Computational fluid and particle dynamics (CFD) techniques were used to simulate the local deposition patterns of the inhaled radon daughters within the model airway bifurcations. The flow field of the mucus layer lining the bronchial airways has been computed by CFD techniques. Trajectories of the radioactive particles propelled by the mucus were computed after their deposition. Radioactive decay was modelled based on the half-lives of the radon progenies. Radiation exposure and activity size distribution parameters were characteristic of a home environment. Polydisperse radioaerosols were considered. Bronchial activity distributions emerging as a result of deposition and clearance were computed. The locations of the alpha-decays were computed.

Results

Our computer simulations revealed that in the large bronchial region of the airways the degree of inhomogeneity due to nonuniform primary deposition of radon daughters is decreased by mucociliary clearance by a factor of about 5. However, a slow clearance zone emerged in the vicinity of the carinal ridge (the central ridge of the bifurcation). As a consequence, the distribution of radio-isotopes still remains nonuniform and the most exposed cells (on a surface area of 1 mm^2) will receive about 10 times higher doses than the average dose corresponding to a given exposure level. The biological consequences of the present results remain to be explored by future research.

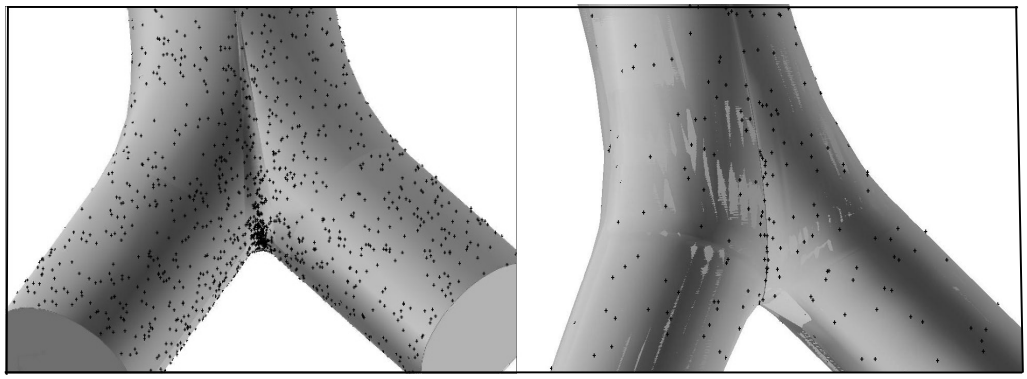

Figure 1: Spatial distribution of the inhaled radon progenies after their bronchial deposition (left panel) and distribution of simulated alpha-decay locations assuming 24 h of radon exposure at 50 Bq/m^3 activity concentration (right panel)

Related publications

[1] P. Füri, I. Balásházy, W. Hofmann, R. Winkler Heil, G. Kudela, Á. Farkas, B. G. Madas: *Effect of mucociliary clearance to radiation burden from inhaled radon progenies in a healthy women's lung*. Submitted to Radiation Protection Dosimetry.

[2] Á. Farkas, I. Balásházy, Á. Jókay: *Numerical modelling of nanoparticle mucociliary clearance in the large bronchial airways.* Inhalation Toxicology (in preparation).

[3] Á. Farkas, P. Füri, I. Balásházy, I. Szőke: *Advanced Models for Internal Dosimetry – Opportunities for Application in Nuclear Emergencies and Decommissioning*. Proceedings of the 40th Enlarged Halden Programme Group Meeting 2017, 24-29 September 2017. Lillehammer, Norway, MTO-3.2, pp. 1-7.

[4] P. Füri, W. Hofmann, Á. Jókay, I. Balásházy, M. Moustafa, B. Czitrovszky, G. Kudela, Á. Farkas: *Comparison of airway deposition distributions of particles in healthy and diseased workers in an Egyptian industrial site*. Inhalation Toxicology **29:(4),** 147-159 (2017)

[5] Á. Jókay, Á. Farkas, B.G. Madas, E. Drozsdik, I. Balásházy: *Numerical computation of internal radon doses for home and mine environments.* Abstracts of the European Radiological Protection Research Week, 10-12 October 2017, Paris, Abstract ID. 86631, pp. 82.

PREPARATION FOR EXPERIMENTS INVOLVING RADON EXPOSURE

Emese Drozsdik, Balázs Madas, József Pálfalvi, Tamás Pázmándi, Andrea Strádi, Julianna Szabó

Objective

The objectives of the present study were to continue our theoretical research [1] on the biological effects of radon exposure, and to evaluate our radon measurement capabilities in order to identify the most important improvements required and the expected opportunities to be exploited.

Methods

For this purpose, we reviewed the active and passive measurement methods, and the legal environment related to radon (in particular the Radon Action Plan to be enacted in early 2018) and participated in international intercomparison campaigns in Italy (Second international radon-in-field intercomparison for passive devices: workplaces and dwellings) and the United Kingdom (2016 Public Health England (PHE) - Intercomparison of Passive Radon Detectors).

In addition, we applied numerical models [2] to estimate the effects of radon exposure on the clonal expansion rate in lung carcinogenesis, and compared it with the outcome of a mathematical analysis of epidemiological data, particularly with the observed inverse exposure rate effects [3].

Results

With computational modelling, we have found that the induction of hyperplasia may result in such a decrease in clonal expansion rate as is expected based on epidemiological data. However, since there are many parameters for which a value has not been measured, there may be other phenomena which provide a better explanation for the inverse exposure rate effect [3].

In the intercomparison campaigns our passive detectors performed better than in the previous year. Improvements were achieved by using a new calibration factor. Table 1 presents the results of the PHE intercomparison. For high and medium exposures, the measured values were in good agreement with the references, while for low exposures the differences were higher. This indicates that more careful handling of the detectors is needed in the future.

Based on the legal changes it is expected that the number of radon measurements in Hungary will increase significantly. It requires an increase in the number of service providers as well as in calibrations and harmonization exercises. It underlines the importance of the few radon chambers in Europe including ours, which could also be used for small animal experiments after being repaired.

Table 1. 2016 PHE intercomparison results

Exposure number	Measured exposure (1 STD) (kBq m^{-3} h)	Reference exposure (kBq m^{-3} h)
1	2572 (89)	2678
2	1333 (265)	1271
3	2 (43)	140
4	338 (230)	384
5	776 (217)	782
6-transit	152 (305)	0

Remaining work

Considering the expected increase in measurements related to radon exposure and the infrastructural and human resources at MTA EK, our role has to be decided and elaborated. In some cases, like the radon chamber, the repair work has to be done.

Related publications

[1] B. G. Madas: *Radonexpozíció és a kis dózisok definíciója*, Fizikai Szemle **67**, 316-318 (2017)

[2] B. G. Madas and E. J. Drozsdik: *Effects of mucus thickness and goblet cell hyperplasia on microdosimetric quantities characterizing the bronchial epithelium upon radon exposure*, International Journal of Radiation Biology. doi: https://doi.org/1 0.1080/09553002.2018.1511931 (in press)

[3] E. J. Drozsdik and B. G. Madas: *Quantitative analysis of the potential role of basal cell hyperplasia in the relationship between promotion and radon concentration*, Radiation Protection Dosimetry (under review)

HEALTH PHYSICS AND ENVIRONMENTAL STUDIES WITHIN THE HUNGARIAN NUCLEAR RESEARCH PROGRAM

Csaba Araczki, Imre Balásházy, Barbara Brockhauser, Sándor Deme, Emese Drozsdik, Margit Fábián, Árpád Farkas, Péter Füri, Felicián Gergely, Ágnes Jókay, Balázs G. Madas, Blanka Nagy-Czitrovszky, János Osán, Tamás Pázmándi, Csilla Rudas, Péter Szántó

Objectives

The Hungarian Nuclear Research Program (2014-2018) is a research and development project funded by the National Research, Development and Innovation Office (project identifier: VKSZ_14-1-2015-0021; homepage: vksz14.kfki.hu). The present report summarizes the health physics and environment related activities carried out in the third year of the project. The activities comprise research on the biophysical effects of low doses of ionizing radiation, modelling the transport of radionuclides in surface water, and conditioning and final disposal of high-level radioactive waste (HLW).

For the third year of the project the following research objectives were set out in the research area of low doses of ionizing radiation:

- further development and application of the stochastic lung deposition and clearance model to compute tissue and cell nucleus dose distributions of inhaled alpha emitters along the human bronchial airways [1],
- quantification of the significance of mucociliary clearance in bronchial radon dosimetry,
- analysis of the potential role of basal cell hyperplasia in the relationship between cell promotion and radon concentration [2,3],
- experimental inspection of the effects of low and moderate doses of gamma-radiation on butterflies and moths.

The dose calculation for the estimation of the environmental radiation burden resulting from an accidental radioactive emission from the Paks Nuclear Power Plant (NPP) includes the evaluation of liquid releases and their consequences. To determine the consequences of a liquid release from Paks NPP, a dynamic aquatic transport model with the local parameters of the Danube is needed. The objective of the 4-year task is to develop such an aquatic transport model and to calculate the dose for different aquatic pathways.

High-level radioactive waste (HLW) produced by spent fuel reprocessing of civil nuclear reactors is currently incorporated into an inert host material. Such vitrification technology is widely accepted for immobilization of HLW materials and borosilicate glasses are generally accepted as proper HLW isolating media. Borosilicate glasses do satisfy the following main requirements: the radioactive elements become immobilized as part of the host material structure; the leaching rate of radioactive elements is acceptably low, and the encapsulation cost is acceptable. The key questions are the crystallization, unknown basic processes and stability of the vitrified compositions. Essentially the most important tasks in this area are to find a better (containing fewer components) starting composition of the host material; to study the incorporation rate of the active elements; and to find a well-controlled vitrification process. Borosilicate-based glasses doped with UO_3 and CeO_2 and Nd_2O_3 (lanthanides used for chemical modelling of the actinides) were studied with the aim to clear up the correlation between structural characteristics, and to find an answer for a possible incorporation mechanism of the U, Ce, Nd elements.

In Hungary, the Boda Claystone Formation (BCF) is the potential rock formation in which to build the future HLW repository. The repository will be a complex system of natural and engineered barriers with the aim of long-term safe disposal of radioactive waste. Studies are going to be performed on the radionuclide retention capabilities of the argillaceous rocks of BCF. A series of macroscopic experiments is planned to quantify sorption of key cationic and anionic radionuclides at constant pH and solid-to-liquid (S/L) ratio at different equilibrium concentrations.

Methods

In the human lung, both deposition and clearance patterns of deposited isotopes are strongly inhomogeneous. A complex dynamic numerical model accounting for both phenomena was developed. The model is able to characterize the radiation burden at both microscopic and macroscopic scales providing a more exact microdosimetric analysis. Gamma-irradiation experiments were conducted on four species of lepidopterous butterflies and *Lymantria dispar* moths.

In order to model the transport of radionuclides in surface water, local and site specific geological and hydrological data were gathered and analysed. These parameters include the local shape of the river's cross-section, the water level dependent flow rate, the flow velocity and also the local sediment data. The local sediment properties are important during a long term release or in an accidental emission when due to flooding, the contaminated sediment could be left on the river shore. To determine the activity concentration of a flooded area the suspended sediment activity concentration is needed, and can be considered to be dependent on the suspended sediment load [kg/m^3]. The sediment load measurements available for 6 years at Dombori (~20 km South of Paks) were analysed and a correlation between the sediment load and the flow rate of the Danube was found as shown in Fig. 1. According to these results, although the correlation is weak, the model uses the plotted line that can be seen in Fig. 1, to calculate the suspended sediment load.

The other hydrological parameter that was investigated was the river stream stage, which effects the other hydrological parameters and has a significant daily change. The analysis of the average monthly stream stage of the Danube at Paks for the last 10 years showed that the highest values occur in late spring, and early summer. The lowest stream stages take place during

autumn and wintertime.

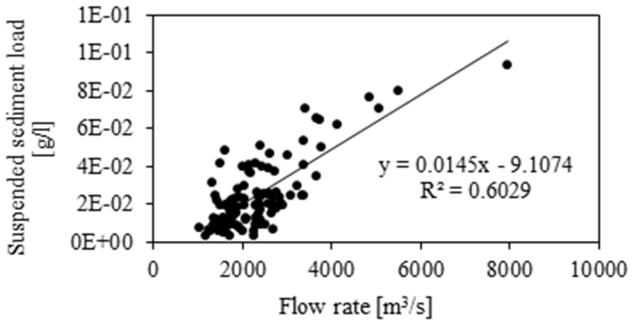

Figure 1: Correlation between the suspended sediment load and the flow rate of the Danube at Dombori from 2007 udntil 2012.

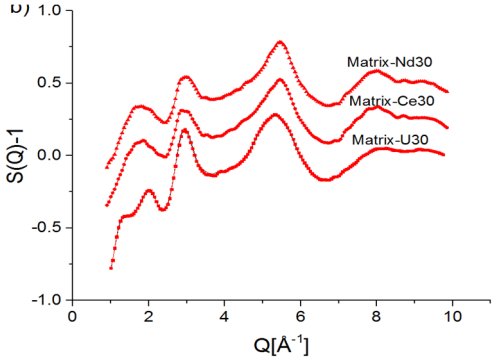

Figure 2: ND structure factors for the Matrix-U,Ce,Nd(30) glasses (red markers) and RMC fits (solid line). (The structure factor, S(Q) is a mathematical description of how a material scatters incident radiation; Q is the scattering vector.)

For studies related to vitrification of HLW, two series of U-, Ce- or Nd-containing glassy samples were prepared and investigated. The composition of the borosilicate matrix (denoted as Matrix) is $55SiO_2 \cdot 10B_2O_3 \cdot 25Na_2O \cdot 5BaO \cdot 5ZrO_2$. The composition of the glassy specimens of the two series are 90wt%[Matrix]+10wt%X, and 70wt%[Matrix]+30wt%X, where X stands for UO_3, CeO_2 or Nd_2O_3. Samples are labelled as Matrix-U10, Matrix-Nd30 etc. Lanthanides were used for chemical modelling of actinides, e.g. Ce(III,IV) for Pu(III,IV) and Nd(III) for Am(III) or Cm(III). The glassy samples were prepared by the melt-quenching technique. The samples were found to be fully amorphous; no crystalline phase was detected.

Based on neutron diffraction (ND) measurements combined with Reverse Monte Carlo (RMC) simulation, a comprehensive structural study of the glasses was possible. The special interest of this system lies in the different glass forming mechanisms of SiO_2 and B_2O_3. One of the main issues is what are the structural changes of the boron-oxygen and silicon-oxygen networks with addition of different kinds of large atoms like U, Ce and Nd. Nuclear Magnetic Resonance (NMR) spectroscopy was also used to get complementary information on the boron environment.

Six clay-rich rock samples were received from core sections of the latest drillings of BCF. Based on the known porewater composition, the measurement circumstances and sample preparation methods were optimized in order to conduct macroscopic sorption investigations.

Results

Based on the stochastic lung model calculations, the deposition of the unattached ^{218}Po and the clearance of the attached ^{214}Po progenies play a crucial role in the final evolution of dose rates. The 6% unattached ^{218}Po results in a radiation burden comparable to that of all the attached progenies. The distribution of radiation burden of the inhaled short-lived radon progenies is strongly influenced by mucociliary clearance. The total radiation burden in the central airways is much higher if mucociliary clearance is taken into account than without it [4,5]. Results suggest a correlation between the local radiation burden and the spatial distribution of bronchial carcinomas.

A result of gamma-irradiation experiments is that the lifetime of the lycaenid imagoes decreased as a consequence of ionizing radiation. In the case of *Lymantria dispars* the lifespan of the larva, pupa and imago states slightly changed at 1 Gy gamma irradiation of the eggs and the change was different between females and males [6].

The geographical and hydrological findings were incorporated into the developed aquatic transport model [7] and dose calculations were made for three scenarios with the released activity of 10^{16} Bq ^{131}I. The following scenarios were calculated at the receptor point of Gerjen (~10 km South of Paks):

- AW: Ingestion dose via consumption of fish originating from the contaminated river (0.3 kg/meal).
- SS: Swimming in, sunbathing near and consuming fish from the contaminated river.
- HMW: Swimming in, sunbathing near and consuming fish from the contaminated river, at highest ever-measured water level.

Table 1 shows the doses from different pathways for the three scenarios calculated for unit Bq release. It can be seen that the internal dose from ingestion of fish and external dose during swimming make the highest contributions to the total dose.

Table 1: Dose conversion values for different pathways

Dose Conversion [mSv/Bq]	AW	SS	HMW
Drinking via swimming	-	2.52E-16	3.95E-17
Fish consumption	4.61E-16	5.64E-16	8.06E-16
Swimming	-	5.68E-16	2.71E-16
Sunbathing	-	3.30E-25	6.77E-26

The multi-component matrix glasses used for HLW vitrification studies have a compact structure, where the network forming Si and B atoms play an important role. It was established that the basic structural units are trigonal BO_3 and tetrahedral BO_4

and SiO_4 groups, and a significant spatial correlation exists between these units. Based on the RMC calculations, the basic network structure was established as formed by mixed $^{[4]}$Si-O-$^{[3]}$B and $^{[4]}$Si-O-$^{[4]}$B linkages. The basic network structure is stable for all studied samples [8]. It is remarkable, that with increasing UO_3, CeO_2 and Nd_2O_3 content the character of the ND structure factors are not changed. The U-O, Ce-O and Nd-O first neighbour distances shows slight concentration dependence, but the average values of the peaks are in the same position, regarding to the two sample series.

From the RMC modelling of ND data (Fig. 2) and NMR spectroscopy it can be concluded that the addition of UO_3, CeO_2 and Nd_2O_3 with different concentrations does not change the basic network configuration. The RMC modelling also provides information on the second coordination sphere. The analysis of the silicon-metal and boron-metal pair correlation functions show pronounced correlations. The relatively shortest second neighbour distances obtained for the Si,B-U, Si,B-Ce and Si,B-Nd pair correlation functions, suggests that uranium and lanthanide ions are involved partly as a network former in the structure. These pronounced correlations show that U, Ce and Nd atoms can incorporate in the matrix glass structure. This result also leads to the conclusion that the compact glassy structure has the ability to include uranium and lanthanide ions with high stability [9].

The design of macroscopic sorption experiments on the recent BCF core samples has been developed and optimized. After grinding the argillaceous rock samples, the particles with size less than 63 μm will be separated. Sorption isotherms are planned to be measured at pH 8.0 using separate samples for the selected ions (Cs^+, Ni^{2+} and SeO_3^{2-}) using both inactive and isotope tracer methods. The high-concentration points of the isotherms will be measured via inductively coupled plasma optical emission spectrometry (ICP-OES) or inductively coupled plasma mass spectrometry (ICP-MS) analysis of the liquid phase separated by centrifugation. The separated solid phase will be available for complementary investigations [10]. The low-concentration range of the isotherms will be recorded using beta scintillation detection of the radiotracers. The optimized S/L ratios and reaction durations were found to be 5 g/L, 8 g/L and 10 g/L; 3 d, 8 d and 21 d for Cs^+, Ni^{2+} and SeO_3^{2-} ions, respectively.

Remaining work

In the field of low doses of ionising radiation, the clearance along the bronchial airways will be modelled by computational fluid dynamic techniques at a local level.

In the last phase of the work on modelling the transport of radionuclides in surface water, the aquatic transport code and dose calculation module will be developed based on the previously established algorithms. A sensitivity analysis will be conducted and the model parameters used will be clarified. The developed program will be tested and the code documentation will be prepared.

Further structural studies are planned on the lanthanide- and uranium-loaded glasses using synchrotron radiation. Leaching of radionuclides from the glasses modelling vitrification of HLW will be studied. Macroscopic sorption experiments will be conducted on the new core samples of BCF.

Related publications

[1] P. Füri, W. Hofmann, Á. Jókay, I. Balásházy, M. Moustafa, B. Czitrovszky, G. Kudela and Á. Farkas: *Comparison of airway deposition distributions of particles in healthy and diseased workers in an Egyptian industrial site.* Inhalation Toxicology **29**(4), 147-159 (2017)

[2] B. G. Madas: *Radon exposition and definition of low doses.* Fizikai Szemle **58**(9), 316-318, in Hungarian (2017)

[3] E. Drozsdik and B. G. Madas: *Quantitative analysis of the potential role of basal cell hyperplasia in the relationship between promotion and radon concentration.* MICROS 2017, 17th International Symposium on Microdosimetry. 5-10 November 2017, Venice, Italy. ID: 91 (2017)

[4] Á. Farkas, P. Füri, I. Balásházy and I. Szőke: *Advanced Models for Internal Dosimetry – Opportunities for Application in Nuclear Emergencies and Decommissioning*. Proceedings of the 40th Enlarged Halden Programme Group Meeting 2017, EHPG 2017, 24-29 September 2017. Lillehammer, Norway, MTO-3.2, 1-7 (2017)

[5] Á. Farkas, Á. Jókay, P. Füri, B. G. Madas, E. Drozsdik and I. Balásházy: *Numerical computation of internal radon doses for home and mine environments.* ICRP 4th International Symposium on the System of Radiological Protection, 2nd European Radiological Protection Research Week, 10-12 October 2017, Paris, France, ERPW Session 6: Internal Dosimetry. Book of Abstracts 82 (2017)

[6] B. Nagy-Czitrovszky, I. Balásházy, P. Szántó, P. Füri, B. G. Madas, G. Szőcs, G. Bozsik, F. Lakatos and K. Tuba: *Effect of low and intermediate dose ionizing radiation on butterflies,* Sugárvédelem, before submission, in Hungarian (2018)

[7] B. Brockhauser, S. Deme, T. Pázmándi, Cs. Rudas and P. Szántó: Poster and full paper: *A Site Specific Accidental Aquatic Transport Model for Radioactive Release in the Danube Under the NPP of Paks*, 5th European IRPA Congress, The Hague, The Netherlands, (2018)

[8] M. Fábián and Cs. Araczki: *Development of Glass Matrix for Radioactive Waste Conditioning,* Materials Science Forum **885**, 48-54 (2017)

[9] M. Fábián and Cs. Araczki. *Optimization of New Glass Matrices for Conditioning of High Level Radioactive Wastes*, ANS Conference International High-Level Radioactive Waste Management, Charlotte, NC, USA, 9-13 April 2017

[10] R. Dähn, J. Osán, M. Marques, D. Grolimund and B. Baeyens: *X-ray absorption investigations of uptake processes by argillaceous rocks. From pure mineral phases to real systems.* Actinide XAS 2017, Oxford, UK, 11-13 April 2017

RESEARCH & DEVELOPMENT ACTIVITIES IN SPACE DOSIMETRY AND SPACE WEATHER

Attila Hirn, István Apáthy, Antal Csőke, Sándor Deme, András Gerecs, Eszter Pálfalvi, József K. Pálfalvi, Tamás Pázmándi, Andrea Strádi, Julianna Szabó, Balázs Zábori

Objective

Space dosimetry and space weather activities of the research centre are concentrated in the Space Dosimetry Research Group of the Radiation Protection Department. Several dosimeter systems developed by the group operate on board the International Space Station (ISS) with the aim of providing information on the dose distribution at different locations with different shielding conditions and also personal dosimetry data during extra-vehicular activities (EVAs) and intense solar events. Maintenance, scientific and technical support during operation and upgrade of these systems are key tasks of the group. In parallel, different types of silicon detector telescope systems have been and are being developed for satellites in low Earth orbit. The objective of the development is to support space weather research and to provide dosimetry data and radiation history for spacecraft components. All these activities are realised in international cooperation.

Methods

The Pille space-qualified thermoluminescent dosimeter system, developed in the institute, provides accurate and high resolution absorbed dose data. Pille-ISS, launched in August 2003 to the Russian segment of the ISS, is operated in cooperation with the Institute for Biomedical Problems (IBMP), Moscow, as part of the service dosimetry system of the Russian Segment. The system comprises 12 dosimeters and an on-board reader. The dosimeters located in different positions are read out monthly. Two of the dosimeters are dedicated to EVAs, as well, and one dosimeter is permanently inserted in the Pille reader and read out automatically every 90 minutes (Fig. 1). For on-board stability analysis, from time to time, all dosimeters are placed on panel No. 327 for two weeks, and the quasi-homogeneous radiation field at that position is used as a natural calibration radiation source. The correction factors for the individual dosimeters are then calculated from the results of the sensitivity measurements. Although the reader is fully operational and it performs correctly without any degradation or malfunctioning, its warranty has expired and the unit will be replaced in 2018.

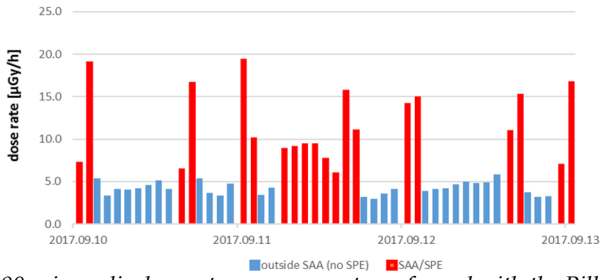

Figure 1: A 3-day sample from the 90-min cyclic dose-rate measurements performed with the Pille dosimeter A0306 on board the ISS Zvezda module. The red double peaks correspond to orbits when the ISS passed the South Atlantic Anomaly (SAA). The increase in the dose rates on 11 September 2017 is due to the September 2017 solar particle event. Accuracy of the measurements is ±10%.

The three-dimensional silicon detector telescope TRITEL was developed by the institute to measure the absorbed dose and the linear energy transfer (LET) spectrum of the space radiation to estimate the average quality factor and hence, the dose equivalent at a given position. The TRITEL-RS system operating on board the ISS includes a data handling interface unit for collection and display of measurement data and a passive detector package comprising a set of thermoluminescent and solid state nuclear track detectors. Passive detectors are also delivered to ISS to support biological experiments [1].

A modified, satellite version of TRITEL was developed to provide measurements of the radiation environment for the European Student Earth Orbiter (ESEO) mission of the European Space Agency (ESA) Education Office.

The objective of the Russian Matroshka-III (MTR-III) experiment will be to study radiation dynamics inside an anthropomorphic phantom exposed to space radiation in different ISS compartments. To estimate the effective dose to the astronauts due to heavy charged particles and secondary neutrons, the development of a silicon detector telescope, LINTEL (LINear TELescope), got underway. The method applied is the measurement of the dose equivalent due to heavy charged particles for 5 critical organs (eye lens, testis, blood forming organs, central nervous system, gastro-enteric system) based on the depth distribution of dose and LET spectra and the thermal neutron flux inside the human phantom. A specific holder is being developed to perform additional absorbed dose measurements with Pille dosimeters inside the phantom.

In the frame of the General Support Technology Programme of ESA, an instrument for measuring space radiation and magnetic field parameters (RadMag) is being developed in cooperation with the Hungarian CubeSat satellite provider C3S Ltd., Imperial College London and the Polish space industry company Astronika [2]. Simulation of the expected radiation field is performed with the Space Environment Information System (SPENVIS) for different orbits and different solar and geomagnetic conditions. In order to simulate the expected energy deposition spectra and dose rates measured with RadMag in orbit, the Geant4 for Radiation in Space (GRAS) Monte Carlo tool is used.

Results

In year 2017, approx. 6000 measurements were performed with the Pille-ISS system. The data obtained were evaluated. After a long time, the effect of a solar particle event (SPE) could be measured with Pille inside the ISS (Fig. 1). Usually, such SPEs do not produce high enough fluxes of penetrating protons that might result in significant increase in the doses measured with passive dosimeters. The new Pille Reader was handed over to the Russian partners for delivery to the ISS. The first pieces of the new type of Pille dosimeters and their universal key used for read-out were manufactured and handed over to the Russian partners for qualification tests (Fig.2).

Figure 2: The new Pille dosimeters (left: universal key and the dosimeter unit, right: the dosimeter inserted in the universal key).

The new interface unit of the TRITEL-RS system was delivered to ISS. The unit was connected to the on-board TRITEL system and successfully switched on in October 2017; the data acquisition with the instrument continued.

ESEO-TRITEL was officially accepted for delivery in June 2017 and it was made ready for the satellite-level environmental tests.

The prototype of the MTR-III Pille holder was manufactured and handed-over to the Russian partners for inspection and testing. The detector concept for LINTEL was elaborated. The LINTEL system consists of two detector heads. The detector head named LINTEL-P uses six 300-μm-thin fully depleted silicon detectors located behind aluminium absorbers of proper thicknesses and it measures the energy deposition of heavy charged particles (mainly protons and α-particles) in each detector and separately energy deposition of particles penetrating through both the gating and measuring detectors. Another detector head, named LINTEL-N, measures the flux of thermalized neutrons inside the phantom. It has two silicon detectors, one covered with a ^{10}B or ^{6}LiF layer to measure the thermal neutrons and primary charged particles, and the other one measures the primary charged particles and serves for compensation in neutron detection. The main interfaces to the phantom were also defined.

The Hungarian RADCUBE space weather microsatellite (CubeSat) project passed its first major milestone, the preliminary design review conducted by a board of space technology and space research experts set up by ESA at the European Space Research and Technology Centre (ESTEC), in the Netherlands. Requirements corresponding to the RadMag instrument and the RADCUBE satellite mission were finalized and the preliminary documentation for the manufacturing was prepared.

Remaining work

Evaluation and interpretation of the measurement data produced by the on-board Pille-ISS and TRITEL-RS dosimeter systems, as well as maintenance of the instruments will be pursued. Qualification tests of the new type of Pille dosimeters and their calibration with gamma rays and protons will be performed. Definition of the LINTEL and Pille experiments for the MTR-III phantom will be finalized and the engineering models will be manufactured and tested. The launch of the ESEO satellite is due in December 2018. The research group will be actively involved in the final satellite-level environment tests, in the commissioning of the ESEO-TRITEL instrument and they will be responsible for the analysis and evaluation of measurement data received from TRITEL during the ESEO mission. The detailed engineering plans of the RadMag space weather instrument will be prepared. An elegant breadboard, an engineering and qualification and a flight model will be manufactured, which will be subjected to thorough qualification and acceptance tests. In addition, another important task is the full calibration of the instrument with radioactive sources and energetic particle accelerators.

Acknowledgements

The authors wish to acknowledge the precious help provided by the colleagues at IBMP and S. P. Korolev, Rocket and Space Corporation Energia. Maintenance and development activities performed in the frame of Russian-Hungarian space cooperation in 2017 were funded by the Government of Hungary, through contract number IKF/694/2017-NFM_SZERZ. The ESEO-TRITEL project was funded through the PECS contract No. 4000112065/14/NL/NDe. The study phase of the development of the RadMag instrument was performed in the frame of the ESA, contract No. 4000117620/16/NL/LF/as. The implementation phase of the project is funded in the frame of the ESA, contract No. 4000120860/17/NL/GLC/as through the subcontract No. 20170630_RCU_MTA_EK_SubCo_i1.0.

Related publications

[1] A. Strádi, J. Szabó, K. O. Inozemtsev, V. V. Kushin, R. V. Tolochek, V. A. Shurshakov, I. B. Alchinovad and M. Yu. Karganov: *Comparative Radiation Measurements in the Russian Segment of the International Space Station by Applying Passive Dosimeters*, Radiation Measurements **106**, 267 (2017)

[2] A. Hirn and B. Zábori: *RadMag – Űridőjárási célú hazai technológia fejlesztés*, Természettud. Közlöny **148(**10), 455 (2017)

PREPARATION OF STANDARD OPERATING PROCEDURES FOR THE OFFICIAL TASKS OF MTA EK CONNECTED TO THE GOVERNMENTAL DECREE 490/2015 (XII.30.)

Éva Kovács-Széles, Csilla Csöme

Objective

In the frame of the Governmental Decree 490/2015 (XII.30.), MTA EK is responsible for the collection of found, lost or confiscated unknown nuclear materials at radiological scenes (e.g. crime scenes), as well as nuclear forensics analysis of these materials. MTA EK has a mobile laboratory and an associated Mobile Expert Support Team (MEST) to perform the tasks of material collection and first in-field categorization. This report focuses on the regulation of MEST's work through the use of different standard operating procedures.

Results

A Conceptional Operation document (ConOps – a kind of manual) was written about the activities of MEST and all the connected needful tasks and requirements. The following topics are described and regulated in the document:

- Standard Operating Procedures (SOP) for Remote alarm assessment
- SOP for On-site alarm assessment
- SOP for Detection Equipment (for all equipment in use)
- SOP for Maintenance of Detection Equipment (for all equipment in use)
- SOP for Necessary tools for sample collection (preparedness package)
- SOP for How to use safety tools/clothing (how to dress up)
- SOP for Roles and Tasks of MEST members
- SOP for Chain-of Custody of collected samples at the Forensic Laboratory (QA/QC)
- SOP for Transportation of the samples
- SOP for Communications
- SOP for Reporting/Notification
- SOP for Exercises

All the documents contain a full description about procedures and requirements for field work. The aim of the ConOps is to help in the training of new members in the team. It also serves to keep permanent MEST members in an up-to-date, trained and experienced condition using various exercises. Figure 1. shows a picture about MEST during field work (collection of unknown radioactive materials at a radiological scene).

Figure 1: In-field operation of the MEST

Remaining work

The next step in this work is to establish a training facility (training and exercise site) with different layouts and possibilities for in-field tests and trainings for law enforcement officers using different scenarios for radiological source recovery.

ASSESSMENT OF CAPABILITIES OF PORTABLE LIBS FOR IMPURITY CONTENT DETERMINATION IN URANIUM BEARING MATERIALS

Éva Kovács-Széles

Objective

As part of the Hungarian Safeguards Support Programme (SP) to the International Atomic Energy Agency, a SP Task (number HUN A2282/17/TND-001) was started with the title and topic of "Assessment of Capabilities of Portable LIBS for Impurity Content Determination in Uranium Bearing Materials". This task supports extending the knowledge and providing of experimental data concerning the analytical capabilities of the promising emerging Laser Induced Breakdown Spectroscopy (LIBS) technology for use in the analysis of the purity of nuclear materials, which can be used for identification of these materials and their origin for safeguards purposes.

Methods

For this task, the portable LIBScan25+ type Laser Induced Breakdown Spectrometer (LIBS) of the MTA EK produced by Applied Photonics Ltd. was used. It contains a 50 mJ Nd:YAG laser and an SSD (solid-state drive) specific optical system.

Results

During this work, once closed laser ablation chambers were designed and fabricated for the field-deployable LIBS analysis of active samples. It is essential to use these chambers for dangerous materials, but the optimization of the structure of the chambers is also a key part for adequate LIBS analysis. Figure 1 shows one of these chambers.

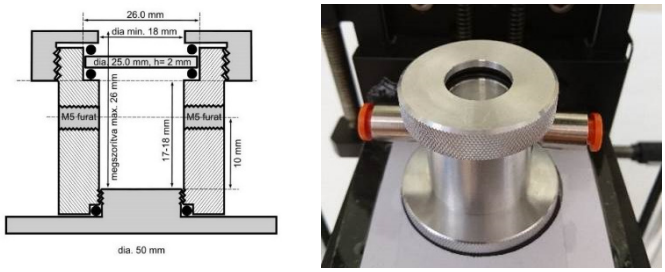

Figure 1: Closed ablation chamber for in-field LIBS measurements

Another part of the work was to perform laboratory experiments using the ablation chamber, the LIBScan 25+ and UO_2 samples available at the MTA EK with the objective of optimizing LIBS measurement conditions to obtain the best analytical performance.

A calibration curve for Zn is shown in Figure 2.

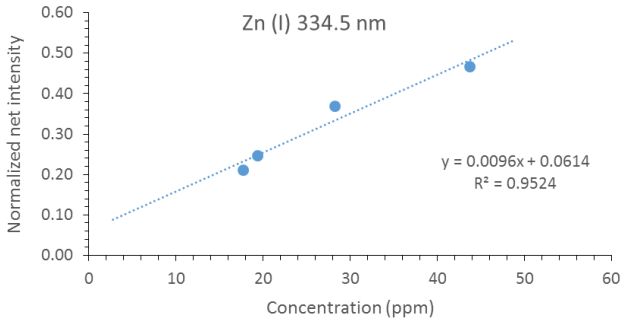

Figure 2: Calibration curve for quantitative analysis by portable LIBS system

The calibration curve clearly indicates the potential for quantitative measurements. In the case of Zn, the limit of detection obtained was 15.6 ppm by the three sigma criteria.

Remaining work

Next steps of the work are the preparation or acquisition of calibration standards for the impurities of interest with a wide range of concentration to perform real measurements. Another aim is to perform quantitative experiments to assess the analytical performance (e.g. limit of quantification, dynamic range, accuracy, repeatability) of the method using several UO_2 samples available at the MTA EK, including reference measurements of the samples by ICP-MS after acid dissolution.

ANALYSIS OF SEALED RADIOACTIVE SOURCES FOR NUCLEAR FORENSICS PURPOSES

Éva Kovács-Széles, András Kocsonya

Objective

The increasing risk of terror attacks using radioactive materials and the support of effective countermeasures against them increases the importance of nuclear forensics. International trends show that not only nuclear materials but even other radioactive materials (e.g. shielded sources) can be used in a possible attack. Due to stricter worldwide regulations of nuclear materials as compared to radioactive materials, which also have got wider application possibilities, their chances for getting out of regulatory control is definitely higher. Therefore, effective methods are necessary for analysis and identification of lost, found, seized, smuggled or other radioactive sources of unknown origin. Since the KFKI campus has several decades' history in the application of artificial radioactive sources, a rather wide variety of sources are available for examination or testing purposes. Due to their wide usage and versatile forms and, moreover, their radiation security aspects, a survey has been started on sealed radioactive sources to identify key nuclear forensics signatures for origin assessment.

Methods

The methods used are based on the standard methods of nuclear forensics, if applicable for sealed sources, with the necessary modifications. Physical characterisation (as a key component) of sealed sources describes the construction, geometric sizes, shape, mass, labels of the sources, and can be determined by visual inspection and by measurements. Since the majority of these data are also available from datasheets and in the registry, a direct comparison is possible to these records. A comprehensive database of this type of data is planned, even on a countrywide level.

The analysis of contaminant radionuclides is a specific application of a widely used method in several analytical areas. The common or different origin of samples is indicated by similarities and differences of elemental, structural, compositional, etc. characteristics of the samples. Since alpha- and beta-decays are often accompanied by gamma-emission, gamma-spectrometry is a powerful analytical technique for identification and quantification of contaminants with the limitation that pure alpha- or beta-emitters cannot be detected. Two high purity germanium gamma-spectrometers were used in the experiments: a high efficiency detector (Canberra GCW6023) located in a well shielded chamber for the measurement of calibration sources and a medium efficiency detector (Canberra BE2825) for the industrial sources. Measurement time was typically 3-4 days/source.

Results

Age (production date) of a source or any radiological material is a key signature in nuclear forensics for origin assessment (to identify or even exclude producers). Therefore, during this work, age dating of sealed radioactive sources was one of the key tasks. E.g. the age of plutonium-beryllium neutron sources (based on the ^{241}Pu (T1/2=14.35 y) → ^{241}Am (T1/2=432 y) reaction) was determined. Another dating possibility is consecutive decay in case of similar half-lives, e.g. the case of ^{95}Zr (64 days) → ^{95}Nb (35 days). Besides, the relative absence of a short(er) half-life daughter radionuclides indicates that the sample is relatively „young". More different sources were analysed using this method.

Two main categories of sealed sources were examined: 1. Calibration standard sources produced typically in the kBq to a few hundred kBq activity range and are typically certified by National Metrology Authorities. These sources are used for detector calibration. Since this is an „analytic" activity, the relatively good radioanalytical purity is a characteristic of these sources and can be an effective tool for the establishment of standard methods and comparative assessment. One other investigated category was the much stronger industrial sources: several ^{60}Co, ^{137}Cs and ^{192}Ir sources were measured. These sources are produced even in TBq activity. The rather high specific activity allows small geometry sizes which is essential for sharp imaging. Since minor impurities are not important for their intended use, the required radioanalytical purity is moderated.

Concerning industrial sources, several ^{192}Ir sources produced by the Hungarian Institute of Isotopes Ltd. Co. (situated on the common KFKI Campus with our institute) were examined. All of them contained ^{60}Co as a contaminant. Two pairs can be selected from the sources with similar ^{60}Co/^{192}Ir ratio, for which the same production series can be supposed. The production technology for these sources on our Campus is under investigation to find the source of ^{60}Co-contaminant.

Remaining work

We will continue the analysis of a wide range of sealed radioactive sources of MTA EK using gamma-spectrometry to build a database for statistical evaluation. The work will also focus on neutron sources such as Cf and PuBe.

EXTENSION OF THE NATIONAL NUCLEAR FORENSICS LIBRARY SYSTEM WITH AVAILABLE TECHNOLOGICAL INFORMATION FROM THE NUCLEAR FUEL CYCLE

Éva Kovács-Széles

Objective

Nuclear and other radioactive materials were smuggled across Europe following the collapse of the former Soviet Union. Illicit trafficking of nuclear and other radioactive material is a subject of serious concern due to the radiological hazard to the public and the environment as well as the security risks associated with nuclear and other radioactive material out of regulatory control. Nuclear forensic science was born to examine these materials, and combines techniques of nuclear and material sciences. The most important aim of these investigations is to determine the specific "signatures" which characterize the unknown material, and which can possibly reveal the origin of the sample. Our experience indicates that it is difficult to determine the origin and history of unknown samples without comparison to data from known samples to facilitate the identification. To increase confidence in determining the origin and history of questioned materials, an analysis of many comparison samples with different origins is necessary. Another necessary element is the development by States of a National Nuclear Forensics Library (NNFL) to aid in national level comparisons of material out of regulatory control. The first prototype of the NNFL was established in Hungary in 2016. However, for more effective origin assessment it is essential to know production technologies in the nuclear fuel cycle. Therefore, our goal was to collect them.

Results

During this work the available technological information from the nuclear fuel cycle was collected from the open literature and using databases of such huge Scientific Centres as Halden. The following parameters and information can be collected during the literature and database study: typical physical characteristics of fuel pellets made by different producers (size, density, shape, form, composition, outlooks, special parameters like holes or edges) following the production trends in the time. Other specific parameters are the pore size and dispersion. They depend on production technologies (indicating theproducers) and the date of the production (pore size has decreased in the last 2 decades). This parameter was typically changed in the last 1-2 decades and by producers in both Russia and Western Europe. A third parameter is the different elemental impurities given by the producers and added directly to the UO_2 powder by the producer, respectively. An example is the Gd or Eu, which are used as reactor poisons. Russian producers are typically using Gd in the production technology.

In Figure 1 we show an example of the data in a diagram about the distribution of pore diameters versus porosity of PWR and WWER fuel pellets.

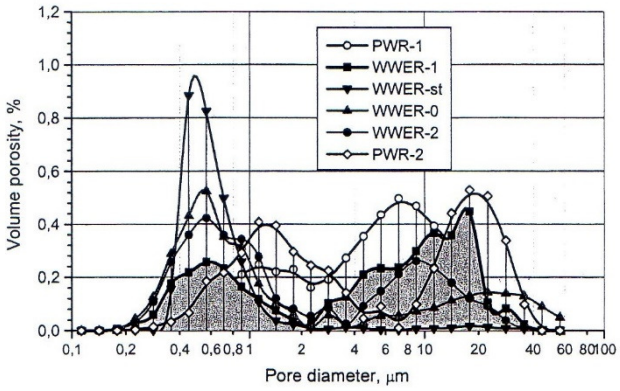

Figure 1: Distribution of pore diameter versus porosity of PWR and WWER fuel pellets

Remaining work

Extension of the NNFL system with more data originating ed from home-use fuel materials (e.g. in Paks Nuclear Power Plant), as well as confiscated nuclear samples for better statistical evaluation is in progress.

CONTRIBUTIONS TO EUROPEAN RADIATION PROTECTION RESEARCH

Andor Andrási, András Kocsonya, Balázs Madas, Anna Pántya, Tamás Pázmándi, Csilla Rudas, Péter Szántó, Péter Zagyvai

Objective

Researchers of MTA EK have been contributing to different projects in European Radiation Protection Research including the CONCERT (European Joint Programme for the Integration of Radiation Protection Research), CAThyMARA (Child and Adult Thyroid Monitoring After Reactor Accident), and CONFIDENCE (COping with uNcertainties For Improved modelling and DEcision making in Nuclear emergenCiEs) projects. In CONCERT, one of our main tasks in 2017 was to identify the current state of datasharing amongst researchers in radiation protection research, and to identify barriers to effective sharing. The general objective of the CAThyMARA project was to improve the capabilities of institutions participating in the response actions during major nuclear emergencies in terms of individual dose exposure monitoring. The rapid determination of uptake of radioiodine in human thyroid glands together with its estimated dose consequence were defined as the main objectives of this European cooperation that lasted 18 months. The objective of the research for the first work package of the CONFIDENCE project was to quantify the uncertainties of atmospheric dispersion calculations, to investigate their effect on the result of a radiological release and to explore methods for their reduction.

Methods

In CONCERT, an electronic survey was prepared, including questions on the providing of post-publication data, on institutional, funding agency, and journal policies, and on awareness of datasharing infrastructures, attitudinal barriers, and technical support. The survey was sent to the members of a mailing list maintained by the CONCERT project funded by the European Commission.

In CAThyMARA, seven work packages were organized; researchers of MTA EK participated in four of them. Two intercomparison runs for determining the radioiodine (mostly ^{131}I) content of the thyroid glands were organized for spectroscopic and rapid non-spectroscopic screening devices, respectively. Mock radioactive sources (containing ^{133}Ba) representing three human age groups were distributed. Monte Carlo calculations were performed in order to modify the calibration factors of measuring (screening) devices for the special requirements of measuring infants and children in the age groups most vulnerable to radioiodine uptake.

In the first year of the three-year-long CONFIDENCE project, the analysis and ranking of the different sources of uncertainties were conducted. Along with the uncertainties of the input meteorological data, the model and source term uncertainties were examined. Concerning the meteorological data, the effects of using an ensemble meteorological forecast or meteorological measurements were analysed. The uncertainties related to the radiological release source term were evaluated and the most influential variables were identified. The uncertainties of the model-specific input variables were also investigated through an extensive literature review, and respective ranges and distributions of the input parameters were determined.

Results

In the CONCERT survey on data management, responses identified that the radiation protection community shared similar concerns with other groups canvassed in earlier studies; the perceived negative impact of datasharing on competitiveness, career development and reputation, along with concern about the costs of data management. More surprising was the lack of awareness of existing datasharing platforms. (See Fig. 1, below.) We find that there is a clear need for education and training in data management and for a significant programme of improving awareness of Open Data issues [1].

In CAThyMARA, participants published several deliverables (ten different guidelines and public reports) on the results of intercomparisons, modelling calculations and – most of all – dose estimations for different age groups making use of revised and re-evaluated uptake and excretion mechanisms of radioiodine species characteristic for the releases of major nuclear accidents. Newly obtained and approved data of model calculations on "dose per content" factors were also included in the respective guidelines, thus providing an excellent practical compilation for crucial and rapid medical response during the urgent and early phases of a major nuclear emergency. The overall availability of the guidelines and reports is implemented by appropriate scientific data sources of the European Union.

In CONFIDENCE, the assessment of meteorological ensembles revealed that these data can provide information on meteorological uncertainties. There are meteorological parameters used in atmospheric dispersion modelling for which the uncertainties are described well in the ensemble data (e.g. wind speed, precipitation) but there are some parameters for which the uncertainties are not captured well in an ensemble (e.g. planetary boundary layer height). With the usage of such ensemble meteorological data, the time and spatial scale needs to be selected carefully since, for example, global ensembles may not reflect local effects. The meteorological measurements and observations can be used to reduce the uncertainty of weather forecasts. The data assimilation of meteorological measurements, that is, the combination of observations with the pre-processing of the weather forecast data appears to improve the quality of the resulting meteorological predictions. The most important uncertain variables of the source term are the timing, position, quantity, isotopic composition and energy of the release. Of these, the timing and the quantity of the release has the largest impact on the results of the atmospheric dispersion

calculation. Based on a comprehensive literature review the most influential model parameters of the atmospheric dispersion calculation were found to be the source term and the wind direction. Other significant parameters, which can have a large effect on the atmospheric dispersion calculation, in some circumstances, are the plume rise, the release height, wind speed, and the release timing. The uncertainty ranges and probability distributions of the model parameters were determined for the turbulent diffusion, the dry and wet deposition, and the surface roughness.

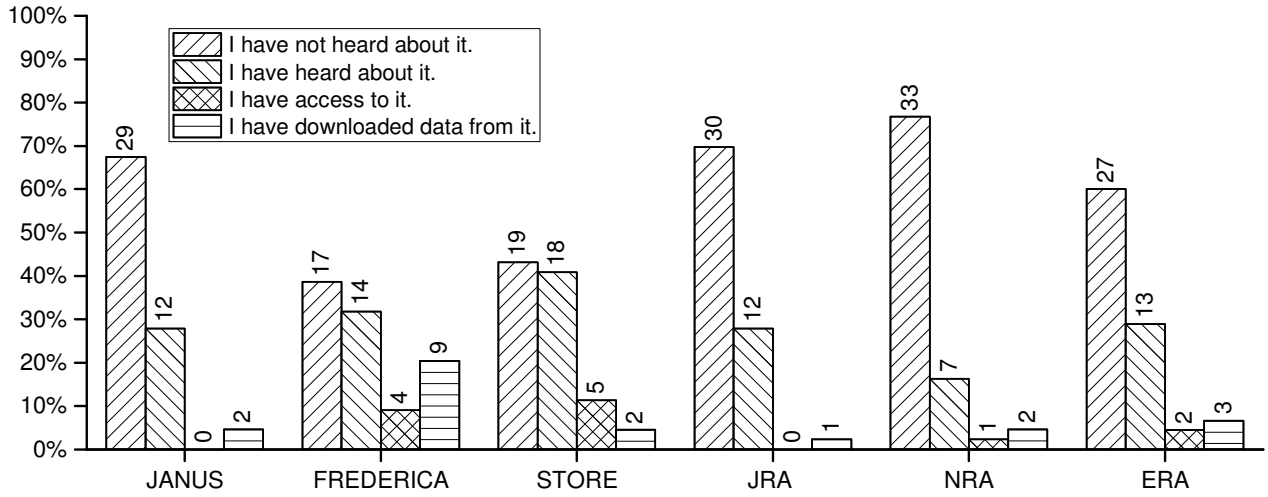

Figure 1: Awareness of extensively reported databases in radiation biology: JANUS - Janus Tissue Archive, FREDERICA - Radiation Effects Database, STORE - Sustaining access to Tissues and data from Radiobiological Experiments, JRA - Japanese Radiobiology Archives, NRA - National Radiobiology Archives, ERA - European Radiobiology Archives.

Remaining work

In CAThyMARA, the outcome and score of the measurements performed with the thyroid-counting device of the Environmental [Health Physics] Service of the Centre for Energy Research is to be utilized in improving the accuracy and precision of the respective analysis. Dose estimation procedures will be further revised in terms of the thyroid uptake and exposure models presented and analysed in work package 6 in order to provide a more accurate dose estimation for all members of the population involved in an emergency. The outcomes will be compared and adjusted to the recent IAEA (International Atomic Energy Agency) recommendations on public protective actions during a nuclear emergency.

Based on the uncertainty evaluations, the input and model parameters used for the atmospheric dispersion calculations will be selected in CONFIDENCE. The calculated release scenarios will be simulated with different input data ranges, representing the uncertainties, to investigate the effects caused in the results of the atmospheric dispersion and the decisions relying on those results. In the following two years of the project, the calculations to determine the effect of different uncertainties will be conducted and the results will be analysed.

Reference

[1] B. G. Madas and P. N. Schofield: *Survey on data management in radiation protection research*, Radiation Protection Dosimetry (submitted), doi: 10.1093/rpd/ncy250

IV. ENERGY AND ENVIRONMENTAL STUDIES

WORKING FLUIDS

Attila R. Imre

Objective

Utilization of geothermal energy is one of the top goals for the Hungarian energy sector. Due to the relatively low temperature for geothermal fluids, the traditional Rankine cycle cannot be used to transform thermal energy to electrical energy. Novel methods – like the Organic Rankine Cycle, ORC – should be used with novel working fluids. For the optimal working fluid selection, one should know the relevant properties of potential working fluids. Basic thermodynamic processes and cycles should be also studied for efficiency maximization.

In a parallel study, the limit of stretching/overheating for various fluids was studied by molecular dynamics; the results can be used for safety calculations.

In the third part, the properties of supercritical methane relevant for Compressed Natural Gas (CNG) application were studied.

Methods

Analytical methods, special computer codes – written for our purpose – and some commercial codes and databases (ThermoC, NIST Webbook) were used for the calculations.

Results

ORC working fluids are traditionally classified as dry, wet or isentropic. Adiabatically expanding them from a saturated vapour phase, dry fluids go to the dry, overheated vapour region, wet fluids expand to the mixed liquid-vapour region while isentropic fluids remain in a saturated vapour state. The transitions between these classes for homologous series are smooth and – using some simple fluid model, like van der Waals fluid – are governed by the molecular degrees of freedom and by the isochoric heat capacity [1].

Although the wet/dry/isentropic classification seems to be good, it does not help us to find a proper working fluid for a given heat source. For this purpose, a novel classification method was developed, using the specific point of the temperature-entropy diagram of the fluids [2].

Although for normal thermodynamic cycles, fluids are always in their stable phases, under some accidental conditions the pressure drop can turn the stable liquid into a metastable one. Metastable liquids have a tendency to relax by explosion-like boiling, causing damage to the equipment. To avoid this problem, the limits of metastability and stability and the properties of fluids in their metastable states should be known. Stability limits of argon and water were determined from their interfacial properties [3]. For water, some experimental results suggest an anomalous region within the metastable region. To describe this region, a novel equation of state should be developed for water. As a first step, a quintic equation state was developed to describe the anomaly in a qualitative manner [4].

Compressed natural gas (CNG) – containing mainly methane - is a potential fuel for cars. Supercritical anomalies (like the maxima of compressibility and heat capacity, the inflection point for the density, and the minimum of the speed of sound) were determined for methane in the temperature-pressure range relevant for CNG-applications [5].

Remaining work

Application of the novel ORC-classification for other thermodynamic cycles is in progress. A description of the transition for more realistic fluids should be developed. For metastable water, the novel equation of state should be not qualitative, but rather quantitative. For methane, the filling process should be optimized to avoid the speed of sound minimum.

Related publications

[1] A. Groniewsky, G. Györke, A. R. Imre: *Description of wet-to-dry transition in model ORC working fluids*, Applied Thermal Engineering **125**, 963–971 (2017)

[2] G. Györke, U. K. Deiters, A. Groniewsky, I. Lassu, A. R. Imre: *Novel Classification of Pure Working Fluids for Organic Rankine Cycle*, Energy **145:** 288-300 (2018)

[3] M. Sega, B. Fábián, A. R. Imre, P. Jedlovszky: *Relation Between the Liquid Spinodal Pressure and the Lateral Pressure Profile at the Liquid-Vapour Interface*, Journal of Physical Chemistry C **121**, 12214-12219 (2017)

[4] A. R. Imre, A. Groniewsky, G. Györke: *Description of the metastable liquid region with quintic and quasi-quintic equation of states*, Interfacial Phenomena and Heat Transfer (submitted, invited paper)

[5] A. Katona, A. R. Imre: *Supercritical fluids in energy storage and consumption*, IEEE Xplore (IYCE'17), 2017 6th International Youth Conference on Energy, 21-24 June 2017, Budapest, Hungary, eISBN: 978-1-5090-6409-0, DOI: 10.1109/IYCE.2017.8003737 (2017)

ELECTROCATALYSTS FOR WATER SPLITTING

József S. Pap, Dávid Lukács, Tamás Ollár, Levente Tapasztó, Antal Koós, Dávid F. Srankó, Zsolt G. Kerner

Objective

Our main scientific goal remained unfolding the structure-reactivity correlations in electrocatalysts designed for the splitting of water. Special attention was paid to collecting experimental evidence on the mechanism of the key steps in the oxygen evolving reaction. The development of new materials for the hydrogen evolving half-cell reaction (HER) has been also among our goals. Beside the in-house finance, the full project gained support in the framework of the VEKOP 2.3.2-16-2016-00011 "Strategic research group for the challenges of renewable energy based power systems" project from July 2017.

Methods

Peptide synthesis by an improved solid phase method, moreover potentiometry, molecular spectroscopy (UV-visible, circular dichroism and X-band electron paramagnetic resonance - EPR) and electrospray ionisation mass spectrometry (ESI-MS) analysis were done by collaborators abroad. Simulation of the EPR spectra, electrocatalysis studies by cyclic voltammetry (CV), square wave voltammetry (SWV) or controlled potential electrolysis (CPE), and dioxygen evolution monitored by an optical probe were all done in our laboratories. Surface-adhesion of the compounds was investigated by X-ray photoelectron spectroscopy (XPS).

Results

In the field of molecular catalysis of the oxygen evolving reaction (OER) two papers were published. In the first one we discussed the crucial role of the carboxylate group of aspartic acid (Asp) building units for metal coordination and OER catalysis. The effect of Asp in the new branched peptides H-Gly-Dap(H-Gly)-Asp-NH_2 (2GD, Dap = 2,3-diaminopropionic acid), 3D (H-Asp-Dap(H-Asp)-Asp-NH_2) and 2DG (H-Asp-Dap(H-Asp)-Gly-NH_2) has been investigated. The ligand 2GD, at increasingly alkaline pH furnishes a single-site catalyst with Cu and the Asp at the C-terminus creates a $\{NH_2, N^-,N^-,O^-\}_{eq}$ set. The changes in speciation with pH accompanied by shifts in the $Cu^{III/II}$ redox potential allowed the calculation of the pK_a values for the Cu^{II} and Cu^{III} forms. The 2GD complex exhibits electrocatalytic activity in the OER in phosphate buffer. However, when Asp residues are present at every termini in 3D, the activity in OER decreases and, if present only at the N-termini in 2DG, the OER ceases. As for Cu^{II} ligated by 2GD, a turnover frequency (TOF) of ~16 s^{-1} was calculated at pH = 11 in 0.2 M phosphate electrolyte, which is crucial for catalysis, but also acts as inhibitor anion according to CV. The system is highly tolerant to the presence of chloride, which is a feature of practical importance in efficient water oxidation catalysis. In a review paper the copper binding abilities of homodetic cyclic peptides (CPs) with histidine (His) moieties has been summarized. This group of ligands is characterized by a cyclic ring composed only of amino acids. It has been highlighted that the application of cyclic peptides should be fruitful in electrocatalysis because of their special structures, stability and resistance against degradation. The cyclic structure promotes the anchoring of metal ions by the amino acid side chains. The impact of peptide cyclization and ring size on the binding abilities toward copper(II) has been reviewed. We also compared the coordinating properties of ligands containing a different number of His residues with His_4-cyclopeptides. The sustainability and stability of nN_{Im} (n = 1–4) complexes depending on the Asp residue in the peptide sequence were also discussed along with the aspects of forming dinuclear copper(II) complexes by cyclopeptides with two separated proline residues in the sequence, since such structures are highly desirable in OER catalysis. We advocated using metallo-cyclopeptides for they enrich the spectrum of available activities or change the properties of these ligands.

In addition to the papers, three invited lectures were given in Hungary and in China. The VEKOP 2.3.2-16-2016-00011 project provides financial support for this research in the upcoming 3,5 years.

On the results of the HER catalysis one manuscript has been submitted. We demonstrated the atomically perfect reduction of the 2D $MoS_{2-x}O_x$ crystals to the pure 2D MoS_2 parent phase by a simple annealing step in an H_2S atmosphere. Significantly enhanced catalytic activity in HER could be observed for the 2D $MoS_{2-x}O_x$ as compared to its pure 2D MoS_2 form. The single oxygen atom substitution sites were identified as the catalytically active sites. Activating the basal plane of MoS_2 is of key importance in developing efficient 2D electrocatalysts.

Remaining work

We wish to continue the above studies of electrocatalytic OER with branched and cyclic peptides: exploring new single site catalysts, characterize 1st gen. pseudo-metallodendrimers and initiate fundamental studies on electrochemical optical waveguide lightmode spectroscopy (EC-OWLS) already in the framework of VEKOP 2.3.2-16-2016-00011 project.

Related publications

[1] Ł. Szyrwiel, D. Lukács, D. F. Srankó, Z. Kerner, A. Kotynia, J. Brasuń, B. Setner, Z. Szewczuk, K. Malec and J. S. Pap: *Armed by Asp? C-terminal carboxylate in a Dap-branched peptide and consequences in the binding of Cu^{II} and electrocatalytic water oxidation*, RSC Adv. **7**, 24657 (2017).

[2] Kotynia, J. S. Pap, J. Brasuń: *The binding abilities of homodetic cyclic His-peptides toward copper ions*, Inorg. Chim. Acta (2017) https://doi.org/10.1016/j.ica.2017.07.028.

[3] J. Pető, T. Ollár, P. Vancsó, Z. I. Popov, G. Z. Magda, G. Dobrik, C. Hwang, P. B. Sorokin and L. Tapasztó: Spontaneous doping of 2D MoS2 basal plane by oxygen substitution during ambient exposure (manuscript submitted)

HIGHLY EFFECTIVE DRY REFORMING ON SODIUM OR INDIUM PROMOTED NICKEL CATALYSTS

Ferenc Somodi, Miklós Németh, Johanna Károlyi, György Sáfrán, Anita Horváth

Objective

The selective conversion of methane with carbon dioxide yields hydrogen and carbon monoxide as reaction products in an equimolar ratio (dry reforming, DRM: $CH_4+CO_2 \rightleftharpoons 2CO+2H_2$). In the present project we aimed to accomplish the following main tasks: 1) development of highly active and stable, noble-metal-free Ni-based catalysts that work under realistic conditions using a model biogas, 2) investigation of the reaction steps with labeled reactants, 3) determination of the coke structure and its formation routes on each catalyst system and finally, 4) building new experimental setups that allow the in-depth characterization to provide feedback for the next catalyst generation.

Methods

Development of a carbon tolerant nickel catalyst for DRM was achieved by alloying Ni with In or Pt or by controlled promotion of the support with a minute amount of Na_2O. A modified impregnation method, sol adsorption and deposition precipitation techniques were used for sample preparation. Structural investigations were carried out by X-ray powder diffraction (XRD), X-ray Photoelectron Spectroscopy (XPS), Transmission Electron Microscopy (TEM) and high-angle annular darkfield (HAADF) STEM for elemental mapping. Reducibility of calcined samples was studied by Temperature Programmed Reduction (TPR) experiments. Metal dispersion was measured by CO pulse chemisorption. Temperature programmed desorption of chemisorbed CO and other species was followed by QMS (Quadrupole mass spectrometer). Diffuse Reflectance Infrared Fourier Transform Spectroscopy (DRIFTS) was applied to detect the surface-adsorbed species in the presence of CO, CO_2 or a dry reforming mixture at atmospheric or under reduced pressure applying a home-made vacuum system attached to the DRIFTS cell. Temperature-programmed or isothermal dry reforming experiments were done i) in a plug flow reactor in excess methane or ii) in a closed loop circulation system using labeled $^{13}CO_2$. Subsequent temperature programed oxidation (TPO) measurements were carried out to compare the reactivity of the deposited carbon. Steady State Transient Kinetic Analysis (SSITKA) was done for the first time in our laboratory on two chosen samples to determine the residence time of intermediates leading to CO product.

Results

Concerning the Na-promoted systems, $^{13}CO_2$-labeled DRM experiments revealed that surface methanation of $^{13}CO_2$ to form some $^{13}CH_4$ occurs only when there is a significant shortage of oxygen/oxidants, although abundant H_2 is available, contrary to the unpromoted catalyst. The same was ascertained in our preliminary SSITKA experiments. However, the residence time of intermediates leading to the CO product was found to be double on the Na_2O-promoted catalyst. Our results proved that we could exploit the high temperature reversible CO_2 capture ability of Na_2ZrO_3 phase (reported in the literature) at nanoscale, which must play a decisive role in the removal of surface coke at the extended Na_2O-ZrO_2-Ni/NiO_xH_y interface via the formation and decomposition of transient carbonates. The coking tendency can be tuned by the decrease of Ni loading at the expense of catalytic activity. The effect of sodium in the case of a well dispersed Pt/ZrO_2 catalyst played a role in hindering inactive carbon formation (as in the case of nickel catalysts), but the activity of Pt was not changed. Alloying Ni with 15%Pt led to a significant activity increase only for the catalyst prepared by impregnation without Na_2O, while coke deposition increased on all bimetallic samples compared to the monometallic counterparts. We speculate that as NiPt particles are easier to reduce, Ni stays fully metallic and accumulates more carbon from CH_4 decomposition (no possibility of NiO_xH_y formation during the reaction).

Concerning the In-promoted system, it was shown that the presence of 2 wt% indium on the surface of a 3 wt%Ni/SiO_2 catalyst prevented coke formation during dry reforming of methane. TPR results pointed out that indium was unstable against sintering without nickel on the silica surface. However, in the bimetallic catalyst it was in metallic state and mixed with nickel after reduction at 700 °C. The presence and uniform distribution of NiIn and Ni2In alloy nanoparticles after reduction at 700 °C of the calcined catalyst was determined by HAADF-STEM, high-resolution transmission electron microscopy (HRTEM) and energy-dispersive X-ray spectroscopy (EDX) analysis. The average particle size of the bimetallic sample was slightly smaller than that of the monometallic catalyst after 24 h time on stream. Based on the presented results, the higher catalytic activity and outstanding carbon tolerance of the bimetallic Ni–In/SiO_2 catalyst is the consequence of structural and electronic effects of indium.

Remaining work

The project will be continued according to the on-going EK 161 project and a new proposal on dry reforming and the related CO_2 utilization routes will be submitted next year. The large amount of unpublished results will be published as well.

Related publications

[1] Y. Lou, M. Steib, Q. Zhang, K. Tiefenbacher, A. Horváth, A. Jentys, Y. Liu and J. A. Lercher: *Design of stable Ni/ZrO_2 catalysts for dry reforming of methane*, Journal of Catalysis **356**, 147 (2017)

[2] J. Károlyi, M. Németh, C. Evangelisti, G. Sáfrán, Z. Schay, A. Horváth and F. Somodi*: Carbon dioxide reforming of methane over Ni-In/SiO_2 catalyst without coke formation*, Journal of Industrial and Engineering Chemistry DOI: 10.1016/j.jiec.2017.09.024, (2017)

[3] M. Németh, D. Srankó, J. Károlyi, F. Somodi, Z. Schay, G. Sáfrán, I. Sajó and A. Horváth: *Na-promoted Ni/ZrO_2 dry reforming catalyst with high efficiency: details of Na_2O–ZrO_2–Ni interaction controlling activity and coke formation*, Catalysis Science and Technology **7**, 5386 (2017)

[4] A. Horváth, F. Somodi, J. Károlyi, D. Srankó, M. Németh and G. Sáfrán: *Low temperature dry reforming of methane over Ni/ZrO2 catalysts: details of the beneficial sodium promotion*, 13th European Congress on Catalysis, poster #P3.115, Florence, 27-31 August, (2017)

[5] F. Somodi, J. Károlyi, M. Németh and A. Horváth: *Dry reforming of methane without coke formation over indium promoted Ni/SiO2 catalysts*, 13th European Congress on Catalysis, poster #P3.78 Florence, 27-31 August (2017)

[6] Co-operating research groups's leaders: J. A. Lercher (Technical University of Munich), G. Rupprechter (Technical University of Vienna) and A. Horváth (FKKL): *Final scientific report of OTKA-EraChemistry NN 107170 project entitled Dry reforming – from understanding the elementary steps to better catalysts* (2017)

RADIOACTIVE LANTHANIDE AND AM DETERMINATION IN LIQUID NUCLEAR WASTE USING EXTRACTION CHROMATOGRAPHY

Dénes Párkányi, László Szentmiklósi

Objective

An easy-to-apply extraction chromatography separation method was developed with DGA (a diglycolamine derivative) resin. The goal was to determine the concentration of difficult-to-measure lanthanide and trivalent actinide nuclides (DMNs) in nuclear waste. These nuclides are usually present in low quantities and they are often pure alpha/beta emitters.

Methods

The separation of lanthanides and trivalent actinides from the main activity of nuclear waste (e.g. Co-60, Cs-134, Cs-137, Ag-110m, Sb-125) was carried out by a co-precipitation step using 5M hydrofluoric acid with La carrier. It is known that lanthanides and trivalent actinides form very insoluble precipitate with fluoride ions. The raw liquid waste was quasi-evaporated and digested with concentrated HNO_3; about 1 kBq of Tb-160 radiotracer was mixed with the sample to indicate the elemental recovery of lanthanides. Therefore, the samples were diluted with 1 M HCl to 200 ml and 60 ml 40% HF together with ~1mg inactive La carrier (1 ml of 1 mg/ml $La(NO_3)_3$ solution) was added to this solution (experience shows it helps the co-precipitation of lanthanides). The mixtures were stirred overnight. After filtration (using a 0.2 µm pore size membrane) the precipitate could be dissolved in 20 ml 3M HNO_3 and 0.5 g H_3BO_3. Activity measurement of the Tb-160 determined the total elemental recovery of lanthanides and trivalent actinides throughout these steps.

The extraction chromatography equipment was a jacketed glass column of 280 mm length and 2.5 mm diameter, filled with about 0.6 g DGA resin. A peristaltic pump was used to flow the solvents through the resin bed. The column was heated with 40°C water flow to maintain a constant and well-regulated temperature. During the elution, fractions were collected with a homemade computer-controlled fraction collector. DGA binding was achieved always from 3 M HNO_3 containing media. The 20 ml load solution was loaded to the column bed with a peristaltic pump at a 0.2-0.4 ml/min flow rate. 1.5 M HCl was found to be the most suitable eluent at a flow rate of 0.1 ml/min. In order to stop the Pu leaking (to keep the Pu oxidation state over +3) 0.03 M $NaNO_2$ was added to the 1.5M HCl eluent.

Certain nuclides (i.e.: Eu-154, Eu-155 and Am-241) emit gamma radiation, but they had only low activities in the investigated samples, therefore they are still regarded as DMN with the conventional instrumentation. These radionuclides could still be detected using high-resolution Ge detectors inside low-level counting chambers, after separation from highly active matrices. Pm-147 is detectable by its beta-radiations. For this purpose, the separated fractions of the nuclear waste were analysed with a Perkin Elmer TriCarb TR 2800 liquid scintillation counter (LSC).

Results

Table 1: Lanthanide and americium activity results of a nuclear waste sample from a nuclear power plant

Nuclide	Bq/l	unc %
Am-241 (59 keV)	164.76	6.6%
Eu-155 (105 keV)	18.95	6.8%
Eu-154 (123 keV)	62.44	6.7%
Pm-147	330.14	14.0%
Sm-151	<LD (~30)	-

Remaining work

Sm-151 is one of the difficult-to-measure lanthanide nuclides with rather long half-life (90 year). At this time, it was under the detection limit with LSC; ICP-MS seems to be a suitable detection method.

Related publication

[1] D. Párkányi, L. Szentmiklósi, N. Vajda: *Lanthanide and americium separation with DGA resin*, 26th Seminar Activation Analysis and Gamma Spectroscopy (SAAGAS 26), 20. - 22. February 2017, Vienna, Austria

REMOVAL OF ANTIBIOTICS AND PESTICIDES FROM WASTEWATER USING HIGH-ENERGY IONIZING RADIATION

Renáta Homlok, László Szabó, Gyuri Sági, Erzsébet Takács, László Wojnárovits

Objective

This study is aimed at clarifying the effect of high-energy-radiation-induced destruction of antibiotics on the changes in biodegradability of antibiotics and it's antimicrobial activity in a synthetic wastewater matrix using electron beam (EB) irradiation [1, 2].

Methods

Irradiation was performed using a Tesla Linac LPR-4 type 4.5 MeV linear electron accelerator. An agar diffusion assay was used to assess the applicability of this process for eliminating the subinhibitory effects of antibiotics on a selection of resistant bacteria. For the *agar diffusion* test, a bacterial suspension was prepared from an overnight culture at 10^6 CFU mL^{-1} concentration. One mL inoculum was measured in each Petri dish and 20 mL molten tryptone-glucose-yeast extract agar was poured on each plate. Holes were punched in the solid agar, each of which were then filled with 100 mL of a treated antibiotic-in-wastewater sample. The agar plates were incubated at 37 °C for 24 h. Due to the low sensitivity of the microbiological tests the antibiotic solute concentrations were 500 times higher than in real wastewater samples.

Results

A synthetic effluent wastewater matrix was designed to be similar to a real sample while containing antibiotics at sufficiently high concentration for the microbiological assay (Fig 1A). We have also performed experiments with no antibiotic present to demonstrate the contribution of the secondary radical species, which are formed in the wastewater matrix, to the antibacterial activity (Fig 1B).

Sample	**0 kGy**	**4 kGy**	**8 kGy**	**16 kGy**	**28 kGy**
A1.	*21.5*	*16.0*	*14.0*	*12.5*	*10.0*
A2.	*21.0*	*16.0*	*15.0*	*12.5*	-

Table 1: The diameter of the inhibition zone in mm as a function of absorbed dose (data corresponds to Fig.1A)

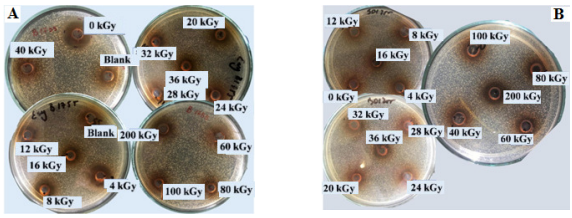

Figure 1: Agar diffusion test showing the killing of S. aureus B.01755 by the synthetic effluent wastewater matrix with antibiotic (A) and without the antibiotic (B) as a function of absorbed dose.

In the presence of antibiotic an inhibition zone appears (Fig. 1A) and it's size starts decreasing already at 4 kGy (Table 1). In its absence (in synthetic wastewater) no inhibition zone appears (Fig. 1B). However, strong inhibition zone-like behaviour was found at 200 kGy. It can be stated that the secondary radicals generated from the synthetic effluent wastewater matrix are causing this phenomenon. In the complex wastewater matrix, despite the high amount of secondary radicals forming from the matrix components, the elimination of the antibacterial activity is suggested to follow the stoichiometry of •OH relative to the antibiotic. Hence, although there are cases when secondary radicals can help in degrading an antibiotic molecule, the technology needs to be designed to the stoichiometric presence of •OH, according to the worst-case scenario approach. By modelling the wastewater effluent with a synthetic matrix we could determine the contribution of secondary free radicals from the matrix to the elimination of the antibacterial activity See Fig. 1B. Despite the high amount of these radicals compared to the antibiotic of interest, OH appeared to govern the elimination of this antibiotic. While there will be cases when other secondary radicals can also be involved in the removal of the pollutant, due to the worst-case scenario approach we always need to plan on the stoichiometric presence of OH. Nevertheless, even in this case a mild (80 Gy) treatment was just enough to reach our goal. This low absorption of energy requirement underlines the economic potential of the EB treatment as an advanced purification technique in wastewater treatment plants.

Remaining work

The continuation of our research is to probe whether EB treatment can eliminate not only the antimicrobial activity but any biological activity resulting in enrichment of antibiotic resistant species in a bacterial population.

Related publications

[1] L. Szabó, M. Steinhardt, R. Homlok, K. Kovács, E. Illés, G. Kiskó, Á. Belák, Cs. Mohácsi-Farkas, E. Takács, L. Wojnárovits: *A Microbiological Assay for Assessing the Applicability of Advanced Oxidation Processes for Eliminating the Sublethal Effects of Antibiotics on Selection of Resistant Bacteria,* Environmental Sci. and Technology Letters **4**, 251 (2017)

[2] L. Szabó, J. Szabó, E. Illés, A. Kovács, Á. Belák, Cs. Mohácsi-Farkas, E. Takács, L. Wojnárovits: *Electron beam treatment for tackling the escalating problems of antibiotic resistance: Eliminating the antimicrobial activity of wastewater matrices originating from erythromycin,* ***321****, 314 (2017)* Chemical Engineering Journal

AU-CONTAINING BIMETALLIC CATALYSTS IN HIGHLY SELECTIVE AEROBIC OXIDATION REACTIONS

Andrea Beck, Gergely Nagy, Somodi Ferenc, Srankó Dávid, László Borkó, Zoltán Schay, Antal Tungler

Objective

The OTKA project #101854 (2012-17) on this subject ended in 2017. We studied supported bimetallic gold catalysts with four different second metals (Ag, Cu, Ru and Ir) to investigate the relationship between structure and catalytic performance in selective oxidation model reactions with special attention to the interaction of the two metals in the catalysts.

Methods

Catalysts were prepared for all four bimetallic systems by the same method, by immobilization of preformed bimetallic nanoparticles (NPs) from bimetallic aqueous sols on alumina and in case of Au-Ag and Au-Cu systems also on silica support. The catalyst structures were investigated by PGAA, (HR)TEM with EDS, UV-vis and ^{197}Au Mössbauer spectroscopies, XRD, XPS, temperature programmed oxidation and reduction, CO adsorption followed by DRIFTS and CO desorption measured by QMS. The catalysts were tested in selective aerobic oxidation of benzyl alcohol in toluene solution (both in base free conditions and with base addition), and of glucose and glycerol in aqueous solutions (with base addition).

Results

The presence of bimetallic particles was confirmed earlier in case of all four systems. In all the catalytic reactions studied the Ag, Cu, Ru, and Ir monometallic analogues of the corresponding bimetallic catalysts had negligible activity in the applied reaction conditions. For the catalytic transformations Au sites must have been available that could be modified by the second metal, likely forming bimetallic active sites favouring the activation of oxygen. The selectivity of glucose and benzyl alcohol oxidations did not vary much between the different samples. In the former reaction the gluconic acid selectivity was 100%, in the latter the benzaldehyde selectivity was above 88%, with benzyl benzoate as the only side product detected on all studied catalysts. In glycerol oxidation many products were formed. Their selectivities were modified on Au-Ag/Al_2O_3 as compared to Au/Al_2O_3. The activity of the bimetallic catalysts and the monometallic gold catalysts were compared by their initial reaction rate related to a 1 mg gold content. In glucose oxidation the Cu, Ru and Ir second metals decreased (with increasing extent in this order) the activity of alumina supported monometallic Au. In benzyl alcohol oxidation in base free conditions (where catalysts deactivated quickly) the order of initial reaction rates of alumina supported samples was AuCu>Au>AuRu>>AuIr. However, if the accessible Au surface estimated by the quantity of CO adsorbed were taken into account, the reaction rates related to the same number of Au sites suggested a synergetic effect of also AuRu beside AuCu bimetallic sites in both reactions. This effect further increased in benzyl alcohol oxidation with added K_2CO_3 (by which means deactivation was eliminated) in case of AuRu, but decreased somewhat for AuCu. In glycerol oxidation alumina-supported AuAg and AuCu catalysts of Au/M=4/1 and 1/1 atomic ratio, respectively, were compared with the corresponding Au/Al_2O_3. In the rate of glycerol conversion, the Ag introduction presented a slight promoting effect, but Cu deteriorated the activity of gold, similar to the effect in glucose oxidation. Ag as a second metal clearly increased the transformation of glyceric acid to tartronic acid.

Significant support effects were observed in comparison of alumina and silica supported monometallic Au and bimetallic AuAg catalysts, and this influenced also the second metal effect. In base free benzyl alcohol oxidation (as also in glucose oxidation) a large synergetic effect of Au and Ag was obtained on AuAg/SiO_2 at Au/Ag: 90/10, 80/20 and 67/33 bulk atomic ratio, while in presence of K_2CO_3 the activity increased accompanied by strong weakening of the synergy. However, in the latter conditions the activities of the corresponding alumina supported catalysts were more than two times higher with even lower synergy between Au and Ag. Also the AuCu/SiO_2 and Au/SiO_2 were much less active than the corresponding alumina supported analogues in base free conditions, showing hardly any conversion.

Remaining work

Completion and submission of the three papers under preparation reporting the results of the project.

Related publications

[1] G. Nagy, F. Somodi, G. Sáfrán, Z. Schay, T. Gál, A. Beck, L. Prati, C. Evangelisti, C. Tiozzo: *Sol derived alumina and silica supported Au-Ag bimetallic catalysts: structure and activity in aerobic selective oxidation of benzyl alcohol*, 33rd European Conference on Surface Science, Szeged, Hungary, 27 August – 1 September (2017) Abstract Book, p. 326

[2] L. Prati, C. Evangelisti, A. Villa, A. Jouve, C. Tiozzo, G. Nagy, F. Somodi, G. Sáfrán, A. Beck: *Gold-Silver catalysts: effect of catalyst structure in the selectivity of glycerol oxidation,* 13th European Congress on Catalysis – EuropaCat-XIII, Florence, Italy, 27-31 August 2017, Abstract Book, chapter 3, p. 38-39

[3] S. Stichleutner, A. Beck, T. Benkó, G. Nagy, G. Sáfrán, F. Schmidt, K. Lázár: *^{197}Au Mössbauer study of bimetallic AuAg/TiO_2 and AuCu/Al_2O_3 catalysts,* ICAME 2017, International Conference on the Applications of the Mössbauer Effect, Saint Petersburg, Russia, 03-08 September 2017, Abstract Book

[4] A. Beck: Final report of the research project #K101854 supported by OTKA and NKFIH, entitled by „Aerobic selective oxidation on gold-containing bimetallic catalysts", 2017

DEVELOPMENT OF SHORT- AND MID-TERM ENERGY SCENARIOS FOR HUNGARY CONSIDERING ECONOMIC AND ENVIRONMENTAL ASPECTS WITH A SPECIAL FOCUS ON THE USE OF RENEWABLE ENERGY SOURCES

Endre Börcsök, Ágnes Gerse, Bálint Hartmann

Objective

This research was motivated by the open questions about the mid-term future of the heating and electricity sectors in Hungary. While the modernization of the heating sector, especially the replacement of inefficient individual heating systems is essential in the mid-term, the power system also needs to undergo a gradual transition, integrating additional renewable energy sources and replacing the recently decommissioned thermal power plants by new, competitive generation capacity. In order to move towards a more sustainable energy supply both in terms of economic and environmental aspects, the comprehensive assessment of future energy supply alternatives is of key importance.

Methods

An optimization method was applied to establish the optimum energy and technology mix for the different scenarios. Starting from a pure techno-economic assessment, the optimization was extended to the external costs of environmental impacts and human health as well. The search for an optimum was implemented as a linear programing problem in the GAMS environment (which models decision problems in a broad way using a high level mathematical modelling language). The scope of modelling covered both heat supply (residential sector) and electricity supply (all sectors); also cogeneration was taken into account among the heat and electricity supply alternatives. A typological approach was used for location and building types to reduce the complexity. For location, two categories were introduced: Budapest and other regions, while the three building typological groups consisted of large-scale and medium-scale multi-flat buildings and single family houses. In a similar way, typical seasonal, monthly and hourly load patterns were computed for modelling the variations in heat and electricity demand. The variability in solar and wind energy infeed was considered with hourly generation patterns. For heat and electricity supply, several technology choices have been implemented in the model including district heating and combined heat and power (CHP) generation. Among the supply alternatives, low-carbon technologies such as renewable energy sources and nuclear energy were considered. The main characteristics of the different technology options included fixed production costs (capital, fixed part of operation and maintenance costs), variable production costs (fuel, variable part of operation and maintenance costs), GHG (greenhouse gas) emission, and the external costs of other environmental impacts and technology constraints. Optimization constraints were specified from the balance of production and demand and from the potential of the installed production capacities. The resulting solution provides an optimum energy and technology mix for the different typological categories.

Results

For an optimal heat supply, fossil energy sources are essential while in the electricity sector, beside the significant nuclear power, fossil and renewable cogeneration has a high priority. While the model is capable to assess the potential electricity generation from wind and solar energy, these variable resources are not part of the optimized electricity generation portfolio due to their limited capacity factors.

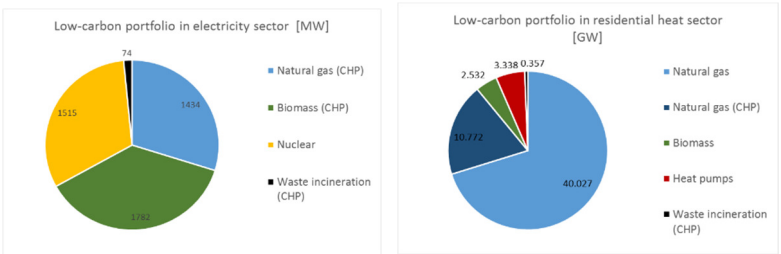

Fig. 1. Low-carbon scenarios in Hungarian electricity and heat sector.

Remaining work

There is some potential for further development, as the present model uses a simplified approach for modelling the energy infrastructure and the different technology alternatives. Due to the large share of imported electricity, the impact of cross-border electricity exchanges needs to be considered in future work, as well.

Related publications

[1] B. Hartmann, E. Börcsök, V. Oláhné Groma, J. Osán, A. Talamon, Sz. Török, M. Alföldy-Boruss: *Multi-criteria revision of the Hungarian Renewable Energy Utilization Action Plan – Review of the aspect of economy.* Renewable and Sustainable Energy Reviews, **80**, 1187-1200 (2017)

[2] E. Börcsök, J. Fülöp: *Possibility of nuclear cogeneration development in the region of Paks.* Acta Polytechnica Hungarica, submitted

EVALUATION OF BIODEGRADABILITY AND TOXICITY DURING IONIZING RADIATION-INDUCED DECOMPOSITION OF ANTIBIOTICS

Krisztina Kovács, Gyuri Sági, László Szabó, Szabina Góger Papné, László Wojnárovits, Erzsébet Takács

Objective

The aim of the present work was to demonstrate the impact of both the degree of mineralization (i.e. the breakdown to CO_2 and H_2O) and the hydrogen peroxide (H_2O_2) content on the biodegradation and ecotoxicity evaluation in the course of using high-energy ionizing radiation to induce degradation of sulfamethoxazole (SMX) by two different sample application approaches.

Methods

Advanced oxidation was carried out at room temperature by a ^{60}Co panoramic type γ-irradiation facility (dose rate = 7.6 kGy h^{-1}) in air saturated, 0.1 mmol dm^{-3} SMX solution. Biological oxygen demand (BOD) experiments were performed by using an OxiTop® Control BOD Respirometer System using the DIN EN 1899-1 (1998) procedure. Chemical oxygen demand (COD) measurements were carried out using a Behrotest TRS 200 COD digestion system according to the International Organization for Standardization (ISO) 6060:1989 (1989) procedure, except that 30 cm^3 sample volumes were used instead of 10 cm^3. Total organic carbon content (TOC) was measured with a Shimadzu TOC–L CSH/CSN analyser. The H_2O_2 concentration was determined with the Merck H_2O_2 test kit (Catalog Nr. 1.18789.0001). To assess the effects of H_2O_2 on *Daphnia magna*, acute mortality tests were executed using the procedure of the Organisation for Economic Co-operation and Development (OECD) Test No. 202 (2004). The growth inhibition on freshwater unicellular microalgae *Pseudokirchneriella subcapitata* was implemented after 72 h, at pH 7–8, according to OECD Test No. 201 (2011). Acute toxicity of SMX and H_2O_2 on *Vibrio fischeri* was evaluated by Microtox® tests performed according to the United States Environmental Protection Agency (2003) approved protocol, on a LANGE LUMIStox 300 equipment using freeze-dried test organisms. In biodegradability and ecotoxicological experiments, technological and biological approaches were both used to study the effects of H_2O_2 and organic content. Statistical significance tests (t-tests) were carried out by using GraphPad scientific statistics software to obtain representative results.

Results

During γ-radiolysis, H_2O_2 forms in irradiated, dilute aqueous solutions with a rather high initial yield of $\sim 3\times10^{-7}$ mol J^{-1} [1]. Residual H_2O_2 in Advanced oxidation processes (AOP) may strongly modify the outcome of the experiments employing living organisms. H_2O_2 concentrations should be reduced to at least ~ 0.05 mmol dm^{-3} in *Vibrio fischeri* and *Pseudokirchneriella subcapitata* measurements due to the strong inhibitory effects on these organisms at higher concentrations. The presence of H_2O_2 in such low concentrations is causing an acceptable impact in manometric evaluation of low BOD. However, *Daphnia magna* was found to be more susceptible: practically complete elimination of H_2O_2 is needed prior to these tests. The H_2O_2 content was removed by catalytic decomposition with manganese dioxide (MnO_2) [2]. Dilution (mineralization) of the initial solutions in the course of AOP cannot be neglected in measuring toxicity or biodegradability as indicated by the results. The technological approach generally applied is not taking into account the presence of H_2O_2, in contrast to the biological approach introduced here. Significant differences were evidenced between the results of these two approaches. For instance, the biological approach showed strong biodegradability, while only moderate biodegradability was seen by the technological approach. Toxicity tests demonstrated differences not only in the extent but also in the tendency of inhibition changes. Such variations may lead to false process optimization and unnecessarily prolonged treatment [3].

Remaining work

Investigation of biodegradability and ecotoxicity is a very important area of research for the evaluation of AOP and persistent organic pollutant removal. Thus further experiments are necessary to get a more comprehensive picture about biological effects of degradation products during the decomposition of different antibiotics.

Related publications

[1] E. Illés, A. Tegze, K. Kovács, Gy. Sági, Z. Papp, E. Takács, L. Wojnárovits: *Hydrogen peroxide formation during radiolysis of aerated aqueous solutions of organic molecules,* Radiation Physics and Chemistry **134**, 8 (2017)

[2] K. Kovács, Gy. Sági, E. Takács, L. Wojnárovits: *Use of bovine catalase and manganese dioxide for elimination of hydrogen peroxide from partly oxidized aqueous solutions of aromatic molecules –Unexpected complications,* Radiation Physics and Chemistry **139**, 147 (2017)

[3] Gy. Sági, A. Bezsenyi, K. Kovács, Sz. Klátyik, B. Darvas, A. Székács, L. Wojnárovits, E. Takács: *The impact of H_2O_2 and the role of mineralization in biodegradation or ecotoxicity assessment of advanced oxidation processes,* Radiation Physics and Chemistry **144:** 361-366 (2018)

MODIFICATION OF CELLULOSE DERIVATIVE-BASED SUPERABSORBENT GELS WITH ACRYLIC ACID AND STARCH

Tamás Fekete, Judit Borsa, Erzsébet Takács, László Wojnárovits

Objective

The aim of this work is the improvement of the properties of various cellulose derivative-based superabsorbents by the partial replacement of the cellulose derivative component with different natural and synthetic polymers. Following our previous work, the effect of the introduction of acrylic acid was investigated for non-polyelectrolyte cellulose derivative systems, as well. For carboxymethylcellulose gels, the partial replacement of the derivative with potato starch was studied for the preparation of a low-cost superabsorbent.

Methods

Hydroxyethylcellulose/acrylic acid and carboxymethylcellulose/potato starch hydrogels were prepared from aqueous solutions via gamma-irradiation. The effect of various synthesis parameters such as the dose, solute concentration, chemical composition and alkali treatment on the gel properties was investigated. The determination of the gel fraction was carried out by washing the samples in distilled water for 48 hours for the removal of sol. The degree of swelling was determined by immersing the dry gels in distilled water and in various salt solutions for 24 hours. The morphology was studied by scanning electron microscopy, while the chemical composition of the gels was characterized by FTIR-ATR.

Results

The introduction of acrylic acid proved to be very efficient for the improvement of the gelling behaviour of hydroxyethylcellulose systems [1]. Significantly lower dose and solute concentration was sufficient for the gelation in the presence of very low concentrations (1-5%) of acrylic acid. Moreover, optimal synthesis conditions led to higher water uptake and higher gel fraction compared to the pure cellulose derivative gels. The molecular properties of the hydroxyethylcellulose also had a major impact on the gelation. Higher molecular weight not only led to easier gel formation, but a higher gel fraction could be reached, as well. A short alkali treatment of the gels resulted in a major increase in the water uptake due to the neutralization of the acrylic acid component. Therefore, the addition of low amounts of acrylic acid allowed the synthesis of superabsorbents with superior properties while keeping the cellulose derivative content very high.

The partial replacement of carboxymethylcellulose with potato starch also led to improved gel properties [2]. However, very high starch content (above 50-60%) had a negative impact on the gelation. The optimal synthesis conditions were similar to the pure carboxymethylcellulose systems, but a higher gel fraction and water uptake was reached. While the improvement is smaller than achievable via the introduction of acrylic acid, the lack of toxic monomers and lower cost makes them an environmentally friendly alternative to the cellulose derivative/acrylic acid systems. Such gels show a large potential in certain application fields such as agriculture where the use of synthetic polymers must be avoided due to their poor biodegradability.

The preparation of the copolymer gels also allowed tailoring the responsive behaviour of the systems. While swelling of hydroxyethylcellulose gels showed no sensitivity to the ionic strength of the swelling agent, the introduction of 5% acrylic acid led to a responsive behaviour and the water uptake decreased significantly in the presence of salt. On the other hand, the sensitivity of the carboxymethylcellulose decreased with the addition of starch. This highlights the potential of cellulose derivative based gels in practical applications as their properties and behaviour can be easily modified depending on the requirements.

Remaining work

The in-depth study of the potential application of the prepared superabsorbents in various fields is planned. Moreover, the further modification of the gels by introducing other components such as clay particles will also be investigated.

Related publications

[1] T. Fekete, J. Borsa, E. Takács, L. Wojnárovits: *Synthesis and characterization of superabsorbent hydrogels based on hydroxyethylcellulose and acrylic acid*, Carbohydrate Polymers **166**, 300-308 (2017)

[2] T. Fekete, J. Borsa, E. Takács, L. Wojnárovits: *Synthesis of carboxymethylcellulose/starch superabsorbent hydrogels by gamma-irradiation*, Chemistry Central Journal **11**, 46 (2017)

TOWARDS SUPPORTED FEPT FERROMAGNETIC NANOPARTICLES

Anita Horváth, Ferenc Somodi, Miklós Németh, András Deák, János Szívós, György Sáfrán

Objective

Ferromagnetic face centered tetragonal (fct) nanocrystals have a regular array of Fe atoms inserted into the Pt rows forming a $L1_0$ superstructure that could be useful as a future ultrahigh-density perpendicular recording medium. However, the as prepared FePt nanoparticles have face centered cubic (fcc) structure and are superparamagnetic. Annealing at about 500 °C or above may convert them into $L1_0$ structured hard magnets. We continued our research tasks of last year which were focused on the production of FePt nanoparticles with wet-chemical methods. Particles prepared were to be investigated after mounting them on nanocrystalline Al_2O_3 or ZrO_2 oxides or a Si surface with the attempt to produce the $L1_0$ phase. An amorphous SiO_x shell was to be built around individual particles already in liquid phase (sol) in order to facilitate the transition to fct structure upon a laser treatment. Catalytic properties were checked in high temperature dry reforming since Pt/ZrO_2 is an excellent catalyst for that reaction.

Methods

FePt sols were prepared in water at room temperature or in organic phase at high temperature using several stabilizer and reducing agents and different Pt and Fe precursors. The complete assembly of a Schlenk line (Fig.1a) was realized that allowed the preparation to be carried out under an inert atmosphere or even in vacuum. The SiO_x layer around the particles was formed by hydrolysis of tetraethylorthosilicate in methanol after adjusting the pH to 11, and the particle size was measured by dynamic light scattering. The size, morphology and the line spacing of the FePt alloy particles were studied by high resolution TEM as well. In addition, XRD measurement was done on chosen samples. Catalytic dry reforming tests were carried out at 600 °C after different calcination/reduction pretreatments on $FePt/ZrO_2$ and $FePt/Al_2O_3$ samples.

Results

FePt nanoparticles prepared in dioctyl ether solvent under an inert atmosphere at 240 °C (FePt-org) were around 2-3 nm with the required Fe:Pt =1:1 composition, but particle coalescence was observed with time. XRD of the as-prepared sol could detect only weakly crystalline/small FePt particles probably with fcc structure. Unfortunately, the SiO_x shell could not be produced in this system. The $FePt\text{-}org/Al_2O_3$ contained tiny particles in strong interaction with the support and also larger particles. A line spacing around 3.7 A representative of the $L1_0$ phase could be discerned only in the larger aggregated metallic islands that were not in strong interaction with the support (Fig.1b). XRD also proved the existence of 25 nm sized FePt crystallites with the $L1_0$ phase. Aqueous sols with fcc FePt particles of very different morphology faced the problem of Fe leaching and particle coalescence. The best aqueous sols with particles between 2-6 nm could be used for SiO_x encapsulating. The SiO_x-modified samples were laser treated, and the bare particles were supported and reduced at 500-600 °C on Al_2O_3 and ZrO_2 as well. However, the $L1_0$ phase was not revealed neither by HRTEM nor by XRD, probably due to the small particle size, and the strong metal-support interaction that seems to limit the transition to fct structure.

Dry reforming catalytic results (Fig.1c) showed that the prereduced (red600) $FePt\text{-}aq/ZrO_2$ is less effective than the $Ptsol/ZrO_2$ reference catalyst (although particle sizes were similar). After calc.600°C/red.600°C the conversion of methane and CO_2 (viz. the catalytic activity) increased, probably due to the surface segregation of Pt and/or destruction of the FePt phase. After calc.750°C/red.600°C, the catalytic activity dropped possibly because of Pt sintering. Carbon deposition was never detected during the calcination treatments. The $FePt\text{-}aq/Al_2O_3$ sample had very low catalytic activity, and it even decreased to zero during the same treatments, although metal dispersions on ZrO_2 and Al_2O_3 were similar. All in all, the small particle size (d<5 nm) and metal-support interaction seemed to hinder the $L1_0$ phase transition which was firmly detected only in the case of aggregated particles of the organic sol-derived sample. The FePt alloy seems to have lower dry reforming activity than pure Pt.

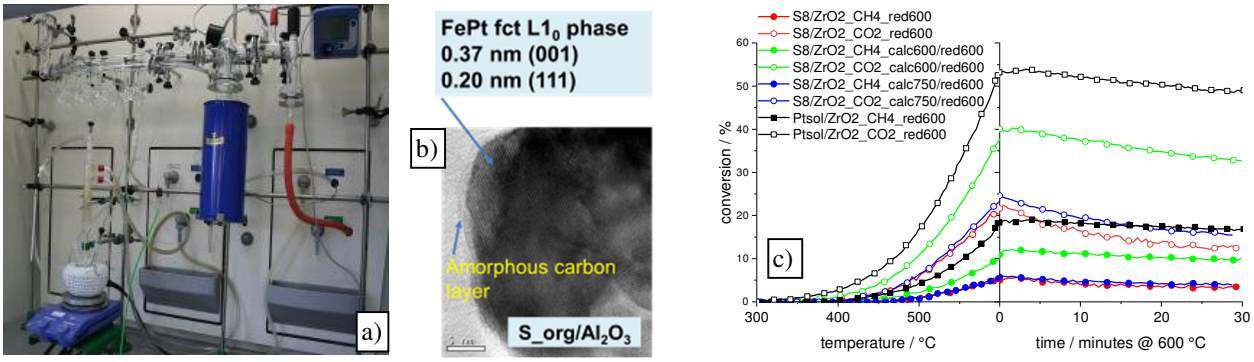

Figure 1: a) The new Schlenk line for sample preparation, b) HRTEM image of $FePt\text{-}org/Al_2O_3$ having the $L1_0$ structure and c) DRM tests on $FePt\text{-}aq/ZrO_2$ catalyst (signed as S8) compared to Pt/ZrO_2

Related publication

[1] A. Horváth, F. Somodi, M. Németh, A. Deák and G. Sáfrán: *FePt nanoparticles: with wet chemical preparation method towards ferromagnetic $L1_0$ phase as possible catalyst components*, 13th European Congress on Catalysis, poster, Florence, 27-31 August (2017)

MIGRATION OF RADIONUCLIDES IN BODA CLAYSTONE SAMPLES

Károly Lázár, János Megyeri, Tibor Szarvas

Objective

The objective of the study was to determine and compare the effective diffusion coefficients (D_{eff}) of various typical long lived radionuclides in order to evaluate the isotope retention properties of Boda Claystone, a potential geological formation for hosting a repository site for nuclear waste. Diffusion of neutral water was studied with tritiated water (HTO, or, more exactly ^{3}HHO), the migration of non-sorbing anions were studied with $^{129}I^-$, $^{36}Cl^-$, $H^{14}CO_3^-$ and $^{75}SeO_3^{2-}$, whereas sorbing cations were represented by $^{137}Cs^+$ and UO_2^{2+} ions.

Methods

D_{eff} values of various isotopes were determined in break-through cells. Diffusion of radionuclides through 5-8 mm thick borecore discs was measured in aqueous media with liquid scintillation detection. Borecore samples were obtained from three zones of the BAF-2 drilling in the Western Anticline region of the Mecsek Mountains (from depths 415, 586 and 724 m). The porosity of the claystone samples was 1-2 %. The time span of the break-through measurements was ca. one year.

Results

For neutral water (HTO), a value of $D_{eff} \sim 10^{-11}$ m^2 s^{-1} was obtained. This value is reliable since it is close to the self diffusion coefficient of water in strong electrolytes. Various experiments were done with the non-sorbing anions. Namely, a high D_{eff} value was determined with hydrocarbonate ($H^{14}CO_3^-$) anion ($\sim 10^{-11}$ m^2 s^{-1}, similar to HTO). $^{125}I^-$ exhibits a slower migration rate ($D_{eff} \sim 10^{-12}$ m^2 s^{-1}), whereas chloride, the anion of the chemically similar halogen element, does not show any break-through within one year. The fourth studied anionic species, $^{75}SeO_3^{2-}$ displayed another type of behaviour, the original concentration of $^{75}SeO_3^{2-}$ drops by 20 – 30 % on the starting side of the cell whereas on the opposite side the concentration increases by one order of magnitude less, a maximum of only 2 - 3 % within one year. Thus, the missing amount of ca. 25 % concentration of ^{75}Se must be stuck in transit inside the borecore sample [1] (Fig.1).

These different characteristics of the migrations of anions can be reasonably explained. For instance, hydrocarbonate anions are already present in a high concentration in the original pore water of the claystone. Thus, chemical equilibria occur earlier, and the migration of $H^{14}CO_3^-$ ions can be interpreted as a simple self diffusion, without any further chemical interaction with the claystone. For this reason, the value of D_{eff} of $H^{14}CO_3^-$ can be similar to that of the neutral water (HTO). Iodide is a large polarizable anion, so its migration is retarded by van der Waals interactions. Curiously, no break-through was detected for $^{36}Cl^-$ during one year. The lack of migration was attributed to anion exclusion in the negatively charged surface layer of clay minerals in aqueous media. The apparent accumulation of ^{75}Se in the borecore sample discs can be attributed to redox processes. In a simplified approach Se(IV) => Se(0) reduction may be combined with the Fe^{2+} => Fe^{3+} oxidation process on ions between the clay layers, resulting in the immobilization of selenium.

As for the studied cations, the expected fast sorption of $^{137}Cs^+$ was observed. The borecore discs chemisorbed irreversibly the caesium cations within a few days. Sorption of uranyl ions was significantly slower; a few months were necessary for completion of the sorption process. The immobilization of uranium was probably connected to formation of insoluble $UO_2(CO_3)$ [2].

A more useful practical representation can also be derived by conversion of the obtained D_{eff} values to corresponding couples of time – distance numbers. For example, the highest D_{eff} value observed on the Boda Claystone sample ($\sim 10^{-11}$ m^2) is equivalent with ca. 20 m migration distance in the claystone within a million years.

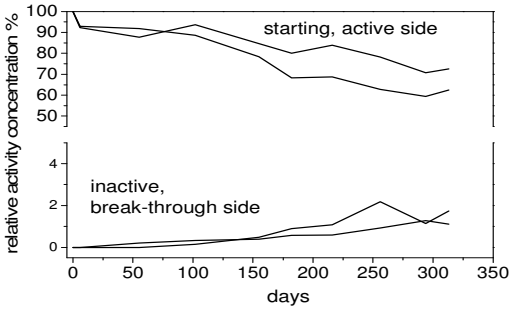

Figure 1:
Relative activities of $^{75}SeO_3^{2-}$ detected in the two compartments of break-through cells

Related publications

[1] K. Lázár, J. Megyeri, T. Szarvas: *Studies on migration of radionuclides in borecore samples from BAF-2,* Report (in Hungarian), MTA EK 22. pp (2017)

[2] K. Lázár, J. Megyeri, T. Szarvas, Z. Máthé: Studies of migration of radionuclides in samples from Boda Claystone, Presentation, "Őszi Radiokémiai Napok" Balatonszárszó, October 25-27, 2017.

PREPARATION AND CHARACTERIZATION OF NANOPARTICLE SYSTEMS CONSIDERED FOR PLANT NUTRITION

Zoltán Klencsár, Sándor Stichleutner, Viktória Kovácsné Kis

Objective

Preparation and characterization of nanoparticle systems to be applied in studies investigating the metal uptake and iron metabolism of plants.

Methods

Samples were prepared using either a sol-gel hydrothermal process (SGHP) or an electric wire explosion (EWE). The investigated spinel type oxides were prepared via SGHP by Gy. Tolnai. Powder X-ray diffractometry (PXRD), ^{57}Fe Mössbauer spectroscopy (^{57}Fe MS), transmission and scanning electron microscopy (TEM, SEM), energy-dispersive X-ray spectroscopy (EDXS) and electron magnetic resonance (EMR) spectroscopy were used to characterize the prepared nanoparticles. EWE and PXRD experiments were performed in cooperation with L. K. Varga at the Wigner Research Centre for Physics, Hungarian Academy of Sciences (MTA). SEM and EDXS measurements were carried out in cooperation with L. Szabó at the Research Centre for Natural Sciences, MTA.

Results

Ferritic steel wire was vaporized in water using electric wire explosion, resulting in a mixture of a colloidal suspension and of promptly settled, larger particles. SEM, TEM, EDXS, PXRD and ^{57}Fe MS measurements revealed that the solid matter so produced consists of spheres of α-iron and the iron oxide wüstite. The spheres exhibited a wide particle size distribution ranging from a few microns down to below 50 nm. Wüstite was identified as having the composition of $Fe_{0.9}O$ with an average crystallite size of 66 nm. The EWE method thus turned out to be able to produce iron particles with a rather wide particle size distribution [1].

^{57}Fe MS, PXRD, TEM and EMR measurements performed on two different samples of $ZnFe_2O_4$ nanoparticle powders revealed spinel nanoparticles with a common characteristic particle size of 5-6 nm, but with different crystallite sizes of ~ 5 nm (single crystals) and ~ 1-2 nm (very low crystallinity). These powder samples are thus promising candidates for the investigation of possible effects of different crystallinity on nanoparticle-plant interactions.

A detailed analysis of ^{57}Fe MS, EMR, TEM and PXRD measurements which were performed previously on a series of magnetite nanoparticles prepared under different experimental conditions was carried out in order to assess the composition of the nanoparticles with respect to the oxidation level of magnetite. A novel method was introduced for the analysis of heavily broadened ^{57}Fe Mössbauer spectra of non-stoichiometric magnetite nanoparticle systems, and the feasibility of the method was demonstrated. According to the results, the application of the coating agent malic acid during preparation hinders oxidation of magnetite nanoparticles [2].

$Mn_xZn_{1-x}Fe_2O_4$ nanoparticle suspensions with $x = 0.25$ and 0.5 were investigated by EMR spectroscopy at different temperatures in the range of 140 to 340 K. Beside the intense ferromagnetic signal, the suspensions revealed a signal of solitary Fe^{3+} ions, which exhibited inhomogeneous broadening in correlation with the magnetization of the nanoparticles, suggesting that it can be associated with an Fe^{3+} complex species attached to the nanoparticles' surface [3].

Remaining work

Preparation, characterization and application of further nanoparticle samples are needed in order to explore the significance of specific material properties in influencing plant-nanoparticle interactions.

Related publications

[1] K. Lázár, L.K. Varga, V. Kovács Kis, L. Szabó, S. Stichleutner, Z. Klencsár: *Vaporization of steel by electric wire explosion in water: phase transitions and oxidation* (lecture), 3rd Mediterranean Conference on the Applications of the Mössbauer Effect (MECAME 2017, Book of Abstracts p. 20), June 05-07, 2017, Jerusalem, Israel

[2] Z. Klencsár, A. Ábrahám, L. Szabó, E.Gy. Szabó, S. Stichleutner, E. Kuzmann, Z. Homonnay, Gy. Tolnai: *The Effect of Preparation Conditions on Magnetite Nanoparticles Obtained via Chemical Co-precipitation* (poster), The International Conference on the Applications of the Mössbauer Effect (ICAME 2017, Conference Programme p. 180), September 03-08, 2017, St. Petersburg, Russia

[3] Z. Klencsár, V. Kovács Kis, S. Stichleutner, Z. May, Z. Sándor, E.Gy. Szabó, E. Bódis, L. Szabó, K. Kovács, E. Kuzmann, Z. Homonnay, F. Pankaczi, Zs. Farkas, Á. Solti, F. Fodor, Gy. Tolnai: *Nanoparticle systems developed for plant nutrition: their composition, structure and effects on cucumber plants* (lecture), International Conference on Functional Nanomaterials and Nanodevices 2017 (NanoMat 2017, Conference Booklet p. 83), 24-27 September 2017, Budapest, Hungary

PREPARATION, CHARACTERIZATION AND APPLICATION OF NANOPARTICLES FOR PLANT NUTRITION

Zoltán Klencsár, Sándor Stichleutner, Viktória Kovácsné Kis

Objective

Preparation and characterization of nanoparticle systems, and their application in studies investigating the metal uptake and iron metabolism of plants.

Methods

Nanoparticle (NP) samples were prepared using a hydrothermal process by Gy. Tolnai. Powder X-ray diffractometry (PXRD), ^{57}Fe Mössbauer spectroscopy (^{57}Fe MS) and transmission electron microscopy (TEM) were used to characterize them. Plant samples were studied among others by Inductively Coupled Plasma Optical Emission Spectrometry (ICP-OES) and electron magnetic resonance spectroscopy (EMR). PXRD experiments were performed in cooperation with L.K. Varga at the Wigner Research Centre for Physics, MTA. ICP-OES measurements were performed by Z. May at the Research Centre for Natural Sciences, HAS. Plant growth experiments were performed by F. Fodor et al. at the Department of Plant Physiology and Molecular Plant Biology, Eötvös Loránd University.

Results

Ferrihydrite/hematite NP suspensions were prepared via forced hydrolysis by adding a solution of $FeCl_3 \cdot 6H_2O$ to solutions of three different surfactants (PEG-1500, Emulsion/104D, LAB 236/2). By the use of TEM, the nature of these applied surfactants was found to influence the composition and particle size of the colloids, resulting, respectively, in 6L (6-line) ferrihydrite of 4-7 nm, hematite of 12-25 nm, and a mixture of 4-8 nm ferrihydrite and 12-20 nm hematite particles.

Magnetite nanoparticle powders were prepared with and without the application of DEXTRAN-40000 stabilizer. ^{57}Fe MS, TEM and PXRD measurements revealed a characteristic particle- and crystallite size in the order of ~ 10 nm in both cases. Differences found between the results obtained for the two samples suggest that the application of the stabilizer is beneficial for the formation/preservation of the smallest nanoparticles.

34 dried cucumber leaf samples were measured by the means of both EMR and ICP-OES in the study of plant regeneration experiments. In the case of plants grown under iron deficient conditions, ICP-OES measurements revealed a strongly diminished Fe concentration accompanied with a greatly enhanced Mn concentration in the leaf samples, indicating a correlation between Fe- and Mn-metabolism of the plant. EMR measurements also reflected this correlation and furthermore confirmed the elevated concentration of solitary Mn^{2+} ions in the Fe-deficient samples. Based on measurements with ICP-OES, we found that plants grown under Mn-deficient conditions exhibited elevated levels of iron, further corroborating the interdependence between Fe- and Mn-metabolism. In the same samples, EMR measurements reflected the strong reduction of Mn^{2+} concentration levels, with no sign of an enhanced Fe^{3+} signal, thereby suggesting that the enhanced level of iron detected in these samples by ICP-OES is due to Fe^{2+} species.

In toxicity experiments performed with a $Mn_{0.25}Zn_{0.75}Fe_2O_4$ NP suspension (nanoferrite) applied in excessive amounts (equivalent with 1 mM of Fe, i.e. one hundred times the Fe concentration applied in the case of the control) to the nutrient solution of cucumber plants, the administered nanoferrite hindered plant growth and resulted in reduced plant fresh weight. At the same time, applying the same amounts of Mn, Zn and Fe in the form of a mixture of iron citrate, $MnCl_2 \cdot 4H_2O$ and $ZnSO_4 \cdot 7H_2O$ inhibited plant growth much more strongly, revealing the considerably less toxic nature of metals when administered in the form of NPs. This result points out that NPs can act as a retarded/prolonged source of metals, by providing access to their metal content solely through their cumulative surface area.

Remaining work

Further nanoparticle samples and plant growth experiments are needed in order to explore the significance of specific material properties in influencing plant-nanoparticle interactions.

Related publications

[1] F. Pankaczi, Zs. Farkas, B. Müller, K. Kovács, Z. Klencsár, Z. May, Z. Sándor, E.Gy. Szabó, E. Bódis, L. Szabó, E. Kuzmann, Z. Homonnay, Gy. Tolnai, Á. Solti, F. Fodor: *Manufactured nanomaterials: new iron based fertilizers or potentially toxic agents?*, A Magyar Növénybiológiai Társaság XII. Kongresszusa, Szeged. Összefoglalók, ISBN 978-963-12-9736-2, p. 18., 2017

[2] V. Halasy, Zs. Farkas, F. Pankaczi, K. Kovács, F. Fodor, Z. Klencsár, Z. Homonnay, L. Tamás, Á. Solti, S. Pólya: *Cucumber and nanoparticles: Can C. sativus utilise nanoferrihydrite as iron source?*, Programme and Abstracts p. 66, Green for Good Meeting G4G IV Conference, 19th-22nd June, 2017, Olomouc, Czech Republic, 2017

[3] Z. Klencsár, V. Kovács Kis, S. Stichleutner, Z. May, Z. Sándor, E.Gy. Szabó, E. Bódis, L. Szabó, K. Kovács, E. Kuzmann, Z. Homonnay, F. Pankaczi, Zs. Farkas, Á. Solti, F. Fodor, Gy. Tolnai: *Nanoparticle systems developed for plant nutrition: their composition, structure and effects on cucumber plants* (lecture), International Conference on Functional Nanomaterials and Nanodevices 2017 (NanoMat 2017, Conference Booklet p. 83), 24-27 September 2017, Budapest, Hungary

CALCULATIONS FOR ENVIRONMENTAL IMPACT ASSESSMENT

Tamás Pázmándi, Péter Szántó, Dorottya Jakab, Csilla Rudas, András László, Sándor Deme

Objective

Two studies were conducted with the objective of evaluating the meteorological uncertainties and their effect on the atmospheric dispersion calculations [1], and determining the radiological consequences for Design Basis Accidents (DBA) and Beyond Design Basis Accidents (BDBA) [2].

Methods

For the evaluation of how meteorological uncertainties effect the results of atmospheric dispersion calculations, the availability of different meteorological data, their reliability and uncertainty was studied and a sensitivity analysis was conducted with the Gaussian puff model of the SINAC code.

In the second phase of the calculations, to determine the radiological consequences of DBA and BDBA events, the effects of six selected severe accidental scenarios were computed. The calculations were made with a modified Gaussian plume model to take into account the effects of the buildings. The atmospheric dispersion was simulated for average meteorological conditions (5 m/s wind speed, Pasquill D atmospheric stability, 5 mm/s precipitation) for the four cardinal and the most frequent wind direction. The environmental consequences were described by the time-integrated ground level air activity concentration, the ground deposition and the external and inhalation dose for unit residence time.

Results

The availability and uncertainty of the meteorological parameters for atmospheric dispersion calculations can be different for various data sources. The meteorological variables used can originate from measurements and observation, but can also be produced by numerical weather prediction (NWP) models. The availability and uncertainty of meteorological data from measurements and observations, and from NWP models were gathered, based on recommendations and general requirements of the World Meteorological Organization (WMO). Sensitivity analysis was conducted for the meteorological parameters of wind direction, wind velocity, Pasquill stability category and precipitation intensity. Fixed value ranges were set for these parameters and each was perturbed separately for the calculation of the time-integrated air activity concentration at different times and locations. The sensitivity analysis showed that using different meteorological parameter values can have different effects on the results at various distances from the release point. For example, changes in wind velocity and direction has a large influence on the air activity concentration, which decreases with distance (Fig. 1 and 2).

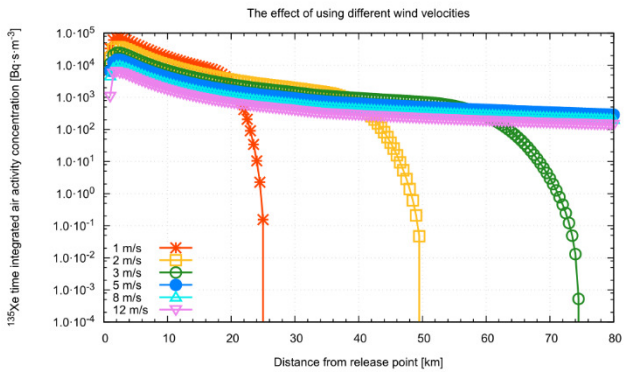

Figure 1: The time-integrated air activity concentrations of ^{135}Xe for different wind velocities.

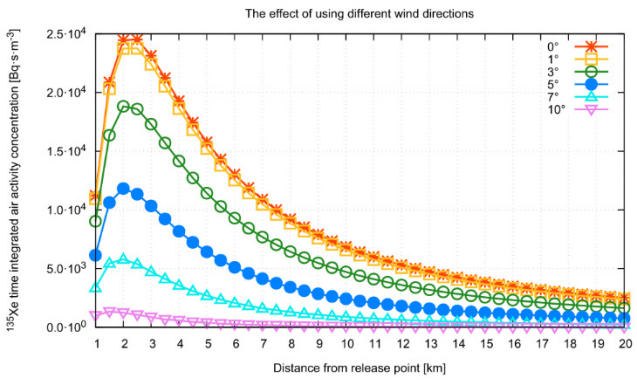

Figure 2: The time-integrated air activity concentrations of ^{135}Xe for different wind directions.

The overall effect of the perturbations of the four meteorological parameters are summarized in Table 1.

Table 1: The maximum ratio of the calculated air activity concentration along the original plume centreline due to the perturbation of meteorological parameters.

Perturbation of the meteorological parameters (exact values)	**The maximum ratio of the air activity concentration in the original plume centreline for different perturbations**		
	Distance from the release point [km]		
	1-5	5-20	20-30
Wind velocity: 11 m/s (1, 2, 3, 5, 8, 12)	$9{\cdot}10^{-2}$	$1{\cdot}10^{-1}$	$3\cdot10^{3}$
Wind direction: 10° (180°, 181°, 183°, 185°, 187°, 10°)	$6{\cdot}10^{-2}$	$1{\cdot}10^{-3}$	no data available
Pasquill category: category 1 (A, B, C, D, E, F)	$1{\cdot}10^{-2}$	$4{\cdot}10^{0}$	$3{\cdot}10^{0}$
Precipitation intensity: 11 mm/h (0, 1, 3, 5, 8, 12)	$7{\cdot}10^{-1}$	$2{\cdot}10^{-2}$	$2{\cdot}10^{-3}$

The results of the radiological consequences analysis for the six severe accident cases were determined for the assumption of a direct release from the containment building without ventilation, and for one scenario, additional calculations were conducted with operating ventilation and stack release. In the stack release case different elemental iodine filtering efficiencies were considered. The highest air activity concentration values occur at the lee side of the main building, where the time dependence of the results correspond with the release timing and the source term. The calculation results show that the largest contributor to the total exposure is the inhalation dose which is about 4-5 orders of magnitude greater than the external dose at the receptor point where the air activity concentration is the highest. The examination of the influence of different elemental iodine filtering efficiencies resulted in an order of magnitude decrease in total dose for elemental iodine with a 90% filtering efficiency compared to the results with a 0% efficiency.

Remaining work

The two mentioned projects have both been completed.

Related publications

[1] D. Jakab, T. Pázmándi, Cs. Rudas, P. Szántó: *Meteorological data uncertainties and their effect on atmospheric dispersion calculation*, EK-SVL-2017-718-01-01-00, in Hungarian (2017)

[2] S. Deme, A. László, T. Pázmándi, P. Szántó: *Radiological Consequences of Design Basis and Beyond Design-Basis Accidents*, EK-SVL-2016-994-03-01-00, in Hungarian (2017)

THE CONTRIBUTION OF DOMESTIC BIOMASS HEATING TO BUDAPEST ATMOSPHERIC AEROSOLS

Szabina Török, János Osán, Endre Börcsök and Csenge Dian

Objective

Extensive use of biomass solid fuel in the domestic sector is risking the compliance with air quality commitments in densely populated areas. The reason of overusing this fuel as a so called renewable energy (RE) source is the fact that the RE directive for EC (elemental carbon) suggest that 15% of the primary energy in Hungary should be from an RE source of which wood logs is the cheapest solution. The presented work aims to show that such widespread domestic solid biomass fuelling has its footprint on the atmospheric aerosol composition and this results in worsening the already poor air quality situation of Budapest.

Methods

Samples were collected over 100 days in a suburban area of Budapest (Gilice tér). Particulate matter (PM) mass and elemental composition, OC/EC content, major anions and organic species of PM were determined, gaseous pollutants (NO_2, SO_2, CO and O_3) and meteorological data (wind speed and direction, temperature and precipitation) were measured. Positive matrix factorisation of the measured date resulted in five reasonable factors/sources: two chemically different biomass burning factors together with soil and traffic related particles as well as secondary aerosols. The trajectories of air masses during the sampling periods were calculated with the Flexible Particle Dispersion Model (FLEXPART). The potential contribution source function was then used to identify the origin over a large geographical region of the PM sources identified with PMF (positive matrix factorization) and the associated gaseous pollutants/precursors.

Results

The aerosol average composition showed that over 45% of the total mass is elemental and organic carbon. The biomass burning (BB) source is the one with the highest share (61%) of levoglucosan a tracer of biomass burning and is also characterized by high levels of K and OC (organic carbon). The BB presents a rather typical seasonal trend for this source with higher contributions in winter that gradually decrease to achieve minimum levels in late spring.

Table 1: Source contribution estimate to PM 2.5 in Budapest
Average values (AV) and standard deviation(SD) for the whole sampling period and seasons

Budapest (BDP) PM2.5 - Source contribution estimation (SCE) μg m^{-3}						
Factor/source	**whole period**		**winter (W)**		**spring (SP)**	
	2015 (09 Feb-18 May)		09 Feb-20 March		21 March-18 May	
	n=94		n=37		n=57	
	AV	*SD*	**AV**	*SD*	**AV**	*SD*
Secondary aerosol **(SEC)**	3.8	*4.1*	7.0	*4.4*	1.8	*2.2*
Biomass Burning **(BB)**	3.8	*3.8*	6.3	*4.6*	2.1	*1.7*
Nitrate rich + BB	2.5	*4.1*	5.1	*5.3*	0.8	*1.5*
Soil	3.2	*3.8*	2.9	*5.3*	3.5	*2.4*
Traffic **(TR)**	2.0	*0.9*	1.7	*1.0*	2.2	*0.7*

Due to the high variability of source contributions in time, SD values calculated for longer periods +can be higher than AV values period.

Remaining work

Methodology for the ultrafine aerosol particles' chemical identification will be elaborated.

Related publication

[1] M.G. Perrone, S. Vratolis, E. Georgieva, S. Török, K. Šega, B. Veleva, J. Osán, I. Bešlić, Z. Kertész, D. Pernigotti, K. Eleftheriadis and C.A. Belis: *Sources and geographic origin of particulate matter in urban areas of the Danube macro-region: The cases of Zagreb (Croatia), Budapest(Hungary) and Sofia (Bulgaria)*, Science of the Total Environment **619–620,** 1515–1529 (2018)

STRATEGIC RESEARCH GROUP ON THE CHALLENGES OF RENEWABLE ENERGY BASED SYSTEMS

Bálint Hartmann, Attila Kazsoki, Lilla Visnovszky, Bálint Sinkovics, Viktória Sugár

Objective

The aim of the first year of our research was to show the effect of intermittency on power-production forecasting for solar photovoltaic units by the use of qualitative examinations. Characteristic, weather-related power-production time series data were formulated by clustering the collected temporal data of photovoltaic units. State-of-the-art forecasting methods were compared, focusing on their typical errors and their potential involvement in system operation. A penetration level was determined, at which the effect of behind-the-meter (non-metered) photovoltaic units can already be identified in the error of system level load forecasting.

Methods

K-means clustering was used to create characteristic groups of solar photovoltaic power-production data. Inputs of the clustering were daily clear sky indices, daily average and maximal cloud cover [%] and average and maximal hourly gradients [kW/m2/h]. Forecasting methods were compared from the aspect of forecast horizon and utilized methodology (physical, statistical of hybrid).

Results

Focal point of the first project year was to perform a qualitative assessment of the effect of intermittent solar photovoltaic power-production forecasts on load forecasting, in order to develop an adequate model of weather-dependency for later research phases. Photovoltaic power-production and related weather data were collected from many locations in Hungary which have been used to determine necessary qualitative indices of the time series data (e.g. clear sky index, variability index) and thus to cluster characteristic behaviour. K-means clustering was used to create three and four groups of data. Quality of clustering has been tested with calculating average distance between data points and cluster means. A literature review has been performed on other grouping methods, and selected methods were also applied to the dataset.

Considering the effect of behind-the-meter solar photovoltaic units on the load curve of the power system, neural networks were used to recreate a forecasting process of the transmission system operator. As the operator currently does not use any learning algorithm, the exact methods have been chosen by comparing effectiveness of multiple structures (e.g. multilayer perceptron, long short-term memory). Forecasting has been created in a Keras environment (a special software for modelling neural networks).

Collection of raw topological data of Hungarian medium voltage distribution networks have been started; all gathered data have been made available by the distribution system operators. Regarding the six distribution areas of the country, representative networks have been received for two areas and complete network data have been received for four of them. A unified data format has to be created due to the different structure of the received information; development of this format has been started.

Remaining work

The research project has a span of four years; focus of the second year is the clustering of medium-voltage distribution networks.

Related publications

[1] G. Ódor and B. Hartmann: *Heterogeneity effects in power grid networks*, Phys. Rev. E **98**, 022305 (2018)

[2] V. Sugár, A. Talamon, A. Horkai, M. Kita: *Architectural style in line with energy demand: typology-based energy estimation of a downtown district*, Energy and Buildings **180:** 1-15 (2018)

REDOX CONDITIONS IN BODA CLAYSTONE SAMPLES USING THE Fe^{2+}/Fe^{3+} RATIO DETERMINED BY MÖSSBAUER SPECTROSCOPY

Károly Lázár, Sándor Stichleutner

Objective

The Boda Claystone Formation (BCF) is a potential host rock for deposition of high level nuclear waste (e.g. spent nuclear fuel). From the point of view of migration of various radionuclides, the redox properties may also play a role. These properties can conveniently be characterized by ^{57}Fe Mössbauer spectroscopy via determination of the Fe^{2+}/Fe^{3+} ratio in minerals of BCF.

Methods

^{57}Fe Mössbauer spectroscopy was used primarily.

Results

Several samples were collected from three different regions of BCF, namely from boreholes drilled in the Western Anticline and Gorica block of the Mecsek Mountains and from an exploratory drift (alpha-1) at ca. 1000 m below ground level in the same region. The oxidative environment of the formation of minerals in the Perm geological period (~ 260 M year ago) is clearly shown in the samples. Namely, most of the samples contain iron oxide (hematite, Fe_2O_3) and the primary oxidation state of iron is Fe^{3+} in other clay minerals as well (e.g. in illite, Fig. 1). In some exceptional cases reductive strata were also formed, and the samples from these regions exhibit solely the presence of Fe^{2+} (Fig. 2). In certain cases, in samples originated from deeper regions (e.g. the alpha-1 drift) the presence of other iron containing minerals (e.g. ankerite) can also be revealed by Mössbauer spectroscopy (Fig. 3) [1].

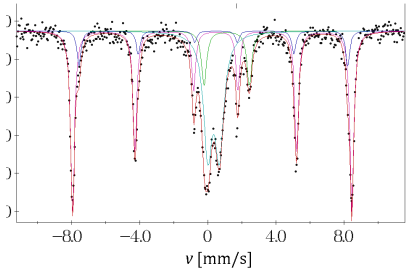

Figure 1: Typical Mössbauer spectrum, displaying the sextet of hematite and doublets of illite.

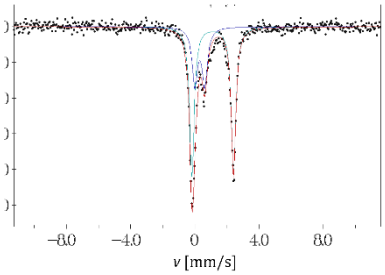

Figure 2: Spectrum from an exceptional strata formed under reducing conditions (Fe^{2+} ions in the doublets of illite and pyrite)

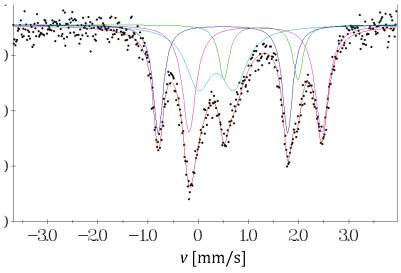

Figure 3: Spectrum of a sample displaying the presence of ankerite ($CaFe(CO_3)_2$) in addition to illite and hematite

The BCF is a consolidated formation, the minerals are well stabilized in it. Participation of iron ions in redox processes is probably restricted, since they are supposed to proceed primarily in the pore filling brine

Related publication

[1] K. Lázár and S. Stichleutner: *Mössbauer spectroscopic studies on samples from Boda Claystone Formation*, Report, 22 pages (2017)

V. NUCLEAR ANALYSIS

COORDINATED RESEARCH PROJECT ON PHOTONUCLEAR DATA AND PHOTON STRENGTH FUNCTIONS

Tamás Belgya, László Szentmiklósi

Objective

The main goals of the IAEA Coordinated Research Project (CRP) are to update the Photonuclear Data Library (1999) and to generate a Reference Database for Photon Strength Functions (PSF). Further goals are to measure photonuclear cross-section data where needed, update existing evaluations and evaluate new photonuclear data (including total photoabsorption cross sections, partial photonuclear cross sections and photoneutron spectra), to measure PSFs where needed, to compile, assess and evaluate existing photon strength function data, to develop and use theoretical tools to make recommendations and extrapolations to mass regions where no data exist, and to propose new measurements where needed [1].

Methods

The methodology is well described in the further goal of the CRP. Out of these tasks our duty is to perform (n,γ) experiments which enables one to test various types of PSFs. To do that we worked out an analysis methodology, including the writing of a spectrum shape modelling software for analysis of (n, γ) spectra that is able to handle any kind of theoretical description of PSFs.

Results

The measurements task is being fulfilled; two results (measurements on ^{232}Th and ^{242}Pu samples) can be found in the report entitled "The CHANDA Transitional Excess' in this yearbook. Beside these experiments, new experiments were performed on enriched ^{73,74}Ge samples and articles have previously been published in high quality journals on the ^{77}Se, ^{196}Pt and ^{114}Cd nuclei. In the past year the simulation software was developed on the ^{113}Cd(n, γ)^{114}Cd spectrum to provide a high resolution result (with 10 keV resolution in gamma energy) instead of the previously published 200 keV resolution. This enables us to view in much more detail the spectrum shape and to check the intensity agreement between modelling and measurements on discrete gamma rays. The achieved best description can be seen in Fig. 1. For level density the Constant Temperature Model (CTM) was used. For PSFs the so called Triple Lorentzian (TLO) was used for E1 gamma transitions, Reference Input Parameter Library (RIPL) prescriptions for M1 and E2 transitions, and a special type of low energy enhancement for E1 transitions were used in the modelling [1-3].

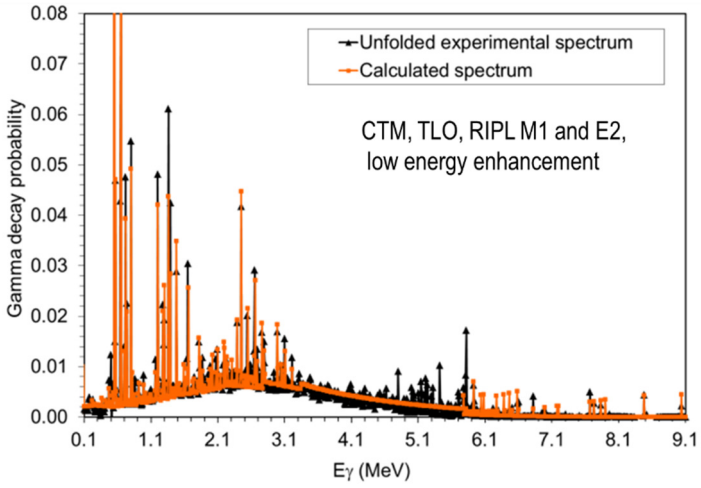

Figure 1: Agreement of a simulation of the unfolded ^{114}Cd gamma-ray spectrum with experiment for the ^{113}Cd neutron radiative capture reaction.

Remaining work

Preparing publications on modelling of unfolded radiative neutron capture spectra to test global prescriptions of PSFs to be determined next year at IAEA 2nd CRP meeting. Based on the quality of the descriptions, make recommendations for model, experimental PSFs, and level densities, which are also needed in the simulations.

Related publications

[1] 2nd year report of the CRP: https://www-nds.iaea.org/CRP-photonuclear/

[2] Talk at the 6th Oslo workshop on PSFs (http://tid.uio.no/workshop2017/) was presented.

[3] T. Belgya, L. Szentmiklósi, R. Massarczyk, R. Schwengner, A. R. Junghans, and E. Grosse: "*High-resolution study of the ^{113}Cd(n, γ) spectrum by statistical decay model with discrete levels and transitions*" in EPJ Web of Conferences, 2017, vol. 146.

IRRADIATION OF HIGH-ENTROPY ALLOYS

Margit Fábián, Dénes Párkányi, Attila Kovács

Objective

To develop and study High Entropy Alloys (HEA), which are loosely defined as solid solution alloys that contain five/six principal elements in equal or near equal atomic percentages. The concept of high entropy introduces a new possibility for developing advanced materials with unique properties which cannot be achieved by the conventional micro-alloying approach based on only one dominant element. The relative complexity seems to be a blessing, it leads to very interesting and useful properties, including high-strength at both room and elevated temperatures, low temperature toughness, high wear-resistance and irradiation resistance, all of which make HEAs attractive for various structural applications, and finally, the general corrosion resistance is much better than that of conventional 304-stainless steel.

Methods

BAGIRA1V1 Reactor irradiation loop – This irradiation rig in the Budapest Research Reactor (BRR), in connection with the hot laboratory, is capable of participating in research projects, as well as being useful for customized irradiation and post-irradiation examination. The gas cooled irradiation rig named Budapest Advanced Gas-cooled Irradiation Rig with Aluminium (BAGIRA) has been operated since 1998 at BRR. Twenty-seven different irradiation campaigns have been performed, testing irradiation ageing of reactor and fusion devices and many structural materials, including low alloyed and stainless steels, Al, Ti and W alloys, ceramics etc. The samples were chosen from materials based on studies done by neutron diffraction (ND), scanning electron microscopy (SEM) investigations, potential radiation hardness for applications in claddings and container systems but for which neutron data is missing or very scarce. Some of their physical properties, mainly structural and optical ones were measured before the irradiation and will be measured after this campaign to evaluate the impact of neutron exposure on these key properties.

Results

Based on the previous considerations we intend to study three samples: Mo6,66-Cr13,88-Fe36-Ni38,33-W5,15, Al8-Mo5-Nb5-Cr22-Fe5-Ni55 and Ni29,5-Fe39,8-Cr20-Mo6-W4,7. 2 target boxes were used for the irradiation of the materials, shown in Figure 1. The HEA specimens were irradiated in the Bagira 1v1 irradiation loop for 576 hours from 11/04/2017 to 08/05/2017.

Figure 1. Target boxes 4. and 5.

Table 1: The measured flux data

Target position	thermal flux $cm^{-2}s^{-1}$ (E<0,025eV)	fast flux $cm^{-2}s^{-1}$ (E>1,5MeV)
4	7.10E+13	4.90E+13
5	5.80E+13	4.40E+13

Table 2: Calculated fluence

Target position	Calculated fluence neutron cm^{-2} (E>1,5MeV)
4.	1.0E+20
5.	9.1E+19

The target boxes were carefully unloaded into a basket and taken down into the hot cells using an elevator, to avoid damage to the sensitive HEA materials. Unfortunately, the activation level is so high that we couldn't measure at this time (2017 November 20). When it's possible, we intend to study the structure of the irradiated samples.

Intense research efforts are underway to develop and study high-entropy alloys with exceptional nuclear engineering properties. The present work addresses the fundamental need to understand the structural properties of HEA alloys.

Remaining work

The evaluation of the chemical-physical and mechanical properties are in progress.

Related publication

Manuscript in preparation.

APPLICATIONS OF NUCLEAR ANALYTICAL METHODS

Zsolt Kasztovszky, László Szentmiklósi, Boglárka Maróti, Ildikó Harsányi, Zoltán Kis, Veronika Szilágyi, Katalin Gméling

Objective

Elemental compositions of various samples have been measured using prompt-gamma activation analysis and instrumental neutron activation. The compositional data provided useful information for diverse fields of research, such as catalysis, material science, geochemistry and heritage science. Within the project, the activities related to an OTKA grant and the EU-funded NMI3-II and IPERION CH projects were supported, too.

Methods

PGAA with cold neutrons has been used in combination with NAA and portable XRF to measure major, minor and trace element components of the samples, so as to benefit from the complementarities of these methods.

Results

Heritage Science (Archaeometry)

- Partly related to a project supported by the Hungarian Scientific Research Fund (OTKA) that finished in March 2017, the compositions of polished stone axes made of metamorphic rocks have been measured. A small set of nephrite, serpentinite, metaandesite, blueschist, etc. archaeological and geological samples from Hungarian museums and from fieldwork have been analysed. The aim of the study is to identify the origin of the raw materials (i.e. provenance of the objects). Two manuscripts have been submitted to summarize the results about stone tools made of high pressure metamorphic rocks [1, 2].

- Chipped stone archaeological objects (fragments of blades, arrow heads, etc.) uncovered in today's Poland and Romania have been analysed by PGAA, in order to determine the provenance of their raw material. A paper about the comparative study of PGAA, pXRF and NAA methods used in provenance of archaeological obsidian has been published in Quaternary International [3]. A similar study has been performed on Korean obsidian, using PGAA and energy-dispersive XRF [4]. Another study of rare mahogany obsidian variety has been performed using the PGAA, SANS, Mössbauer Spectroscopy and Transmission Electron Microscopy, in order to understand the formation process and determine the object's provenance [5].

- Various sets of historical Byzantine, Medieval and Murano glass fragments have been analysed to trace the evolution of coloured glass production. With PGAA and PIXE it was possible to associate chemical elements with different colours [6].

- In the frame of different projects coordinated by other users (Lendület, OTKA, "Bakota"), different historical bronze objects, such as axes, a spearhead, spirals, were analysed by PGAA and pXRF to determine their chemical composition. Additional information was obtained using neutron radiography. Based on the results (e.g. the Sn, As and Ni content), conclusions regarding the production technique (casting and annealing) can be drawn. [7]

- 20 pieces of 6th century ceramics from Szólád were analysed with PGAA and NAA methods. During the pottery analysis, additional thin section petrography was carried out at the Eötvös Loránd University. Using petrographic and chemical data in a mixed-mode statistical analysis, a more precise grouping of the objects was possible to be achieved. Two main groups and four non-grouped samples were defined. The two groups were probably made in the same geological area, while the latter unique samples can be defined as import wares. These results will be a part of the PhD thesis of Katalin Bajnok (Wigner Research Centre for Physics).

Geology and Environmental research

- We measured the boron content in aleurolit samples from the Boda Claystone Formation. The clay minerals preferentially build boron into their crystal structures; thus their boron contents (≥ 200 μg/g) are well above that of normal rocks which are forming the earth crust.

- There were 7 more andesite rocks from the King George Island, Antarctica to analyse with PGAA and NAA to compare and complement previous results from other geoanalytical laboratories and complete the geological conclusions.

- Pieces from the Allende meteorite were measured with PGAA as a preliminary study for long-term reactor irradiation studies and neutron activation analysis of different types of meteorite samples to be made at a later date. Short PGAA, long PGAA and decay measurements provided the results similar, within the uncertainty limits, to those results measured in 2007 in our laboratory (and also to those in literature).

- Using PGAA and NAA measurements, our laboratory took part in an IAEA organized inter-laboratory comparison

study of WEPAL (*Wageningen Evaluating Programs for Analytical Laboratories*) soil (ISE - *International Soil-Analytical Exchange*) and plant (IPE - *International Plant-Analytical Exchange*) samples with the excellent results agreeing with the reference data and that of other participating laboratories.

- A pilot study on 3 fossilized echinoids (sea urchins from the Middle Miocene) has been done at the NIPS-NORMA station. Neutron tomography, as well as bulk PGAA of a restricted volume within the investigated specimens is expected to provide compositional information both on the calcium carbonate shell and the inner part (stomach, divided into five parts) of the sea urchins. Such information could help ecologists and sea biologists to reconstruct the ancient paleo-environment.

Chemistry and Material science

- The compositions of orthodontic archwires were measured by PGAA at BNC and with pulsed-beam PGAA at ISIS (Neutron and Muon Source at the Rutherford Appleton Laboratory of the Science and Technology Facilities Council, on the Harwell Science and Innovation Campus in Oxfordshire). The two techniques were found to be complementary for some elements, while for most cases steady-state PGAA still offered better detection conditions [10]

Remaining work

We will continue the applications of PGAA and NAA related to thematic research projects and also ad-hoc proposals coming from international TNA projects (IPERION CH, C-ERIC).

Related publications

[1] Zs. Bendő, Gy. Szakmány, Zs. Kasztovszky, K. T. Biró, I. Oláh, A. Osztás, I. Harsányi, V. Szilágyi: *High pressure metaophiolite polished stone implements from Hungary: Na-pyroxenites, eclogites and related rocks*, submitted to Archaeological and Anthropological Sciences (in press)

[2] B. Váczi, Gy. Szakmány, E. Starnini, Zs. Kasztovszky, Zs., Bendő, F. A. Nebiacolombo, R, Giustetto R. Compagnoni: *Characterization of HP meta-ophiolite boulders and cobbles from northern Italy primary outcrops and secondary deposits, as possible raw material sources for the production of "greenstone" prehistoric tools: petrographic investigation and archaeological assessment,* European Journal of Mineralogy (accepted)

[3] Zs. Kasztovszky, B. Maróti, I. Harsányi, D. Párkányi, V. Szilágyi: *A comparative study of PGAA and portable XRF used for non-destructive provenancing archaeological obsidian*, Quaternary International **468** 179-189 (2018)

[4] Y-J. Jwa, Yi, S; M-E. Jin, Zs. Kasztovszky, I. Harsányi, G-M. Sun: *Application of prompt gamma activation analysis to provenance study of the Korean obsidian artefacts*, Journal of Archaeological Science: Reports **20** 374–381 (2018)

[5] Zs. Kasztovszky, K. Lázár, V. Kovács Kis, A. Len, J. Füzi, A Markó, K T. Biró: *A novel approach in the mineralogy of Carpathian mahogany obsidian using complementary methods*, Quaternary International **467** 332-341 (2018)

[6] B. Constantinescu, D. Cristea-Stan, Z. Szőkefalvi-Nagy, I. Kovács, I. Harsányi, Zs. Kasztovszky*: PIXE and PGAA – Complementary methods for studies on ancient glass artefacts (from Byzantine, late medieval to modern Murano glass),* Nuclear Instruments and Methods in Physics Research B **417** 105–109 (2018)

[7] B. Maróti, Z. Kis, Zs. Kasztovszky, G. Szabó, J. G. Tarbay, G. Wilhelm, Á. Király, V. Kiss: *Production and use of bronze spirals in the 2nd Millennium BC Carpathian Basin* (poster), NINMACH 2017, 11-13 Oct 2017, Budapest, Hungary

[8] D. Atkins, J. Beaucour, T. Pirling, U. Koester, N. Kardjilov, F.Ott, E. Ando', A.Tangettini, I. Tomandl, I. Groutso, C. Montet-Beaucour, I. Matuschevskaya, V. Danilovitch, S. Dernovitch, V. Kochman, V. Lakiza: *Neutron and laboratory x-ray characterization of excavated Napoleonic artefacts from the Berezina Battlefield in Belarus* (oral presentation), NINMACH 2017, 11-13 Oct 2017, Budapest, Hungary

[9] M. I. Dias, M. I. Prudencio, Zs. Kasztovszky, Zsolt, B. Maróti, I. Harsányi, P. Flor*: Nuclear techniques applied to provenance and technological studies of Renaissance majolica roundels from Portuguese museums attributed to della Robbia Italian workshop,* Journal of Radioanaitical and Nuclear Chemistry **312** 205–219 (2017)

[10] K. V. Tian, G. Festa, L. Szentmiklósi, B. Maróti, L. Arcidiacono, G. Lagana, C. Andreani, S. Licoccia, R. Senesi, P. Cozza*: Compositional studies of functional orthodontic archwires using prompt-gamma activation analysis at a pulsed neutron source,* J. Anal. At. Spectrom. *2017, DOI: 10.1039/c7ja00065kr*

[11] M. Rogante, L. Rosta, Gy. Káli, Zs. Kasztovszky, Z. Kis, I. Kovács, B. Maróti, Z. Szőkefalvi-Nagy*: Neutron based archaeometallurgical investigation of Picenan and Roman age metal objects from the Academia Georgica Treiensis collection (Italy), STAR: Science & Technology of Archaeological Research,* ***3:2****, 1-14,* (2017) *DOI: 10.1080/20548923.2017.1372933*

[12] Several oral and poster presentations at the NINMACH 2017 conference, in 11-13 October 2017, Budapest, Hungary

Media appearance:

[1] A PGAA mérések bemutatása (B. Maróti): *Bronzkori rejtélyek c. film. MTA BTK Lendület Kutatócsoport (Kiss Viktória), Real Pictures Production*

DEVELOPMENT OF NUCLEAR ANALYTICAL TECHNIQUES, NUCLEAR DATA MEASUREMENTS & DISSEMINATION ACTIVITIES

László Szentmiklósi, Tamás Belgya, Boglárka Maróti, Katalin Gméling, Zoltán Kis, Dénes Párkányi, Ildikó Harsányi

Objective

To develop our analytical capabilities and know-how in Prompt-Gamma Activation Analysis (PGAA), Neutron Activation Analysis (NAA), X-ray florescence analysis (XRF), to accurately determine related nuclear data, to do basic research on nuclei, and to provide training and education for guest researchers and students

Methods

(n,γ) measurements, PGAA, NAA, portable XRF spectrometry (pXRF), evaluation of nuclear data and comparison to literature, computer programming, Monte Carlo modelling, teaching

Results

The measurement of new calibration data for high-energy detector calibration in NAA was completed. We produced ^{24}Na, ^{56}Mn, and ^{72}Ga by reactor-irradiation, and ^{116}In by guided cold neutron beam irradiation and determined relative emission probabilities. At a PGAA station, where the detector calibration is done on a routine basis up to 12 MeV gamma energy with a precision of about 1% for efficiency and about 0.01 keV for energy measurement, one can find ideal conditions to measure energies and relative intensities for such high-energy gamma emitters. We produced a coherent dataset of such energies and intensities for various nuclides and applied them for efficiency and energy nonlinearity calibration of other gamma spectrometers at the NAA and DÖME counting stations [1]. In combination with Monte Carlo calculations, they could form a basis of a more advanced detector calibration procedure in NAA.

A computer program to fit special spectrum regions of PGAA, i.e. the annihilation peak at 511 keV, the boron peak at 478 keV, the Ge-triangles, as well as complicated multiplets was programmed and validated [2]. This resulted in a substantial improvement in the precision of the peak fitting methodology, improving the trueness and precision of the analytical results for many elements. This software is linked to the ProSpeRo concentration calculation macro to facilitate its easy application in the daily routine.

The nuclear physics research program continued with the measurement, analysis and publication of ^{56}Fe [3], ^{239}Pu [4-5] and ^{54}Fe [6] isotopes. The latter study used accelerator mass spectrometry (AMS) to detect the trace amounts of isotopes produced by neutron capture. A new compilation of spectroscopic data for nuclear non-proliferation [7] applications was prepared and published with Lawrence Livermore National Laboratory and Lawrence Berkeley National Laboratory. In the framework of an IAEA Coordinated Research Project (IAEA CRP), the strength functions of Cd-114 [8] and Th-232 are under analysis. As a partner of an international collaboration a technical paper was published about the multi-detector facility and related data treatment [9] at Institute Laue-Langevin (ILL).

Digital pulse shape analysis using a CAEN digitizer's list mode was applied to study the rising edge of a gamma detector signal, in order to discriminate between single site and multiple site events, with the vision of improving the Compton suppression performance. The resulting 4 TB of data are still under analysis. This work was done in framework of a transnational access proposal at the PGAA station of Forschungs-Neutronenquelle Heinz Maier-Leibnitz, Munich (FRM II).

Several pieces of electronic waste were characterized by the joint use of neutron imaging and element analysis [10]. It was demonstrated that X-ray and Neutron Imaging, as well as prompt-gamma activation imaging and in-beam neutron activation provide complementary information to characterize such complex objects, and can reliably estimate their toxic- and valuable element contents.

The Termo RadEye SPRD dosimeter was calibrated with neutron-activated radioisotope sources at the pneumatic rabbit irradiation facility of the Budapest Research Reactor Facility.

Education and dissemination activities

- PhD course at Eötvös University, 'Nuclear Analytical Methods and their Application in Earth Sciences and Archaeometry I-II.'
- Central European Training School on Neutron Techniques 2017 (also with hands-on training materials [11])
- Iperion CH training school, Paris
- PGAA laboratory training for BME and ELTE students

Related publications

[1] L. Szentmiklósi, B. Maróti, D. Párkányi, I. Harsányi, Zs. Révay, *High-energy detector calibration data for k_0-Neutron Activation Analysis*, J Radioanal Nucl Chem **315** (3), 743–750 (2018), DOI: 10.1007/s10967-017-5651-x

[2] L. Szentmiklósi, *Fitting special peak shapes of prompt gamma spectra*, J Radioanal Nucl Chem, **315** (3) 663–670 (2018), DOI: 10.1007/s10967-017-5589-z

[3] R. B. Firestone, T. Belgya, M. Krticka, F. Becvar, L. Szentmiklósi, I. Tomandl: *Thermal neutron capture cross section for $^{56}Fe(n,\gamma)$*, Phys Rev C **95**, 014328 (2017)

[4] A. Gatera, T. Belgya, W. Geerts, A. Göök, F.-J. Hambsch, M. Lebois, B. Maróti, A. Moens, A. Oberstedt, S. Oberstedt, F. Postelt, L. Qi, L. Szentmiklósi, G. Sibbens, D. Vanleeuw, M. Vidali, and F. Zeiser: *Prompt fission gamma-ray spectral characteristics from $^{239}Pu(n_{th},f)$*, Phys. Rev. C **95**, 064609 (2017), DOI: 10.1103/PhysRevC.95.064609

[5] A. Gatera, T. Belgya, W. Geerts, A. Göök, F.-J. Hambsch, M. Lebois, B. Maróti, S. Oberstedt, A. Oberstedt, F. Postelt: *New prompt fission gamma-ray spectral data from 239Pu (n_{th}, f) in response to a high priority request from OECD Nuclear Energy Agency. The European Physical Journal Conferences.* ISSN 2101-6275. ***146*** . doi:10.1051/epjconf/201714604020

[6] A. Wallner, T. Belgya, K. Buczak, L. Coquard, M. Bichler, I. Dillmann, R. Golser, F. Kappeler, A. Karakas, W. Kutschera, C. Lederer, A. Mengoni, M. Pignatari, A. Priller, R. Reifarth, P. Steier, and L. Szentmiklósi*: Precise measurement of the thermal and stellar $^{54}Fe(n;g)^{55}Fe$ cross sections via accelerator mass spectrometry*, Phys. Rev. C. **96,** 025808 (2017), DOI: 10.1103/PhysRevC.96.025808

[7] A. M. Hurst, R. B. Firestone, B. W. Sleaford, D. L. Bleuel, M. S. Basunia, F. Becvar, T. Belgya, L. A. Bernstein, J. J. Carroll, B. Detwiler, J. E. Escher, C. Genreith, B. L. Goldblum, M. Krticka, A. G. Lerch, D. A. Matters, J. W. McClory, S. R. McHale, Zs. Revay, L. Szentmiklosi, D. Turkoglu, A. Ureche, and J. Vujic: *Developments in capture-γ libraries for nonproliferation applications*, EPJ Web of Conferences **146**, 09008 (2017), DOI: 10.1051/epjconf/201714609008

[8] T. Belgya, L. Szentmiklósi, R. Massarczyk, R. Schwengner, A. R. Junghans, and E. Grosse: *High-resolution study of the ^{113}Cd (n,γ) spectrum by statistical decay model with discrete levels and transitions.* The European Physical Journal Conferences **146,** 05009 (2017), DOI: 10.1051/epjconf/201714605009

[9] M. Jentschel, et al: *EXILL - a high-efficiency, high-resolution setup for gamma-spectroscopy at an intense cold neutron beam facility*. Journal of Instrumentation **12**, P11003 (2017)

[10] L. Szentmiklósi, M. Papp, Z. Kis, D. Párkányi, B. Maróti: *Characterization of electronic waste by nuclear analytical and imaging techniques*, SAAGAS26, Vienna, 21 Feb 2017, oral presentation

[11] 2 chapters (*Neutron imaging, Prompt Gamma Activation Analysis*) in Research Instruments at the Budapest Neutron Centre, Handbook of the Central European Training School on Neutron Techniques, ISBN 978-963-12-8757-8 (2017)

[12] T. Belgya, Z. Révay: *Prompt Gamma Activation Analysis (PGAA)*. Book chapter in Neutron Methods for Archaeology and Cultural Heritage, Springer International Publishing: 221-234 (2017)

SELECTED APPLICATIONS OF MÖSSBAUER SPECTROSCOPY

Károly Lázár, Sándor Stichleutner, Zoltán Klencsár

Objective and Methods

The potential for applications of two types of Mössbauer spectroscopy are demonstrated.

^{57}Fe transmission spectroscopy was used to track the migration and relocation of iron ions in a microporous zeolite analog and in mesoporous ferrisilicates. In another study on similar substances, the method of ^{57}Fe Mössbauer spectroscopy was combined with positronium lifetime measurements. Also products of a particular method used for preparation of nanodisperse metallic particles (Electric Explosion of Wires, EEW) were analyzed in order to track the simultaneous dominant processes in the procedure. Iron and various steel wires were exploded under paraffin oil, ethylene glycol and dimethyl siloxane. Finally, *^{197}Au Mössbauer spectroscopy* was used to study AuCu/Al_2O_3 (1:1 Cu:Au ratio) catalysts prepared by different procedures (with consecutive deposition or with co-precipitation) and used for selective oxidation of glucose and benzyl alcohol.

Results

^{57}Fe transmission spectroscopy: The coexistence of Fe^{2+} and Fe^{3+} ions and their relocation among various sites was observed both in microporous Fe-FER and Fe-MFI structures and in mesoporous Fe-MCM-41. Furthermore, the existence of combined μ-oxo dimers, $Fe^{3+}_{framework}$-O-$Fe^{2+}_{extra\text{-}framework}$ was also suggested in the microporous systems [1]. The results of the positronium annihilation measurements reveal a modest dependence of lifetime in the microporous pore structure, whereas in mesoporous structures the influence is more enhanced. The siting of iron was determined by Mössbauer spectroscopy. Addition of iron significantly shortened the lifetimes in mesoporous Fe-SBA-15 [2]. Beside metallic nanoparticles, a mixed oxidic-carbidic residue is also formed in various amounts in the EEW processes carried out in various media. Globules are primarily formed from molten droplets of the metal wire. The residue is formed from the interaction of the vaporized metal atoms with atoms of the decomposed liquid media (C, H, O), all in excited states in a short life-time plasma. As a typical example, the Mössbauer spectrum of the dominant fraction of products (metallic globules) is shown in Fig. 1. The spectrum can be decomposed to contributions of various Fe-carbide components, without any signal from the starting pure metallic iron [3,4].

^{197}Au spectroscopy was used to characterize nano-sized bimetallic AuCu/Al_2O_3 catalysts prepared by different procedures. The spectrum of the sample prepared with consecutive deposition is shown in Fig. 2. The Au_{core} species (central singlet) was attributed to a AuCu alloy with a modest (~ 5 at%) Cu content based on the isomeric shift value of this line. The Cu content of the bimetallic particles formed in the co-precipitated sample was slightly larger (~ 10 at%) [5]. Spectra of both catalysts can be decomposed into several components, namely to bare $Au_{surface(I)}$ (bright green doublet), to surface atoms interacting with the alumina support $Au_{surface(II)}$ (green doublet), and to an electron deficient $Au^{\delta+}$ state (purple doublet), induced and stabilized by CuO_x partly surrounding the AuCu nanoparticles.

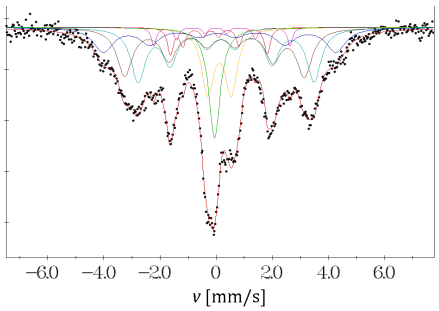

Figure 1: ^{57}Fe Mössbauer spectrum of metallic globules of the dominant fraction of products in electric explosion of iron wire in paraffin.

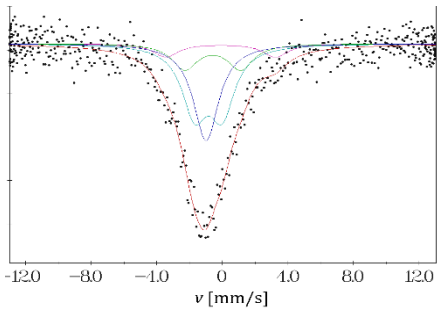

Figure 2: ^{197}Au Mössbauer spectrum of AuCu (1:1)/Al_2O_3 catalyst prepared by consecutive deposition at 4.2 K temperature

Related publications

[1] K. Lázár: *Redistribution of iron ions in porous ferrisilicates during redox treatments,* Pure and Applied Chemistry **89**, 471 (2017)

[2] Tran Quoc Dung and Károly Lázár: *Positronium lifetime measurements in micro- and mesoporous ferrisilicates,* Radiation Physics and Chemistry **139,** 49 (2017)

[3] K. Lázár, L. K. Varga, V. Kovács Kiss, Z. Klencsár and S. Stichleutner: *Vaporization of iron wires by electric explosion: Influence of cooling media,* ICAME 2017 conference (St. Petersburg, Russia, 03-08, Sept. 2017)

[4] K. Lázár, L. K. Varga, V. Kovács Kiss, Z. Klencsár, S. Stichleutner and L. Szabó: *Vaporization of steel by electric wire explosion in liquids,* MECAME 2017 conference (Jerusalem, Israel, 05-08, June 2017)

[5] S. Stichleutner, A. Beck, G. Nagy, D. F. Srankó, G. Sáfrán, F. Schmidt, and K. Lázár*: 197Au Mössbauer study of bimetallic Au-Cu/Al_2O_3 catalysts,* ICAME 2017 conference (St. Petersburg, Russia, 03-08, Sept. 2017)

NON-DESTRUCTIVE ANALYSIS OF METALLIC SAMPLES USING PGAA AND COMPLEMENTARY METHODS

Boglárka Maróti, László Szentmiklósi, Tamás Belgya

Objective

To determine the elemental composition of contemporary and ancient metal alloys non-destructively. To investigate the inner structure of heterogeneous metal objects as well as their method of manufacture. To extend the available Prompt Gamma Activation Analysis (PGAA) library for the more precise determination of alloying elements.

Methods

Different analytical methods were used for the extensive characterization of valuable objects. For the surface composition determination, a handheld X-ray fluorescence (XRF) spectrometer was used. Based on the visual information obtained with cold neutron tomography, different parts of the heterogeneous object were selected for bulk local chemical PGAA. For the PGAA library measurements, pure metal samples were analysed as well as their chlorine containing stoichiometric compounds.

Results

An ancient statue was characterized using the surface XRF technique, PGAA and neutron tomography. The monkey figure of the statue was found to be homogeneous tin-bronze, while the palm stub showed a more complex macroscopic structure. With the combination of PGAA, XRF and neutron imaging, important compositional and structural information were determined. Fig 1b shows the vertical cross section of the palm stub. Based on the neutron attenuation properties, three different regions could be distinguished (Fig 1b). From *A* to *C* the neutron attenuation increases. The least neutron absorbing part marked with *A* can be attributed to the tin-bronze material. Fig 1a demonstrates the three analysed volumes within the palm stub. For region 1 (Fig. 1a), besides iron, large amounts of Pb, S and H were detected. A smaller amount of Pb and S was detected at region 2, though the Pb/S ratio remained the same as in region 1, and some Sn and Cu were also seen. Neither Pb nor S was detected in region 3, but Sn and Cu were both there in large amount. Fe, H and Cl were found in all three regions. Surface-concentration measurements were carried out at several places using a handheld XRF spectrometer. In the surface region 5 to 10-times less Pb and S were detected, relative to the Fe, than in the bulk. All this means that the regions marked with *C* are rich in iron and hydrogen, while the material with an increased amount of Pb and S can be linked to the part *B* with intermediate neutron attenuation [1].

Previously a set of certified reference copper alloys was analysed with different PGAA setups (conventional PGAA, attenuated PGAA, high-resolution PGAA, in-beam NAA). During this research on reference materials, a discrepancy was observed between the tin results obtained by PGAA and the certified reference tin alloy composition values. This deviation was successfully overcome by introducing additional copper prompt gamma peaks and taking them into account when doing the interference correction (Fig 1c) [2].

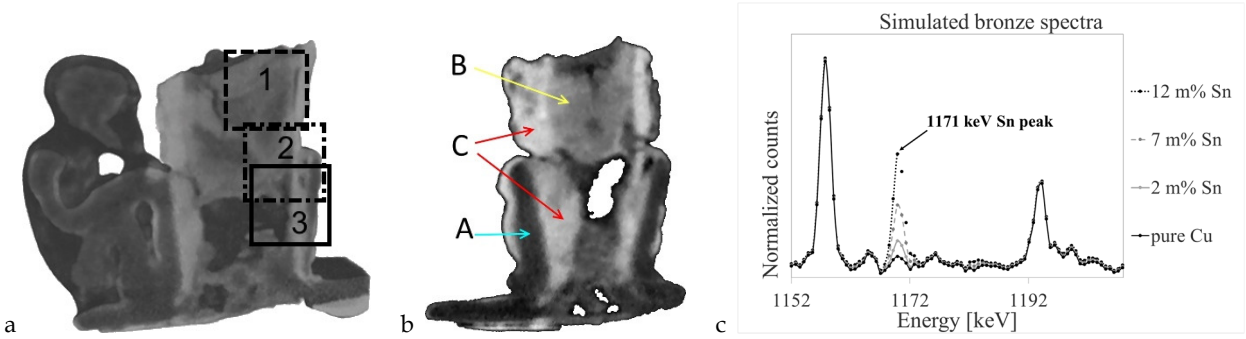

Figure 1: a) regions used for local chemical PGAA analysis at different parts of the palm stub, b) virtual cross section of the palm stub showing regions with different neutron attenuation (dark means low attenuation), c) low intensity Cu prompt gamma peak at the same 1171 keV energy as tin.

Remaining work

To summarize all the PGAA, pXRF, and neutron imaging results on certified reference copper alloys as well as on real ancient heterogeneous objects to finish the PhD thesis.

Related publications

[1] B. Maróti, Z. Kis, L. Szentmiklósi, E. Horváth, Gy. Káli and T. Belgya: *Characterization of a South-Levantine bronze sculpture using position-sensitive prompt gamma activation analysis and neutron imaging*, Journal of Radioanalytical and Nuclear Chemistry **312**, 367-375 (2017)

[2] B. Maróti, Zs. Révay, L. Szentmiklósi, K. Kleszcz, D. Párkányi and T. Belgya: *Benchmarking PGAA, in-beam NAA, reactor-based NAA and handheld XRF spectrometry for analysis of archeological bronzes,* Journal of Radioanalytical and Nuclear Chemistry **317**, 1151-1163 (2018)

and *1 poster and 2 oral presentations*

RADIOGRAPHY AND TOMOGRAPHY AT BRR

Zoltán Kis, László Horváth, László Szentmiklósi

Objective

To develop and apply imaging instrumentation and methodology at the Budapest Research Reactor (BRR).

Methods

The *energy distribution of the neutron beam* at the Neutron and X-ray Radiation (RAD) station has been measured by the activation foil method. In collaboration with the Paul Scherrer Institute (PSI), Switzerland, the development and improvement of *fast neutron sensitive screens* is being started. A systematic *investigation of casting defects* for ancient and modern objects and the *systematic study of porous materials* (geology, paleontology, ceramics) were carried out by evaluating tomographic datasets. T*he quality assurance of Budapest Research Reactor (BRR) control rods* continued. The *imaging of several objects with high importance* from cultural heritage organizations and from industry were carried out.

Results

During *fast neutron tomography* experiments a typical industrial object (a large part of an auto gear shift) was imaged by the best available commercial screen. The image (**Fig. 1.a**) clearly shows the advantage of the fast neutrons: both the metal and the H-containing parts can be visualized at once. A systematic *investigation of casting defects* for a Late Bronze Age axe (**Fig. 1.b**) revealed its porous structure and an inclusion, for which the material was measured by PGAI to be a region of lead enrichment formed during the casting process. The distribution of pore sizes was categorized into main regions: a small-pore region (numerous pores with a large cumulative volume) and a large-pore region (a few pores with less cumulative volume). The casting process of spheroidal graphite iron can be improved using our imaging results, which showed casting defects localized in a *brake system* (**Fig. 1.c**). Among the *porous materials* Nubian ceramics were investigated by neutron tomography. As a pilot study, the orientation of the voids and sherds in the space were visualized, as one can see in **Fig. 1.d**. This information is of primary importance for the study of the fabrication technique. These results suggest the use of coil-building in a group of samples, and possibly percussion forming in another sample group. In collaboration with the Museum of Fine Arts, Budapest, the neutron tomography of the statuette "Budapest Horse and Rider" attributable to Leonardo DaVinci was carried out. For the first time ever, we could show the detailed 3D inner structure and the remains of the lost wax casting technique **Fig. 1.e-f**, which helps in the interpretation in art history issues.

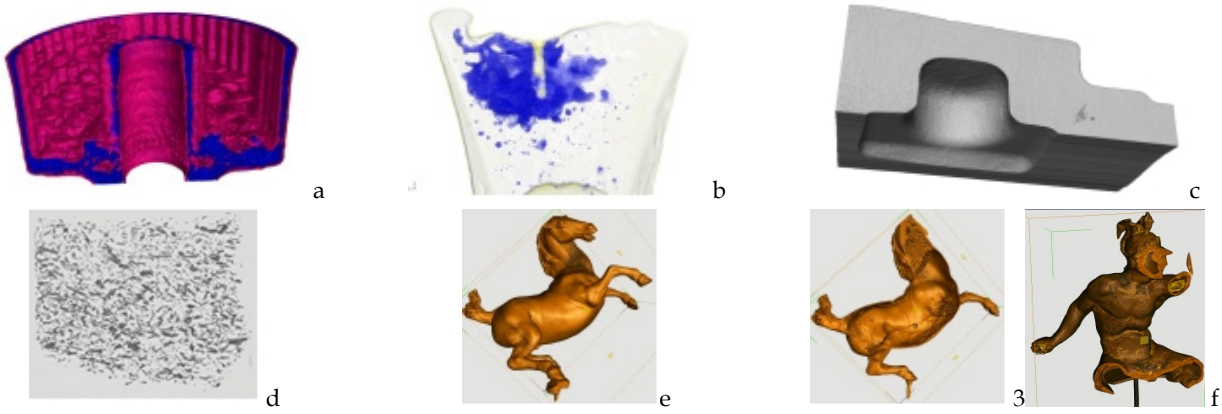

Figure 1: Neutron tomography results: see text for further information

Remaining work

In 2017 the *BRR was out of operation* for half a year. This fact has caused postponement of several experimental programs planned earlier. The evaluations of both the *energy distribution of the neutron beam* at the RAD station and the characteristics of the fast neutron scintillation screens were postponed to 2018. The investigation of the *phase transition of a supercritical fluid* by real-time imaging was postponed to a later time because of the lack of availability of the reactor and of human resources.

Related publications

[1] A. P. Kaestner, Z. Kis, M. J. Radebe, D. Mannes, J. Hovind, C. Grünzweig, N. Kardjilov, and E. H. Lehmann: *Samples to Determine the Resolution of Neutron Radiography and Tomography*. Physics Procedia **88**, 258-265 (2017)

[2] Z. Kis, F. Sciarretta, and L. Szentmiklósi: *Water uptake experiments of historic construction materials from Venice by neutron imaging and PGAI methods*. Materials and Structures **50**, 159 (2017)

[3] Z. Kis, L. Szentmiklósi, R. Schulze, and E. Abraham: *Prompt Gamma Activation Imaging (PGAI)*. In: N. Kardjilov, and G. Festa, (eds.): Neutron Methods for Archaeology and Cultural Heritage. pp. 303–320. Springer (2017)

[4] A. Kiss, M. Balaskó, L. Horváth, Z. Kis, and A. Aszódi: *Experimental investigation of the thermal hydraulics of supercritical water under natural circulation in a closed loop*. Annals of Nuclear Energy **100**, Part 2: 178–203 (2017)

[5] L. Szentmiklósi, Z. Kis, T. Belgya, B. Maróti, L. Z. Horváth, and M. Papp: *Roncsolásmentes képalkotás neutronokkal és röntgensugárzással a Budapesti Neutron Centrumban*. Fizikai Szemle **7-8**, 240-244 (2017)

[6] J. G. Tarbay, Z. Kis, and B. Maróti: *The Bottom of a Looted Cauldron: Part I.* Acta Archaeologica Academiae Scientiarum Hungaricae **68**(2), 219–240 (2017)

PROVENANCE STUDY OF LITHIC RAW MATERIALS OF STONE TOOLS FOUND IN THE CARPATHIAN BASIN

Zsolt Kasztovszky[1], György Szakmány[2], Zsolt Bendő[2], Katalin T. Biró[3], András Markó[3], Bálint Péterdi[4], Ildikó Harsányi [1]

[1]Centre for Energy Research, [2]ELTE Department of Petrology and Geochemistry, [3]Hungarian National Museum, [4]Mining and Geological Survey of Hungary

Objective

Prompt Gamma Activation Analysis (PGAA) has been used to investigate various lithic assemblages, chipped and polished stone tools made of obsidian, flint, radiolarite, and greenschist-metabasite varieties (high-pressure metamorphite, nephrite, serpentinite and greenschist). The aim of the research was fingerprinting, characterising and identifying important lithic sources of the most significant rock types. The results will contribute essentially to the knowledge on the „long distance" raw material sources and the system of contacts between the prehistoric communities in the Central European region. The absolute non-destructive feature of PGAA is highly important in the study of intact museum pieces. The project has started in April 2012, and finished – after a one-year extension – in April 2017.

Methods

The research plan consisted equally of geological sample collection in the field, conventional petrography (macroscopic and microscopic investigations), and instrumental analytical measurements. The principal analytical method used was PGAA. PGAA can quantify all the major elemental components and some trace elements in various rocks. It is unique in its capability for determination of the elements H and B. Occasionally we performed complementary measurements using portable X-Ray Fluoresence (XRF), Instrumental Neutron Activation Analysis (INAA) and Electron Para-Magnetic Analysis (EPMA). One other very important new method, the non-destructive Scanning Electron Microscope SEM/EDX analysis was developed and used to study the elemental and mineralogical composition of polished stone tools.

Results

During the whole project, we were able to perform all the planned field work and also most of the planned non-destructive analysis of the field samples as well as of the museum objects. However, in the fifth year, partly because of the limited number of reactor operational days, we could not make any further PGAA measurements for the project. We have summarized the analytical data in different databases, in order to draw conclusions. Altogether, about 500 samples were analysed by PGAA and about 170 by SEM/EDX.

Particular results: 1, Obsidian: The raw material of artefacts found in Romania, Poland and Hungary have been identified as Carpathian 1 type. Methodological studies about the complementarity of PGAA and XRF, as well as about the origin of mahogany obsidian were published [6, 7]. 2, Chipped stone tools made of silex: Various flint and radiolarite objects found at a Copper Age excavation in Erősd, Romania have been analysed by PGAA. Based on their composition we have shown thatmost of the pieces' raw materials are from long distance trade (Prut flint, Volhynian flint or Balkan flint), and only a small portion has a local origin (Eastern Carpathians). 3, Polished stone tools: The long distance import of Neolithic polished stone tools is proved by PGAA and SEM/EDX measurements. Raw material sources of nefrite, serpentinite, greenschist, blueschist and contact-metabasite objects found in the Carpathian basin, were identified in the surroundings (i.e. in the Western Alps, Jordanow mts., Eastern Alps, Apuseni Mts., etc. See Figure 1.

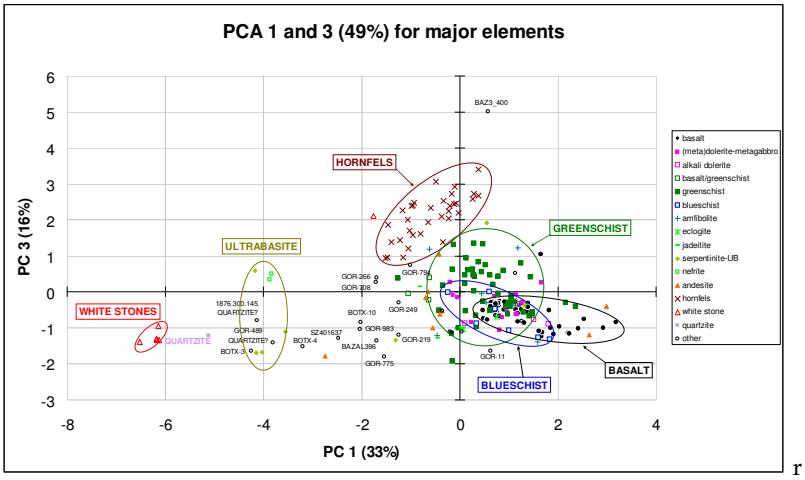

Figure 1: Classification of the measured rocks applying Principal Component Analysis

Related publications

[1] M. I. Dias, Zs. Kasztovszky, M. I. Prudêncio, A. C. Valera, B. Maróti, I. Harsányi, I. Kovács, Z. Szőkefalvi-Nagy: *X-ray and neutron-based non-invasive analysis of prehistoric stone artefacts: a contribution to understand mobility and interaction networks*, Archaeological and Anthropological Sciences **9,** 1-15 (2017)

[2] Y. Suda, A. V. Grebennikov, Y. V. Kuzmin, M. D. Glascock, K. Wada, J. R. Ferguson, J. C. Kim, V. K. Popov, S. V. Rasskazov, T. A. Yasnygina, N. Saito, H. Takehara, T. Carter, Zs. Kasztovszky, K. T. Biró, A. Ono: *Inter-laboratory validation of the WDXRF, EDXRF, ICP–MS, NAA and PGAA analyticaltechniques and geochemical characterisation of obsidian sources in northeast Hokkaido Island, Japan*, Journal of Archaeological Science: Reports **17,** 379-392 (2018)

[3] B. Váczi, Gy. Szakmány, Zs. Kasztovszky, E. Starnini, F. A. Nebiacolombo: *Előzetes eredmények a magyarországi nagynyomású metaofiolit anyagú csiszolt kőeszközök származási helyének pontosításához*, Archeometriai Műhely, XIV.2. 69-84 (2017)

[4] Zs. Kasztovszky: *Áttekintés a „Kárpát-medencében fellelt kőeszközök nyersanyagainak roncsolásmentes eredetvizsgálata" c. projektről,* Archeometriai Műhely, XIV.2. 61-68 (2017)

[5] F. Bernardini, E. Sibilia, Zs. Kasztovszky, F. Boscutti, A. De Min, D. Lenaz, G. Turco, R. Micheli, C. Tuniz, M. Montagnari Kokelj: *Evidence of open-air late prehistoric occupation in the Trieste area (north-eastern Italy): dating, 3D clay plaster characterization and obsidian provenancing*, Archaeol Anthropol Sci, DOI 10.1007/s12520-017-0504-7

[6] Zs. Kasztovszky, B. Maróti, I. Harsányi, D. Párkányi, V. Szilágyi: *A comparative study of PGAA and portable XRF used for non-destructive provenancing archaeological obsidian*, Quaternary International **468,** 179-189 (2018)

[7] Zs. Kasztovszky, K. Lázár, V. Kovács Kis, A. Len, J. Füzi, A. Markó, K. T. Biró: *A novel approach in the mineralogy of Carpathian mahogany obsidian using complementary methods*, Quaternary International **467,** 332-341 (2018)

[8] E. Kereskényi, Gy. Szakmány, B. Fehér, Zs. Kasztovszky, F. Kristály, P. Rózsa: *New archaeometrical results related to Neolithic blueschist stone tools from Borsod-Abaúj-Zemplén County, Hungary*, Journal of Archaeological Science: Reports, **17**, 581-596 (2018)

[9] Y-J. Jwa, S. Yi, M-E. Jin, Zs. Kasztovszky, I. Harsányi, G-M. Sun: *Application of prompt gamma activation analysis to provenance study of the Korean obsidian artefacts*, Journal of Archaeological Science: Reports **20,** 374–381 (2018)

[10] K. T. Biró, Zs. Kasztovszky: *Stone artefacts and neutrons - Case studies from Hungary*, Journal of Archaeological Science: Reports **19,** 669–673 (2018)

[11] Zs. Kasztovszky, V. Szilágyi, K. T. Biró, J. Zöldföldi, M. I. Dias, A. Valera, E. Abraham, M. Bessou, F. LoCelso, V. Benfante: *Chapter 6: Ceramics, Marbles and Stones in the Light of Neutrons: Characterization by Various Neutron Methods*, pp. 89-140. in Neutron Methods for Archaeology and Cultural Heritage, Eds. N. Kardjilov and G. Festa, Springer International Publishing Switzerland, 2017

DETERMINATION OF ^{235}U IN NANOGRAM QUANTITIES USING DELAYED NEUTRON COUNTING AT THE PNEUMATIC RABBIT SYSTEM OF THE BUDAPEST NEUTRON CENTRE

Szentmiklósi László, Hlavathy Zoltán, Janik József, Katona Csaba, Párkányi Dénes, Gméling Katalin, Kocsis Tímea

Objective

Delayed neutron counting (DNC) is an analytical technique for detecting the fissile content of unknown samples. The active interrogation, based on the neutron-induced fission of ^{235}U, requires an external source of neutrons. During this work, the pneumatic rabbit system of the Budapest Research Reactor was used for irradiation; this yielded a tremendous sensitivity improvement over neutron-generator and radioisotope-based devices.

Methods

The sample was sent into the reactor core for 1 minute. After irradiation it was transferred into the neutron detector via the pneumatic system. When the sample leaves the core, the system gives a timer signal. The Pulse Train Recorder (PTR-32) stored the neutron detector pulses and the associated time signals in list mode, and the time dependence of the neutron decay was restored by a program written for this project. The fitting amplitude A, after calibration, gives the amount of uranium.

Results

The reliable quantification of 100 ng of natural uranium (i.e. 1 ng ^{235}U) has become possible. As a continuation of the previous work in 2016-17, we optimized the equipment and the measurement procedure. The new pipeline of the pneumatic transfer system has shortened the return time of the sample from the reactor core to the detector; we have developed a better logging platform of the irradiation data; we modified the trigger electronics in order to eliminate the false triggers, which cured the previously observed timing uncertainties. We also worked out an evaluation method for the time dependence and quantification based on the nonlinear least squares method and derived the statistical errors of the measurement results. This was compared with the conventional time-window integration evaluation. The fluctuations of the measured concentration values were checked with repeated measurements; the observed standard deviation was higher than the fitted-model predictions by about a factor of 2 to 5. The method was finally tested on a geological sample series. It was also concluded that the uranium content of swipe samples can be quantified in this way.

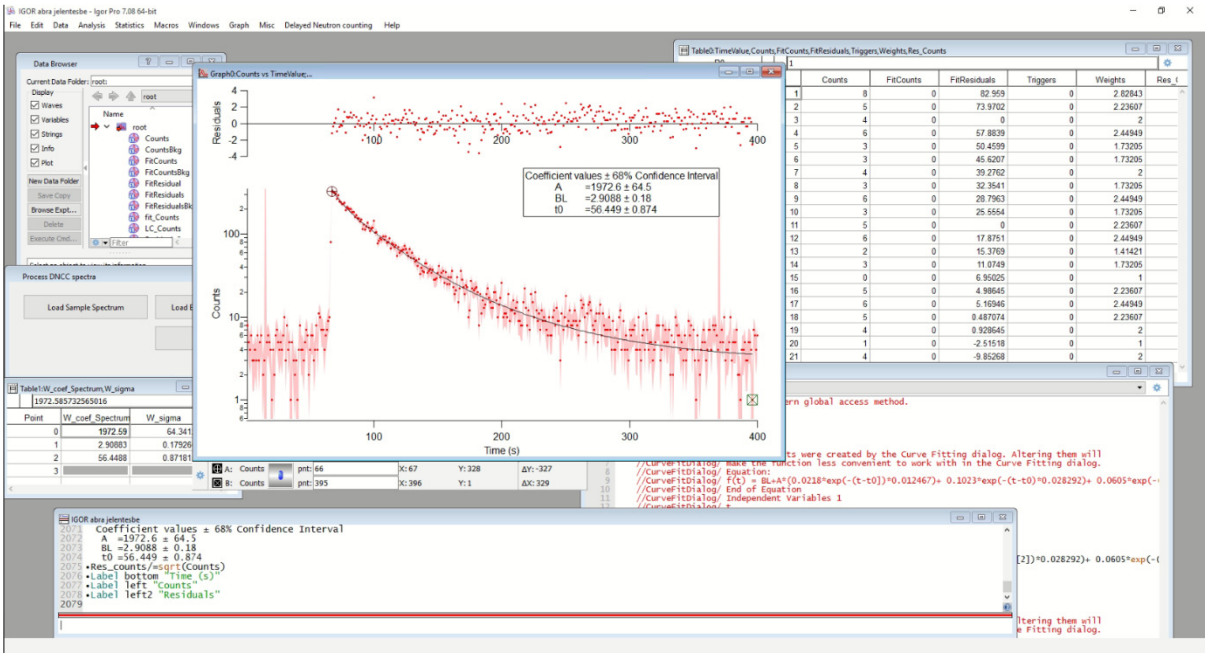

Figure 1. Data evaluation with a fitted model function

Related publication

[1] L. Szentmiklósi, Z. Hlavathy, J. Janik, Cs. Katona, D. Párkányi, K. Gméling, T. Kocsis: *Determination of ^{235}U in nanogram quantities via delayed neutron counting at the pneumatic rabbit system of the Budapest Neutron Centre,* OAH-ABA-14/17-M, EK-NAL-2018-275-001-M01, in Hungarian (2018)

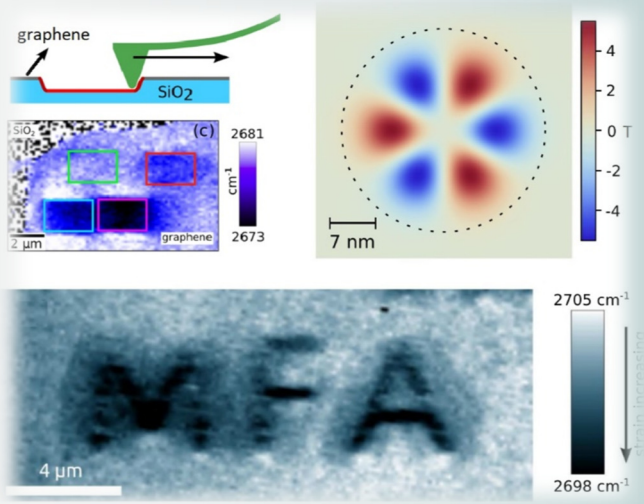

VI. RESEARCH AND DEVELOPMENT IN INSTITUTE OF TECHNICAL PHYSICS AND MATERIAL SCIENCES

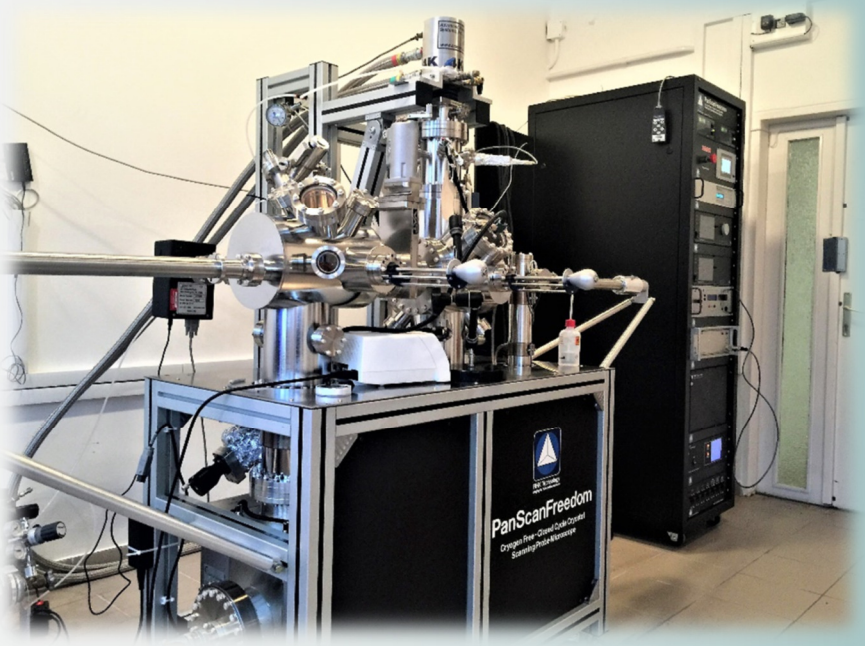

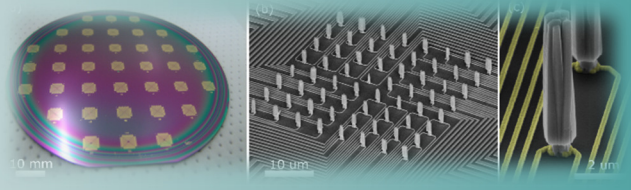

FORCE FEEDBACK AND TACTILE SENSING FOR ROBIN HEART SURGICAL ROBOT

(Intelligent Catheters in Advanced Systems for Interventions, ENIAC INCITE 621278, NEMZ_12-1-2014-0005)

J. Radó, Cs. Dücső, P. Földesy, Kamil Rohr, Z. Nawrat, and P. Fürjes

Minimally invasive robotic surgery (MIS) offers several advantages for the patients, although the lack of sensory feedback for the surgeon is one of the main barriers in its progress and widespread application. Gathering immediate multi-parametric information about the physical and anatomic conditions of tissues is crucial for the operator to precisely control the robotic actions. “Smart” laparoscopes with integrated MEMS sensors can provide such feedback and to improve the safety of these interventions.

Our goal was to develop a novel smart laparoscope for surgery robots with integrated 3D force sensors inside the grasper and on the tip of the device to measure the gripping strength and to provide tactile information about the different organs and tissues touched.

Force sensor chips for force feedback and tactile sensing applications

Piezo-resistive transduction principle is used to design and fabricate the 3D force chips. Accordingly, the piezoresistors were formed in the device layer of the SOI substrate wafer by ion implantations. Deformable membranes were formed by DRIE (deep reactive ion etching) process to minimize the lateral size of the chips. The SOI wafers provide uniform membrane thickness over the whole wafer. Anodic wafer bonding was applied to integrate the active Si to borosilicate glass for parallel formation of rigid substrate and ohmic contact between piezo-resistors embedded in the Si element and wire bonding pads on boron glass. The fabricated force sensor chips are shown in Fig. 1.

Electro-mechanical and system level integration

Two 3D MEMS force sensors were integrated in the laparoscopic head on a flex-PCB with dedicated preamplifiers and ADCs forming the pre-processing electronic circuitry. One sensor chip is on the tip of the lower jaw of the tweezers and the other one is inside the same element. The electrical connections were produced by wire bonding according to the architecture of the silicon-glass bonded structure. The MEMS force and tactile sensors were embedded in flexible polymer covering to ensure adequate mechanical stability and provide reliable force/load transfer to the silicon membrane. Fig. 2. shows the packaged sensor array on the flexible PCB.

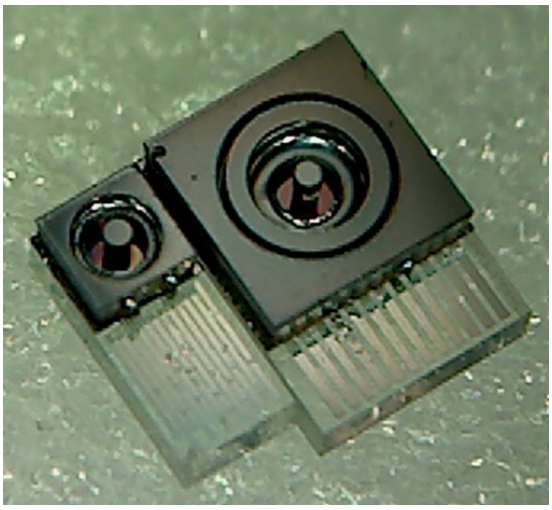

Figure 1: Individual force sensor chips: 1×2.5mm² chips for head mounted tactile sensing (left) and 2×3mm² for gripping force detection (right).

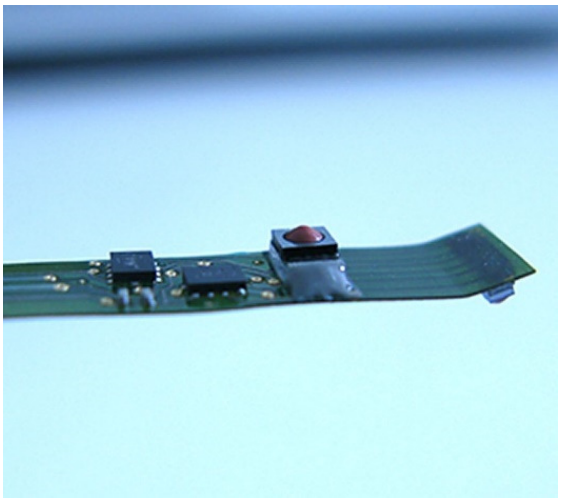

Figure 2: The flexible PCB with the packaged sensor array containing the tip mounted tactile sensor and the force sensor dedicated for force feedback measurement inside the laparoscope tweezers.

The laparoscope prototypes were printed by direct metal LASER sintering (DMLS) from EOS Stainless Steel GP1 medical grade stainless steel. For demonstration and to check the quality of the cast coverage, transparent silicone was used, whereas in the final prototypes black, medical grade colorant masterbatch was mixed in silicone to eliminate the effect of light on the noise, stability and accuracy of the piezoresistors in the MEMS chips.

Figure 3: The medical grade stainless steel laparoscopic tweezers with the integrated electronics covered in the (transparent) flexible biocompatible elastomer.

The developed MIS tool was mounted on the robotic arm, and the robot control as well as the sensing capability were analysed using the force feedback. The fabricated stainless steel tweezers were integrated into the mechatronic system of the proposed smart laparoscope tool. The full functional laparoscopes are capable to drive the tweezers by motor and transfer the electronic signals from the signal processing electronics to the I2C-CAN communication board.

RobinHeart Minimal Invasive Surgery robot with force / tactile feedback

The laparoscope was fixed on the arm of the ROBIN HEART surgery robot and connected to the manipulator via CAN BUS communication. Preliminary tests were accomplished to evaluate the force and tactile signals of the integrated sensors during interventions. The information was successfully applied to provide haptic feedback for the operator by a specific controller (Fig. 4). In the preliminary test the signals of both sensors were utilized to control the movement of the arm and the jaw of the gripper. When the laparoscope touches a surface and the emerging force in the tip tactile sensor reaches a pre-set value, an actuation routine stops the forward movement, regardless the actions of the operator with the manipulator head (Fig. 4.) Tactile measurements were also implemented on artificial and real animal tissues to prove the applicability of the device for biomechanical screening during MIS surgery.

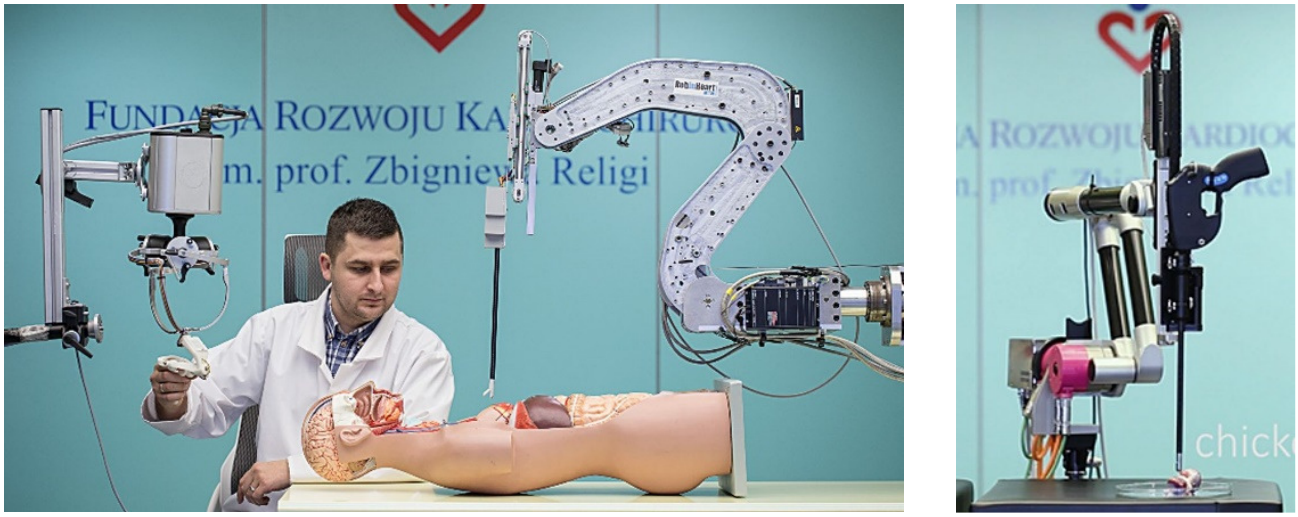

Figure 4: „Smart laparoscopes" integrated in the ROBIN HEART surgery robot systems.

Summary

In this work the project partners demonstrated the design and manufacturing of the MEMS force sensors, the near-chip signal pre-processing and digital communication electronics, reliable electrical and mechanical packaging of all components and mainly the functional validation of the integrated sensor array system. The functionality of the electronics components was validated and the whole laparoscope mounted sensor system (including the electronics) was integrated with the robot control systems. By integration of this "smart" tool into the surgery robot system an advanced human-machine synergy was demonstrated applying two-directional haptic control. The first demonstration of force feedback in ROBIN HEART robotic surgery system was successfully achieved.

CORROSION RESISTANCE OF NANO-SIZED SiC-RICH COMPOSITE COATINGS PRODUCED BY NOBLE GAS ION MIXING

A.S. Rácz, Zs. Kerner, A. Németh, P. Panjan, L. Péter, A. Sulyok, G. Vértesy, Zs. Zolnai, and M. Menyhárd

Silicon carbide (SiC) is a material that has attracted considerable interest for a long time, particularly due to its high temperature strength, thermal shock resistance, good thermal conductivity and its inertness to exposure in corrosive environments. In thin film form SiC is used in micro/nano-electromechanical system (M/NEMS) which are operating in harsh-environments e.g. automotive and aerospace applications such combustion processes or gas turbine control. Different methods can be used for producing SiC thin films e.g.: physical and chemical vapour deposition. However, these methods need elevated temperature which might be disadvantageous by certain substrates. Ion beam mixing might also be used to overcome the high activation barrier of the compound formation since it creates far from equilibrium conditions, where the apparent activation barrier might be much lower.

We have applied noble gas Ar^+ and Xe^+ ion irradiation on different C/Si/C/Si/C/Si (substrate) multilayer structures (with individual layer thicknesses falling in the range of 10-20 nm). The irradiation took place at room temperature in the energy and fluence ranges of 40-120 keV and 1-6x10^{16} ion/cm^2, respectively. The effects of ion irradiation including the in-depth distribution of the SiC produced was determined by AES depth profiling. The thickness of the SiC-rich region was only some nanometers and it could be tailored by changing the layer structure and/or the ion irradiation conditions.

Fig. 1 presents the effect of the ion irradiation process on a 6x10^{16} Ar^+/cm^2, 40 keV irradiated sample.

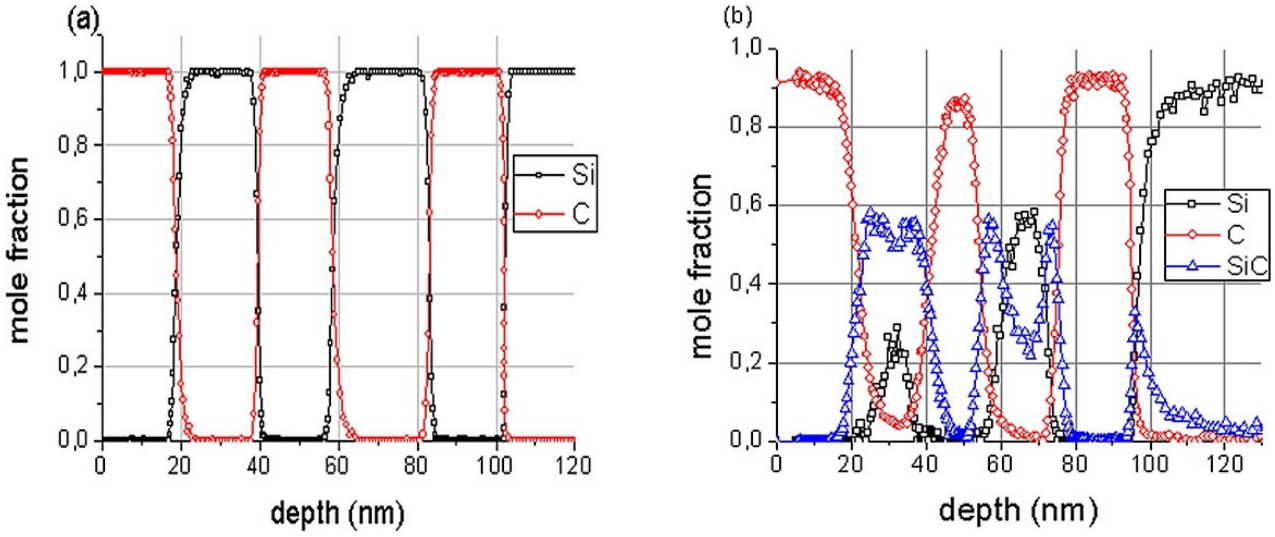

*Figure 1: AES depth profiles of the **(a)** pristine, and **(b)** irradiated (6x10^{16} Ar^+/cm^2, 40keV).*

An AES depth profile is also shown of a non-irradiated sample as a comparison (Fig. 1a). In this case all initial interfaces are sharp but due to irradiation serious changes occur. The first Si layer (below the topmost C layer) practically disappears; it was consumed by the SiC production. On the other hand, only a part of the second Si layer was converted to SiC. This can be understood considering the projected range of the 40 keV Ar^+ being about 40 nm. The last carbon layer remained more or less untouched. Considering the shape of the SiC distribution e.g. at 50 and 70 nm one can conclude that the SiC is growing from the Si/C interface.

To check the corrosion resistance of the SiC rich layer potentiodynamic electrochemical test in 4M KOH solution were performed. The potentiodynamic corrosion test provides the quantitative characterization of the coating layer. The measured corrosion resistance of the SiC-rich layers was orders of magnitude better than that of pure silicon. To find the correlation between the amount of SiC and corrosion resistance a new quantity, the effective areal density, was introduced. Fig. 2 shows that a reasonable correlation between these two quantities has been established. In this way a connection between IBM and the corrosion resistance of the layer was given. Since the amount and distribution of SiC can be determined by TRIDYN simulation [G. Battistig, et al., J. Phys. D: Appl. Phys. 2016, 49, 185303-185311] one can predict the corrosion resistance for given sample and irradiation conditions. The method thus can be utilized to make tailored SiC coatings for e.g. sensors operating in harsh environments.

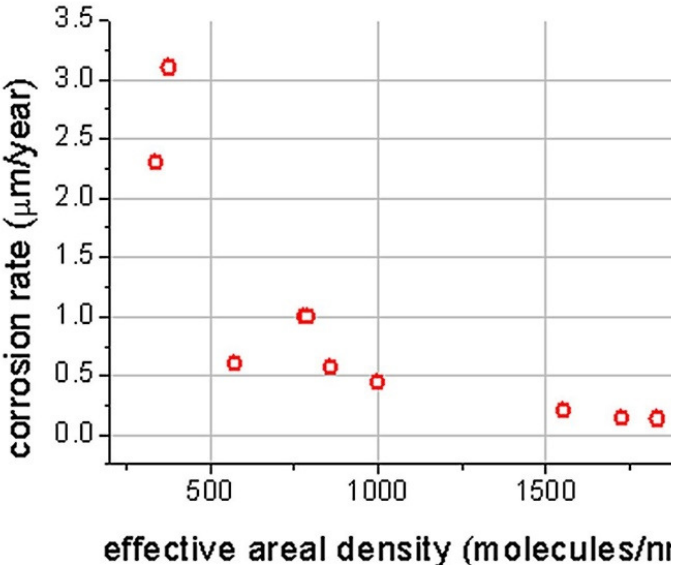

Figure 2: Corrosion rate vs effective areal density.

CATALYTICALLY ACTIVE SINGLE OXYGEN SITES IN THE BASAL PLANE OF 2D MoS_2 CRYSTALS

(ERC StG NanoFab2D 680263, Lendület LP2014-14)

J. Pető, P. Vancsó, T. Ollár (EK-FKL), P.B. Sorokin (MISis-Moscow), and L. Tapasztó

A major objective in catalysis is the atomic level identification and control of catalytically active sites for a specific reaction. Here we propose that this can be realized in molybdenum disulfide (MoS_2) through a simple oxidation process. In contrast to the generally accepted view of environmentally inert basal plane, we found that during ambient exposure oxygen gradually incorporates into the basal plane of two-dimensional (2D) MoS_2 crystals by replacing individual sulfur atoms. These O substitution sites were identified as single-atomic active reaction centres for H_2 evolution, extending the catalytic activity of MoS_2 crystals from edges over the entire basal plane. The substitutional oxidation of 2D MoS_2 crystals provides a novel chemical engineering method of unprecedented control to design highly efficient 2D electrocatalysts with a high density of single-atomic active basal plane sites.

We have investigated the catalytic activity of 2D $MoS_{2-x}O_x$ crystals for the electrochemical hydrogen evolution reaction (HER). Polarization curves (I-E) on both $MoS_{2-x}O_x$ and MoS_2 single layers were measured. This way, catalytic activity of the very same flake both with and without O substitution sites in the basal plane manifested itself, as revealed by STM characterization.

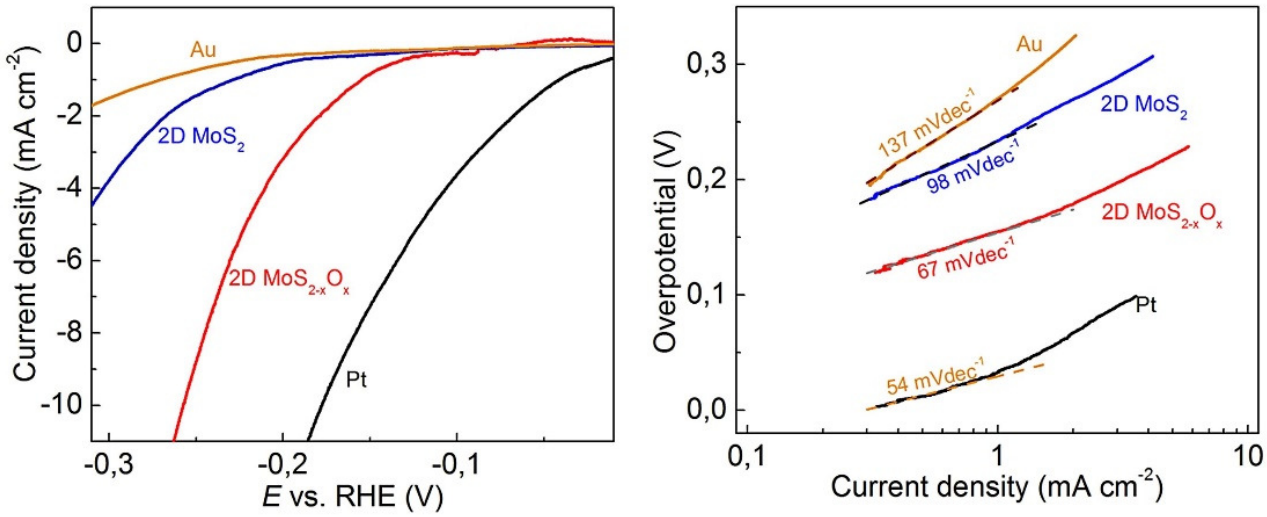

Figure 1: Catalytic activity of 2D $MoS_{2-x}O_x$ in the hydrogen evolution reaction (HER). Linear sweep voltammograms (a) and the corresponding Tafel plots (b) for: Au substrate, MoS_2 single layer, $MoS_{2-x}O_x$ single layer, and Pt substrate, revealing the significantly higher catalytic activity of the 2D oxy-sulfide phase as compared to the pure MoS_2 phase, attributed to the novel catalytically active oxygen substitutional sites incorporated into the basal plane during the ambient exposure.

Measured polarization curves and the corresponding Tafel plots shown in Fig. 1 evidence a highly increased catalytic HER activity of the 2D $MoS_{2-x}O_x$ solid solution crystals, as compared to the reduced pure 2D MoS_2 phase. Consequently, this enhanced catalytic activity can be clearly related to the presence of substitutional O sites. STM measurements following the catalysis confirmed that structural integrity of the 2D $MoS_{2-x}O_x$ crystals was preserved even after several hundreds of cycles. Our DFT calculations in accordance with the literature show that the mid-gap states characteristic to S vacancies that are proposed to play an important role in catalytic activity are absent for oxygen substitution sites (Fig. 2). In this light, it might seem surprising that O substitution sites still display a similar or even higher catalytic activity as S vacancies. A possible explanation is that a different mechanism is responsible for enhancing the catalytic activity of the O saturated vacancies. The Bader charge analysis (Fig. 2) reveals a strong acceptor type behaviour of the O substitution sites, implying a local negative charge surplus of about - 0.88 *e*. This, combined with the experimentally measured overall n-doping of the flakes imply the presence of highly localized negative charges on the O substitution sites, which, through electrostatic interaction, can enhance binding of protons. Furthermore, after the charge transfer, neutral hydrogen atoms are less attracted to the O sites, facilitating their release for the subsequent recombination step to H_2.

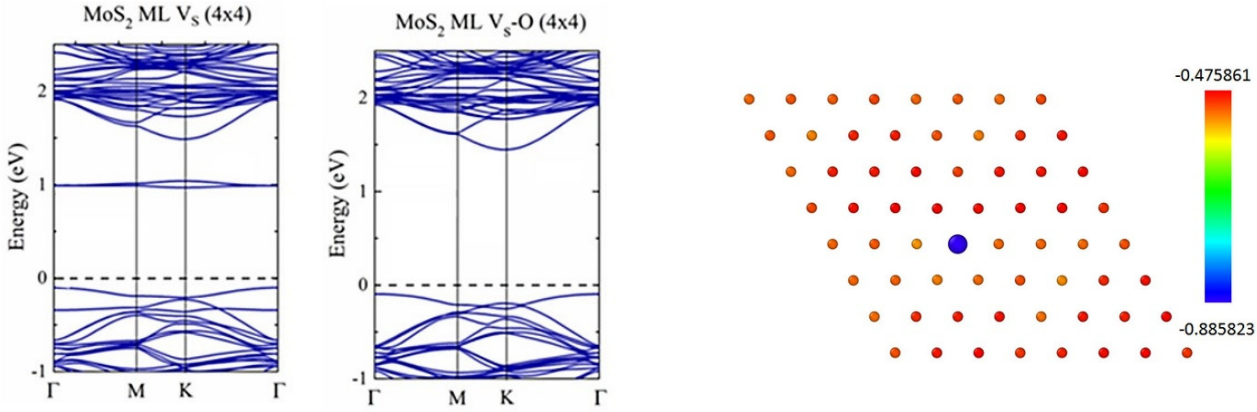

Figure 2: Calculated DFT band structure of the, sulfur vacancy site MoS_2-V_S, and oxygen substitution site MoS_2-V_S-O. Bader charge analysis of the $Mo_{64}S_{127}O$ surface revealing the electron acceptor nature of the O substitution site characterized by -0.88e excess negative charge.

Understanding catalytic processes is a highly challenging task, in big part due to the complexity of the systems experimentally investigated being in strong contrast to the idealized theoretical models. 2D $MoS_{2-x}O_x$ provides an ideal model system for understanding atomic level relations between active sites and catalytic HER activity, as it is characterized by a single type of active site. The site with experimentally known atomic structure, while edges and previously investigated more disordered MoS_2 structures can host a variety of active sites with complex atomic configurations and often little experimental insight into their precise atomic nature. These findings clearly evidence that the substitutional oxidation process of the MoS_2 basal plane reported here can open new routes for engineering 2D electro-catalysts with single oxygen atom active sites of a much higher site density than previously achieved for individual hetero-atom catalysts.

OBSERVATION OF LARGE BAND GAP MODIFICATION IN SINGLE-LAYER MoS_2 DUE TO FORMATION OF NANOBUBBLES

(Lendület LP2014, ERC StG NanoFab2D 680263, OTKA K 108753, Korea-Hungary Joint Laboratory)

J. Pető, G. Dobrik, P. Nemes-Incze, G. Kukucska, J. Koltai (ELTE), and L. Tapasztó

The family of transition metal dichalcogenides has received much research interest in the last few years owing to unique properties when stripped to only one layer. Some of the members exhibit semiconductor behaviour with a direct bandgap (MoS_2, $MoSe_2$, WS_2 etc.), which makes them particularly useful in electronic and optoelectronic applications. In case of direct band gap materials, as there is no need for a simultaneous photon-electron-phonon interaction, quantum efficiency can increase even by a factor of 10^4. In order to fully exploit the potential of these materials in future applications however, it is necessary to find ways to tune the bandgap. One of the promising methods to accomplish this task is engineering the band gap by applying mechanical strain to the 2D crystal structure. This allows us to make a fully reversible change of the band gap that leaves chemical composition intact. DFT calculations predict a band gap decrease of 0.2 eV for 1% strain. The method can be effective if the application of considerable strain is possible. Our investigations revealed that highly strained areas naturally occur within MoS_2 single layers upon van der Waals interaction with substrates. The contamination trapped at the interface is squeezed into nanoscale bubbles by the van der Waals forces. The pressure in such nanobubbles can reach high values, which imparts a significant mechanical strain to the MoS_2 monolayer.

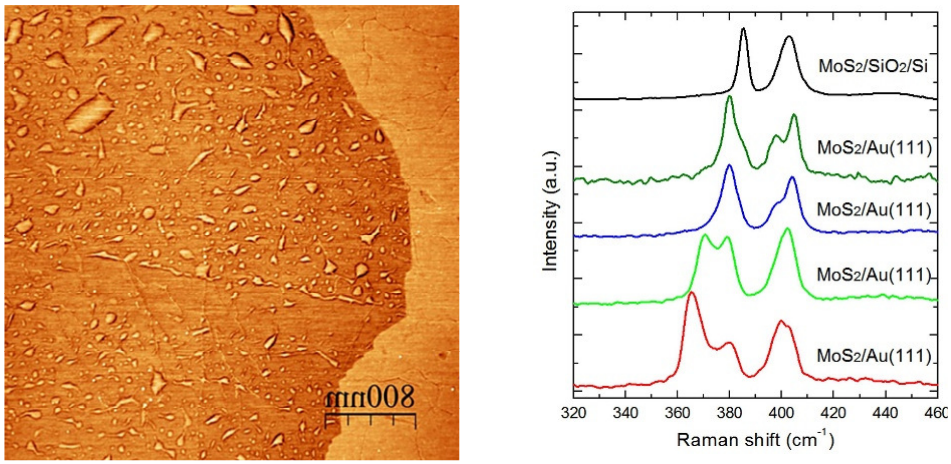

Figure 1: AFM (phase) image of nanobubbles within the MoS_2 single layer exfoliated onto Au (111) substrate. Raman measurements display strong shifts og the MoS_2 main peaks that can be attributed to the large (1 - 5%) mechanical strain within the bubbles.

We have also investigated the MoS_2 nanobubbles by Scanning Tunneling Microscopy. The diameter of the bubbles is typically in the 10-300 nm range with an aspect ratio (h/R) of 0.5 - 1.5. An example can be seen in Fig. 2.

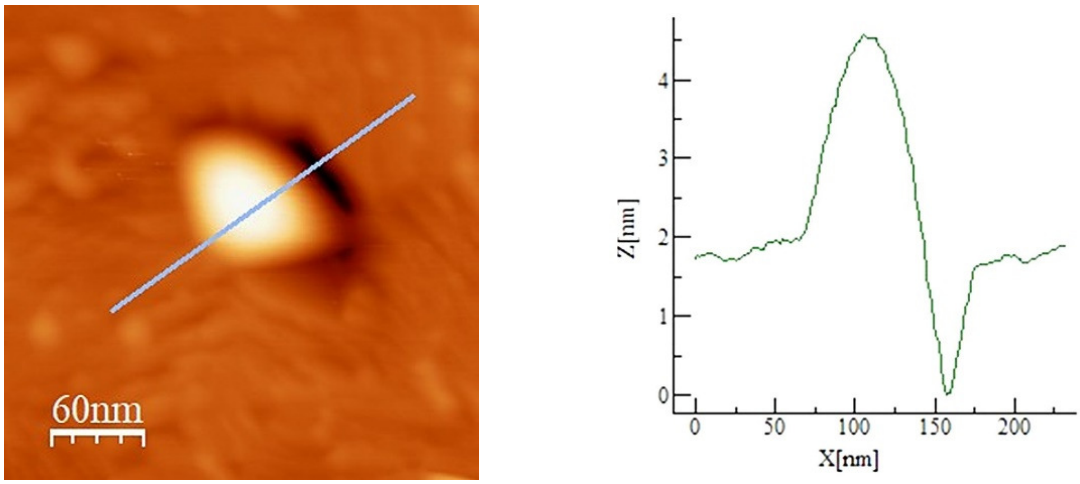

Figure 2: STM image of a nanobuble formed in the MoS_2 monolayer on Au (111) substrate (left). A line profile can be seen in the image and its plot shows the size of the bubble to be 75 nm in diameter with the top of the bubble reaching a 2.5 nm height.

In order to test the theoretically predicted and significant decrease of band gap upon strain, we performed Tunneling Spectroscopy measurements on the nanobubbles where deformation of the lattice was significant.

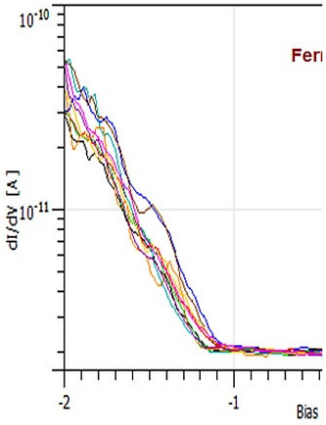

Figure 3: Tunneling spectra at the centre of a nanobubble displaying a band gap is only 1-1.1 eV, and the Fermi level shifted out of the gap into the edge of the conduction band.

While the intrinsic bandgap of the strain-free MoS_2 monolayer is about 2 eV, the nanobubble shows only a 1-1.1 eV band gap. Thus the band gap is decreased due to strain by about 0.9 eV. Our experimental findings clearly evidence that strain engineering is a very powerful tool also for engineering the band gap of transition metal dichalcogenides.

INTERACTION EFFECTS IN A CHAOTIC GRAPHENE QUANTUM BILLIARD

(EU FP7 GraNaRip 334377, OTKA K 119532)

I. Hagymási (Wigner FK), P. Vancsó, A. Pálinkás, and Z. Osváth

The appearance of two-dimensional materials like graphene has renewed the interest in the properties of quantum dots and quantum billiards made of these materials. Here we examined a quadrilateral shaped graphene quantum dot, which is a truncated triangle having three zigzag and one armchair edges (see Fig. 1a). This peculiar shape resembles the theoretically well-studied Sinai billiard. In this joint experimental and theoretical study, we use scanning tunneling microscopy (STM) and perform theoretical calculations to understand the experimental results. Our main finding is that the electron-electron interaction must be taken into account to reproduce the STM images and the local density of states (LDOS) measurements, which highlight the important role of the interactions in quantum dots in graphene even at room temperature.

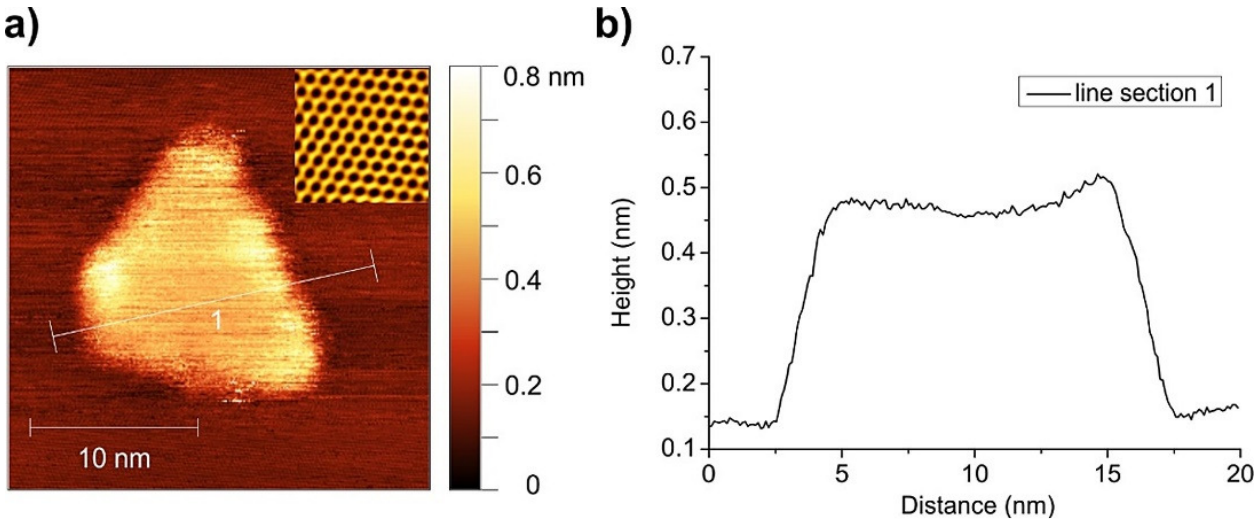

Figure 1 (a): STM image of the investigated graphene quantum dot. Tunneling parameters: U = 200 mV, and I = 1 nA. The atomic resolution inset image shows the crystallographic orientation in the dot. (b): Height profile taken along the line section 1 in (a), showing monolayer thickness.

Graphene grown by chemical vapor deposition (CVD) onto electropolished copper foil was transferred onto a highly oriented pyrolytic graphite (HOPG) substrate using thermal release tape. Graphene nanostructures were obtained by annealing the graphene/HOPG sample at 650 °C for two hours in an argon atmosphere. STM and scanning tunneling spectroscopy (STS) measurements were performed using a DI Nanoscope E operating under ambient conditions. Atomic resolution images on the dot (inset of Fig. 1a) reveal that the nanostructure has three zigzag edges and one armchair edge.

In Fig. 2 (first row), we can see different superstructure patterns within the quantum dot measured at various voltages. The well-known ($\sqrt{3}\times\sqrt{3}$)R30° superstructure (marked by white circles) appears in addition to the atomic structure.

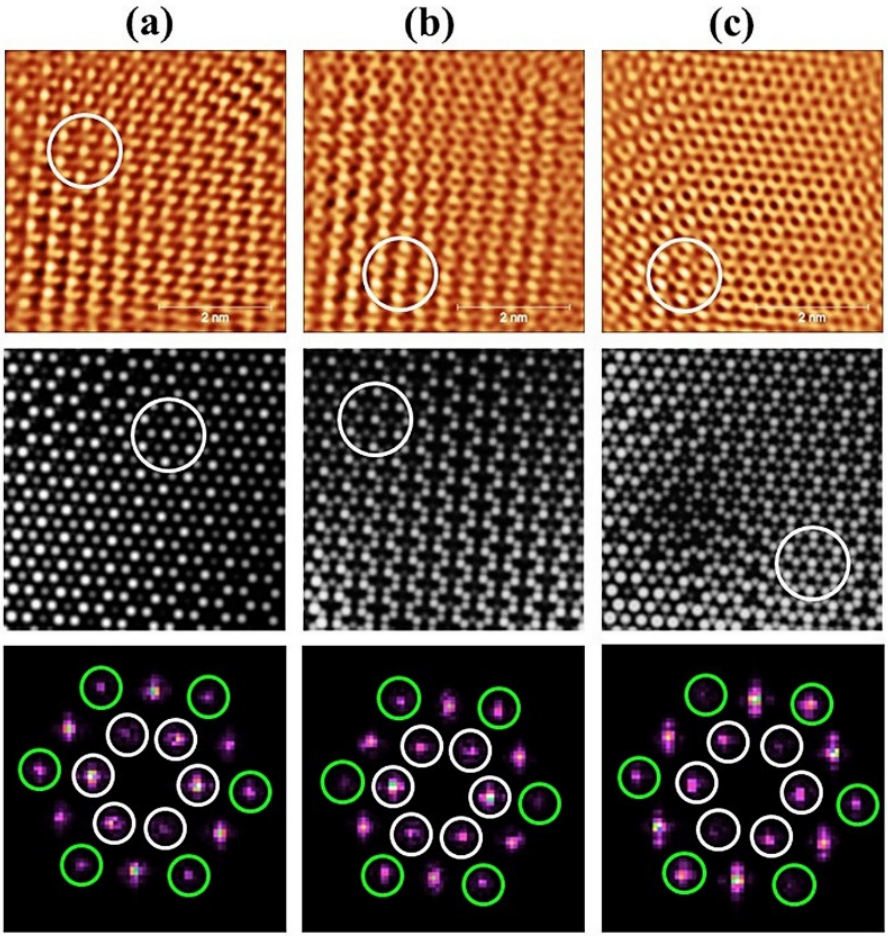

Figure 2: Topographic STM images within the quantum dot. Each column corresponds to a different voltage where the measurement was done: (a), (b), and (c) belong to U = 100, 25, and -50 mV, respectively. The first row shows the measured images, the second one contains the simulated images, while the third row displays the Fourier spectra of the measured images. The spots inside the white circles in the Fourier spectra are the components of the (√3×√3)R30° superstructure, while the green circled spots are their overtones. The noncircled spots correspond to the periodicity of the atomic lattice.

Additionally, stripes parallel to the armchair edge and rings are observed in the measured STM images. In order to simulate these distinct STM images, a finite electron-electron interaction was considered. STM images were simulated with the simple Tersoff-Hamann approximation and by using calculated LDOS of the interacting system. Taking into account the electron-electron interaction, we can quantitatively reproduce the measured STM images, including the (√3×√3)R30° superstructure, the stripes, and the rings at different voltages (Fig. 2, second row). Fourier spectra of the measured images (Fig. 2, third row) show that the Fourier components of the (√3×√3)R30° superstructure are always present (inner hexagon, white circles). Moreover, their harmonics (marked with green circles) appear with various amplitudes, which results in the formation of different, more complex patterns in the topography images. The emergence of the harmonics measured by STM is attributed to Umklapp scattering processes, which serve as a further evidence for the presence of electron-electron interaction in our system.

ATOMIC SCALE ELECTRONIC PROPERTIES OF SINGLE LAYER $MoSe_2$ CRYSTALS GROWN ON GRAPHITE

(János Bolyai Research Scholarship, ERC StG NanoFab2D 680263)

A. A. Koós, Z. Osváth, A. Pálinkás, G. Dobrik, K. Kertész, L. P. Biró, and L. Tapasztó

Unique properties of 2D materials like graphene and transition metal dichalcogenides offer unprecedented opportunities in a wide range of applications, for example designing better electronic devices, faster sensors, more efficient catalysts or optoelectronic devices. The combination of layered materials in hybrid nanostructures allows us to further improve applicability of these materials. For example, hybrids of graphene with zero-gap character and semiconducting $MoSe_2$ are expected to become building blocks of next generation high performance nanoelectronic devices. In order to understand properties of graphene-$MoSe_2$ hybrids, the $MoSe_2$ sheets were grown by chemical vapour deposition (CVD) on highly ordered pyrolytic graphite (HOPG). The hetero-structures formed were investigated with Scanning Tunneling Microscopy (STM) and Scanning Tunneling Spectroscopy (STS) at atomic resolution.

The $MoSe_2$ flakes grown on HOPG follow the crystallographic orientation of the substrate (Fig. 1a). It was found that the apparent height of the flake edges was higher than the apparent thickness of the flake, which indicates that the electronic properties at edges are different (Fig. 1b). In order to exclude artifacts due to contamination of the edges during the CVD growth, we formed freshly cut edges by nanolithography, and found that the apparent height increase was the same.

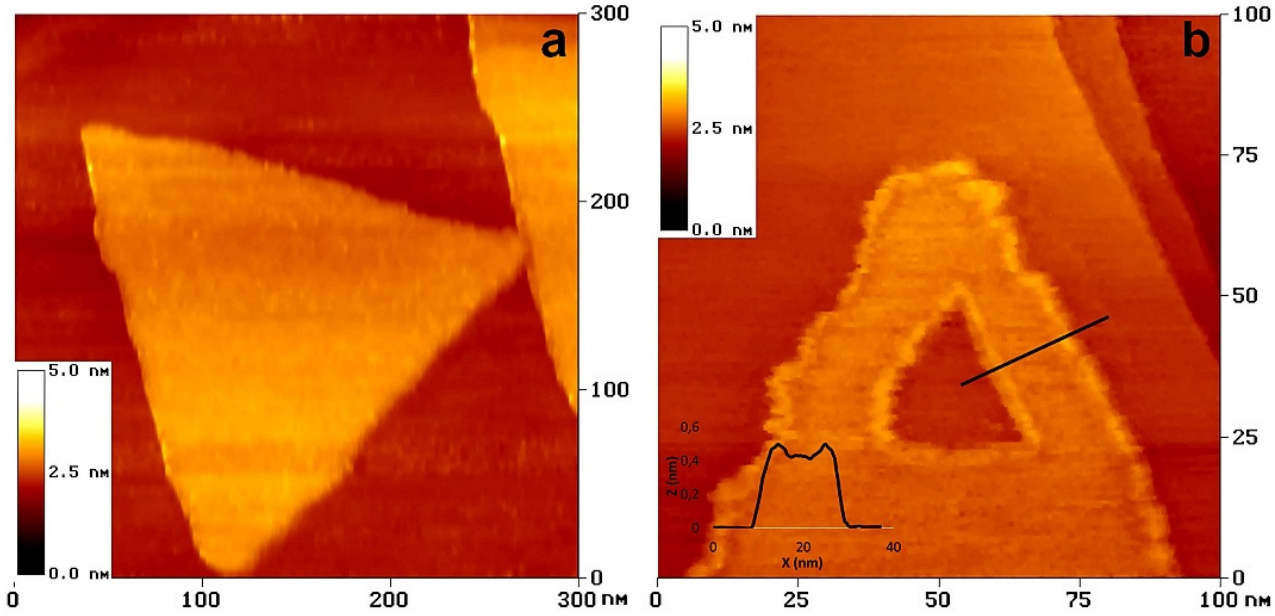

Figure 1: a) STM image of a $MoSe_2$ flake grown on HOPG. b) Higher resolution STM image of a $MoSe_2$ crystal with a cut made by nanolithography. Inset: Height profile along the black line.

We have investigated the effect of tunneling current and voltage on the quality of STM images. We found that at negative voltages it was possible to highlight the grain boundaries between $MoSe_2$ single crystals. Interestingly, number of visible defects strongly depended on STM imaging voltage (Fig. 2a-c). This suggests that defect-localized electronic states of certain energy are present. From tunneling spectroscopy measurements, it became obvious that at a defect site the conduction band slightly decreased at defects and a localized defect induced midgap states to appear at about -600 meV (Fig. 2d). Consequently, defects become visible only when imaging at negative bias voltages are below -600 meV, in accordance with topographic images. These effects must be considered during the design of 2D $MoSe_2$-based nanoelectronic devices.

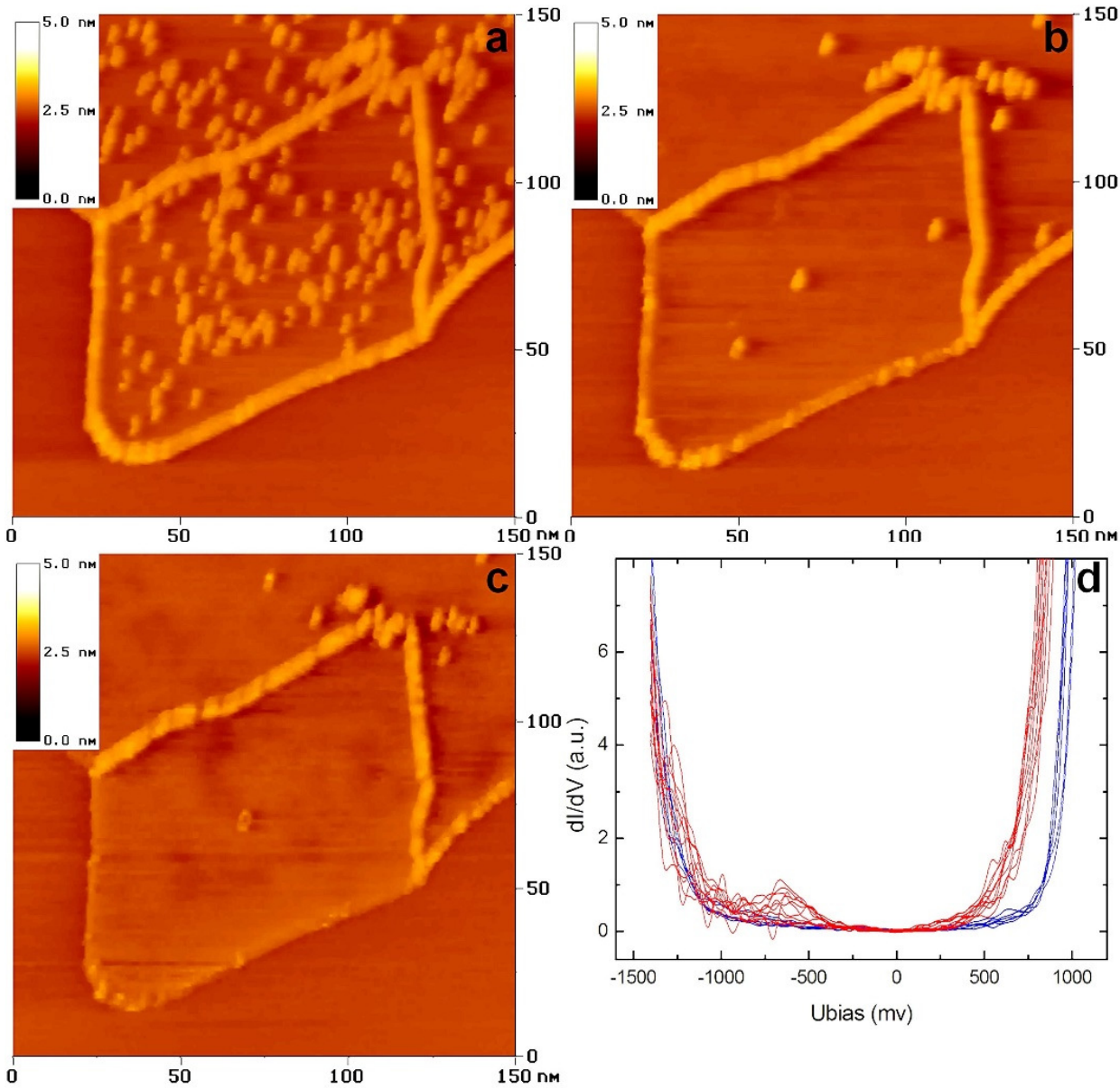

Figure 2: a-c) Effect of bias voltage on the visibility of $MoSe_2$ defects. The images were recorded at 200 pA. The voltage was selected -1V (a), -0.5 V (b) and -0.1 V (c), respectively. (d): STS recorded above $MoSe_2$ flake (blue) and defects (red).

In conclusion, CVD offers the opportunity to produce high quality graphene-2D MoSe2 heterostructures, their structure and properties, however, should be carefully investigated when developing reliable applications.

NOVEL GRAPHENE/SN AND GRAPHENE/SnO_X HYBRID NANOSTRUCTURES: BAND GAPS REVEALED BY SCANNING PROBE MEASUREMENTS

(EU FP7 GraNaRip 334377, OTKA K 119532, TÉT_12_SK-1-2013-0018)

A. Pálinkás, Gy. Molnár, G. Zs. Magda, C. Hwang (KRISS, Korea), L. Tapasztó, P. Samuely (IEP SAS Slovakia), P. Szabó (IEP SAS Slovakia), and Z. Osváth

Graphene has attracted substantial research interest due to its outstanding properties. Hybrid nanostructures integrating graphene with metallic or semiconducting nanoparticles (NPs) could potentially display versatile and tuneable properties, as well as novel or enhanced functionalities arising from the synergy between the properties of graphene and those of NPs. In this work, graphene covered Sn and SnO_x nanoparticles were synthesized and characterized by AFM, and STM/STS. We showed that metallic Sn NPs induce electrostatic doping by transferring electrons to graphene. We also demonstrated that the graphene cover layer prevented oxidation of tin NPs. Graphene/SnO_x hybrid nanostructures were also prepared and the electronic band gap of SnO_x NPs was measured by STS.

Tin was evaporated (7 nm) onto highly oriented pyrolytic graphite (HOPG) surface. Due to the low wetting properties, the evaporated tin film self-organized into nanoparticles. The NPs were covered with CVD-grown graphene, the transfer was done using thermal release tape method. Later the sample was annealed in electric furnace at 500 °C for 30 min in Ar atmosphere. The graphene-covered tin NPs were tested by STM and STS in ambient conditions both before and after annealing. The STM image in Fig. 1a shows graphene covered closely spaced Sn NPs.

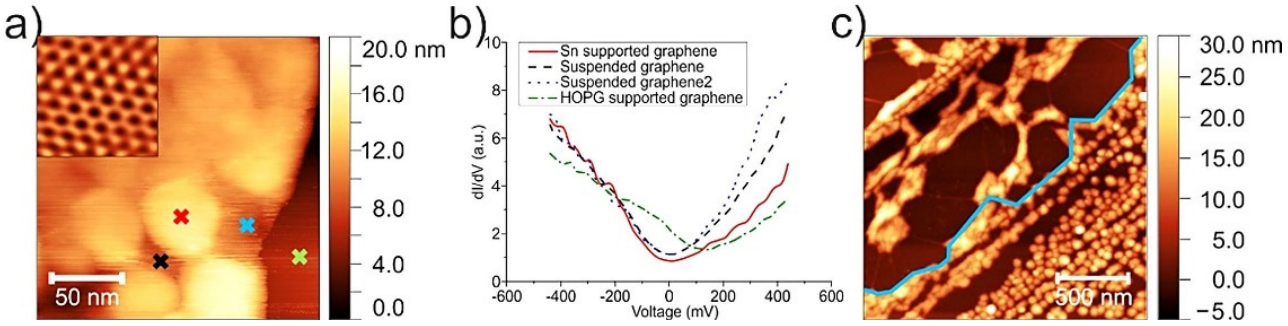

Figure 1 (a): STM topography image of graphene covered Sn NPs. The inset shows an atomic resolution image of the Sn supported graphene. (b): dI/dV spectra measured at the positions marked with colored symbols in a) as follows: Sn supported graphene (red), suspended graphene (black, blue), graphene on HOPG (green). (c): AFM Topography image of a partially graphene covered area after annealing at 500 °C. The edge of the graphene is marked with blue line.

STS measurements were carried out on both Sn supported graphene, and graphene suspended between the Sn NPs. The room temperature STS spectra in Fig. 1b show that the pre-existing environmental p-doping of graphene (see the HOPG supported graphene) can be significantly reduced by the Sn NPs, an effect which prevails in the suspended graphene parts as well.

After annealing at 500 °C the graphene covered regions transformed drastically, the NPs merged into nanorods and other new nanostructures (Fig. 1c), while on the uncovered regions, the sphere-like shape of NPs was preserved. The melting point of Sn, SnO and SnO_2 are at around 230 °C, 1080 °C and 1630 °C, respectively. This phenomenon demonstrates the shielding efficiency of graphene. When annealing was performed three months after the initial tin evaporation, and graphene was able to protect efficiently the Sn NPs from oxidation in this time frame. On the other hand, non-covered NPs exposed to air oxidized completely, and thus they did not melt during annealing at 500 °C.

We also prepared a graphene/SnO_x nanoparticle hybrid material in the same way, except that the evaporated Sn NPs were annealed (oxidized) before covering with graphene. A topographic AFM image of both graphene covered and non-covered NPs is shown in Fig. 2a. Here, the non-covered NPs are observed in the area between the two blue lines.

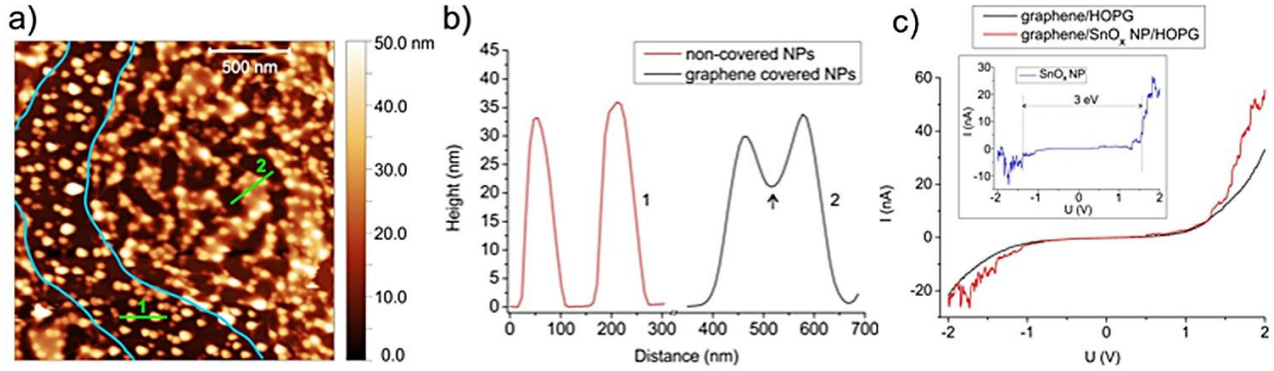

Figure 2 (a): AFM topography of graphene covered SnO_x NPs. Graphene edges are marked with blue lines. (b): Height profiles taken on non-covered (red) and graphene covered (black) NPs. ***(c):*** *Tunneling spectra on graphene/HOPG (black) and a graphene covered SnO_x nanoparticle (red). Subtracting the graphitic contribution we obtain the tunnelling conductance through the NP (inset, blue line), which shows a band gap of 3 eV.*

Many nanoparticle groups are observed when graphene is suspended between the NPs. This is shown, for example in Fig. 2b, where height profiles taken on non-covered and graphene covered NPs are compared. We investigated the graphene/SnO_x hybrids by STM and STS. The non-covered oxidized nanoparticles could not be imaged with low voltages (U < 1 V) due to the high electronic band gap of SnOx. In contrast, graphene covered SnO_x NPs could be well investigated using such low bias voltages also, since graphene immobilizes the NPs and good tunneling conductance is achieved through it. STS measurements revealed band gaps of 2.7 – 3.2 eV, which are better observed when subtracting 'graphenic' contribution of the current (inset of Fig. 2c). In this setting, graphene facilitates the STM investigation of semiconducting NPs by fixing them to the substrate and enabling the study of their density of states by STS.

CHANGES IN STRUCTURAL AND PIGMENTARY COLOURS IN RESPONSE TO COLD STRESS IN POLYOMMATUS ICARUS BUTTERFLIES

(OTKA K 111741, OTKA K 115724)

K. Kertész, G. Piszter, Z. E. Horváth, Zs. Bálint, and L. P. Biró

While numerous papers investigated effects of thermal stress on the pigmentary colours of butterfly wings, such studies regarding structural colours were mostly lacking, despite their important role in sexual communication. To gain insight into the possible differences between responses of the two kinds of colouration, we investigated the effect of prolonged cold stress (cooling at 5 °C for up to 62 days) on the pupae of Polyommatus icarus butterflies. The wing surfaces coloured by photonic crystal-type nanoarchitectures (dorsal) and by pigments (ventral) showed markedly different behaviour. On the dorsal wing surface of the males, with blue structural colouration, a smaller magnitude response was found with much more pronounced individual variations (Fig. 1a vs. 1b, & Fig. 1e vs. 1f) possibly revealing hidden genetic variations. The ventral wing surfaces of both sexes exhibited stress responses proportional in magnitude to the duration of cooling and showed the same trend for all individuals, irrespective of their sex (Fig. 1c vs. 1d, & Fig. 1g vs. 1h).

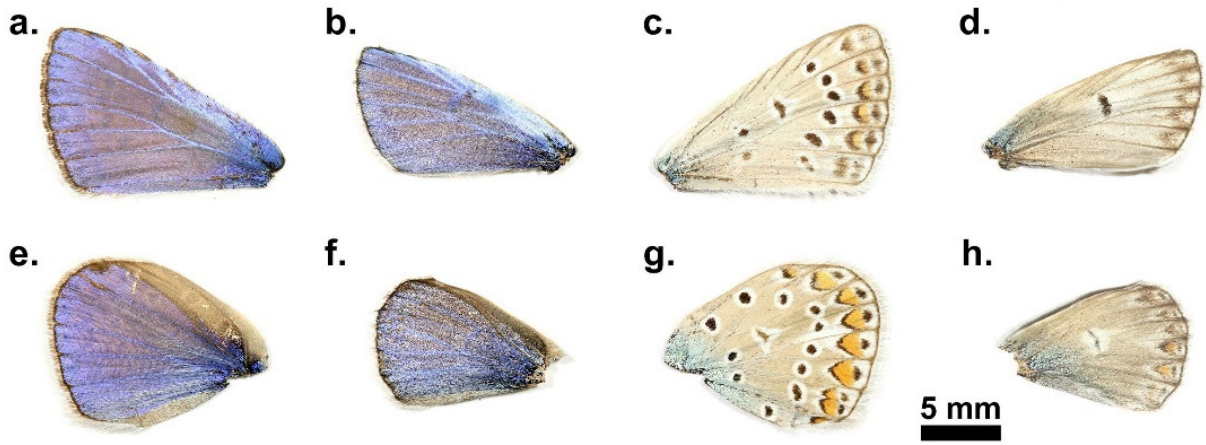

Figure 1: Wings of wild butterflies and of butterflies eclosed from pupae subjected to prolonged cooling at 5 °C in dark. ***(a)****: Dorsal forewing of a wild male;* ***(b):*** *dorsal forewing of a male merged from a pupa cooled for 62 days;* ***(c):*** *ventral forewing of a wild male;* ***(d):*** *ventral forewing of a male eclosed from a pupa cooled for 62 days;* ***(e):*** *dorsal hindwing of a wild male;* ***(f):*** *dorsal hindwing of a male emerged from a pupa cooled for 62 days;* ***(g):*** *ventral hindwing of a wild male;* ***(h):*** *ventral hindwing of a male eclosed from a pupa cooled for 62 days.*

The reflectance of the dorsal (blue) wing surfaces (all four wings of each individual) was measured using UV-VIS spectroscopy. Position of the reflectance maximum in the blue region (365–432 nm) was located and plotted as a function of the time they were kept cooled for all the pupae in Fig. 2a. Cold stress for 10 days did not produce significant deviations in the peak position of the blue reflectance. Cold stress for longer durations (>10 days) caused higher deviations from the normal biological variation of the blue colour of the male P. icarus and induced the appearance of blue scales on all the females, which have brown dorsal wing surfaces in the wild population. The possible cause of the shift in the spectral position of the reflectance maximum may be related to the slight alteration of the dimensions of the photonic nanoarchitecture, or to changes in the scale arrangement.

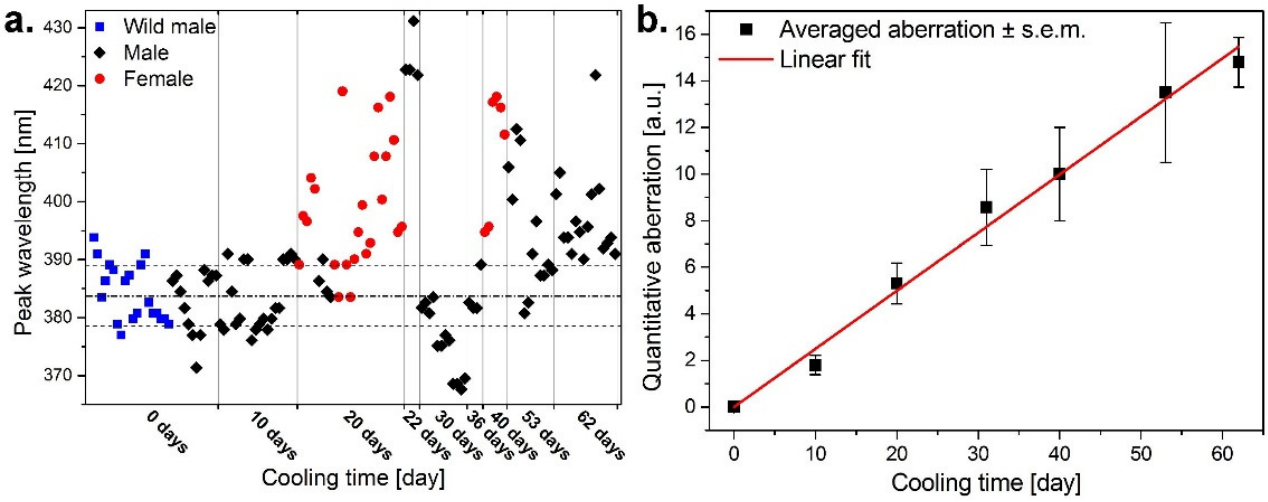

Figure 2: (a): Spectral position of the blue reflectance peak for all the investigated exemplars. Horizontal broken lines indicate the range of wild males with centre at 384 nm marked by dotted broken line. (b): The averaged quantitative aberration of the ventral wing surfaces versus the cooling time of the pupae shows linear relationship.

The ventral side of the wing surfaces of both the males and females exhibited similar complex pigmentation (Fig. 1c and 1g). In fact, this pattern is used by taxonomists to identify these species. It is possible to assign a certain numerical value to any deviation (Fig. 1d and 1h) from the standard pattern observed on normal individuals, enabling quantitative evaluation of the degree of aberration of the pigment colours. We qualified and coded the wing size, ventral wing-surface colouration and pattern in comparison with individuals of the control group as a standard. Numerical value of the aberration was averaged for butterflies eclosed from pupae cooled for the same number of days, and the results are plotted in Fig. 2b. One may observe that the quantitative value of the aberration shows a very closely monotonic and linear variation with the length of the cooling period endured by the pupae.

Clearly, colouration generated by nanoarchitectures and the colouration generated by pigments reacted differently to the stress produced by prolonged cooling of the pupae. This finding may be less surprising if one considers that the two processes, scale formation and pigmentation, are well separated in time, and also perform different functions in the life of these butterflies. The blue colouration, used for sexual communication, is much more stress resistant than the pigment-generated pattern of the ventral wing surface, which is used for camouflage: significantly smaller magnitude changes were induced by the prolonged cooling in the blue colour of the males, as compared to the alteration of their ventral wing patterns.

DETECTING PATCHY NANOPARTICLE ASSEMBLY AT THE SINGLE-PARTICLE LEVEL

(OTKA K 112114, and OTKA K 119532)

S. Pothorszky, D. Zámbó, D. Szekrényes, Z. Hajnal and A. Deák

Patchy colloids allow the development of a spatially inhomogeneous interaction profile and depending on the number and arrangement of the patches, the valence and directionality of the interaction can be controlled. Due to their intense light scattering, noble metal nanoparticles represent an ideal class of model system for the investigation of self-assembly processes at the single particle level.

Relying on the unique optical properties of the heterodimers composed of a patchy gold nanorod and a nanosphere, direct, in situ information on the structure of the assembly can be obtained using single particle scattering spectroscopy combined with correlative electron microscopy investigations. This combined technique opens the possibility to correlate optical properties with relative position of the particles in the heterodimer. In situ measurements performed in a liquid cell give direct information about how the self-assembled structure evolves in the aqueous phase (Fig. 1). Furthermore, both the directing feature of colloidal interactions and immersion type capillary forces can be investigated separately.

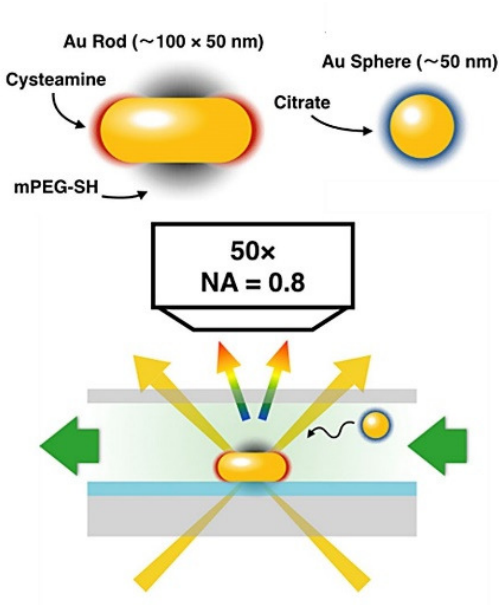

Figure 1: The prepared nanoparticles (top) and the measurement arrangement (bottom). The patchy nanorods are first immobilized on ITO covered substrates, then the aqueous nanosphere solution is introduced and changes in the scattered spectrum upon binding detected.

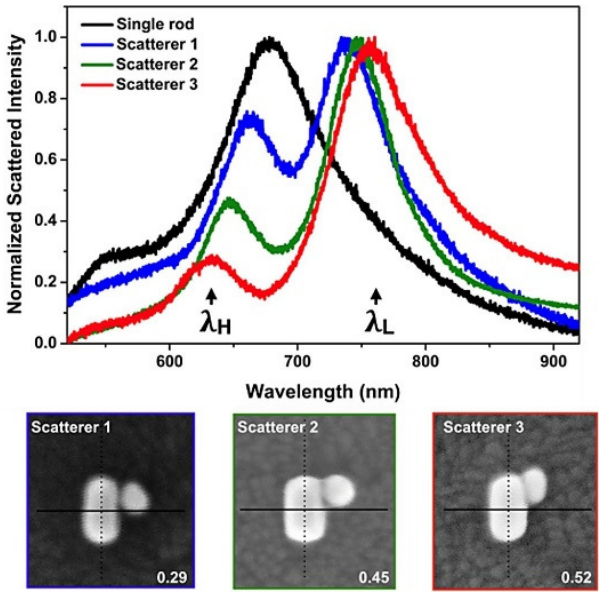

Figure 2: Typical scattering spectra measured in situ in the liquid cell and the corresponding SEM images. The numbers indicate their respective relative displacement.

During *in situ* measurements, a blueshifted higher (H) and a redshifted lower (L) energy peak were appeared at around the initial longitudinal plasmon peak of the rod indicating the formation of a heterodimer (Fig. 2.). Based on the energy difference between the two peaks, the spheres were attached to the side region already in the aqueous phase. The side-localization of the spheres and its distribution for the given rod/sphere heterodimer can be interpreted based on the combined effect of dispersion, electric double layer and steric interactions. The results can contribute to the rational design of nanoscale patchy particles for a better control over the resulting assembly structure.

MAGNETIC FLUX SIMULATION FOR THE INSPECTION OF LOCAL THINNING OF FERROMAGNETIC PLATES – EXPERIMENTAL VERIFICATION

(OTKA K 111662)

S. Pothorszky, D. Zámbó, D. Szekrényes, Z. Hajnal and A. Deák

For pipes used in industry, wall thinning is one of the most serious defects. Detection of the thickness reduction is a very important issue for prediction of lifetime of the pipes in order to avoid severe accidents. The inspection should be done from the outer side of the pipe. A recently developed nondestructive method called Magnetic Adaptive Testing (MAT), which is based on systematic measurement and evaluation of minor magnetic hysteresis loops, was successfully applied for the detection of local wall thinning in ferromagnetic plates. It was shown, that even a relatively small, local modification of the plate thickness could be detected from the other side of the specimen with an adequate signal/noise ratio.

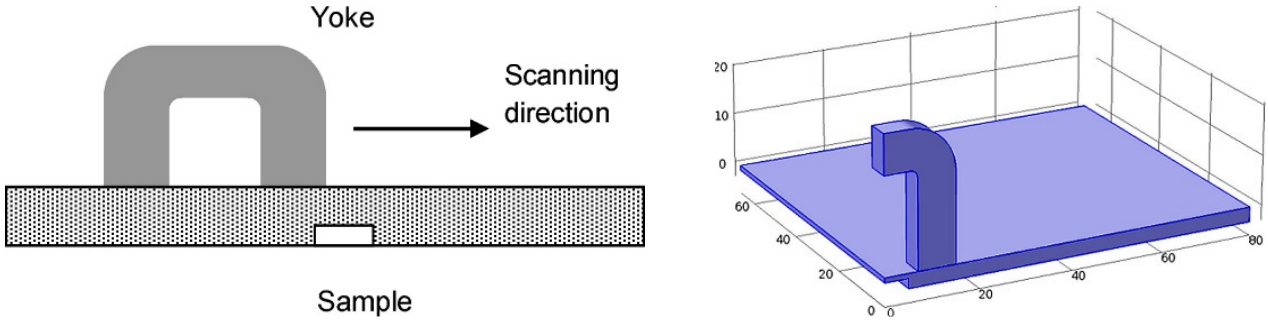

Figure 1: Configuration used both for measurement and simulation. The geometry on the right represents a quarter-view of the arrangement, showing only part of the whole plate, and with the yoke in central position right above the slot.

To improve applicability of MAT, the measurement conditions should be optimized. It is important to study, how modification of the measured hysteresis loops, caused by the presence of an artificial slot in the investigated ferromagnetic plate(s), and are influenced by the parameters of the measurement arrangement. Previously we calculated how geometry of the measured arrangement affects change of the magnetic flux inside the magnetizing yoke. Result of the simulation helped to find optimal parameters of the experimental arrangement.

The purpose of the present work is to perform numerical simulations of the measurement on a single ferromagnetic steel plate which contains various artificial slots of different size, and to compare results of the simulations with the experimental data. Measurements were done by MAT, by moving the magnetizing yoke over the surface. A ferromagnetic steel plate of size 500 mm × 300 mm × 6 mm was considered, which contained an artificial rectangular slot, the size of which is varied. Fig. 1 shows the configuration of the measurement and simulation.

Change of the magnetic flux density in the cross section of the magnetizing yoke, which occurs due to the presence of the artificial slot, was calculated as a function of the size of the slot. The AC/DC Module of the Comsol Multiphysics® finite element software was used for the simulations. By the simulations we investigated how this flux change depends on the size of the slot. Three slot widths (5, 10 and 15 mm) were combined with three slot depths (1, 2 and 3 mm) resulting all together in nine different cases. The result of simulation can be seen in Fig. 2(a), while the results of the measurements are given in Fig. 2(b).

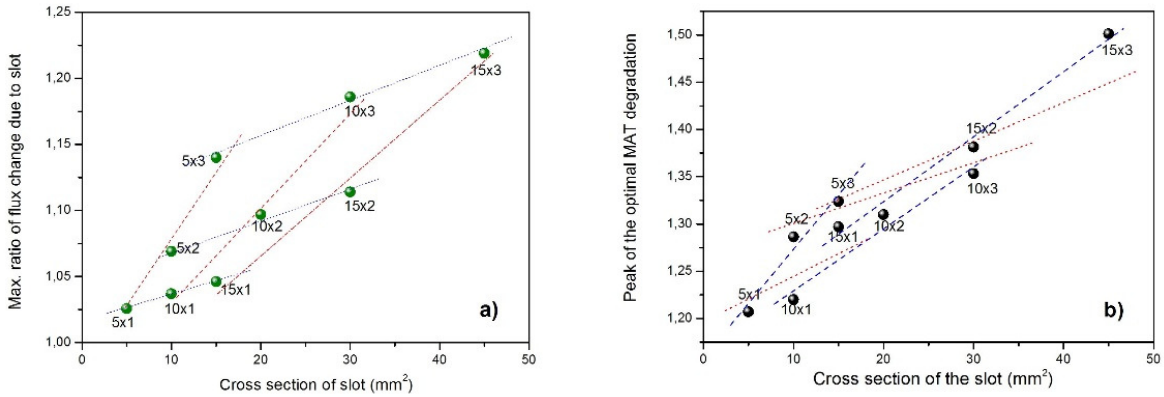

Figure 2: Maximum values of flux change for different cross sections of the slots. a): calculated, b): measured.

It was found that existence of the investigated artificial slots can be detected with a good signal to noise ratio by MAT method. The evaluated parameters indicate presence/absence of the slot and are able even to reflect size of the slot quantitatively. Numerical simulation confirmed that detection of the slot by a magnetic inspection head (i.e. the magnetic yoke with the necessary coils) attached to the investigated steel plate from the side opposite to where the slot is situated makes sense. The signal measured inductively by the experimental method in the pick-up coil originates from variation of the magnetic flux inside the magnetic circuit composed of the magnetizing yoke and of that part of the ferromagnetic plate, which contains the investigated slot.

The results of both the simulation and of the experimental measurement showed nearly linear correlation between the evaluated parameters and the cross section of the slots. This was true both for the case when depth of a given slot was fixed and its width was modified, and also when width of a given slot was fixed and its depth was varied. However, the slopes were significantly different. Consequently, we can conclude that depth of the slot has a larger influence on the measurable signal than its width, considering the same slot volume. Good qualitative correlation was found between the *calculated* maximum relative change of the magnetic flux, and the peak values of the optimally determined *measured* MAT normalized parameters. A useful message of the present work is to show the tendency, that is, how parameters of the testing arrangement affect the measured magnetic flux. This result can also be important for identification of the slots from the measured signal.

The good correlation between the calculated and measured quantities also means the experimental validation of the used simulation method.

DEVELOPMENT OF OPTICAL METROLOGY TOOL FOR IN-LINE QUALIFICATION OF THIN FILMS ON LARGE AREA

(EU FP7 SEA4KET-611332, ENIAC E450EDL-325613, NEMZ_12-1-2013-0001)

Cs. Major, Gy. Juhász, P. Petrik, and M. Fried

We were involved in 2 EU-projects („SEA4KET" and the ENIAC-2012-2 "E450DL") to develop "Imaging Optical Inspection Device with a Pinhole Camera". Our tool is unique for the characterization of thin films over large area. Using this tool developed in the Photonics department, thin film properties such as the thickness, the refractive index and related physical properties from the spectroscopic measurement, such as the conductivity or the crystallinity, can be determined within several minutes on a large area. We developed 30, 45-60 and 60-90 cm wide prototypes for mapping the optical properties of thin films of big area samples measuring in approximately 1000 points.

Figure 1: We installed our optical mapping device in the clean-room of IISB (Erlangen, Germany). A 300 mm diameter wafer can be seen on the robotic arm (left side).

300 mm diameter SiON-on-Si wafers were measured on the robotic arm in clean room environment. We determined the thickness maps on these big wafers and compared it with reference measurements on a commercial Woollam M-2000DI spectroscopic ellipsometer. The results show a good agreement between our maps and the reference one, both having a good fit quality (mean squared error, MSE) or the spectra. For the sake of brevity, the fitted spectra are not shown.

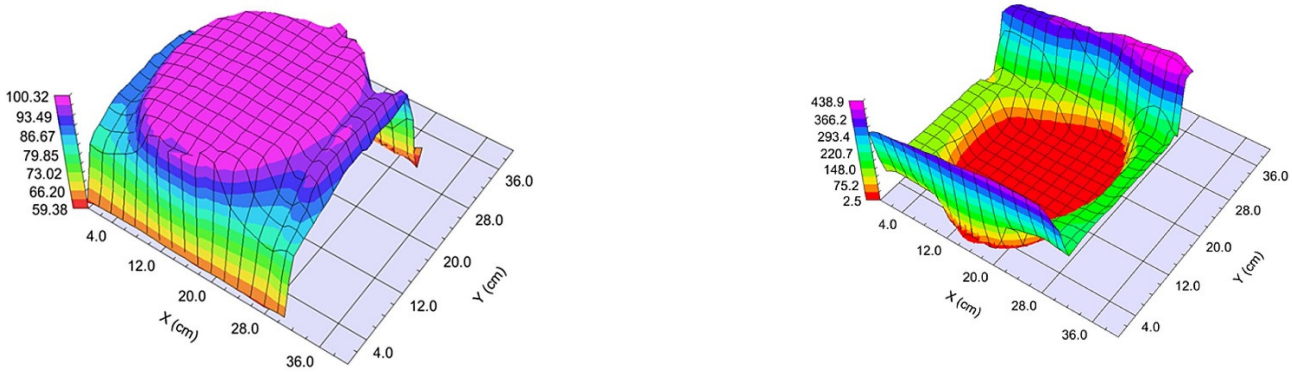

Figure 2: Thickness map of a nominally 100 nm sample of a 300 mm diameter SiON-on-Si wafer (with automatic scale, left). The mean squared error (MSE) map shows the area of the sample (right).

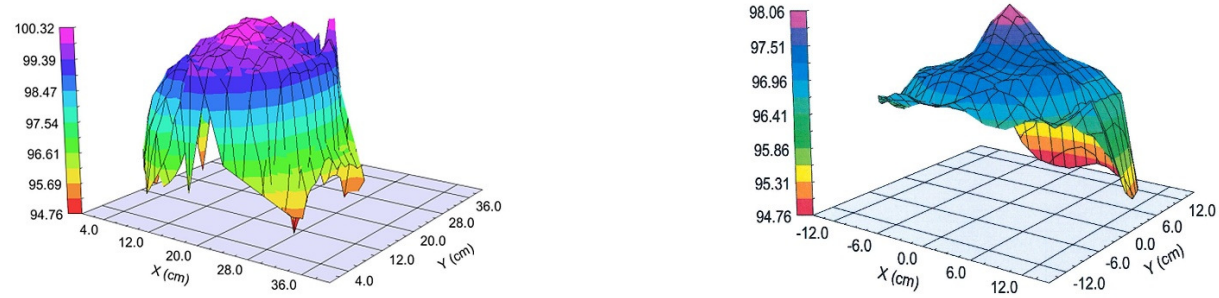

Figure 3: Thickness map with the same limited scale as the results of checking spectroscopic ellipsometry measurements by a Woollam M2000DI ellipsometer (1 color = 0.29 nm).

FABRICATION OF GENETICALLY MODIFIED BACTERIAL FILAMENT COATINGS TO DEVELOP SENSOR SURFACES FOR DETECTING WATER POLLUTION

(M-ERA.NET WaterSafe/No. 39/2016, OTKA NN 117849, OTKA NN 117847, OTKA K 115852 and EU (ERDF) INFRANANOCHEM No. 19/01.03.2009)

J. Nádor, B. Kalas., A. Saftics, L. Illés, B. Kovács, Cs. Moldován, A. Romanenko, M. Gartner, M. Fried, F. Vonderviszt, and P. Petrik

In modern technology the developments in environmental areas become more important and current. Freshwater stocks and pollution are in the most relevant topics, as they can be crucial in the future of humankind. Within the "WaterSafe" international project, we take part in the development of a device for detecting various water pollution molecules (mainly heavy metals and nitrogen oxide ions). The surface of the disposable sensor can be a mix of dielectrics, nanostructures or genetically modified bacterial flagellar filaments (FF) that have specific binding sites for specific molecules. The adsorption of the target molecules to the immobilized filaments induces a change in the conductance of the electrode which can indicate the presence of the pollution.

The main aim of our group is to create the sensing layers by immobilizing the FFs on the gold electrode of the sensor surface, for which we applied two different methods. Either genetically modified FFs were used, which have an enhanced number of thiol groups on their surface in order to create covalent interactions with the gold surface. Or we used unmodified wild type FFs, and applied chemical crosslinker DSP (dithiobis(succinimidyl propionate)) molecule for immobilizing the FFs to the gold surface.

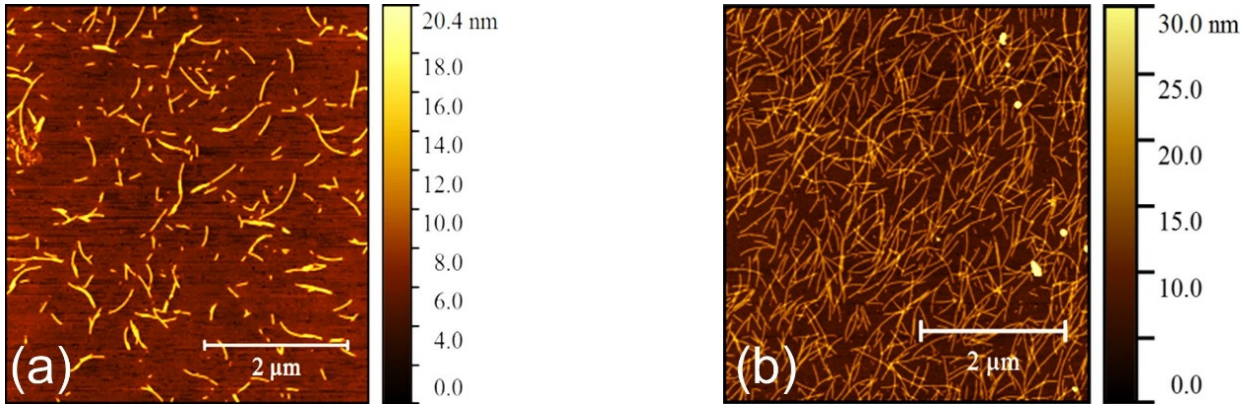

Figure 1: AFM images of flagellar filaments immobilized on gold coated glass substrates applying (a): genetically modified filaments with an enhanced number of thiol-groups on their surface and (b): wild type filaments immobilized by DSP crosslinker molecules.

Both types of the FFs were immobilized on various surface nanostructures. Using in situ plasmon enhanced spectroscopic ellipsometry, AFM, SEM and ex situ scanning ellipsometry, we have shown that those nanostructures (e.g. titanate nanotubes, TiO_2 nanoparticles and ZnO nanorods) can facilitate the adsorption of protein.

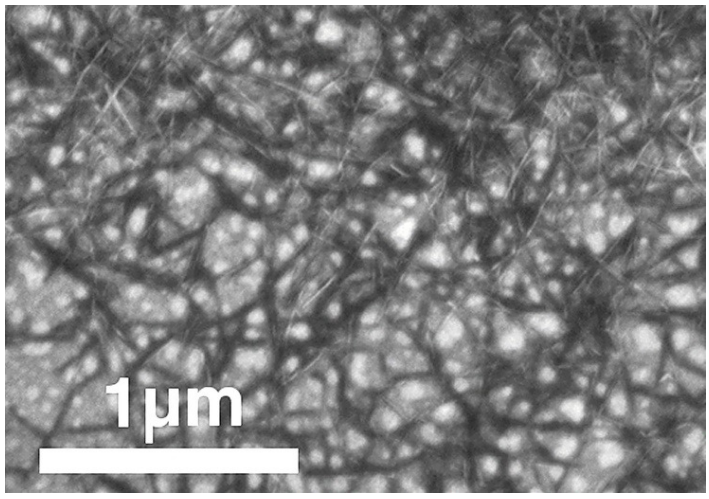

Figure 2: SEM image of a flagellar filament layer (dark fibers) prepared on titanate nanotube coating (lighter fibers) on gold surface.

INVESTIGATION OF WETTING PROCESSES BY THE CAPILLARY BRIDGE PROBE TECHNIQUE

N. Nagy

The research aims the development of a highly sensitive measuring method, which enables to characterize flat solid surfaces by accurate determination of the contact angle even in case of very low or high contact angles. The proposed capillary bridge probe method is based on the capture and analysis of the shape of the liquid bridge formed between the cylindrical probe and the investigated surface, and on the measurement and analytical calculation of the capillary force. Advancing and receding contact angles can be determined by changing the distance between the probe and the surface even in case of very low contact angles.

The appropriate measuring setup was constructed and built up. The main advantage of the method emanates from the use of the probe: the contact angle can change continuously at the edge of the probe oppositely to the recent apparatuses. A further uniqueness of the construction is the closed sample chamber providing close-to-saturated atmosphere.

The evaluation is based on the accurate image analysis of the liquid bridges and on the analytic calculation of their properties during one approach-retraction cycle. The evaluation program was implemented for nodoid-shaped bridges, i.e., for surfaces of contact angle less than 90°.

Close to the ideal surfaces (freshly cleaned glass slides, SiO_2, Si_3N_4) and surfaces with significant hysteresis are analysed (Al_2O_3, GaO_2) and the contact angle values are compared to the results of the sessile drop method. Furthermore, the behaviour of these r-ϑ capillary bridges are investigated first and compared to the statements and models of the literature on ϑ-ϑ capillary bridges between identical planes.

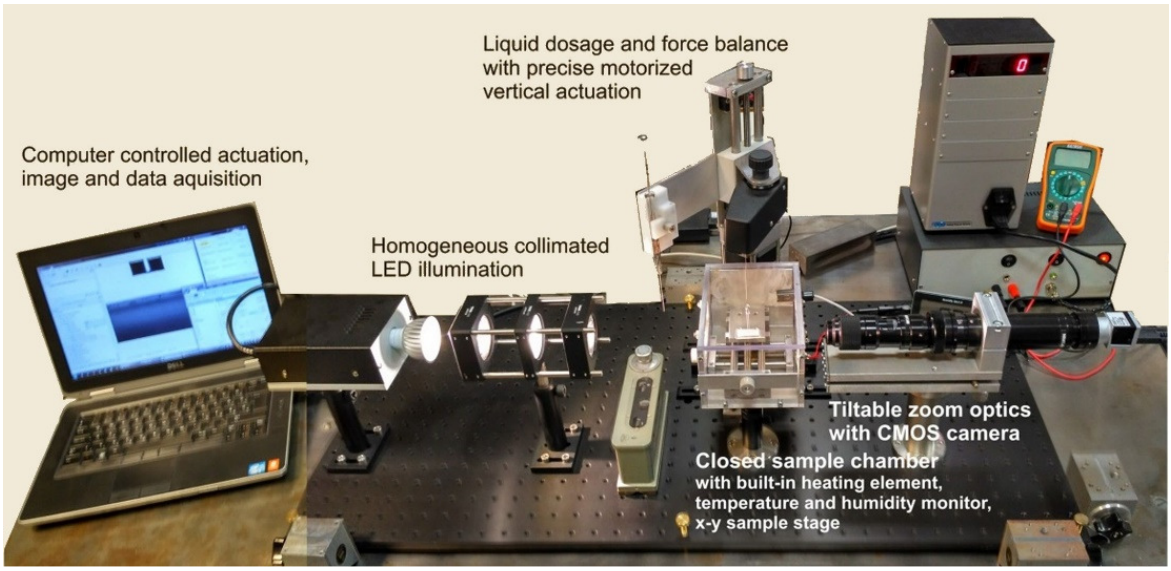

Figure 1: The accomplished apparatus for highly sensitive characterization of solid surfaces by the sessile drop or by the capillary bridge probe method, furthermore for investigation of r-ϑ capillary bridges.

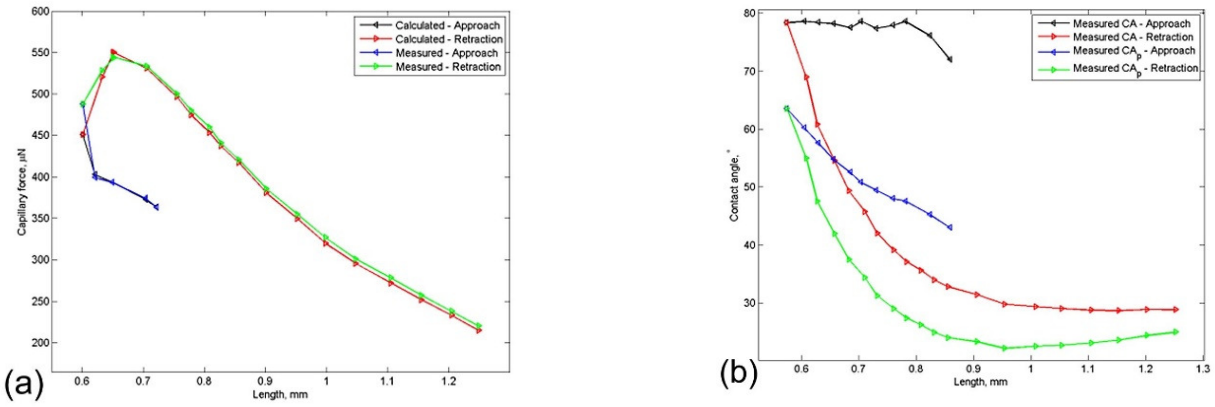

Figure 2: Measured and calculated capillary force (a): and the determined contact angles (b): on the investigated surface and on the probe (CA_p) in the function of bridge length during one approaching-reversal cycle, measured on a GaO_2 thin film with high hysteresis.

OPTICAL AND STRUCTURAL CHARACTERIZATION OF GE CLUSTERS EMBEDDED IN ZrO_2

(OTKA K 115852, M-ERA.NET WaterSafe No. 39/2016, OTKA NN 117847)

E. Agócs, Z. Zolnai, A. K. Rossal, J. A. van den Berg, B. Fodor, D. Lehninger, L. Khomenkova, S. Ponomaryov, O. Gudymenko, V. Yukhymchuk, B. Kalas, J. Heitmann, and P. Petrik

Recently, a promising application of Ge-NCs embedded in ZrO_2 matrix for nanocrystal-based memory devices has been shown, since Ge has a smaller band gap than Si, and ZrO_2 has a higher k value than SiO_2 that increases the electric field across the tunneling oxide. This material system may also be interesting for third-generation solar cells, since Ge has a higher exciton Bohr radius. Therefore, a stronger quantum confinement effect is expected than for e.g. Si nanocrystals, and the band gap can better be adjusted.

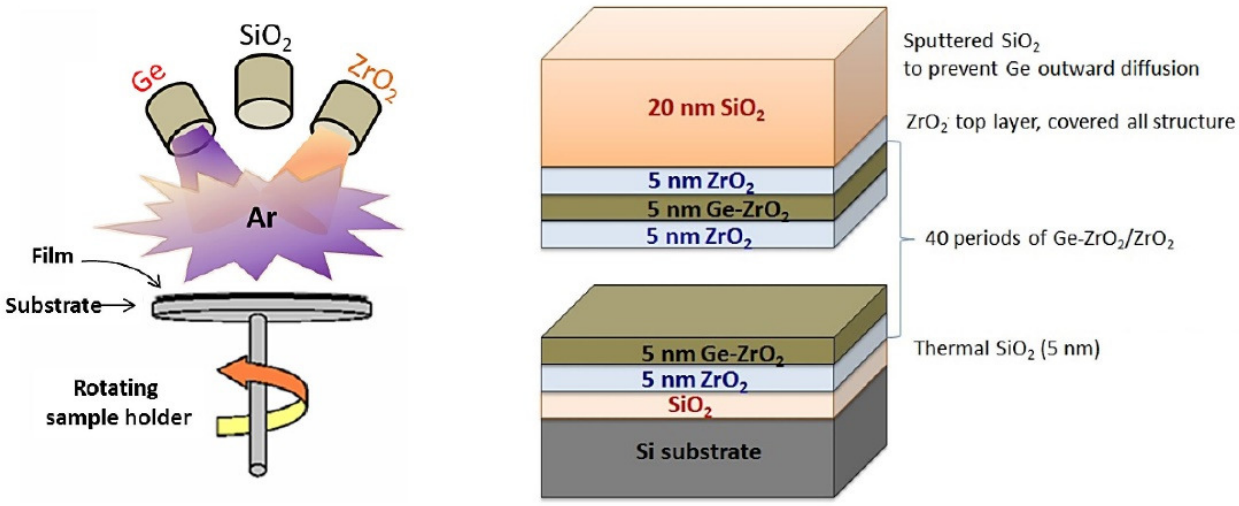

Figure 1: Shematic graph about the sample preparation (left), and the structure of samples (right).

The present study has two major aims. First, to develop and to test proper optical models to determine Ge nanocrystals in a single Ge-rich-ZrO_2 layer as well as in a multi-layer structure. Second, to demonstrate the validity of this method by the optical investigation of the evolution of the samples structure caused by annealing.

The samples were fabricated using a radio-frequency (RF) magnetron sputtering system equipped with a confocal arrangement of 3-inch targets (Ge, ZrO_2 and SiO_2) (Fig 1). The ellipsometric measurements were performed by means of a Woollam M-2000DI rotating compensator ellipsometer. Raman scattering spectra were excited with a 488.0 nm line of an Ar^+ laser and recorded using a LabRam HR800 micro-Raman system equipped with a Peltier-cooled CCD detector.

References for both ZrO_2 and pure Ge were determined on single-layer samples prepared with the same deposition conditions as those used for multilayer structures. The dielectric function of the ZrO_2 component was described by the Cauchy parametrization (Result: A = 1.988, B = 0.0092 μm^2 and C = 0.000812 μm^4.).

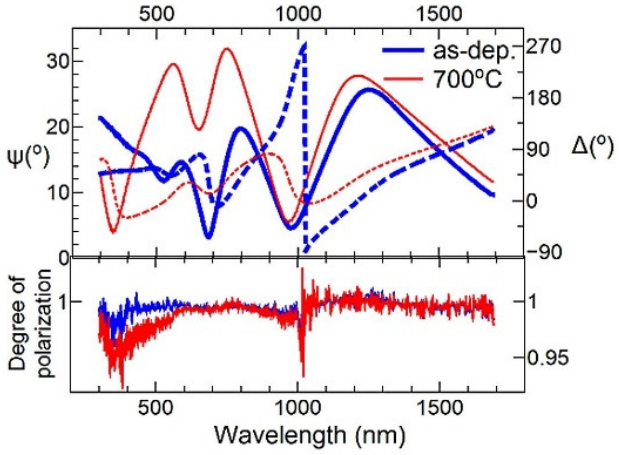

Figure 2: Measured Ψ (solid lines) and Δ (dashed lines) spectra for Sample Ge-ZrO_2 annealed at 700 °C as well as without annealing.

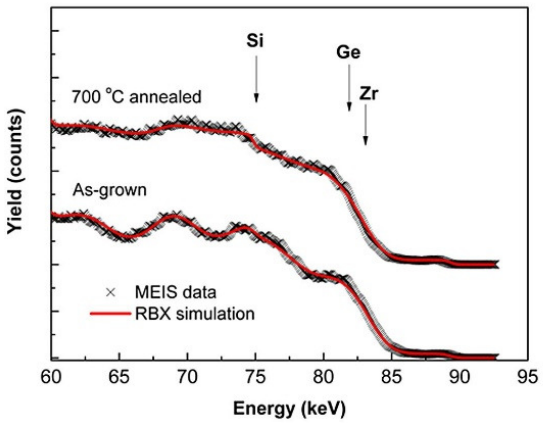

Figure 3: Medium Energy Ion Scattering spectra and the corresponding RBX simulations of as-deposited and annealed Ge-ZrO_2 samples.

References for both ZrO_2 and pure Ge were determined on single-layer samples prepared with the same deposition conditions as those used for multilayer structures. The dielectric function of the ZrO_2 component was described by the Cauchy parametrization (Result: A = 1.988, B = 0.0092 μm² and C = 0.000812 μm⁴.). Germanium requires more complex parameterization of the dielectric function for the modelling. For the as-deposited Ge layer the Urbach-Cody-Lorentz parameterization was used. The superlattice samples have been modeled using either a single-layer (MsL) or a multi-layer (MmL) approach. Both of them utilize a layer stack of Si(substrate) / SiO_2 / SL / SiO_2, whereas the 'MsL' and the 'MmL' models use a Bruggeman-Effective Medium Approximation (B-EMA) layer and 40 pairs of B-EMA layers, respectively, describing the superlattice (SL) structure (Fig. 1 right). In the B-EMA layer, we used the Ge and ZrO_2 references determined above.

It has been shown that ellipsometry offers a characterization method of Ge/ZrO_2 and Ge-rich-ZrO_2/ZrO_2 multi-layer structures with high sensitivity. The as-deposited structure was successfully modeled using reference optical constants determined from single-layer characterizations. It has also been shown that the surface region (several layer-pairs from the top) can sensitively be measured by Medium Energy Ion Scattering (MEIS), that revealed substantial diffusion during annealing.

ELLIPSOMETRIC AND X-RAY SPECTROMETRIC INVESTIGATION OF FIBRINOGEN PROTEIN LAYERS

(TÉT-12-DE-1-2013-0002, OTKA K 115852, M-ERA.NET WaterSafe No. 39/2016, OTKA NN 117849)

B. Kalas, B. Pollakowski, A. Nutsch, C. Streeck, J. Nádor, M. Fried, B. Beckhoff, and P. Petrik

The quantitative measurement of thin protein layers is of primary importance from both the metrology point of view and for many applications. Bovine fibrinogen monolayers on thin gold films and glassy carbon substrate were investigated using grazing incidence X-ray fluorescence (GIXRF) and spectroscopic ellipsometry (SE). The aim was to determine the amount of protein and to develop models and references for the SE measurement. Both methods were capable of measuring protein amount in the range of µg/cm² with a sensitivity below 10%, which suggests the use of both techniques as complementary, combined methods. To do it with a high confidence, the lateral uniformity and the stability of the layers during transportation has to be investigated in more detail in the future. The surface mass density and homogeneity were determined using X-ray and optical methods. Reference refractive indices have been measured and models have been developed in order to measure the thickness and the uniformity of the protein films quickly and accurately on surfaces. A fair agreement was found between the quantities determined by grazing incidence X-ray fluorescence and spectroscopic ellipsometry, however, the lateral homogeneity might also influence the results considerably.

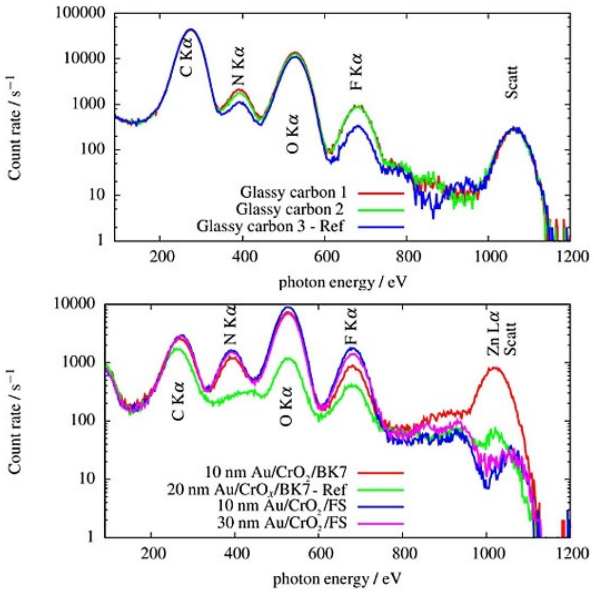

Figure 1: GIXRF spectra are exhibited recorded at a photon energy of about 1060 eV. Top: Spectra measured at glassy carbon. Bottom: Spectra measured at fused silica and glass substrate.

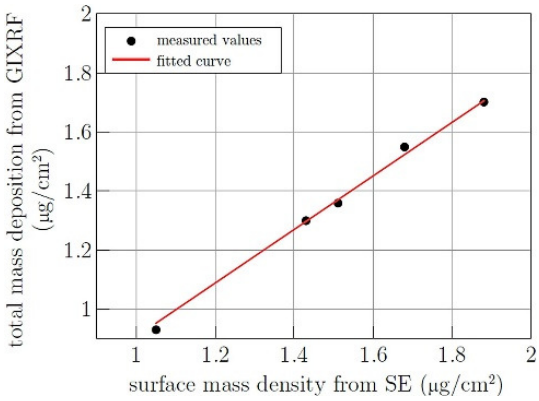

Figure 2: Comparison of the GIXRF and the SE results using the Cauchy expression. The data show a good agreement between the two methods, within their measurement errors.

VEGARD'S-LAW-LIKE DEPENDENCE OF THE ACTIVATION ENERGY FOR BLISTERING ON THE SI/GE RATIO IN HYDROGENATED A-SI_XGE_{1-X}

M. Serényi and A. Hámori

The relationship between the activation energy of blistering and the Si-to-Ge ratio has been determined in hydrogenated amorphous a-Si_xGe_{1-x} by employing layers deposited by radio frequency sputtering. To this aim the blistering activation energy was determined in several samples with different compositions, including x=0 and x=1. Each sample was submitted to heat treatment up to the temperature where the onset of blistering was observed by change of the surface reflectivity. A linear dependence of the activation energy on x has been established similar to the Vegard's law. The experimental result is supported by reaction kinetics modelling. It is suggested that the key step for the formation of blisters is the breakage of the SiH and GeH bonds. The related energetic reaction leading to the formation of H_2 molecules in a-Si_xGe_{1-x} follows a linear law as a function of the x composition similarly to the activation energy.

The activation energy E_a for blistering was determined by Arrhenius plots reporting the minimum time needed to make the blisters optically visible as a function of the temperature. The hydrogenated samples have been heated in air on a plate at constant temperature while illuminated by a 3 mW He-Ne laser beam with a diameter of 3 mm and angle of incidence of 60° which resulted in an elliptically illuminated sample area with size of about 3x6 mm² (Fig. 1). The reflected light fell onto a Si PIN detector blended with diameter of 3 mm. During the heating process the specular reflection transforms into a spread one, which has a dominant directional component that is partially diffused by surface irregularities. The onset of blistering was identified with the decrease of the reflected intensity caused by the outgoing rays reflected at many different angles. The activation energy Ea of the a-Si_xGe_{1-x} is displayed in Fig. 2 as a function of the x composition.

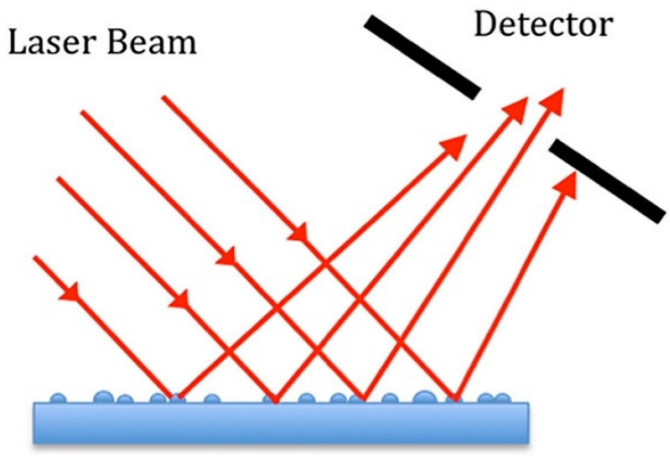

Figure 1: Sketch of the experimental procedure for detecting the onset of blistering.

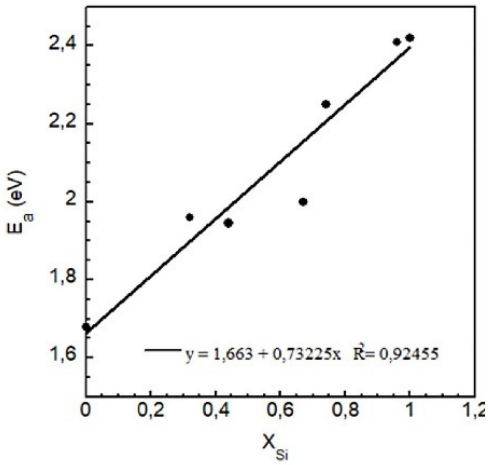

Figure 2: Blistering activation energy $E_a(Si_xGe_{1-x})$ in Si_xGe_{1-x} as a function of x.

POROUS SI DEGRADATION IN PHYSIOLOGICAL SOLUTION

B. Fodor, B. Kalas, T. Defforge, M. Fried, G. Gautier, and P. Petrik

Cooperation is being continued with the GREMAN laboratory of the University of Tours. Our long-term goal is the development of an accurate and selective biosensor. For this purpose, in situ ellipsometric characterization can be performed with the help of a flow cell, where the solution containing the particles would be adsorbed onto the substrate material, causing a detectable variation in the optical properties of the surface. Silicon-based nanostructured frameworks could be used as adsorbing substrates to increase the sensitivity and selectivity of proteins. However, without adequate surface treatment, these materials remain unstable in physiological solutions, i.e. degradation occurs. Therefore, the degradation in different solutions must be investigated, and appropriate stabilizing methods should be found by applying different surface chemistries (oxidation, carbonization). In a first step, we investigated the degradation by a flow of PBS solution (7.4 pH) for ~90 min. In Fig. 1, the effect of the degradation can be seen on porous silicon with an initial porosity of 68%. It is yet unsure if the collapse of the skeleton frame occurs during the *in situ* experiment or because of the drying step, but ellipsometric signal intensity was lost after 80 min.

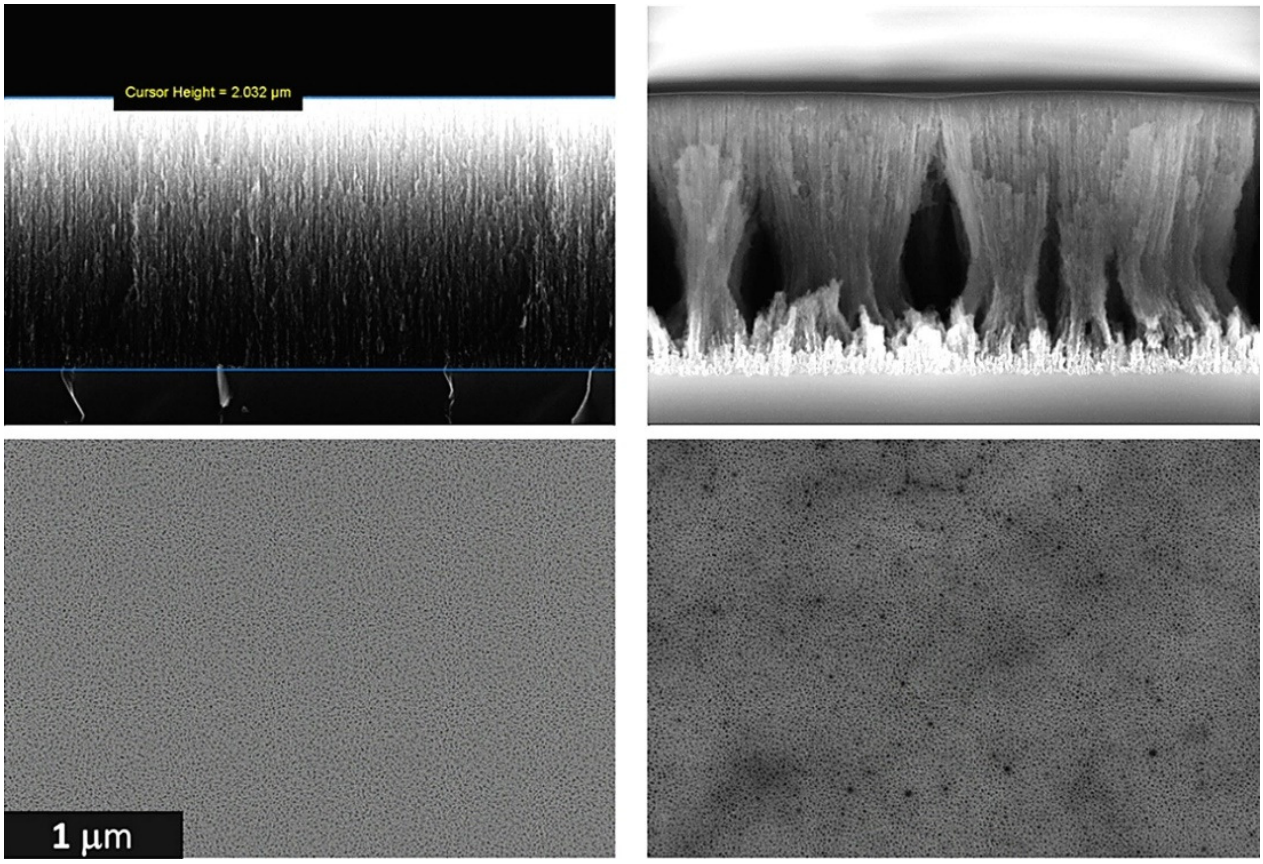

Figure 1: SEM images showing the degradation effect before (left) and after (right) a 100 min buffer solution flow experiment in a cross-sectional (top) and a top (bottom) view.

DEVELOPMENT OF MICRO GAS SENSORS

Cs. Dücső, Z. Baji, I. Bársony, G. Battistig, P. Földesy, P. Fürjes, Z. Hajnal, G. Molnár, A.E. Pap, V. Rakovics, J. Radó, Z. Szabó, I. Réti, Z. Zolnai, F. Biró, M. Takács

Solid-state gas sensing microstructures were developed aiming at the detection of hydrocarbons below their lower explosion limits as well as for measuring NH3 and H2S in the ppb – 00 ppm range.

Degradation mechanisms of microhotplates operated above 500°C

In calorimetric sensors for hydrocarbons a high T_c Pt micro-heater is coated with catalyst to initiate combustion of hydrocarbons in the presence of oxygen. The generated chemical reaction heat modifies the temperature, thereby the heater resistor. The transduction principle is based on resistance read-out. Our previous results show that the most efficient catalyst is Pt, however, the minimum temperature required is 500°C and 700°C for LPG and CH_4, respectively. A detailed investigation revealed the degradation mechanisms of the Pt filament. We found three phenomena of different activation energies leading to the continuous resistance change and finally the fatal degradation. First the TiO_2 adhesion layer beneath the Pt filament forms TiO_2 nanocrystals which penetrate the bulk of Pt. Parallel to the well-known electromigration effect, thermally driven Pt migration dominates in regions, where the local temperature exceeds ~850-900K and the temperature gradient approx. 0.5K. The coincidence both of thermo- and electromigration driven by temperature, and potential gradients precisely determine the position of the filament rupture. The phenomenon was proven by statistical analysis of experimental measurements. We determined the operation limits of the filaments and concluded that highest allowable temperature for a device expected being operational at least for one year is ~540°C (Fig.1).

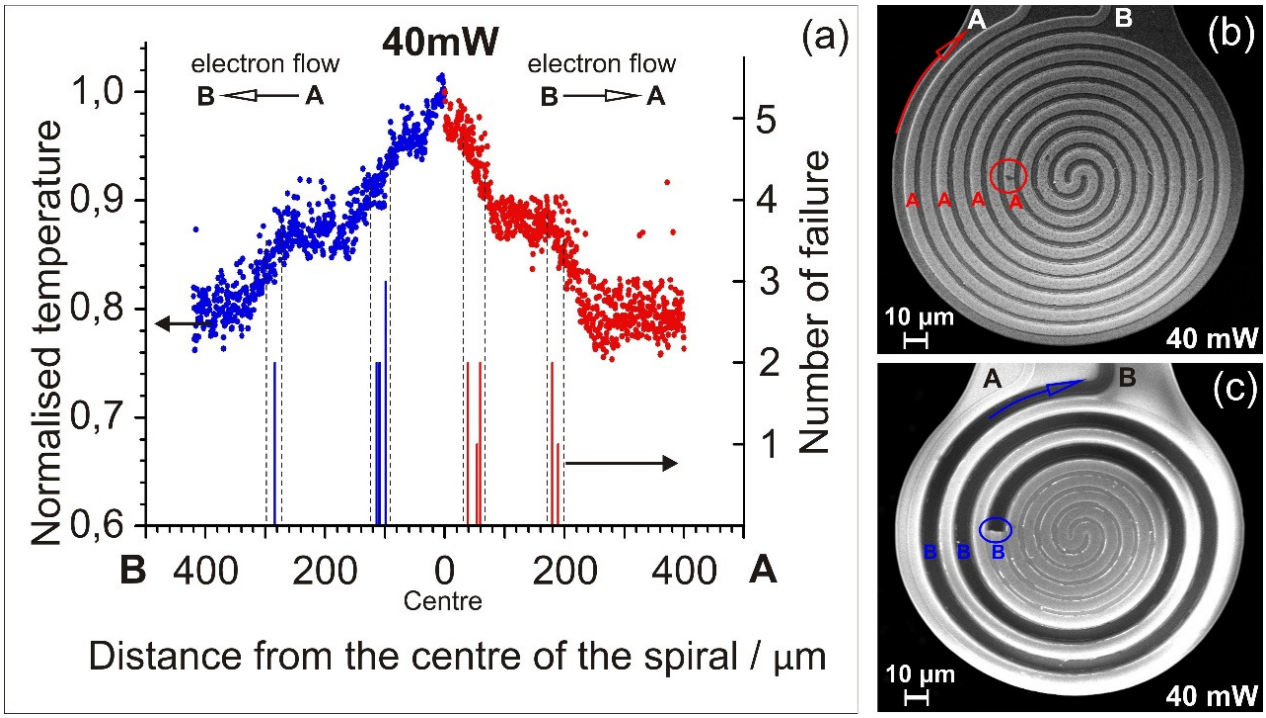

Figure 1: Graphical illustration of correlation between the temperature distribution and breakdown positions. Graphs on the left indicate the temperature profile as a function of the distance from the centre point along the filament as measured by pyrometry for 40 mW heating powers The number and position of ruptures for each of the hotplates are marked by bars. Corresponding SEM micrographs are shown on the right. Potential contrast mode image better reveals the location of the rupture. Blue and red colours denote the spiral arms, the electron flow direction (blue and red arrows) are indicated.

We also elaborated ALD technique to deposit 2-4 nm sized Pt nano-catalyst in the porous alumina surface formed by electrochemical etching of thin Al layer on top of the hotplate. Functional tests revealed another degradation mechanism, i.e. the coalescence of Pt nanocrystals at elevated temperature, and the thermo-migration of Pt due to the inhomogeneous temperature profile of the hotplate. Pt migrates in radial direction from the hottest centre towards the colder perimeter of the hotplate leading to the sensitivity loss.

From the above degradation mechanisms, we conclude that the investigated meander and coil-type filament heated hotplates covered with ALD Pt catalyst are capable to measure LPG (T_{max}<540°C), but for methane (T_{min}>700°C) the lifetime of the device is ~160hrs only at continuous loss of sensitivity. The best way for improvement is definitely to apply a new catalyst active at reduced temperature and to use pulse mode operation. Nevertheless, some improvement in lifetime is expected from novel geometric and possibly material design.

Conductivity type sensors for NH_3 and H_2S

Nanostructured WO_3 layers were synthetized, sensitized and characterized for their performance in detection of NH_3 and H_2S. In 2016, we elaborated a hydrothermal method for formation of hexagonal WO_3 nanorods and demonstrated the efficiency of Au and Pt doping. Reliable detection of H_2S down to 25 ppb was demonstrated.

As the drop deposition of the separately synthetized sensing layer is a bottleneck in reproducible mass production, thus, we elaborated wafer level processing methods to form uniform, nanostructured WO_3 layer on top of the microhotplates. Two alternatives were investigated; sol-gel process with spin-coating and electrochemical (anodic) etching of thin W layer. The sol-gel process results in sponge-like porous structure with 12-20 nm characteristic pore size, whereas 50-70nm diameter pores grown perpendicularly to the surface can be formed by the electrochemical process. Both techniques were integrated in the MEMS sequence using lift-off technique or selective anodization for lateral patterning. ALD Pt was deposited for sensitizing and the performance of all WO_3 structures was investigated. The operation temperature of the best sensors was found between 180-220°C. The electrochemically processed sensors doped with 2-4 nm Pt nanoparticles exhibited the best performance in terms of sensitivity and stability as well as regarding response and recovery time (Fig 2).

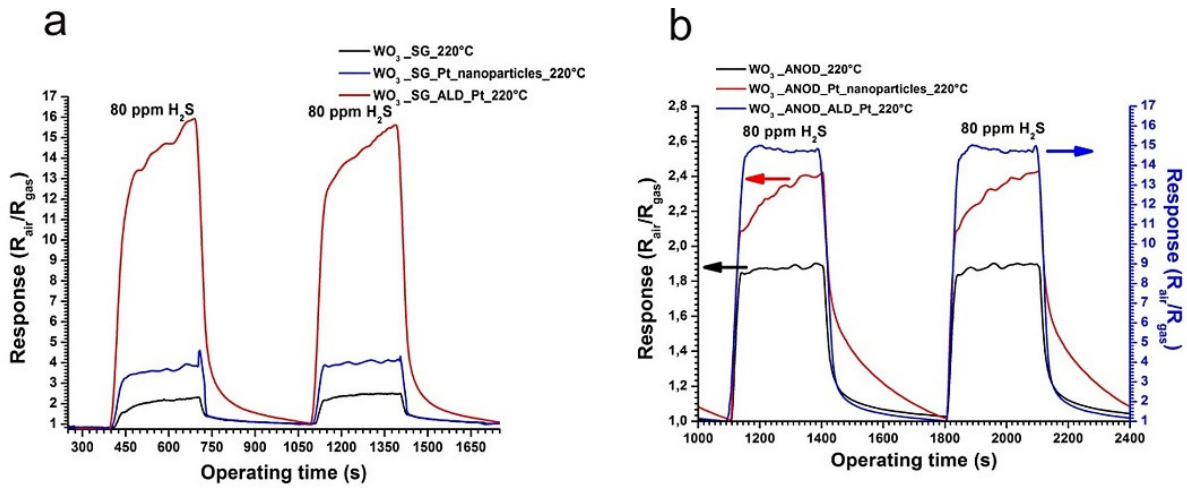

Figure 2: Transients of sol-gel (a), and electrochemically (b) formed sensors for exposure of H_2S.

In summary, we conclude that by low enough operation temperature we meet the sensor standards in terms of the hotplate stability and read-out dynamics. By proper selection of WO_3 nanostructure and sensitizers both NH_3 and H_2S can be detected in the 5-100 ppm range. ALD gold doping of electrochemically formed mesoporous WO_3 promises dynamic, reliable H_2S detection far below the ppm level.

Development and production of Near Infrared LEDs

This year, the activity was focused on further improvement of the multiple wavelength GaInAsP/InP NIR light source reported in 2016. Following structural/processing improvements demonstration activities were intensified to establish a cooperation-network for exploitation of the application potential of NIR LEDs.

Appropriate measures to increase our production capacity for the standard single wavelength, and the novel multiple wavelength NIR LED design were introduced.

POLYMER MICROFLUIDIC SYSTEMS FOR MEDICAL DIAGNOSTICS

P. Fürjes, O. Bálint-Hakkel, Cs. Dücső, P. Földesy, Z. Hajnal, E. Holczer, E.L. Tóth, J. Radó

Precise and fast Point of Care, PoC monitoring of disease related blood protein marker levels could be crucial in effective therapies. Due to the specific tools and novel microtechnology processes the cost-effective, complex but miniaturised analytical systems, such as Lab-on-a-Chip (LoC) and microfluidic devices have become available and can be implemented in the overall sample analysis from the preparation to the molecular diagnostics. The use of biological sample requires bio-inert surface properties with minimized non-specific adsorption and coagulation in the channels. The perspective of our work is to develop a polymer based microfluidic cartridge suitable to autonomously controlled sample transport and preparation of integrated bioanalytical devices.

Accordingly, microfluidic system was designed and manufactured for whole blood or plasma transport by precisely controlled sample rate. These autonomous sample transport systems can be integrated into PoC Lab-on-a-Chip based diagnostic devices. The developed systems are planned to be applied for detection of inflammation and cardiovascular diseases, in cooperation with "Diagnosticum Inc." and "77 Elektronika Ltd.".

Characterization of blood protein adsorption on modified PDMS surfaces

Polymer based microfluidic sample transport system with multiple functions was developed for application in bioanalytical devices detecting blood protein biomarkers or cells. Significant flow controlling subparts of the overall microfluidic system were designed, fabricated and characterized in the function of different surface modifications and microscale geometries. In order to fulfil the requirements, the polydimethylsiloxane (PDMS) base material was modified by embedding PDMS-b-PEO molecules into the PDMS matrix. PDMS-b-PEO molecules change the inherent hydrophobicity of the polymer ensuring adequate capillary pressure for self-driven transport and affecting also the level of the non-specific protein adsorption simultaneously.

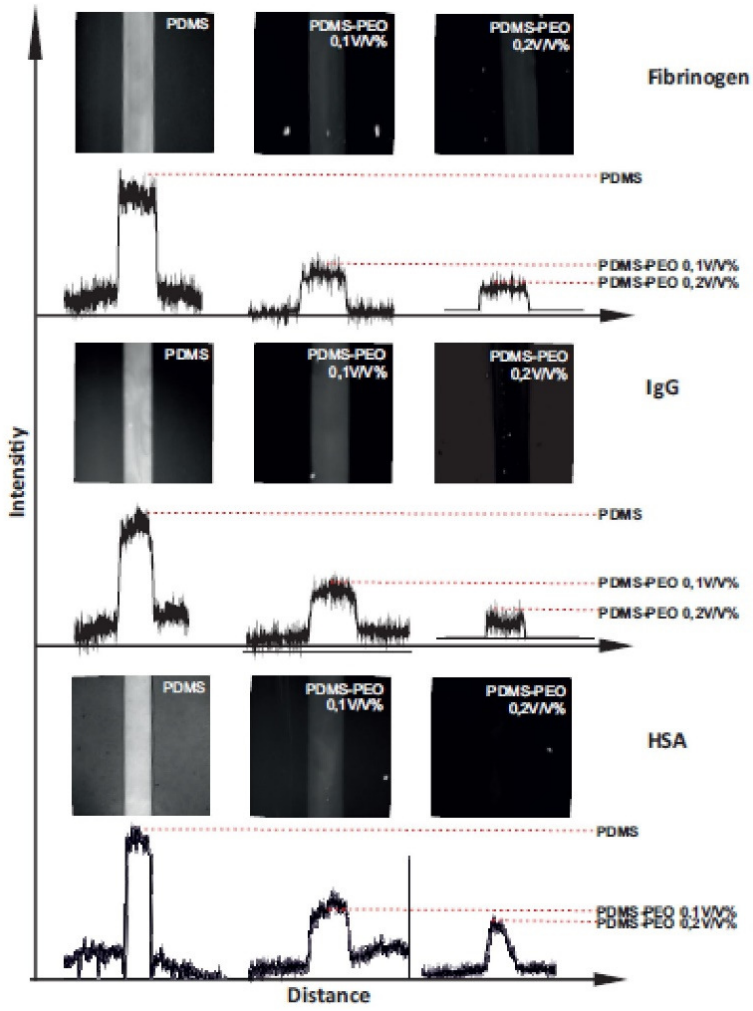

Figure 1: Recorded fluorescent intensities indicating the presence of irreversibly bonded fluorescent labelled protein molecules on the microchannel surfaces.

In order to modify the surface characteristics of PDMS, PDMS-b-PEO block-copolymer was added in different concentrations into the non-polymerized raw mixture. The embedded copolymer molecules can not only enhance the wettability of the surface, but also reduce the non-specific protein adsorption, significantly and permanently. The embedded molecule concentration dependent surface adsorption of typical human blood proteins (HSA, IgG, fibrinogen) were characterized by

fluorescent microscopy and BCA colorimetric protein assay in the function of the modified PDMS surfaces. The applied methods enable quantitative determination of the relative and absolute amount of irreversibly bonded proteins. Based on the results material compositions were defined in order to avoid the non-specific adsorption of different proteins in autonomous microfluidic systems. Embedding non-ionic surfactants in the PDMS effectively changes the surface characteristics of the material. The non-specific protein adsorption can also be significantly decreased by the developed surface modification method. By embedding PDMS-b-PEO molecules above 0.5V/V% concentration the irreversible protein binding can be completely terminated. (Fig. 1)

Fabrication of hybrid microfluidic system on transparent substrates

High complexity polymer or hybrid microfluidic structures open the way towards fabrication of cheap, disposable analytical cartridges. Glass and polycarbonate were considered as primary transparent substrate material for metal (Au, Pt) electrode deposition, whereas the microchannels were formed in multi-layered SU-8 negative photoresist. PDMS layer was proposed as cover layer for proper sealing and sample inlet formation (Fig. 2). Our aim was to modify both the SU-8 and PDMS surface in order to form covalent bond between the substrates. According to the literature the feasible SU-8 / PDMS binding is evolving through the reaction of the epoxy groups and amino groups, however our attempts to reproduce the published recipes failed in most cases. Several bonding strategies were characterized in terms of their adhesion and stability, considering plasma processes (O_2, N_2) and silanization treatments. Chemical composition of the SU-8 and PDMS bonding surfaces were analysed by sensitive analytical methods in molecular level. The appropriate materials and processes were defined to achieve reliable formation of complex hybrid polymer microfluidic systems. Accordingly, SU-8 series can be bonded to PDMS layer after silanization of its surface and oxygen plasma treatment of PDMS. This method enables to form integrated hybrid microfluidic cartridge on transparent substrates.

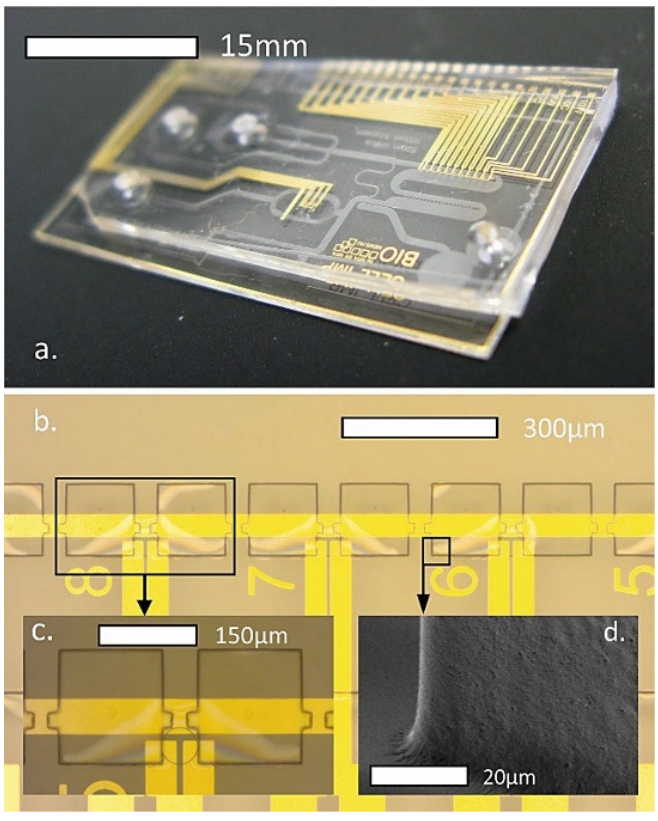

Figure 2: Metal (Au) electrodes integrated in SU-8 based hybrid microfluidic system (a). For proper alignment, electric insulation and transparency the channels are formed in multi-layered SU-8 (b, c). SEM view presents the interface between the thin insulation and the thick channel forming SU-8 layers (d).

CELL AND PARTICLE MANIPULATION AND SCREENING IN MICROFLUIDIC SYSTEMS

P. Fürjes, O. Bálint-Hakkel, Cs. Dücső, P. Földesy, Z. Hajnal, E. Holczer, E.L. Tóth, J. Radó

The rapid development of microscale diagnostic (Lab-on-a-Chip) devices has underlined the importance of microfluidics enabling fast and effective preparation and analysis of liquid samples. Nevertheless, due to the governing physical phenomena on microscale, classical sample preparation methods might become challenging, such as the effective mixing of fluids as well as the size-dependent separation of corpuscles and their sorting or filtering from the liquid samples. This leads to the development of novel microfluidic structures based on the physical laws of this size domain.

Modelling and characterisation of cell and molecule advection in continuous microfluidic systems

Lab-on-a-Chip applications often require separation of particles of specific properties e.g., shape, size, density or other physical, chemical or biological properties. Microfluidic chip with special channel layout was developed for hydrodynamic particle sorting by their cell size or density for optical scattering based pollution monitoring applications. Finite Element Method (FEM) was used to model the hydrodynamic properties and the behaviour of the microfluidic system including their effects on particle movement. COMSOL Multiphysics software was used to calculate the laminar flow field and particle trajectories having different parameters along the channel. The microfluidic chip was fabricated by fast prototyping using SU-8 photoresist and polydimethylsiloxane (PDMS) for replica moulding. The developed chip was evaluated using fluorescent microscopy with two particles of 10 and 16 µm diameters labelled with different fluorescent dyes. Measurement was in good agreement with the modelling predictions and successful size-dependent particle sorting was demonstrated.

Particle separation and trapping in micromagnetic separation (MMS) systems

Bioanalytical methods based on detection of receptor / marker protein interactions are widespread in today's clinical diagnostics. Determination of specific receptor molecules with high affinity (such as antibodies or artificial aptamer molecules) is a key issue of assay development. Aptamers can recognize a wide range of targets, from ions to complex cellular macromolecules, although their synthesis by in-vitro SELEX (Systematic Evolution of Ligands by Exponential Enrichment) method is a time and money consuming process. Using microfluidic SELEX method, the aptamer selection process can be improved and accelerated, and pave the way for development specific diagnostic devices. The aim of this work is to adapt, study, and optimize magnetophoretic separation and trapping methods in microfluidic systems to be applied in mSELEX process. Microfluidic Magnetic Separation (MMS) devices use the effective magnetophoresis based magnetic bead manipulation by applying microfabricated paramagnetic patterns to locally amplify the magnetic field. With the integration of ferromagnetic (FeNi) microstructures into a microfluidic platform the lateral magnetic field gradient can be altered and locally enhanced, thereby enabling the precise manipulation of small amount of magnetic beads.

Different micromagnetic separation (MMS) systems with various ferromagnetic pattern and microfluidic channel geometry were designed, modelled, fabricated and characterised. The studied microfluidic structures were manufactured by the combination of traditional micromachining and soft lithography methods in heterogeneous glass-polymer (PDMS, polydimethylsiloxane) systems. Different micromagnetic separation (MMS) systems were characterised considering their separation and trapping parameters using superparamagnetic beads.

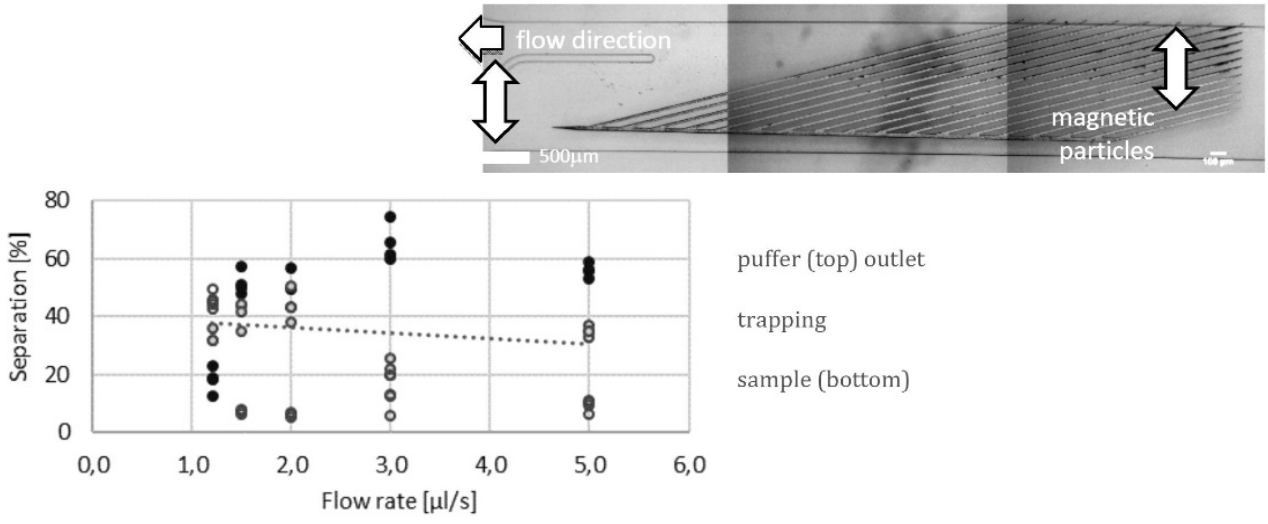

Figure 1: MicroMagnetic Separation structure in the microfluidic channel (top) and the flow rate dependent separation efficiency (bottom).

MMS systems were proved to be applicable for temporal (trapping) and spatial separation of superparamagnetic particles. Based on the experiments an efficient micromagnetic separation architecture was proposed including the special layout of the ferromagnetic microstructure and the geometry of the fluidic system.

Droplet generation and trapping for cell analytical two-phase microfluidic system

Multi-phase flows have numerous applications in the growing field of Lab-on-a-Chip (LOC) technology. In these multi-phase flow devices, monodisperse sheath emulsion helps to manipulate, focus and separate encapsulated chemical reagents or living cells. Therefore, cell-analytical and diagnostic procedures can be automatized on microscale, although the precise control of droplet parameters and movements are essential for their reliable application. Present work focuses on the design and characterisation of a two-phase microfluidic device with integrated electrode system (Fig. 2) for impedance analysis. The system is capable to create and manipulate droplets having pre-determined size aligned to the cell diameter of 4-20 μm.

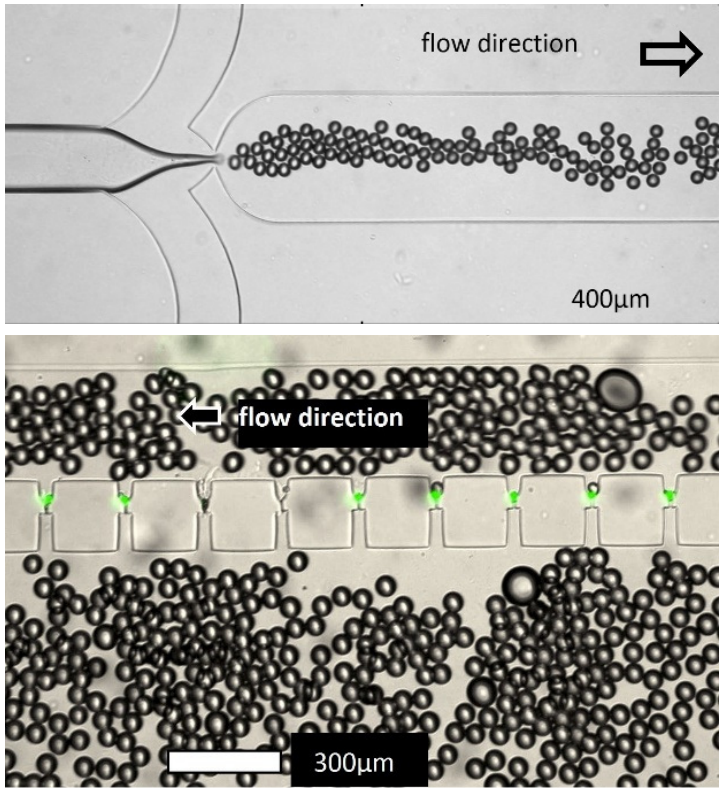

Figure 2: Droplets generated in the two-phase microfluidic system (top), and encapsulated fluorescent beads trapped in the perforated cavities of the model microfluidic system (bottom).

Present study analysed the influence of flow characteristics of special water-oil two-phase microfluidic systems on the droplet generation, cell encapsulation and trapping processes. Water droplets were dispersed in a continuous phase oil targeting precise size distribution to enable effective cell entrapment. The evolving droplet size and the number of encapsulated cells were examined considering the applied flow rate ratios of the two phases. Droplet size dependency on geometrical and flow parameters has been investigated experimentally with special focus on the influence of flow rates and their ratios. Yeast cells were encapsulated in water droplets and distribution of their number in a single containment was also recorded. Direct dependency on the flow rate ratios with multiple maximum was observed versus the size distribution of the yeast cells.

Model was built in the simulation code COMSOL Multiphysics ©. The hydrodynamic environment of the trapping zone and droplet trajectories were calculated. The hydrodynamic behaviour of the microfluidic system was modelled by Finite Element Method (FEM) coupled with particle trajectory. Flow velocity field and decreasing flow rates in the perpendicular perforations demonstrate decreasing trapping efficiency of the cavities in the direction of the main flow. The suspected effect was verified by encapsulation and trapping fluorescent particles (Spherotech, 10 μm diameter): the trapping probability was experienced to be highest near the inlet of the trapping zone. The experimental results were compared to the simulation and the applicability of our droplet based cell microfluidic system was characterised.

CONCENTRATION GRADIENT GENERATION FOR CELL POPULATION ANALYSIS

P. Fürjes, O. Bálint-Hakkel, Cs. Dücső, P. Földesy, Z. Hajnal, E. Holczer, E.L. Tóth, J. Radó

The chemical environment plays significant role in controlling biological, physiological processes in the living organism at molecular level. Accordingly, several biomedical researches aim to study the behaviour of cells in artificial chemical concentration distributions. Such as studying the mechanism of chemotherapy in cancer research can be highlighted. Due to the low sample volumes and accelerated reactions in microfluidic environment, this apparatus is highly suitable for advanced analysis of cell populations. These Lab-on-a-Chip (LoC) microfluidic systems are suitable for more realistic and accurate reproduction of extracellular microenvironment as well as for the manipulation and examination of cell populations with limited, but representative size. Flow-based concentration gradient generators (CGGs) are capable to maintain a stable spatial and temporal concentration distribution, which can be dynamically changed. Note, that due to the laminar flow conditions the molecular diffusion is limited, thereof special geometric design is needed to improve the performance of these microfluidic systems.

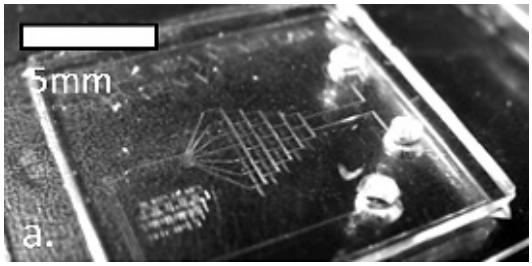

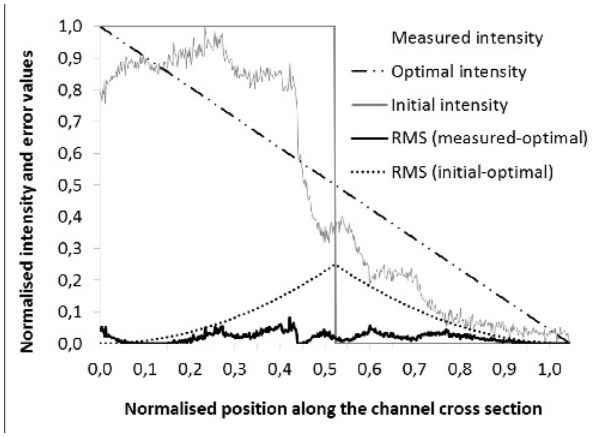

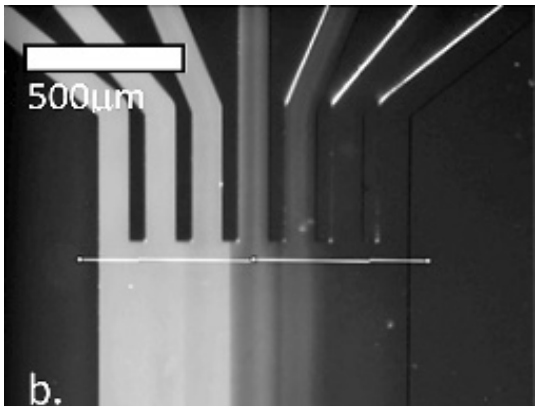

Figure 1: Enhanced pyramid type CGG structure with Herringbone mixer (a), and the fluorescent intensity distribution (b, c) of the HSA concentration (at 0.1µL/s flow rate).

Microfluidic chemical concentration gradient generators (CGGs) were designed with advanced geometric structures to establish a stable gradient along the gradient chamber at the output region. Basic structures were combined with secondary Herringbone mixers to improve the efficiency of distinct structures. The resulted concentration distributions were characterized for different flow rates and the performance of a given generator was defined as the root-mean-square of the difference between the measured and the ideal linear concentration values. The quality factors of the different structures were compared and the advantage of the integrated Herringbone mixer structures were proved.

SERS ACTIVE PERIODIC 3D STRUCTURE FOR TRAPPING AND HIGH SENSITIVE MOLECULAR ANALYSIS OF PARTICLES OR CELLS

P. Fürjes, O. Bálint-Hakkel, Cs. Dücső, P. Földesy, Z. Hajnal, E. Holczer, E.L. Tóth, J. Radó

SERS (Surface Enhanced Raman Spectroscopy) evolves in close vicinity of metallic nanostructures where the interaction between the electromagnetic field of photons and the surface plasmons results in several orders of magnitude enhancement of the Raman signal. This effect extremely improves the sensitivity of Raman spectroscopy achieving the limit of molecule detection in attomolar (10^{-18} M) concentrations.

The highly sensitive molecule recognition performance of a specially designed surface SERS substrate was demonstrated. The general inverse pyramid structures were perforated as cavities in perforated membrane applicable for particle and cell filtering, sorting and trapping. In the voids of the gold covered substrate size compatible particles functionalised by different molecules were trapped, their SERS signal was detected and the different molecules were recognised (Fig.1).

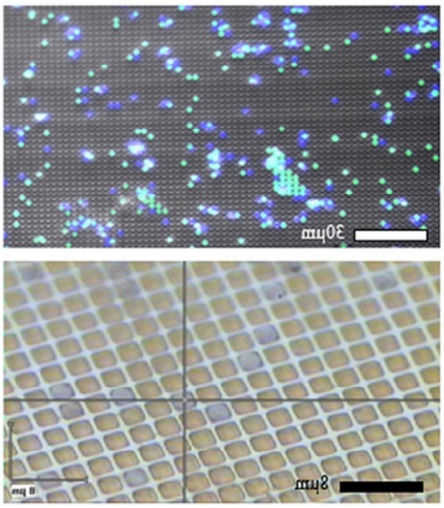

Figure 1: Fluorescent beads with appropriate 2µm diameter (Sigma Aldrich - green and Spherotech - blue) entrapped in the periodic array of perforated pyramidal structures: multichannel fluorescent image (top) and upright optical micrograph (bottom).

The fluorescent molecules were analysed by SERS taking advantage of the plasmonic enhancement by the structured surface of the traps. The definite and sensitive differentiation of the molecules immobilized on the polystyrene bead surfaces are presented in Fig. 2, where a huge increase in the Raman signal can be observed on the SERS surface.

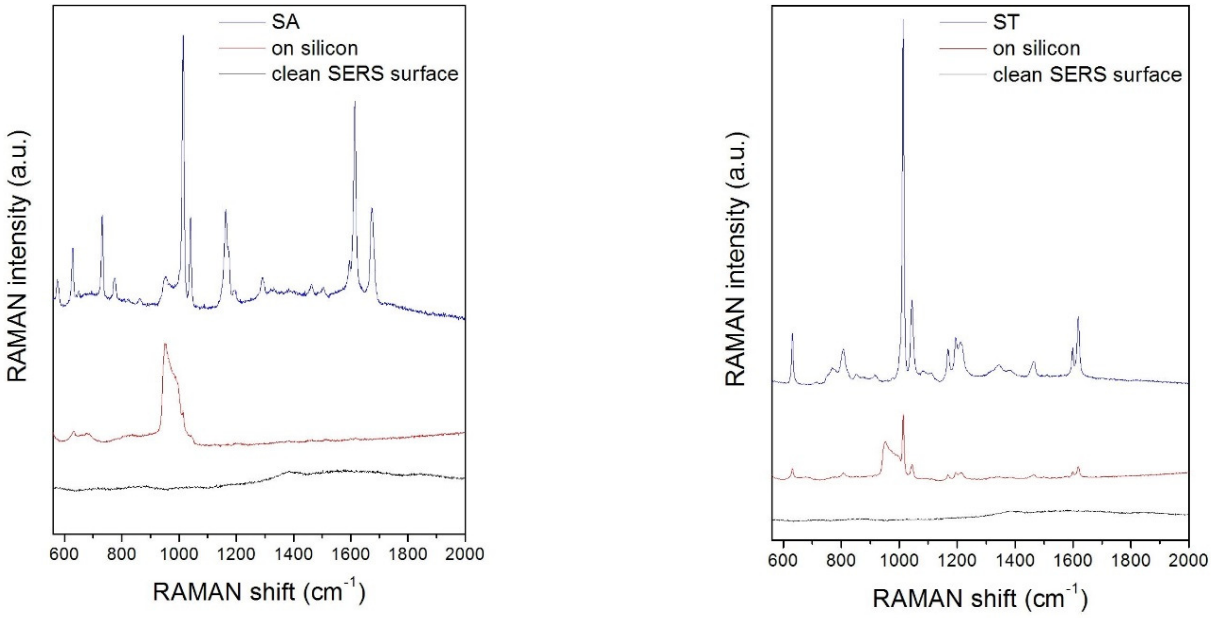

Figure 2: Comparison of the SERS spectra recorded on the clean SERS substrate (black) and different fluorescent beads on silicon (red) and trapped in the periodic array (blue). SA – Sigma Aldrich and ST - Spherotech fluorescent beads, respectively.

The advantage of the 3D structure was demonstrated for simultaneous particle (or cell) trapping and extremely sensitive SERS-based detection of molecules immobilized on the surfaces of the confined beads.

INTELLIGENT WOUND PATCH FOR ONLINE MONITORING WOUND HEALING PROCESSES – WOUNDER

P. Fürjes, O. Bálint-Hakkel, Cs. Dücső, P. Földesy, Z. Hajnal, E. Holczer, E.L. Tóth, J. Radó

In the clinical practice, the proper care of wounds is of primary importance in the case of accidents, postoperative and ulcerative ulcers. It is a basic expectation of the treating physician or nurse to provide continuous or regular information on the healing of the wound. In case of a home-based hospitalization, the control of wound is time consuming and difficult for the physician, but remote monitoring of the appropriate parameters can help in effective curing. The role of the intelligent bond is to facilitate the work of both the physician and the patient by monitoring the process of healing and, in the event of a problem, warns the user and the physician about the need for a check or a replacement.

In this work an intelligent tool was developed to provide continuous information about various parameters of the wound healing, such as temperature, humidity, and the tightness of the bandage. These are the major parameters determining the condition of the recovery of the injury. Aiming at the final wireless, point-of-care application we focused on the minimization of the energy consumption. Appropriate sensors were chosen and integrated into a flexible PCB. Low power consumption electronics solve the preliminary signal processing and communication tasks using Bluetooth protocol. Data processing and visualisation software was also developed (Fig.1). Functionality tests, calibrations and the influence on the patient behaviour are in progress.

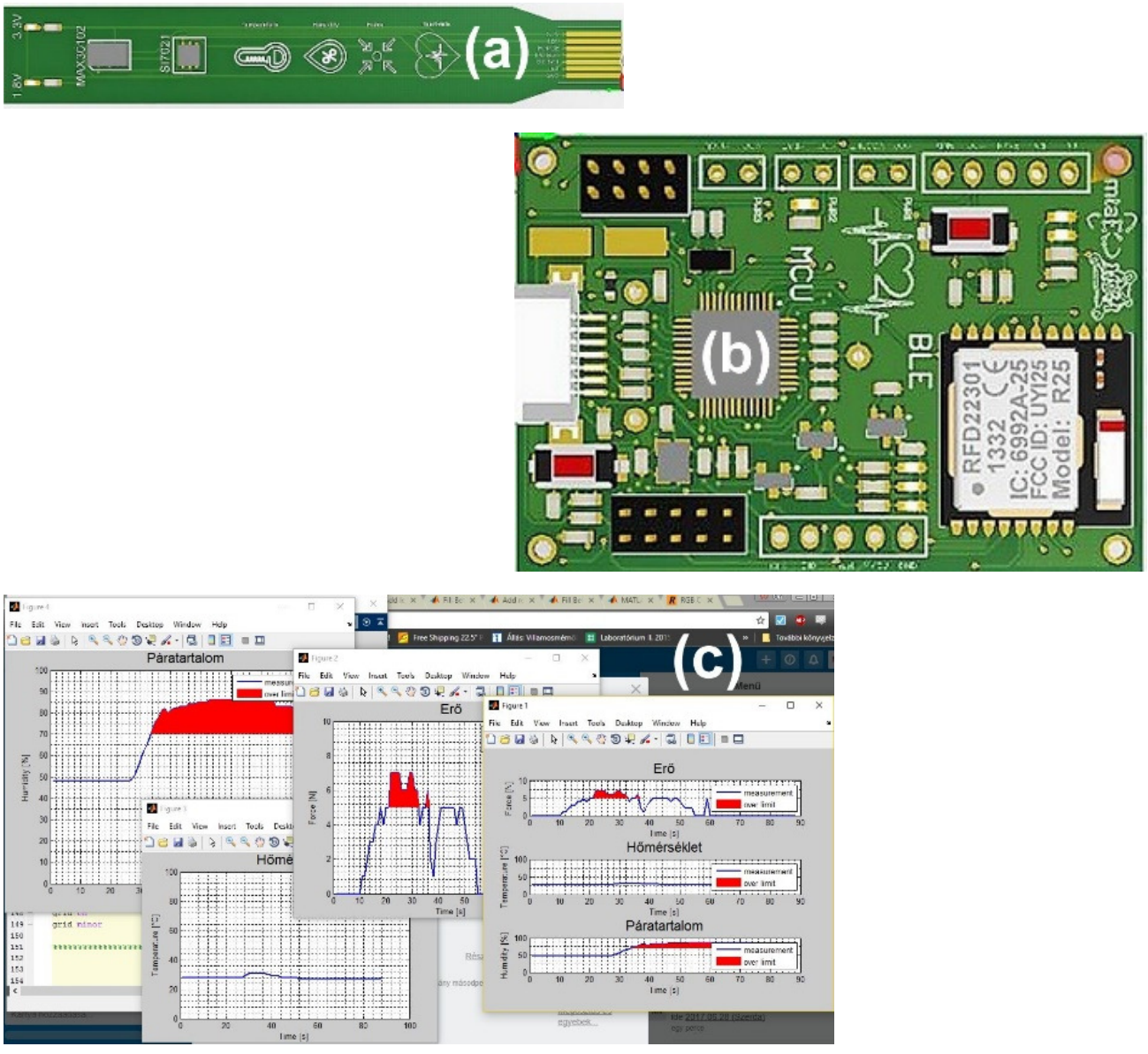

Figure 1: Flexible PCB for sensors (a), and signal processing electronics (b), for wound healing monitoring system. The sensor data can be visualised in the application specific software (c) – WoundER / PC.

PRECISELY CONTROLLED FOCUSED ION BEAM MILLING OF SOLID STATE NANOPORE ARRAY FOR MOLECULE SENSING

P. Fürjes, O. Bálint-Hakkel, Cs. Dücső, P. Földesy, Z. Hajnal, E. Holczer, E.L. Tóth, J. Radó

Nanoporous membranes are fundamental components of the transport modulation based label free electrochemical biosensors envisioned for high sensitive molecule detection. The sensitivity and the specificity of these sensors are significantly affected by the pore geometry what has to be fitted to the size and conformation of the target molecules. Precise tailoring of nanopore geometries and alignment to target molecule conformation and size improves the signal-to-noise level of the identification method - in our case the impedance spectroscopy. This pore geometry engineering is essential for reliable and reproducible manufacturing of solid state nanopore-arrays in integrated molecule diagnostic devices. Commercialization of the nanopore based biosensors or Lab-on-a-Chip devices seem to depend on the development of the high throughput nanofabrication techniques enabling reliable and reproducible shaping nanopore geometries in solid state membranes.

During this work, FIB milling process was exploited and the resulting time dependent nanopore geometries were characterized to achieve reliable and reproducible manufacturing nanoporous dielectric membranes. The time dependence of the evolving pore diameter in different layer structures was studied during ion beam milling. A pore diameter evolution rate parameter (γ) was defined, its continuous regression during the milling process verified and interpreted by the Gaussian profile of the spatial ion intensity distribution of the ion beam. Adequate milling parameters (current, time) must be defined to achieve precise and predictable pore evolution in the applied membrane structure. The reproducibility of the FIB nanoprocessing was improved by neutralization (electrostatic grounding) of the sample surface. By this technique the distortion of the pore diameter could be reduced significantly, and the pore size variations reproducibly kept below 5 nm (Figure 1).

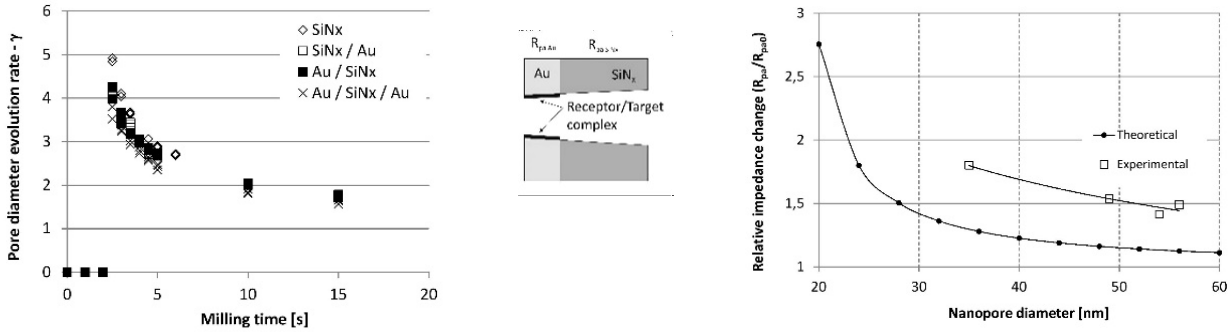

Figure 1: Pore diameter evolution rate parameter (γ) as a function of the milling time (10 pA ion current and 30 keV ion energy) (left). Theoretical and measured relative impedance variation of the solid-state nanopore array as a function of the nanopore-diameter after avidin binding (right).

The performance of membrane impedance analysis based molecule detection was studied by avidin-biotin binding in the nanopore array. The application of uniform pores is a major importance, since the sensor response depends on both the concentration of the target molecule and the pore size as well. Development of precise nanoprocessing techniques of predictable yield is therefore an elementary requirement for molecule sensing.

PIEZOELECTRIC NANOWIRE ARRAYS FOR HIGH RESOLUTION TACTILE MAPPING

J. Volk, Zs. Baji, A. Békési, G. Battistig, Cs. Dücső, P. Földesy, N. Q. Khánh, I. Lukács, Gy. Molnár, A. L. Tóth, Zs. Zolnai, Z. Szabó, and I. Bársony

In 2017 our main contribution to the project was the completion of the fabrication process and the functional characterization of a high-resolution fingerprint sensor, where all the 250 nanowire (NW) pixels are contacted vertically (top-bottom contact). The base chips with Ga doped ZnO (GZO) seed layers and bottom contact were produced by project partner CEA-LETI. The subsequent fabrication steps, including the wet chemical NW growth, encapsulation, and top contact formation (Fig. 1) were optimized by the MFA team.

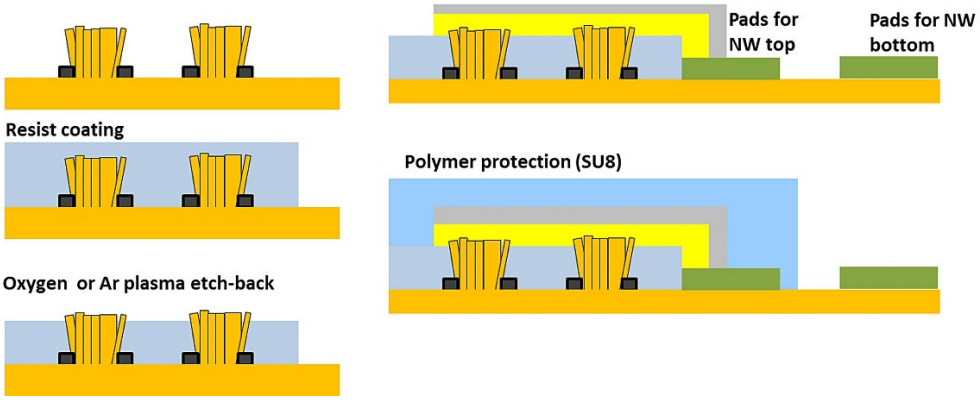

Figure 1: Schematic representation of the process steps for top-bottom contacted NW: selective area wet chemical growth, polymer encapsulation, plasma etch-back, top contact deposition and patterning, deposition of a protective coating.

The process started with the selective area wet chemical growth (SAWCG) of ZnO NWs where the nucleation windows were patterned by e-beam lithography. It resulted in an almost parasitic crystal free chip surface with bundles of vertically oriented NW in each matrix position (Fig. 2). The height of the NWs was approximately 3.5 µm.

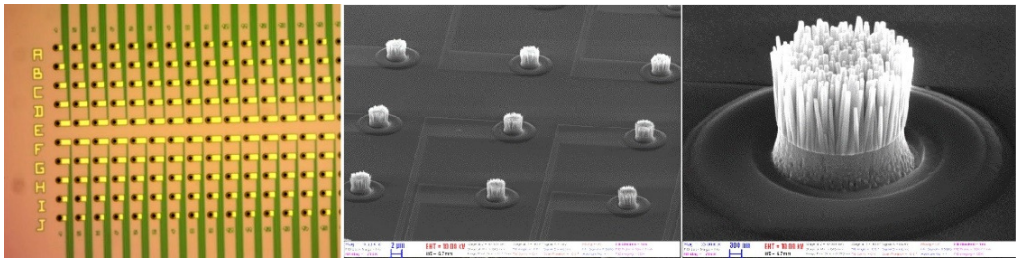

Figure 2: Optical micrograph of the left half of the matrix (a), and SEM images of ZnO nanowire pixels after wet chemical growth through e-beam lithography patterned nucleation windows (b-c).

SAWCG was followed by polymer spin-coating and hot plating, where three conventional polymer materials were tested: SU8 negative epoxy based photoresist, PMMA e-beam resist, and S1818 positive photoresist. The polymer matrix was etched in oxygen (or Ar) plasma until AFM observation confirmed that the tip of the NWs got released. An Au layer of 100-250 nm was then deposited onto the chip using e-beam evaporation method through a handmade stencil mask to obtain Schottky-type rectifying junction. Similar results were found for PMMA, however, SU-8 negative epoxy resist was found to leave an unwanted residue on the top of the NWs. Though it can be removed by physical dry etching using e.g. Ar plasma, due to the ion bombardment of ZnO top surface it results in an Ohmic contact with Au.

The photograph of chip in Fig. 3a shows the square shaped, reddish photoresist coating and the cross-shaped yellow top metal coating, which is connected to four metal pads through its arms. SEM observation of an FIB cut NW pixel confirmed the quality of the polymer encapsulation and direct contact between the top metal and ZnO NW (Fig. 3b). Before wire bonding of the chips randomly selected NW pixels were tested electrically. Most of the circuits demonstrated high quality Schottky type I-V characteristics with the expected polarity (Ohmic at the bottom and Schottky on the top). In case of the best chip the calculated ideality factor scattered in the 2.6 - 3.6 range which is rarely found in the literature for contacted NWs.

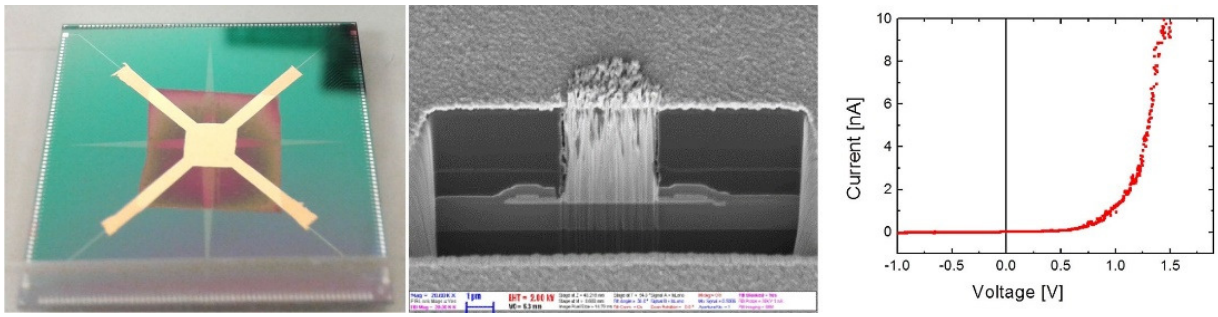

Figure 3: Photo of the fabricated chip after top Au deposition (a), SEM image on the FIB cross section of a NW pixel (b), and a characteristic I-V curve showing Schottky type electrical junction (c).

In accordance with the original research plan most of the completed chips were sent to our consortium partners for automatic wire-bonding and for a subsequent direct piezoelectric test (zero-bias voltage type). However, a few were kept at MFA to carry out manual wedge bonding and an alternative, 'non-zero bias voltage' characterizations. These chips were wire bonded to a test printed circuit board with limited number of contact pads (128). Hence, roughly only every second pixel was connected among the available 250 matrix elements.

In Fig. 4, the macroscopic characterization setup purposely built for the alternative demonstration is shown. During the loading tests, simple stamps were pressed against active matrix of the chip (225 µm x 600 µm). The magnitude of the loading force was continuously monitored by a calibrated force gauge. The electrical signal of each wire bonded pixel was collected one-by-one through two ribbon cables by a high-density matrix switch which was connected to a source measure unit (National Instrument, PXI).

The photograph of chip in Fig. 3a shows the square shaped, reddish photoresist coating and the cross-shaped yellow top metal coating, which is connected to four metal pads through its arms. SEM observation of an FIB cut NW pixel confirmed the quality of the polymer encapsulation and direct contact between the top metal and ZnO NW (Fig. 3b). Before wire bonding of the chips randomly selected NW pixels were tested electrically. Most of the circuits demonstrated high quality Schottky type I-V characteristics with the expected polarity (Ohmic at the bottom and Schottky on the top). In case of the best chip the calculated ideality factor scattered in the 2.6 - 3.6 range which is rarely found in the literature for contacted NWs.

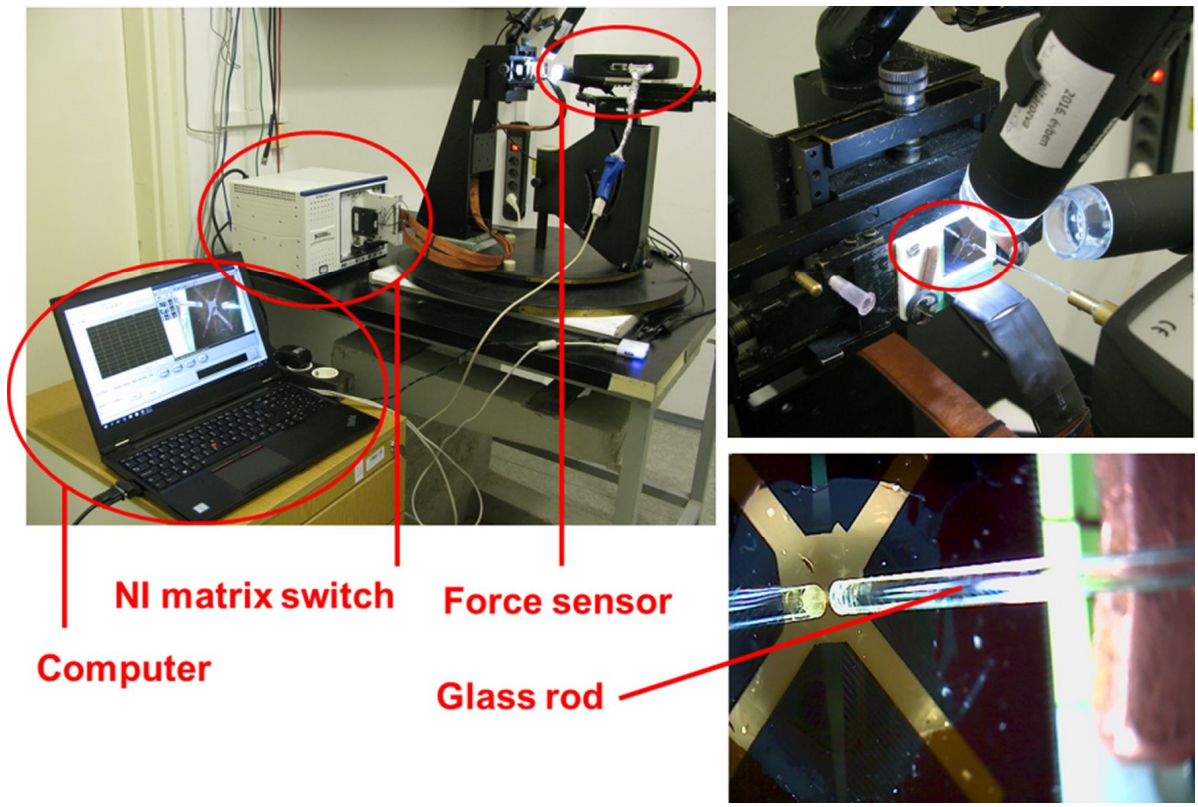

Figure 4: Macroscopic setup for pressing tests using calibrated force sensor, source measure unit connected to a 128 channel high density matrix switch (NI PXI) and a controller computer with LabVIEW based data acquisition software.

A LabVIEW based data acquisition and evaluation software was written to take I-V curves from each pixel, to monitoring time domain current/voltage signals, applying bias voltage, drawing response maps, and to monitor the signal of the force

gauge. About 4.5 s is needed to collect current/voltage data for all the 128 channels at fix bias voltage/current and to refresh the chess pattern map.

At first I-V curves were collected from each pixel in relaxed state. It confirmed that most of the pixels, around 117 have Schottky type rectifying curves. By applying this current monitoring method on every channel we could monitor the whole matrix and may have a chance to recognize simple patterns. However, as we found, the measurement is less noisy in current generator mode, i.e. a constant current (e.g. 100 nA) was forced through each pixel and the generated voltage was monitored and visualized by the software. Prior to pressing, reference voltage (V_0) was taken from each pixel. Afterwards, only the absolute value of the relative change ($\Delta = |V_1 - V_0| / V_0$) was shown by a color scaled matrix.

In order to demonstrate pattern recognition and position sensitivity a fine Al wire was pressed (Ø= 200 µm) against the NW matrix. The Al wire was looped around the apex of a Cu cone mounted on the horizontal force sensor. It was aligned such a way that the long axis of the Au wire was perpendicular to the long edge (600 µm) of the rectangular matrix. During the demonstration at first the wire was pressed near to the left edge of the matrix. The applied loading force was 500 mN. After releasing the stamp it was moved manually towards the right side of the matrix along the x-axis using micro-meter positioner and pressed the matrix again. This sequence was repeated until reaching the right side of the matrix.

Fig. 5 shows the color maps taken at each loading event. Black pixels in a chess pattern indicate the un-bonded inactive elements. Deep blue color corresponds to the unchanged voltage signal ($\Delta = 0$), while red is set to show a relative change of 7%
($\Delta = 0.07$) in this particular experiment. On the right side of Fig. 5 snapshots were taken by a USB camera to show the position of the pressing stamp relative to the chip. For clarity, two dotted red lines indicate the initial and final position of the Au wire. The recorded maps on the left side clearly show the perpendicularly elongated shape of the Au wire and its position. Even though some of the unloaded pixels are also red due to the voltage drift, the pattern recognition concept, at sufficiently high loading force, seems to be feasible.

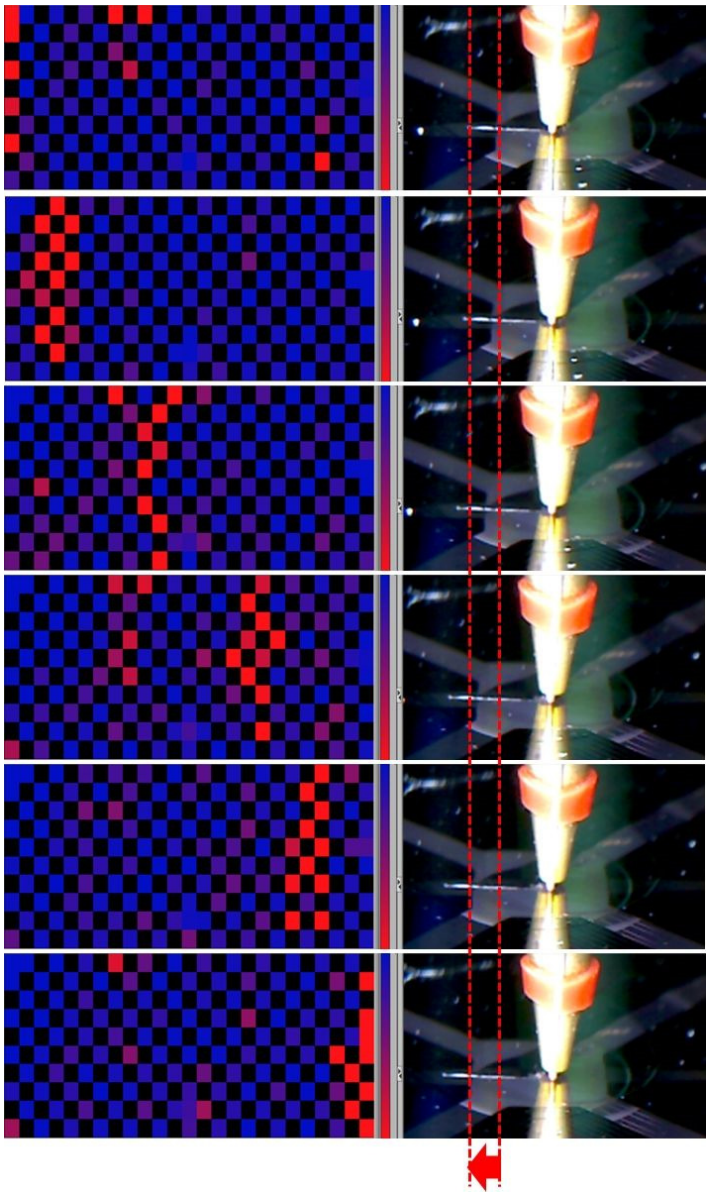

Figure 5: Relative voltage change maps at a bias current of 100 nA at different positions of the perpendicularly aligned AI wire type stamp. Position of the stamp was changed from left to right of the matrix with incremental steps of approximately 100 µm.

SPIRAL-SHAPED PIEZOELECTRIC MEMS CANTILEVER ARRAY FOR FULLY IMPLANTABLE HEARING SYSTEMS

J. Volk, Zs. Baji, A. Békési, G. Battistig, Cs. Dücső, P. Földesy, N. Q. Khánh, I. Lukács, Gy. Molnár, A. L. Tóth, Zs. Zolnai, Z. Szabó, and I. Bársony

Fully implantable, self-powered hearing aids having no external unit could significantly increase the life quality of the patients suffering from severe hearing loss. This highly demanding concept, however, requires a strongly miniaturized device which is fully implantable in the middle/inner ear and includes the following components: frequency selective microphone or accelerometer, energy harvesting device, speech processor, and cochlear multielectrode.

In this work we demonstrated a low volume, piezoelectric MEMS cantilever array which is sensitive even in the lower part of the voice frequency range (300-700 Hz). The test array consisting of 16 cantilevers (Fig. 1b) has been designed using Comsol Multiphysics © simulations and fabricated by standard bulk micromachining on a Si-on-Insulator (SOI) wafer with AlN as a CMOS and biocompatible piezoelectric material. The low frequency and low device footprint (2×2 mm²) were achieved by Archimedean spiral geometry and Si seismic mass (Fig. 1a).

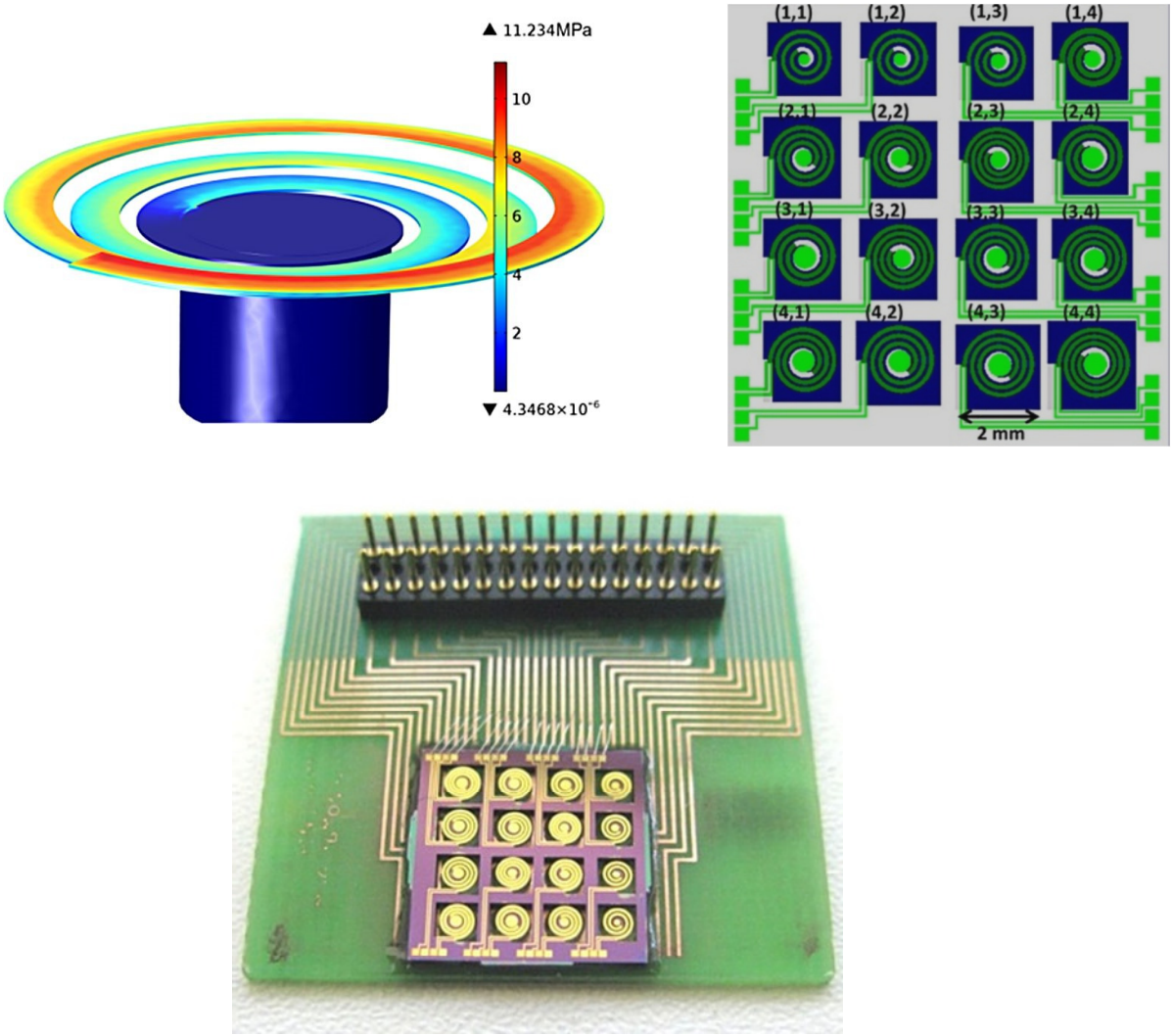

Figure 1: Tensile stress distribution along the beam, calculated by finite element method (a), layout of the selected 4x4 spirals (b), and the wire bonded chip ready for shaking tests (c).

On the 4" wafer most of the chips with the sensitive spirals survived the fabrication process of over 30-steps; an example is shown in Fig. 1c. Scanning electron micrograph of two typical spiral cantilevers situated in the (1,3) and (3,4) array positions are shown in Fig. 2a and b, respectively. The darker region on the cantilever beam corresponds to the metal-piezo-metal stack covered region. A reflecting Au disk in the centre was designed for additional laser beam deflection tests. As shown in both SEM images the diameter of the seismic mass is decreasing from the back side towards the membrane, i.e. the sidewall of the DRIE etching was not perpendicular.

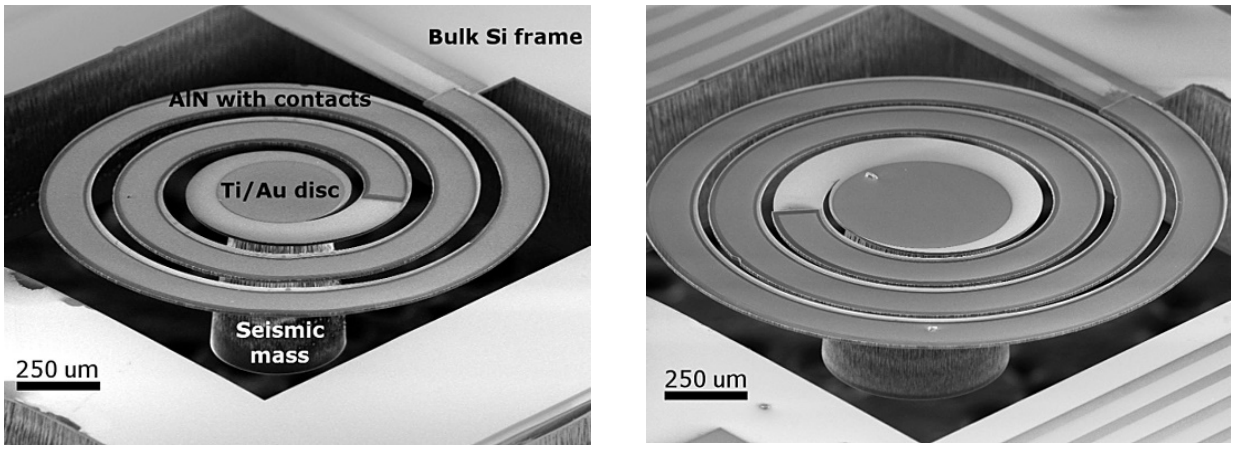

Figure 2: Tilt-view SEM images of two typical suspended spiral-shaped cantilevers (1,3) (a) and (3,4) (b) with contacted AlN layer (darker region) on their top surfaces and a wafer thick 3D-micromachined Si seismic mass beneath.

Vibration tests, performed at a fix acceleration of 1g (9.81 m/s^2) using a PID controlled mini-shaker confirmed the frequency selectivity of the cantilever array (Fig. 3). Most of the spirals (12 out 16) showed sharp resonance peaks scattering in the range of 281-672 Hz. For clarity, the spectra were ordered according to their resonance frequency from low to the high (Channel 1-12). The calculated Q-factors ($f_0/\Delta f\sqrt{2}$) in air vary in the range of 117-254.

As shown in the inset image of Fig. 3 the recorded time-dependent open circuit signal is purely sinusoidal without any vertical offset which indicates stress-free cantilevers. The inactivity of the remaining 4 devices can be attributed to the low electrical resistance of the metal/AlN/metal stacks. That may be the result of random defects in the AlN layer. The generated open circuit voltages fell in the range of 3.0-9.6 mV.

The frequency selectivity demonstrated in the lower half of the voice frequency range and the relatively high Q-factor measured in air are promising for next generation fully implanted cochlear implants (FICI). Moreover, due to the low volume and weight several cantilevers (>12) could be placed inside the human middle ear. Nevertheless, there are still several challenges to be solved: the generated voltage and especially the power are too low for the direct excitement of the hearing nerves, the piezo-cantilevers have not been tested at low accelerations (<1 mg), and overtones may generate unwanted signals.

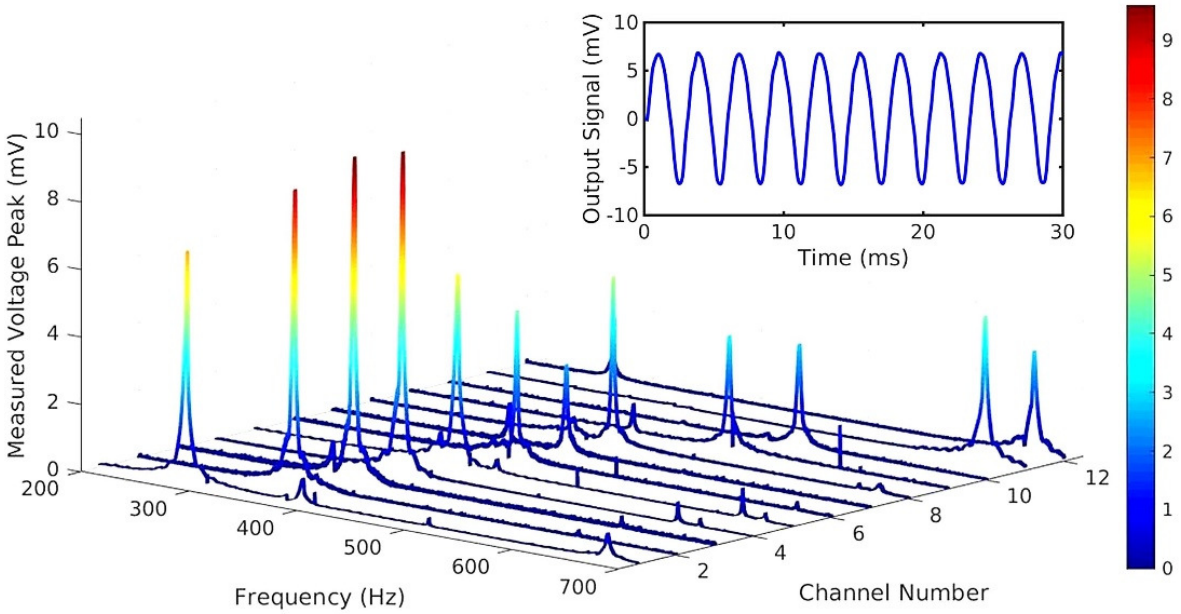

Figure 3: Piezoelectric output voltage during continuous sinusoidal excitation at a feedback controlled acceleration of 1g. Depending on the geometry the base frequency of the cantilevers falls in the range of 281-673 Hz. Inset shows the sinusoidal output waveform of channel 1 at resonance.

VIBRATIONAL ENERGY HARVESTER POWERED SENSOR NODE

J. Volk, Zs. Baji, A. Békési, G. Battistig, Cs. Dücső, P. Földesy, N. Q. Khánh, I. Lukács, Gy. Molnár, A. L. Tóth, Zs. Zolnai, Z. Szabó, and I. Bársony

The aim of this work is to demonstrate a wireless accelerometer sensor node which can operate autonomously even in dark and hardly accessible places in a continuously vibrating ambient such as industrial machine, vehicle, heavy traffic road, bridge, railway etc. In such environments vibrational energy harvesting (VEH) seems to be a reasonable choice to power 'place and forget' type systems.

In this bread-board demo set-up a commercially available piezoelectric energy harvester was applied to investigate limits and challenges for microscopic piezo-MEMS based energy harvesting. The development of the latter one is currently in progress in the KoFAH project.

The developed sensor node (Fig. 1a) consists of a purpose designed electronics and a tuneable VEH holder. The former one was optimized for low power consumption and continuously varying charging voltage level. The PCB, shown in Fig. 1b, includes a microcontroller, an RF module for short-range wireless communication, an energy management unit, two supercapacitors, and an accelerometer. During operation it is powered by the piezo VEH (Midé) whose resonance frequency can be adjusted to the characteristic resonance peak of the ambient by changing the clamping position, i.e. the free length of the vibrating cantilever beam.

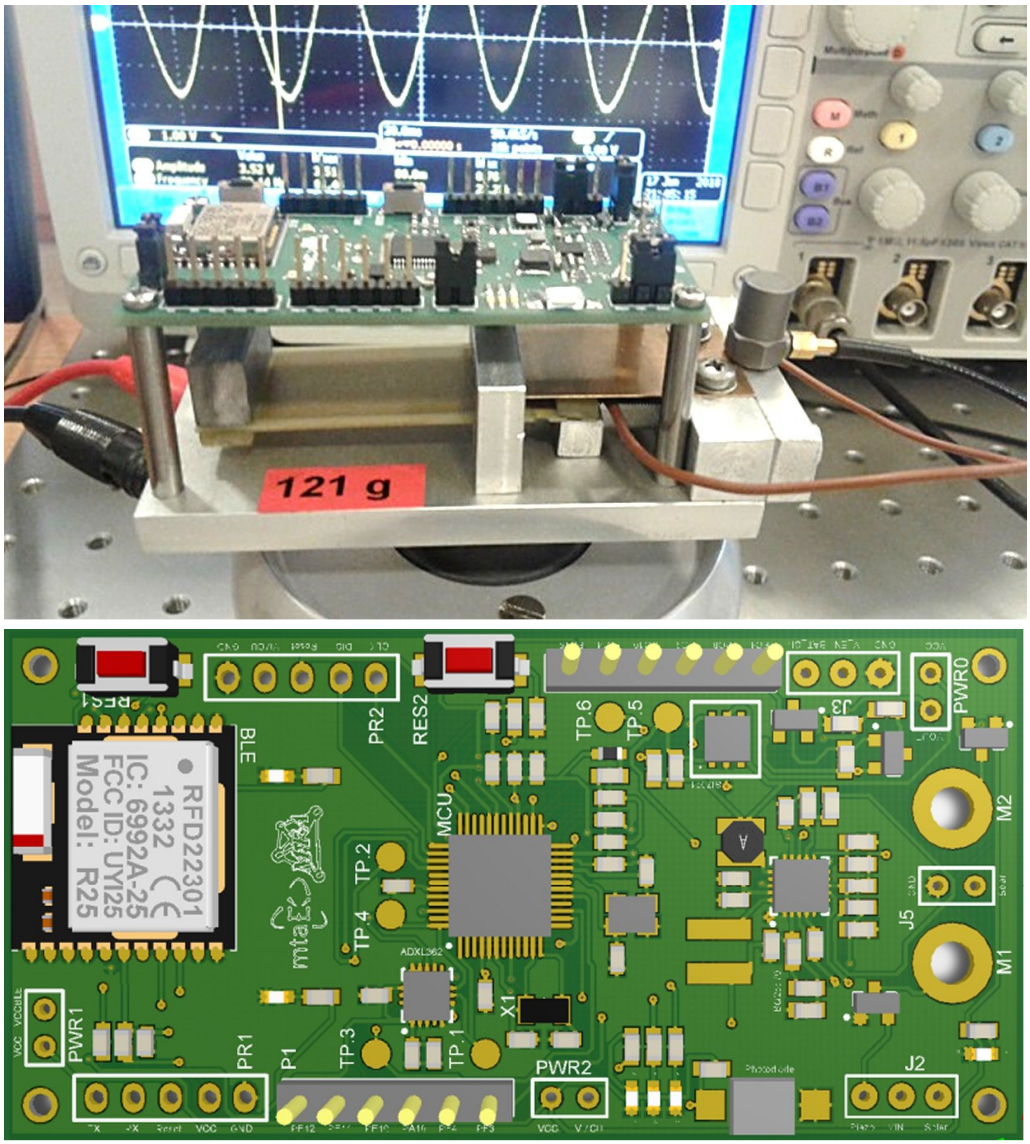

Figure 1: Vibrational energy harvester powered wireless sensor system (top) and the electronics of the purposed designed electronics (bottom).

TEM STUDY OF THE AS-DEPOSITED AND ANNEALED Ga_2O_3 FILMS GROWN BY VAPOUR PHASE EPITAXY

(MTA Postdoctoral Fellowship and bilateral scientific agreement between CNR and MTA)

I. Cora, B. Pécz, M. Bosi, F. Mezzadri, F. Boschi, G. Calestani, R. Fornari, M. Čaplovičová, and A. Rečnik

Ga_2O_3 is a wide bandgap semiconducting oxide (~4.7 eV), promising for UV optoelectronics and power electronics. Ga_2O_3 layers were grown onto (001) surface of α-Al_2O_3 by vapour phase epitaxy and were annealed at 1000 °C for 2 and 6 hours. The as-deposited layers and the two annealed samples were studied by high-resolution transmission electron microscopy (HRTEM), X-ray diffraction (XRD) and Differential Scanning Calorimetry (DSC). *In situ* heating was also performed in TEM in order to follow the κ→β structural transformation. A previous XRD study [F. Mezzadri et.al. Inorg. Chem. 55, 12079. (2016)] on *as-deposited films* showed that these films are single crystalline epitaxial layers and exhibit hexagonal $P6_3mc$ space group symmetry, characterized by partial occupation of the Ga sites, which corresponds to the ε phase, with disordered Ga atoms in the structure. The studies coupled with simulations by JEMS allowed us to investigate the real structure of this phase on the nanoscale The structure is ordered in 5-10 nm large (110)-twinned domains, and each domain has an orthorhombic structure with $Pna2_1$ space group symmetry, called κ-Ga_2O_3. This phase is a new polymorph among the Ga-oxides. Parallel XRD analysis carried out on thicker samples (9-10 μm layer thickness) confirmed the same results, and refined structural parameters were provided.

Crystalline structure of these Ga_2O_3 layers consists of an ABAC oxygen close-packed stacking, where Ga atoms in between occupy octahedral and tetrahedral sites forming two types of polyhedral layers parallel to (001) (Fig. 1). The edge-sharing octahedrons and the corner-sharing tetrahedrons form zig-zag ribbons along the [100] direction. Anti-phase boundaries are common inside the domains. Polar character of the structure was confirmed, in agreement with the characteristics of the $Pna2_1$ space group and explaining the ferroelectric nature. Differential Scanning Calorimetry (DSC) up to 1100 °C was carried out on fragments of pure κ-Ga_2O_3 taken from a very thick layer. This polymorph can tolerate long-lasting thermal treatments up to 700 °C, although some weak traces of lattice modifications were detected by DSC (endothermic bent) starting from about 650 °C. A complete transition to β-phase is observed for annealing temperatures ≥900 °C while at intermediate temperatures of 800 °C the films showed very disordered noisy diffraction spectra, with no evident diffraction peaks of either κ or β types. The detailed structural transformation was studied by TEM during *in situ* heating (results are under publication).

The duration of *ex situ* thermal treatment at 1000 °C strongly influenced the crystallinity of the samples: while for a 2 hours annealing, the sample remained polycrystalline and strongly textured, samples annealed for 10 hours were found almost single crystalline. In more detail, the sample that was *annealed ex situ for 2 hours*, consists of pure β-Ga_2O_3. The layer is polycrystalline and strongly textured: [-201] direction of each β-Ga_2O_3 crystal is perpendicular to the (001) of the α-Al_2O_3. The *10 hours-long, ex situ annealed sample* is pure β-Ga_2O_3 and almost single crystalline: β-Ga_2O_3 grow onto the α-Al_2O_3 with epitaxy: (310)/[-13-1] β-Ga_2O_3 || (001)/[1-10] α-Al_2O_3. The upper part of the layer grows with epitaxy but with a different orientation: (310)/[-130] β-Ga_2O_3 || (001)/[1-10] α-Al_2O_3.

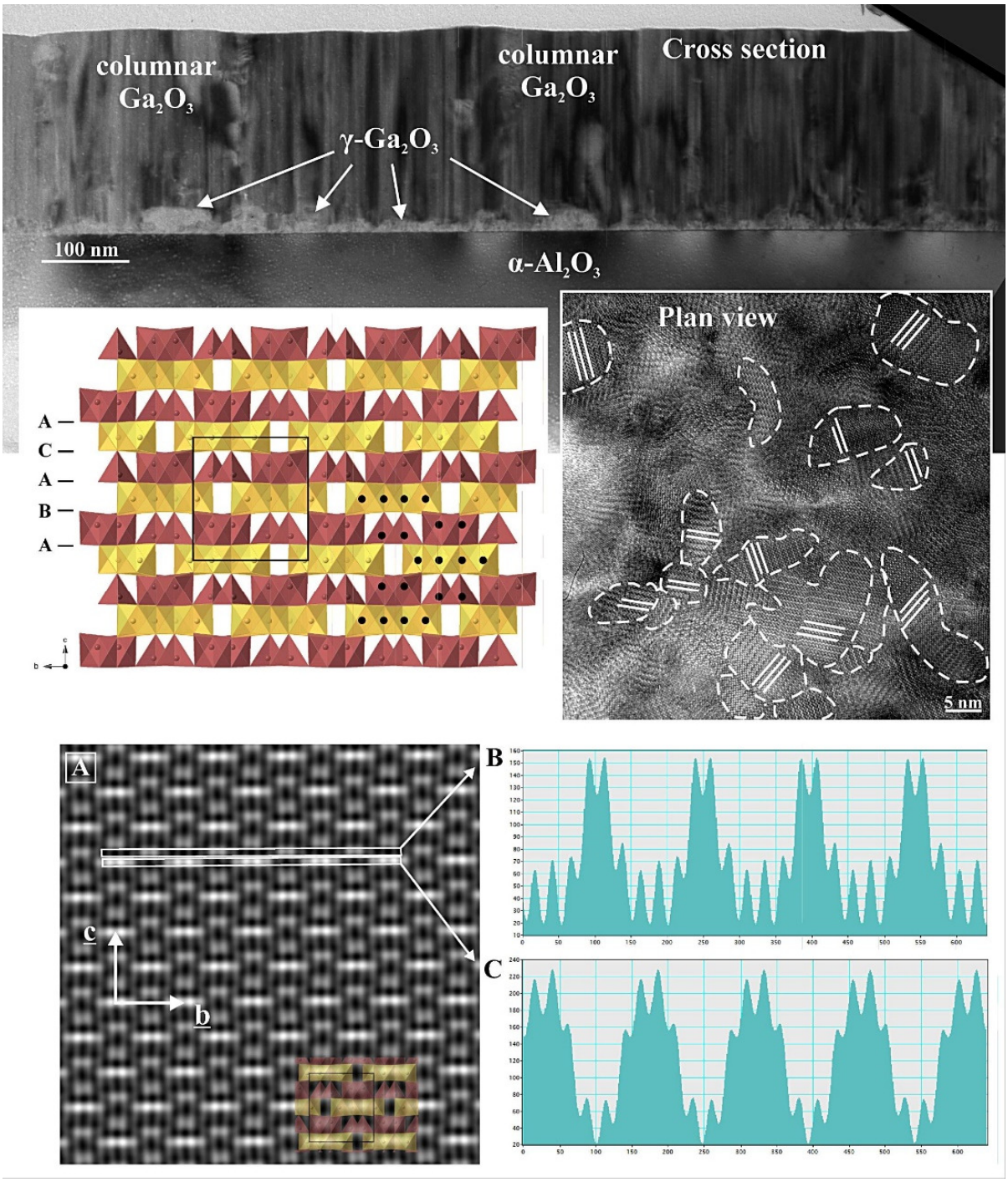

Figure 1: TEM images of the cross-section and the plane view TEM specimens of the as-deposited layers with the corresponding crystal structure of κ-Ga_2O_3. The structure is textured consisting of 5-10 nm large (110)-twinned orthorhombic domains. STEM image (at the bottom) with the corresponding line scans shows the Ga atoms in [100] projections. Spurious peaks are due to overlapping of the twin domains.

PHASE FORMATION SEQUENCE IN THE TI/INP SYSTEM DURING THIN FILM SOLID-STATE REACTIONS

J. L. Lábár, M. Menyhárd, E. Ghegin, Ph. Rodriguez, S. Favier, I. Sagnes, and F. Nemouchi

Continuous demand for increasing data rates necessitates switching to optical devices and interconnections. Due to the indirect bandgap of Si, the III-V semiconductor compounds are considered and introduced as candidates in optical applications. Integration of these devices in the Si CMOS technology (called "Si Photonics") requires a change of material of electrical contacts, as those traditionally contain Au or Pt (elements which are not even allowed to enter into Si cleanrooms, thus are excluded from the integration procedure). Ohmic contacts with low specific contact resistivity are needed. The main process flow consists of a surface preparation (wet and/or plasma treatments), one or several metal layer depositions and a heat treatment. These processes aim to control formation of intermetallic compound(s), thereby modifying the contact resistivity.

In this paper, the phase formation sequence of various observed phases obtained on the Ti (20 nm and 50 nm)/InP systems under rapid thermal processes (RTP) was investigated to identify mechanisms responsible for their formation. Sample preparation consisted of wet etching for 30 s in dilute $HCl:H_2O$ (1:2) solution followed by a direct Ar^+ plasma etching (RF) prior to the metal deposition process. The 20 and 50 nm-thick titanium films were deposited by physical vapor deposition (magnetron sputtering in DC mode) at 100°C and capped by 7 nm thick TiN protecting films deposited at the same temperature.

Investigations on this system highlight the initiation of a reaction between the Ti and the InP substrate during deposition process performed at 100°C. Simultaneous formations of two binary phases, namely, Ti_2In_5 and TiP is detected by XRD and confirmed by electron diffraction (SAED) in the TEM (Fig. 1). TEM image corresponding to a sample subjected to Ar pre-clean, features important roughness with a discontinuous TiN film, which morphology is determined by individual TiN grains. An amorphous layer of about 10 nm is also identified. Because of the important roughness, the corresponding Auger electron spectroscopy (AES) depth profile (Fig. 2) is highly smeared and the signals emanating from the InP, the amorphous layer, and the TiN top layer are not clearly distinct. Nonetheless, a compositional gradient can be observed in the profile. It, therefore, appears that this kind of plasma leads to a phosphorus depletion of the InP surface consistently with what was previously reported in the literature [E. Ghegin et.al., Microelectron. Eng. 156, 86 (2016).]. Formation of the Ti_2In_5 and TiP phases is attributed to the compositional gradient induced in the InP by the wet surface preparation and enhanced by the subsequent in situ Ar^+ pre-clean. Once formed, the TiP layer acts as a diffusion barrier inhibiting further reaction up to 450°C in spite of the presence of an important Ti reservoir (Fig. 3). Consequently, the layer system is stable up to 450°C. At higher temperature, however, i.e., from 550°C, a reaction is enabled either by the enhancement of the species diffusing through the TiP layer or by its agglomeration. This reaction gives rise to the total consumption of the Ti_2In_5 and Ti while the TiP and In phases are promoted.

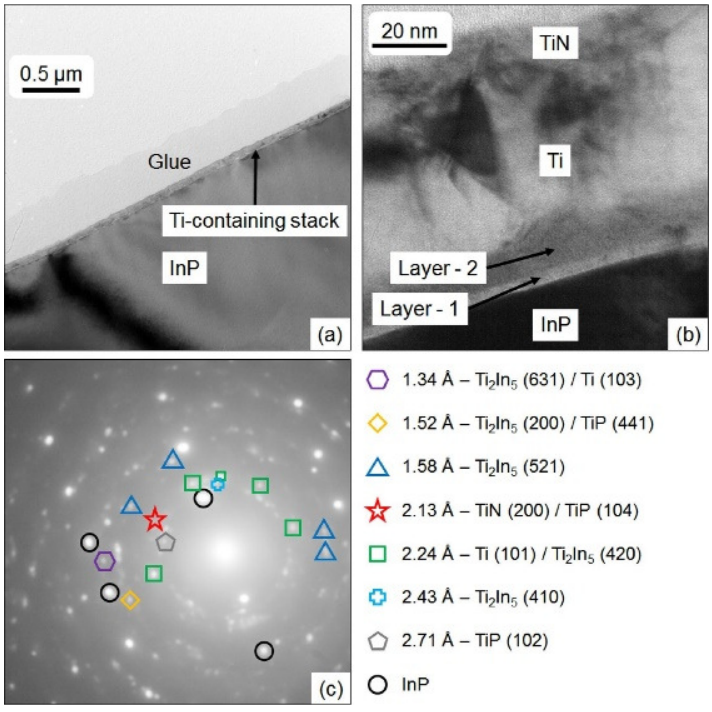

Figure 1: Bright field TEM cross section of (a) the TiN (7 nm)/Ti (20 nm)/InP as deposited sample in low magnification, (b) the TiN (7 nm)/Ti (50 nm)/InP as deposited sample in high magnification and (c) the corresponding SAED pattern highlighting the presence of four different layers in the system.

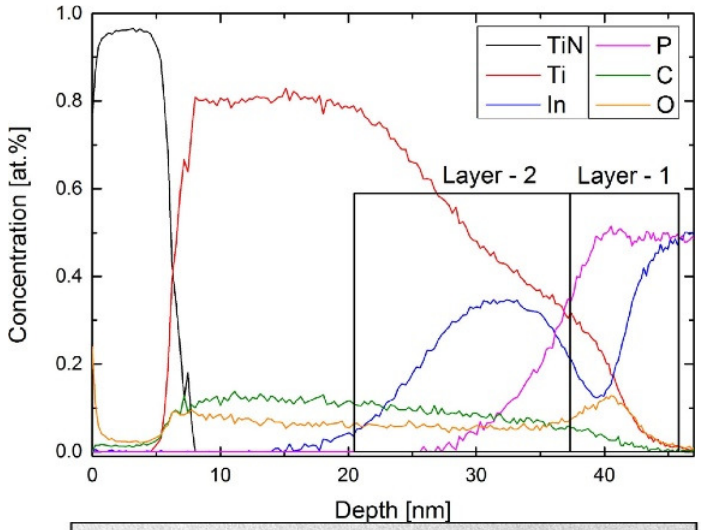

Figure 2: AES depth profile corresponding to the as deposited TiN (7 nm)/Ti (20 nm)/InP system.

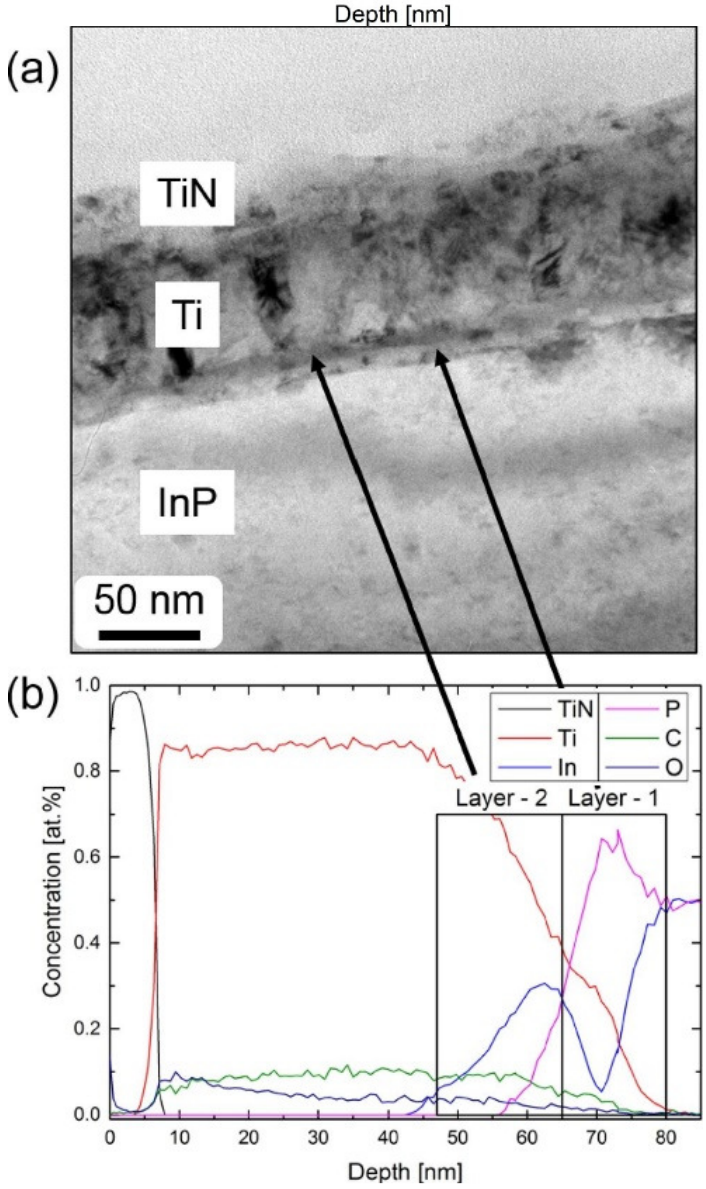

Figure 3: above (a) TEM cross section of the TiN (7 nm)/Ti (50 nm)/InP system annealed at 450°C and (b) corresponding AES depth profile.

EFFECT OF DEPOSITION PARAMETERS ON CUBIC TiC AND HEXAGONAL T FORMATION IN TiC/A:C THIN FILMS

Z. Fogarassy, N. Oláh, I. Cora, Z. E. Horváth, T. Csanádi (IMR SAS), A. Sulyok, and K. Balázsi

Formation of TiC and Ti phases and their influence on their mechanical properties were studied. Thin layers were deposited by DC magnetron sputtering at room temperature in ultrahigh vacuum from two targets (Ti and C).

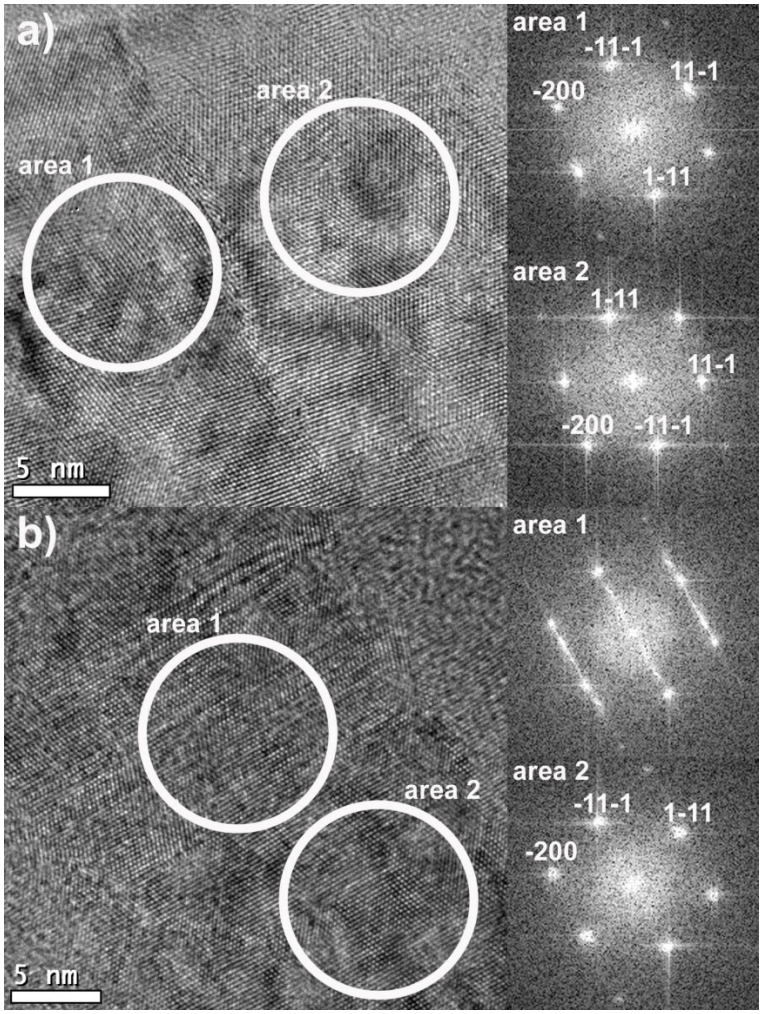

Figure 1: HRTEM images of the TiC layer with 86 at % Ti content. In the a) HRTEM image of an incoherent twin boundary and the FFTs from twin boundary two side. In the b) HRTEM image, stacking faults in the c-TiC are forming h-Ti structure, as seen on its associated FFTs (in one FFT area are from twin boundaries, in the other FFT area twin boundaries are not present).

Thin films with columnar structure containing Ti between 58 at.% and 95 at.% were obtained in dependence of the sputtering power of the carbon (C) and titanium (Ti) target. Previous studies by us covered mechanical and structural properties of the a-C/TiC and TiC films with Ti content from 0 to 58 at.% [N. Oláh et.al., Surface and Coatings Technology, vol. 302, (2016), pp.410-419.]. Cubic TiC phase (c-TiC) was formed in films with Ti content from 58 to 86 at.%. Formation of hexagonal Ti (h-Ti) occurred first from 86 at.% of Ti content and was observed for all films with Ti content between 86 and 95 at%. The c-TiC disappears at 90 at. % and higher Ti content, where only h-Ti crystallizes. Both the h-Ti structure and the c-TiC structure can be formed in the layer with 86 at.% titanium content. The HRTEM investigation shows that dominantly c-TiC structures are formed in the film. However, c-TiC grains contain several stacking faults. There are some areas where after a single stacking fault the orientation of the grain changes in one part of the grain (Fig. 1a right). In such areas where the two grains with different orientations meet, they form (112) type incoherent twin boundary perpendicular to the surface of the substrate (Fig. 1). In certain areas the density of stacking faults increases and locally the crystal structure of c-TiC can pass through h-Ti structure. The TEM and the XRD studies confirmed the dominance of c-TiC (111) texture with increasing Ti content.

The hardness of thin films agrees with structural observations. The highest hardness value (~26 GPa) showed the c-TiC thin film with 67 at.% Ti content. A hardness of ~25GPa was measured in films with 58 to 70 at.% Ti content. The nanohardness showed decreasing character with increasing Ti content over 70 at.%. The lowest values of nanohardness (~10 GPa) was observed for thin films with only h-Ti phase.

The present phases will have a large influence on mechanical properties: the films with pure cubic TiC phase exhibited two times higher hardness than films with the softer hexagonal Ti phase. It was proven, that the lowest hardness value of around 10 GPa in films with 90-95 at.% Ti is still 2-4 times higher than the hardness of various Ti alloys like the TiAl6V4 alloy that is often used as implant material.

STRUCTURE AND MECHANICAL PROPERTIES OF HARD YET FRACTURE RESISTANT W-B-C COATINGS WITH VARYING W AND C CONTENT

Zs. Czigány, M. Alishahi, S. Mirzaei, P. Soucek, L. Zábransky, V. Buršíková, M. Stupavská, V. Peřina, P. Vašina and K. Balázsi

Sputter deposited WBC films were investigated in cooperation with Department of Physical Electronics of Masaryk University, Brno, Czech Republic (Brno) and Nuclear Physics Institute of Academy of Sciences of the Czech Republic, Řež (Řež). Preparation of coatings simultaneously exhibiting high hardness and enhanced fracture toughness is currently a hot topic, as nowadays used ceramic based protective coatings show difficulties to cope with increased demands due to their inherent brittleness. Materials exhibiting such seemingly contradictory combination of mechanical properties - high hardness and moderate ductility - was already realized in Mo2BC and recently predicted by ab initio calculations in crystalline X_2BC system (X = Ti, V, Zr, Nb, Mo, Hf, Ta, W). The WBC films were deposited by RF magnetron sputtering of W, C and B4C targets in Ar at 500°C. The coatings were systematically synthesized to contain a constant amount of boron. The effect of C/W ratio on the bonding structure, microstructure, hardness, stiffness, scratch behaviour and fracture toughness of the coatings was studied. The films with C/W ratio of 0.11 and 0.78 have amorphous structure, however, the films also exhibit a certain short range ordering that is manifested in irregular curved lattice fringes with short extension in HR images. The films with C/W ratio of 0.48 and 0.61 contain crystalline clusters inside the near-amorphous matrix (Fig. 1). These clusters of 1-2 nm size with lattice fringe contrast are clearly visible in the HRTEM images. In the diffraction patterns sharper textured segments at 2.41 are observable within the inner diffuse ring. The textured segments indicate lattice planes parallel with the substrate surface. Therefore, coatings with the C/W ratio the furthest from W2BC stoichiometric composition were near amorphous with no obvious crystallites, coatings closer to the W_2BC stoichiometry were nanocomposites with small grains embedded in an amorphous matrix. A gradual roughening of the microstructure from dense close packed to a porous columnar structure was observed with increasing of the C/W ratio and was attributed to a decrease of the energy flux and momentum transfer to the growing coating during the deposition with the increasing C/W ratio. All of the presented coatings classified as hard coatings with hardness > 20 GPa (Fig. 2). The level of crystallinity played no crucial role in determining the hardness of the coating, while the effect of the coating structure was clear – the densest coating with the highest relative amount of W-B bonds exhibited the highest hardness of ~ 29 GPa. The presented coatings furthermore exhibited high adhesion to industrially important substrates as well as scratch and crack resistance unmatchable by current top-of-the-shelf industrial protective coatings of comparable hardness. Therefore, W-B-C coatings might pave the way to the next generation of coatings for tool protection.

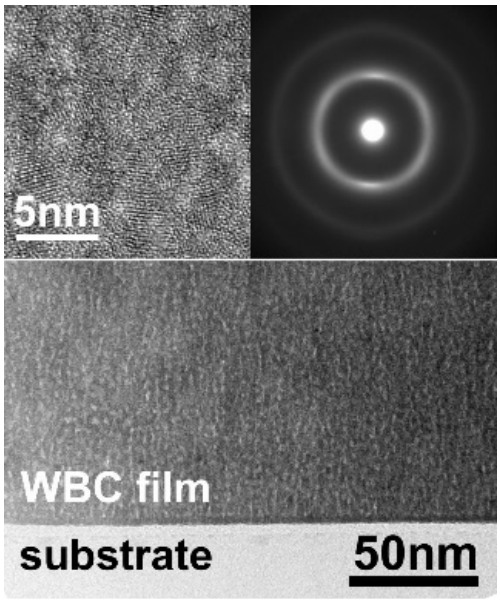

Figure 1: Cross-sectional TEM image of WBC film with C/W=0.61. Porous column walls are visible. Nanocrystallites are observed by HRTEM and SAED pattern (insets).

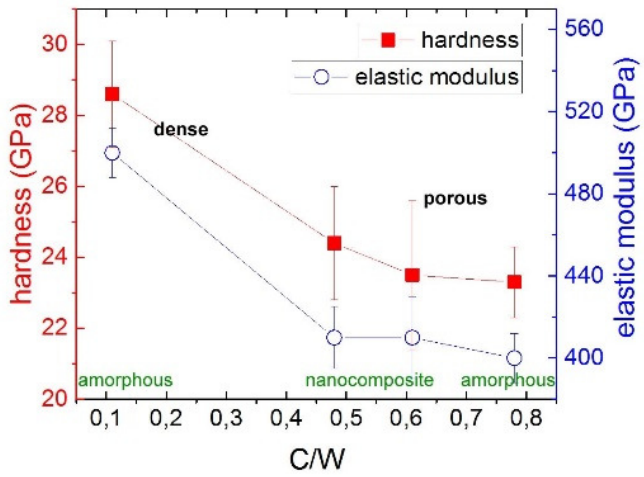

Figure 2: Hardness and elastic modulus of WBC films with different C/W ratio. The mechanical properties show correlation with the density of the microstructure rather than with the degree of the crystallinity of the films.

DOT PATTERNING OF COPT FILMS BY RF PLASMA ETCHING FOR HIGH CAPACITY MAGNETIC MEDIA (PH.D. WORK)

J. Szívós, G. Sáfrán, Sz. Pothorszky, J. Soltys,
M. Serényi, H. An, Tenghua Gao, A. Deák, and J. Shi

In a Ph.D. work new, cheap and green solution for the nanopatterning of FePt and CoPt films was searched for to implement Bit Patterned Magnetic Media (BPM) as a potential candidate to increase bit density in present-day hard disk drives. As for template Langmuir-Blodgett (LB) films of silica nanospheres self-organized in hexagonal structure were applied. In 2015, excimer laser pulses were used for surface modification through the template [J. Szívós et.al., Vacuum 109, 200 (2014)]. In 2016, RF plasma-etching was introduced that removes the layer only at the uncovered areas, and separated islands are formed behind the silica nanospheres. The technique was demonstrated through nanopatterning metallic, semiconductor and insulator films and the influence of plasma parameters was revealed on the depth, morphology and resolution.

RF plasma etching technique was applied in 2017 for dot-patterning CoPt magnetic layers prepared in cooperation with the Tokyo Institute of Technology. We obtained hexagonally distributed individual magnetic domains of sizes below 100 nm. TEM (Fig. 1), VSM (Fig. 2) and MFM studies revealed that our films exhibit the hard magnetic L10 (fct) CoPt phase in separated and magnetically decoupled, islands. Such nanopatterned layers are candidates for dot patterned magnetic media [G. Sáfrán, Applied Surface Science 435 (2018) 31–38].

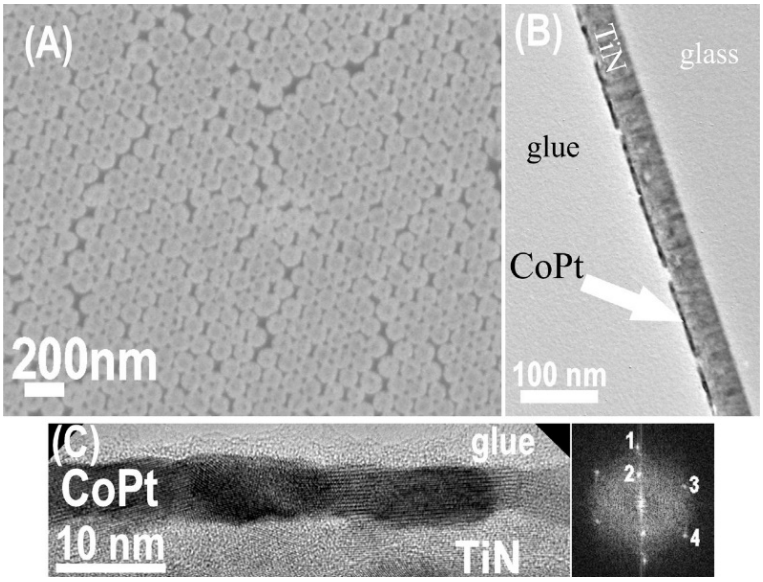

Figure 1: (a) SEM and (b) XTEM of dot-patterned L10 (fct) CoPt film. ***(c)*** *HRXTEM image and its Fast Fourier Transform. Marked reflections: 1 – fct CoPt(002); 2 – fct CoPt(001); 3 – fct CoPt(011); 4 – fct CoPt(110).*

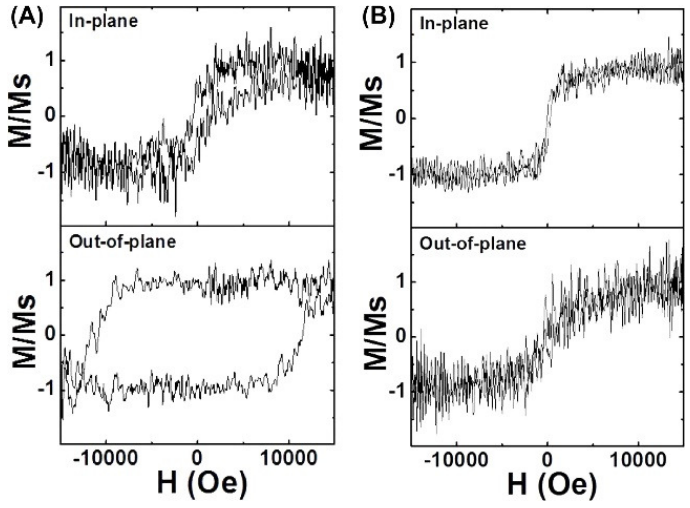

Figure 2: Vibrating Sample Magnetometry (VSM) results. VSM of nanopatterned CoPt films measured parallel and perpendicular to the surface, respectively (a) heat treated sample, (b) non-heat treated sample.

FORMATION AND PROPERTIES OF SELF-FORMING DIFFUSION BARRIER LAYERS

(OTKA K 81808)

K. H. Nagy and F. Misják

Cu-Mn films are perspective contact and interconnect material [J. Bogan et.al., J. Appl. Phys. 120 (2016) 105305]. However, their application on low-κ dielectrics (carbon doped oxides, CDO) has difficulties since Mn can react with carbon present in the dielectric, which complicates interface chemistry. Thermal stability and solid phase reaction between amorphous Cu-Mn films and carbon substrates were investigated by in-situ TEM. Amorphous Cu-Mn films (with 50 and 70 at% Mn content) were deposited by DC magnetron sputtering at room temperature. Evaporated carbon foils were used as substrates to model low-κ carbon doped oxides in their reaction with Cu-Mn films. In-situ TEM revealed that the amorphous state is stable below 300°C, where the films crystallize into Cu(Mn) and α-Mn-based solid solutions. While Cu-based solid solution remains stable up to 600°C, Mn-based phases alter. Mn carbide phases appear at 400°C accompanied with the disappearance of α-Mn phase and the decrease of Mn content of Cu(Mn) phase. In the temperature range of 400-500°C $Mn_{23}C_6$ and Mn_5C_2 carbide phases are present. As temperature increases more carbon diffuses into the film and hence the compound of lower C:Mn ratio ($Mn_{23}C_6$) disappears and a new phase of higher C:Mn ratio, the Mn_7C_3 appears. Mn_5C_2 carbides have lamellar structure and show Arrhenius-type grain growth in the temperature range of 400-600°C.

The activation energy of Mn_5C_2 growth is 101±20 and 88±22 kJ/mol respectively in the film containing 50 and 70 at% Mn indicating that carbide growth is facilitated with increasing Mn content. In addition to carbide formation, surface oxidation occurs as well in the system. Thermodynamic considerations indicate that Mn carbide formation can only occur in the Cu-Mn-C-O system when the Mn is not fully oxidized, and there are free metallic Mn atoms left. Our results suggest that a thin, uniform barrier layer without carbide formation can be formed on the surface of CDOs when sufficient O is available for full oxidation of Mn within diffusion distance to the Cu(Mn)/CDO interface and when the diffusion of Mn into the CDO is prevented.

TEM STUDY OF NICKEL AND COPPER SILICIDES

E. Dodony and Gy. Z. Radnóczi

Microelectronics and semiconductor industry has a growing appetite for the use of nickel and copper silicides in their products, because of their favorable properties. For example, nickel is used for metal induced lateral crystallization (MILC) processes, and nickel silicides in various nano-, and microelectronic devices as contact material. Cu_3Si is used as contact material as well as catalyst in making semiconductor nanowires and ultrapure silicon suitable for photovoltaic devices.

Due to their importance, we have studied formation of nickel and copper silicides in thin amorphous silicon (a-Si) films. A 10 nm thick a-Si film was transferred onto Cu and Ni grids and heated in-situ in a Philips CM20 transmission electron microscope. During heating, the Cu and Ni grids acted as unlimited sources for the diffusion of metals into the a-Si. Copper silicides started forming at 500 ^{o}C, and nickel silicides at 560 ˚C. We observed two competing phases, Ni_3Si and one of the low temperature polymorphs of the Cu_3Si (Fig. 1). Both forms are superstructures. Available structural models for both phases were compared to the measurements, and was found that they do not match properly, similarly, as calculated diffraction patterns using published models do not match our experimental data.

Now we focus our efforts to collect diffraction data and high-resolution electron microscopic images of both phases. Our goal is to make new crystal structure models for both the η″-Cu_3Si and Ni_3Si.

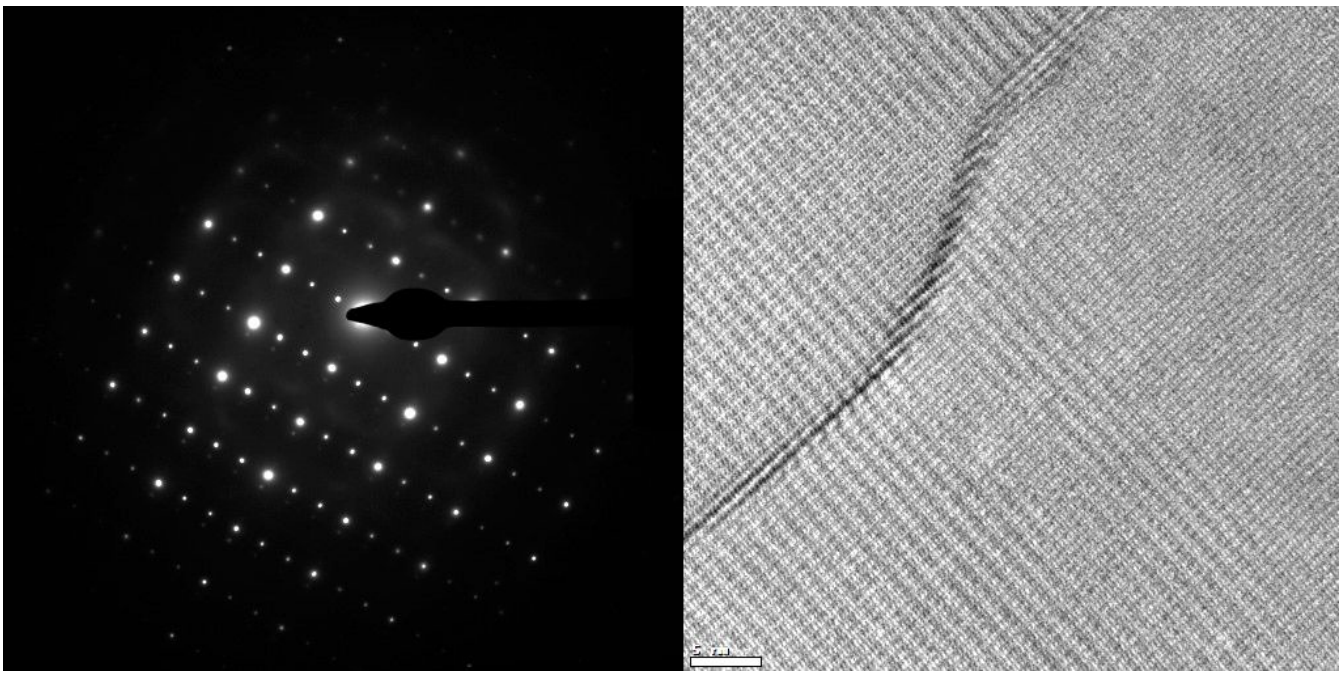

Figure 1: Diffraction of η″-Cu_3Si [110] projection and a HREM image of the same phase.

CHARACTERIZATION OF DEFECT STRUCTURE, MECHANICAL PROPERTIES AND STABILITY OF ELECTRODEPOSITED NANOCRYSTALLINE NI FILMS

T. Kolonits, Zs. Czigány, J. Gubicza (ELTE Univ.), P. Jenei (ELTE Univ.), S. Zsurzsa (Wigner Res. Centre), L. Péter (Wigner Res. Centre), and Bakonyi (Wigner Res. Centre)

Effect of various organic additives on defect structure and mechanical properties of electrodeposited Ni films was investigated by X-ray diffraction (XRD) line profile analysis (eCMWP model), transmission electron microscopy (TEM) and energy disperse spectroscopy (EDS). Main task in the project is to investigate the effect of the additives on the grain structure and defect (dislocation and twin) density which influence macroscopic properties of the layers and their applications.

Electrodeposited layers were prepared at room temperature and at low current density onto copper substrates. The basic electrolyte mainly contained nickel-sulphate ($NiSO_4 \cdot 7\ H_2O$) and boric acid (H_3BO_3). XRD and TEM grain size and phase analysis was carried out to determine the microstructure. Hardness tests were made to examine mechanical properties. Heat treatment (at 500, 750 and 1000 K) was also applied to investigate the stability of the micro and macro properties.

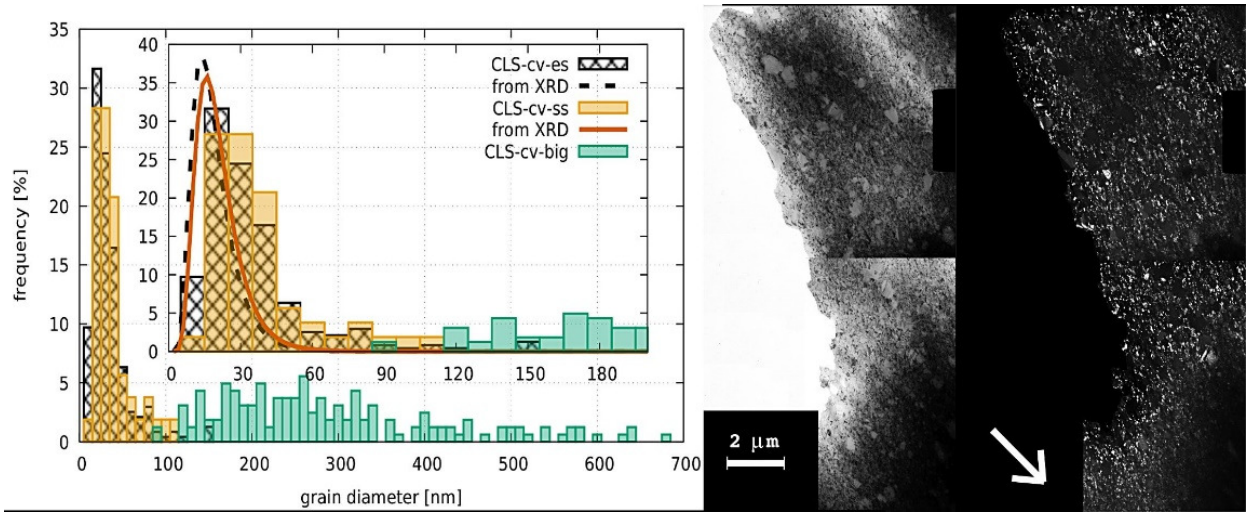

Figure 1: Grain size distribution of nanocrystalline Ni film deposited from electrolyte based on nickel-sulphate and nickel-chloride with saccharine additive determined by TEM (left). A bimodal grain size distribution can be observed by TEM (right). Arrow indicates the growth direction of the layer.

According to our former research [T. Kolonits et.al., J Electrochemical Society (2016), 163(3): D107-D114] in the film deposited without additives, a columnar structure was observed, textured into direction <220>. Varying additives in the bath, various microstructures were observed: textured (both in direction <220> or <200>), non-textured, twinned, ultrafine grained and nanocrystalline, etc. EDS revealed that mainly the low quantity of (~0.1 at%) incorporated sulphur, sodium and chlorine is responsible for the different microstructures. Due to the synergic effect of nickel-chloride and saccharin, an interesting bimodal grain size distribution could be observed: a smaller one due to saccharin, and a larger one corresponding to the effect of nickel-chloride (Fig. 1). Hardness test was compared with the microstructure both before and after heat treatment. One of the additives (trisodium-citrate) showed outstanding hardness and thermal stability, meanwhile in samples deposited with saccharin (which showed the smallest grain size, largest defect density and best hardness) the recrystallization process occurred between 750-1000 K and took place in a few minutes.

NEW TYPE FUNCTIONAL ALLOY FILMS

(OTKA NN 112156)

F. Misják, B.R. Braeckman, K.H. Nagy, G. Radnóczi, D. Depla

A new type of material, high-entropy alloy (HEA) thin films were investigated in this project. High-entropy alloys processed by non-equilibrium methods such as splat quenching, ball milling or magnetron sputtering exhibit in most cases simple structures. HEA prepared in the form of thin films or coatings can have favourable functional properties like relatively high hardness and plasticity, good electrical or magnetic as well as anticorrosion properties making them suitable for different applications. The phase formation in HEA films depends on the alloy composition and the synthesis methods.

Nb_x-(CoCrCuFeNi) thin films were synthesized by sputtering from compacted powder targets. The films were deposited at room temperature onto Si substrates with a deposition rate of ~10 nm/min. The structure formation mechanism of the Nb_x-CoCrFeNiCu (HEA) model system was investigated by transmission electron microscopy (TEM) to reveal nanostructure of the films. Fig. 1 shows the cross-sectional bright field HR-TEM images and the electron diffraction patterns of the deposited thin films as a function of Nb content. The CoCrCuFeNi alloy without Nb exhibits a single phase face centred cubic (fcc) solid solution [Braeckman BR, et.al., Thin Solid Films 616, pp. 703-710. (2016)]. When adding Nb, the diffraction rings are broadened with increasing Nb content and the higher order diffraction rings eventually vanish. The bright-field images reveal the presence of nanocrystallites in the film with 5, 7, and 9.6 at.% Nb, while films with 15.2 and 24.3 at.% seem amorphous. However, a thorough HREM investigation of the 15.2 at.% sample revealed nanocrystallites of 2–3 nm in size, and with a lattice spacing corresponding to the observed FCC phase in samples with a lower Nb content. These crystallites are embedded into an amorphous matrix. It is also observed that the size and density of the crystallites decreases with increasing Nb concentration. A comparison between grain sizes (as determined from HRTEM, and XRD) is shown in Fig 1f. The XRD grain size was calculated using Scherrer's equation, and a continuous decrease with increasing Nb concentration is observed. The HREM analysis shows apparently the same result.

Structural changes in the nanostructure as a function of Nb content can be understood from topological point of view: such alloys can be regarded as binary alloys. The addition of Nb with a larger atomic radius (143 pm) as compared with the five base elements (between atomic sizes of 125 and 128 pm) introduces lattice strains. When the Nb concentration becomes too high, the FCC lattice cannot accommodate the atomic level strains, and the amorphous configuration becomes more favourable.

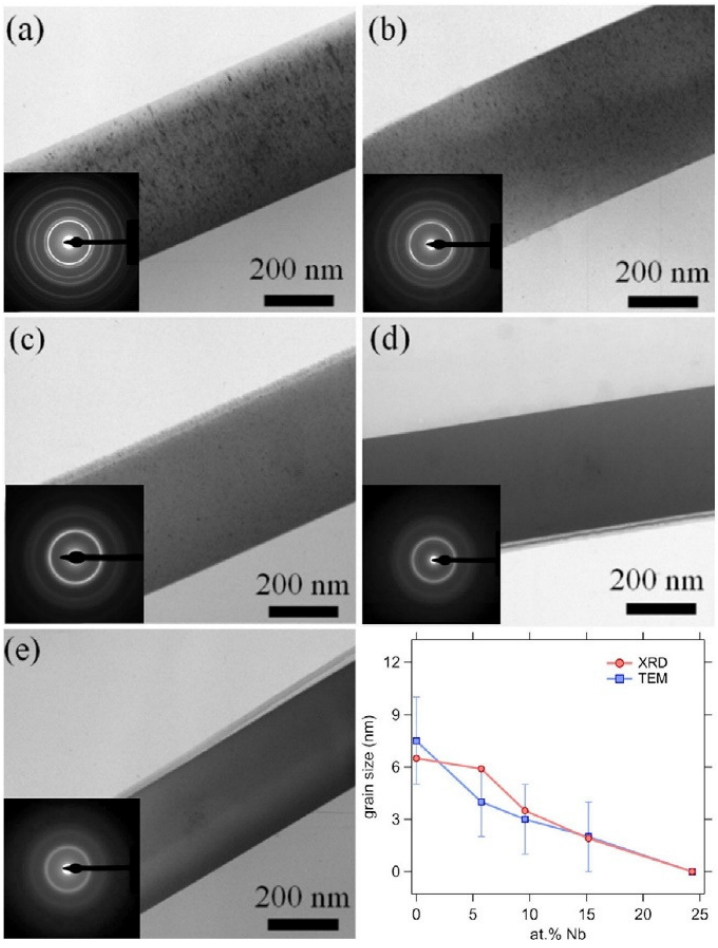

Figure 1: Cross-sectional bright field TEM images and electron diffraction patterns of the Nbx-(CoCrCuFeNi) thin films for (a) 0 at.% Nb, (b) 5.7 at.% Nb, (c) 9.6 at.% Nb, (d) 15.2 at.% Nb, and(e) 24.3 at.% Nb. The grain size as determined from XRD and TEM is shown in (f). The grain size of the amorphous film with 24.3 at.% Nb was set to 0 nm.

GRAPHENE-CERAMIC COMPOSITES FOR TRIBOLOGICAL APPLICATION IN AQUEOUS ENVIRONMENTS

(M-ERA.NET GRACE, OTKA NN 114422, OTKA PD 121368)

C. Balázsi, O. Tapasztó, Zs. Fogarassy, V. Varga, M. Knoch (FCT), J. Dusza (IMR SAS, Slovakia), A. Kailer (IMW Fraunhofer, Germany), K. Balázsi

Main objective of the project was to develop tribological systems on the basis of functionalized graphene and ceramic-graphene nanocomposites and their qualification for technical applications, e.g., for slide bearings and face seals in aqueous media. Our current knowledge in the field of ceramic nanocomposites shows that it is possible to make ceramic materials with improved mechanical and tribological properties by incorporating graphene both into the Si_3N_4 (Fig 1) and the SiC structure. During the last period, we tested six different types of graphene as additions in SiC and Si_3N_4. The multi-layered graphene (MLG) was prepared by attritor milling at 10 hours intensive milling of few micrometer sized graphite powders in large quantities (few kilograms). The large quantity, very cheap and quick preparation process are the main strengths of our MLG. The Si_3N_4/MLG and SiC/MLG nanocomposites were prepared by attritor milling and sintered by hot pressing (HP) in Slovakia (laboratory scale, diameter of samples was 3 cm) and in FCT lab, Rödental (industrial scale, for industrial testing). The laboratory scale Si_3N_4 ceramics were produced with 1 wt%, 3 wt%, 5 wt% and 10 wt% content of MLG. In all composites, densities between 97 and 100 % were obtained.

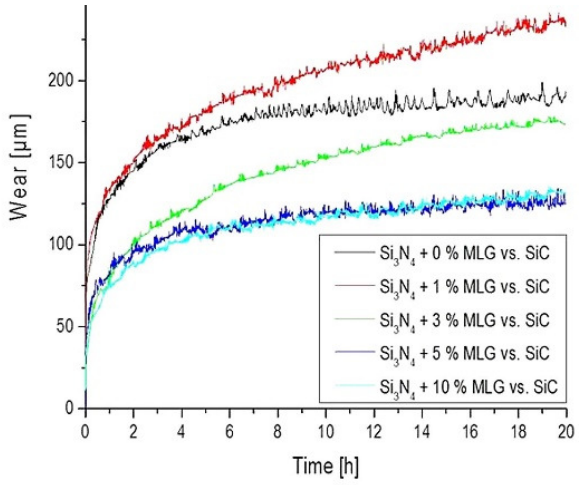

Figure 1: Development of the total wear depth of the multi-layered graphene containing Si_3N_4-pins on SiC-rings and structure of Si_3N_4/5 wt% MLG.

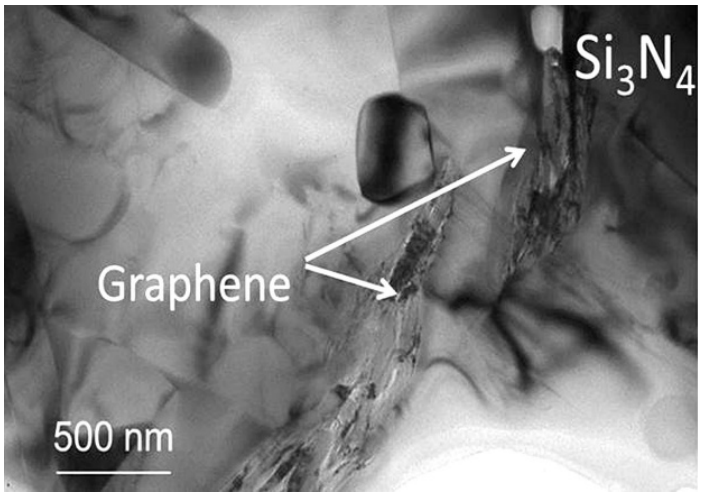

Figure 2: TEM image of Si_3N_4 / 5 wt% MLG showed the dispersion of MLG between silicon nitride grains after milling and sintering.

The α-Si_3N_4 to β-Si_3N_4 phase transformation was completed during hot pressing. The structural investigations and phase analysis measurements confirmed the presence of MLGs in all composites after the HP sintering process (Fig. 2). Presence of very fine nanostructured zirconia on the silicon nitride grains is the consequence of the highly efficient milling process. HV values decreased with increasing of MLG content from 18.86 GPa to 9.69 GPa. The small increase to 18.86 GPa of HV at 1wt% MLG content in comparison to 17.01 GPa reference Si_3N_4 might be attributed to smaller grain sizes. The results showed that improved tribological properties, more stable frictional behaviour and a significant increase of the wear resistance at MLG contents beyond 5 wt% can be achieved (Fig. 1). This new approach is very promising, since ceramic microstructures can be designed with high toughness and provide improved wear resistance at low friction.

NEW APPROACHES IN THE DEVELOPMENT OF HYPOALLERGENIC IMPLANT MATERIAL IN ORTHOPAEDICS: STEPS TO PERSONALISED MEDICINE

(EU FP7 HypOrth 602318)

K. Balázsi, N. Oláh, Zs. Fogarassy, V. Varga, T. Sopcák, T. Zagyva, L. Illés, D. Delfonse (Mathys, Switzerland), C. Lohman (Magdeburg Un., Germany), J. Lorenzen (Teknologisk Inst., Denmark), A. Wielowiejska-Giertuga (INOP, Poland), Cs. Balázsi

Joint replacement is one of the most successful in current orthopaedics. Although many improvements have been made, tissue reactions to biomaterials, infection and lacking osseointegration are still the main reason for the failure of implants and for revision surgery. Various materials - considered as "ideal" to wear resistance (e.g., CoCr-alloys) or "bioinert" (Ti-alloys) – are found to induce adverse tissue reactions or to support biofilms. Patients with a known metal allergy are at a higher risk of developing sensitivity against biomaterials. HypOrth project helps understanding local adverse reactions around artificial joint replacements and to improve integration of potential hypoallergenic implants with improved biocompatibility.

HypOrth has already developed bioactive implant surfaces including bioceramics. Those surfaces and implant materials are being tested in material tests as well as cell culture experiments. From these results, prototypes are being designed. A very unique surface coating will be realized by using eggshells and seashells as a source for calcium/hydroxyapatite coating to enhance osteointegration and mimic biocompatibility. This technology has been proven to be efficient and effective in simulator tests.

It can be assumed that the initiative HypOrth has direct impact on the health of European citizens but also on the technology transfer by stimulating metal forming industries. Already today, the prototype surfaces are expected to show superior properties as compared with existing technologies. The main part of the project´s results is confidential.

INVESTIGATION OF BIOCOMPATIBLE GLASSES FOR BIOMEDICAL APPLICATIONS

(EU FP7 HypOrth 602318)

V.K. Kis, M. Fábián, J. Lábár, I. Székács, A. Sulyok, Zs. Dallos, Zs. Horváth, F. Misják and Zs. Kovács

Synthesis and optimization of Ca and P containing bioactive glasses which, due to their composition, structure and mechanical properties, are suitable for biomedical application. Bioactive glasses has been prepared by melt-quench technique in the compositional range SiO_2(45)CaO(25)Na_2O(30-x)P_2O_5(x), x=0, 1, 3, 5. Using DTA/DSC analysis, the glass transition and crystallization temperatures were determined for the different samples. Mechanical properties, such as Vickers hardness and Young's modulus were measured by nanoindentation tests at different positions in the as-cast glasses.

Structure of the bioactive glasses was characterized using electron and neutron diffraction. TEM studies supported amorphous structure on the nanoscale in case of glasses with 0, 1 and 3 mole% P content, while the sample with 5 mole% P, contained nanocrystals with size <30 nm (Fig. 1). Partial atomic correlation functions and coordination numbers were revealed from RMC modelling based on neutron data (Fig. 2). Structure forming bonds of Si–O and P-O exhibit narrow distance distribution, while those corresponding to Ca–O, Na–O and O-O bonds show broader and more asymmetric distributions.

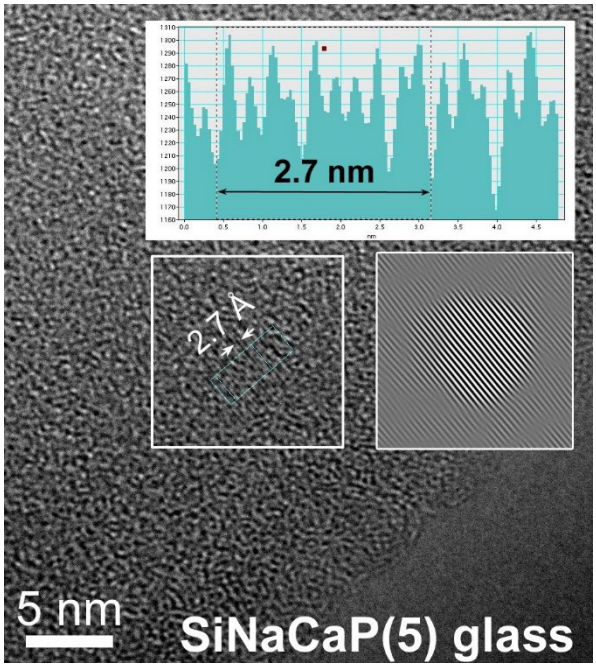

Figure 1: HRTEM: Nanocrystal in bioglass with 5 mole% P.

Interference functions and e-PDFs obtained from NBD were compared with bulk neutron RMC results. To validate e-PDF analysis, the effect of sample thickness and mean free path was analysed using a reference pure SiO_2 glass with different thickness at 200 and 300 keV. The probe size was 1.5 µm and 25 nm in case of 200 keV and 300 keV respectively. According to our results the atomic distances obtained from e-PDFs are in good agreement with neutron based RMC data and independent of sample thickness and the applied Q-range. Thus, e-PDF proved to be suitable for semi-quantitative characterization of amorphous structure on the nano scale. e-PDFs of the 5 mole% P sample obtained from NBD using 25 nm probe size at 300 keV imply inhomogenities in the amorphous structure which is in agreement with HRTEM observations.

To test the bioactivity of the glasses, samples have been treated in simulated body Fluid (SBF, following the protocol of Kokubo and Takadama, 2006) for different soaking times (3h, 3days, 7days, 21 days). After three hours all P containing samples exhibited a Ca and P rich layer on their surface, which proves the bioactivity of the glasses. At the same time, on the surface of the P-free glass a silica-rich layer was formed. According to XPS, this silica-rich layer contains Mg and P, which implies the ion-exchange between SBF and glass.

Characterization of the bioactive layer as a function of composition and soaking time in comparison to bone mineral component is still in progress. A 30 min soaking experiment is also planned parallel to nanoindentation measurement to reveal the initial stage of glass transformation and related changes of mechanical properties in SBF.

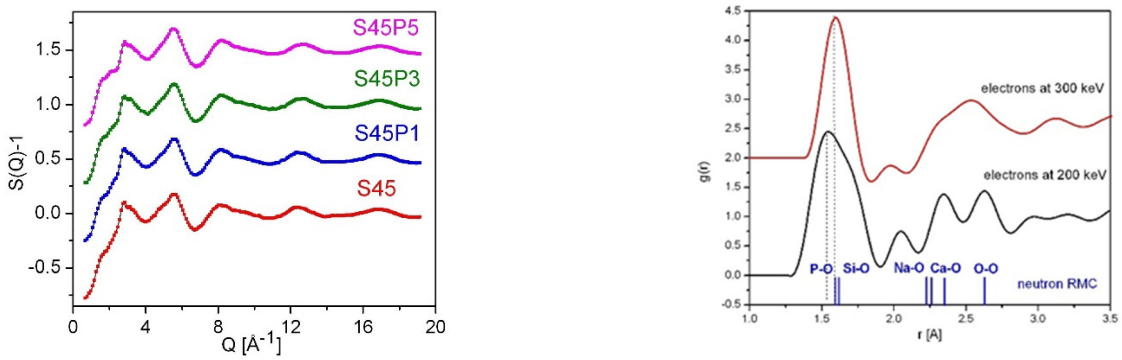

Figure 2: (left): Neutron diffraction structure factors, experimental data (colour) and RMC simulation (black solid line). (right): Comparison of total pair distribution functions from electron and neutron diffraction data (local vs. bulk, respectively) in the 5 mole% P content sample (S45P5) indicate the spatial inhomogeneities observed by HRTEM.

DEVELOPMENT AND CHARACTERIZATION OF MULTI-ELEMENT DOPED HYDROXYAPATITE COATINGS ON METALLIC IMPLANT MATERIALS

M. Furkó and Cs. Balázsi

The aim of this research work is to develop coatings onto implant materials which possess simultaneous antimicrobial and biocompatible properties. The coatings were prepared by applying pulse current deposition technique (Fig. 1). The pure hydroxyapatite (Hap) layer was doped and co-deposited with Ag^{+}, Zn^{2+}, Mg^{2+} and Sr^{2+} ions (multi-element Hap, mHap). The corrosion and biodegradable properties of the layers were studied by carrying out potentiodynamic polarization measurements in simulated body fluid (SBF) using three-electrode open cell over a long time period. The biocompatible characteristics of the layers were investigated by seeding osteoblast-like MG-63 cells onto the sample surface.

Fig. 2 clearly demonstrate that the most corrosion resistant material is the substrate (Ti6Al4V) while the least corrosion resistant (the highest corrosion current measured) is the multi element doped HAp coating, proving its biodegradable properties.

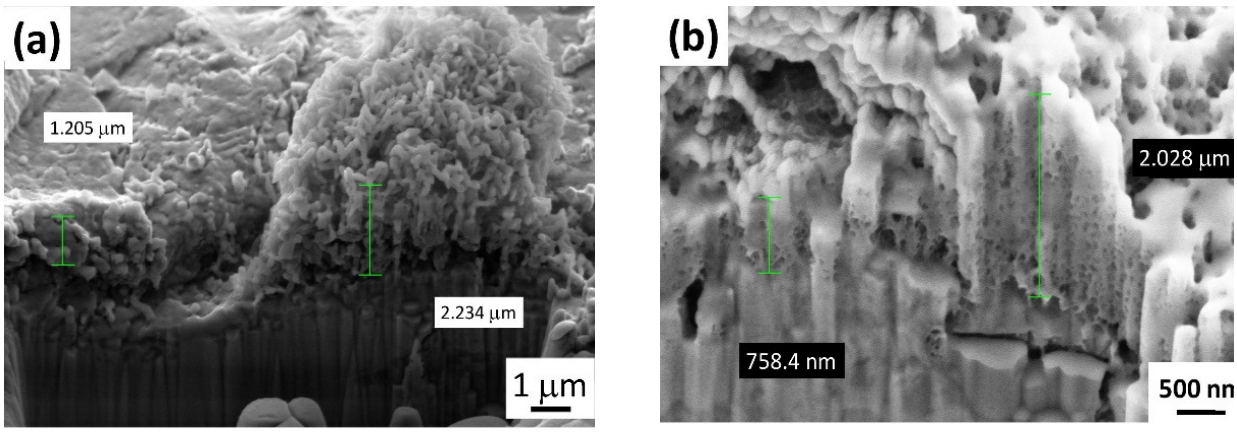

Figure 1: SEM-FIB images on HAp coating (a), and on multi-element doped HAp (b).

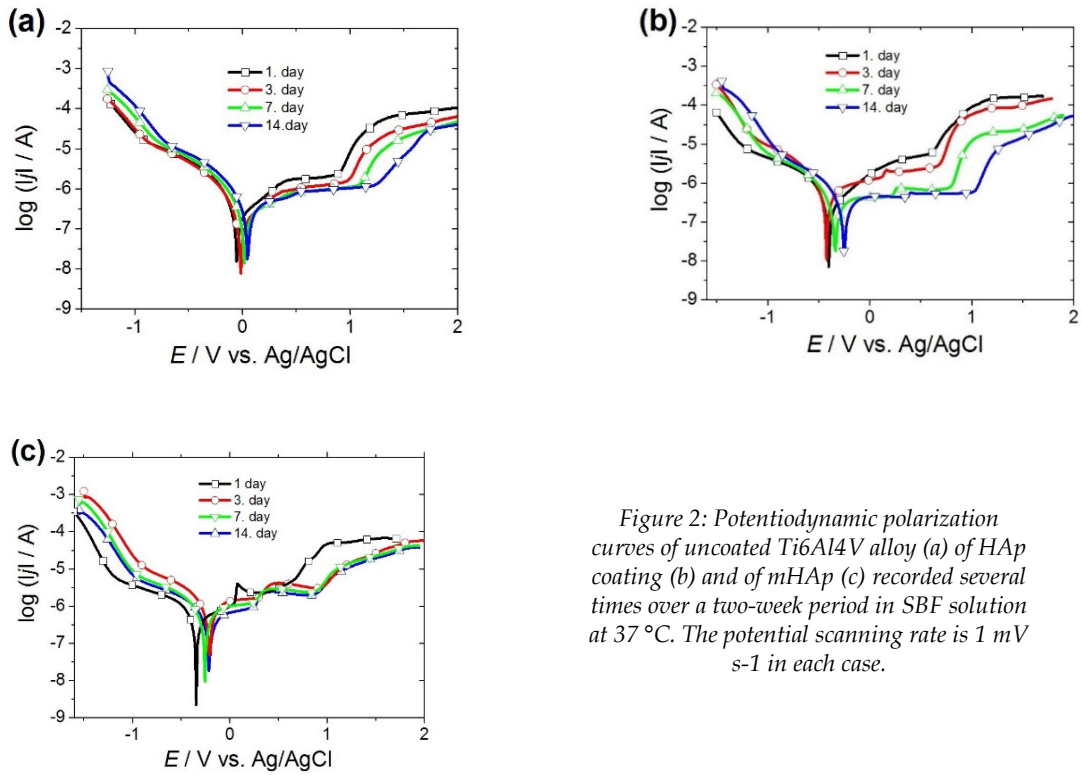

Figure 2: Potentiodynamic polarization curves of uncoated Ti6Al4V alloy (a) of HAp coating (b) and of mHAp (c) recorded several times over a two-week period in SBF solution at 37 °C. The potential scanning rate is 1 mV s-1 in each case.

DEVELOPMENT OF PROTECTIVE TIC/A:C THIN FILMS PREPARED BY DC MAGNETRON SPUTTERING

N. Oláh and K. Balázsi

Most of the metallic medical implants are made of titanium (Ti) or of its various alloys because of the favourable biocompatibility. However, after implantation, Ti ions (and / or alloying elements) can be detected in the body – due to corrosion or metal scraping – which may cause inflammation, and may lead to allergic symptoms, or in the worst case, the implant must be removed. In order to increase the metal insulation, corrosion resistance, and thus biocompatibility, several methods can be used. One of them is the passivation of the surface with different nanocomposites. Ceramic titanium carbide / amorphous carbon (TiC/a:C) protective nanocomposite thin film may be a potential candidate for such a surface protection coating to the different implant materials serving as barrier layer. The main goal of this work was to develop and produce TiC/a:C nanocomposite thin film coatings by DC magnetron sputtering, electron microscopic examination of growth mechanisms, determination of relationship between the structure and the physical - biological properties, as well as the sample preparation.

It was shown that the TiC/a:C thin films produced by DC magnetron sputtering at room temperature follow the morphology characteristic of the two- component system zone diagram but they do not follow the phase transformations expected based on the macroscopic Ti - C phase diagram. Based on structural examination it was found that the globular TiC nanocrystals began to take shape until 25 W of Ti target power and above this value, the films were grown by columnar crystals. The diameter of the columns increases with the thickness increase, the higher the Ti content is widening faster. As the Ti content increased, the thickness of the amorphous carbon matrix decreased from 10 nm to 1 – 2 nm and the size of the TiC nanocrystals grew from ~ 0.5 nm to 26 nm (Fig. 1). FFT confirmed the presence of the only identifiable face-centred-cubic (fcc) TiC crystal phase. Further increasing of Ti content, up to ~ 60 at% showed the disappearance of amorphous carbon from the full length TiC columns, and any other Ti phase, such as hcp Ti, was not manifested.

The effect of TiC/a:C thin films on the mechanical (hardness (H), modulus of elasticity (E)) and tribological properties was also analyzed and it was detected that these properties show a distinct variation depending on Ti content. The highest H of ~ 26 GPa and E of ~ 140 GPa with friction coefficient of 0.268 was observed in case of the film prepared at ~ 38 at% Ti content (Fig. 2).

Most important result of the corrosion tests was that the TiC/a:C protective coating on various substrates, while providing a high hardness to the surface, was also sensitive to electrochemical processes. The TiC/a:C coated sandblasted TiAl6V4 alloy possesses the highest polarization resistances over time while the lowest resistances belong to coated polished wafers. It was observed from the ICP-OES results that the TiC/a:C coated sandblasted TiAl6V4 alloy prevents dissolution of both Ti and Al into simulated body fluid.

Based on the biocompatibility and viability tests of the thin films, it was found that the cells like the surface of the coating, are proliferated on the TiC/a:C thin film, so the films become non-toxic, biocompatible and the viability of the cells is excellent after 3 days. Furthermore, based on the results of the hydrophilicity tests on the coatings it was found that all films exhibited hydrophobic behaviour regardless of the composition.

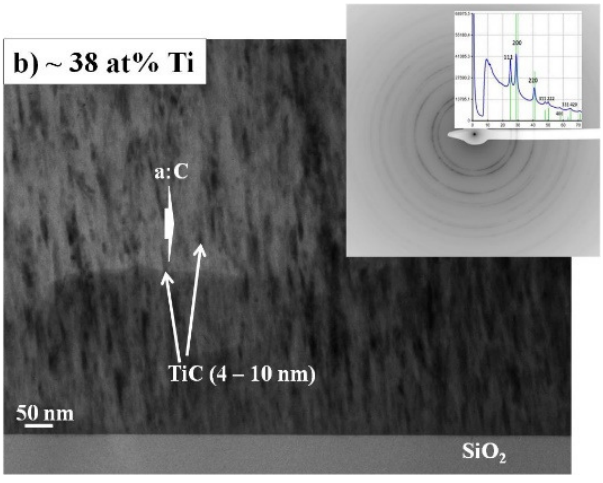

Figure 1: Cross section TEM image of TiC/a:C thin film deposited consisted at 40 W PTi.

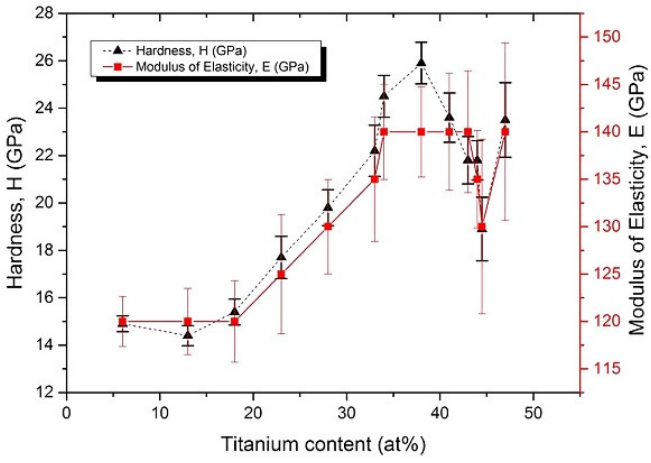

Figure 2: Effect of structure on mechanical properties of TiC/a:C thin films.

EFFECT OF OXIDIZATION OF Si_3N_4 PARTICLES ON STRUCTURE OF SINTERED Si_3N_4 CERAMICS

A. Qadir, K. Balázsi, and Cs Balázsi

Materials made of silicon nitride (Si_3N_4) are used in high-temperature oxidizing environment, thus, it is necessary to investigate the oxidation mechanism on structural, mechanical and tribological properties. The effect of hot isostatic pressing (HIP) on nanosized oxidized silicon powder particles on the structural and mechanical properties of Si_3N_4 was studied. The starting α-Si_3N_4 powders were oxidized for 10 and 20 hours at 1000 ˚C in ambient air. Amorphous oxide layer formation was observed on the surface of Si_3N_4 powder particles by high-resolution transmission electron microscopy (HRTEM). Thickness of the oxide layer on the surface of powder particles increased with oxidation time. These powders were densified at 1700 ˚C in nitrogen gas environment under 20 MPa for 3 hours using HIP technique. The complete α to β transformation was observed in Si_3N_4 samples which were sintered at 1700 ˚C under 20 MPa for 3 hours. Silicon oxynitride (Si_2N_2O) phase was found in sintered samples and the amount increased with the oxidation time (Fig. 1). The β phase decreased with the increase of Si_2N_2O phase in the sintered samples. We showed that the oxidation influenced the mechanical properties of sintered composites as well. The flexural strength of samples at 1700 ˚C sintering temperature is higher due to the higher amount of β- Si_3N_4 phase than that of samples which were sintered at 1500 ˚C. Decreasing tendency in flexural strength of the samples was observed with oxidation time. Higher amount of oxygen in the base powders results in higher tendency of formation of Si_2N_2O in the sintered Si_3N_4.

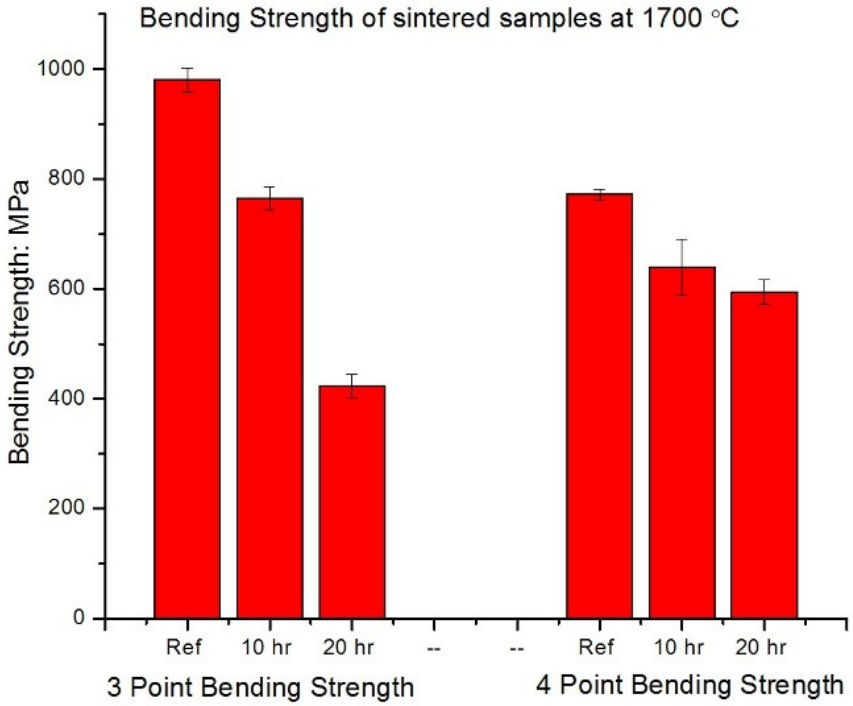

Figure 1: The bending strength of sintered samples decreased with the increase of oxidation time.

ADVANCED CERAMIC AND THEIR COMPOSITS FOR ENERGY APPLICATION

S. Lamnini, K. Balázsi, Cs. Balázsi, Zs. Fogarassy, E. Zs. Horváth, and S. Tóth

Several applications in energetics are known where yttria-stabilized zirconia (YSZ) and zirconia / multiwall carbon nanotube (MWCNT) composites were useful used as parts of solid oxide fuel cells (SOFC), photovoltaic solar cells, supercapacitor or hydrogen storage materials. The Ni – YSZ cermets are widely accepted as anodic materials in SOFCs with high catalytic activity and electrical conductivity. Research works showed drawbacks when with hydrocarbon fuels carbon build-up, sulphur poisoning or low tolerance to redox cycling is found. These irreversible processes damage the microstructure of anodes and reduce cell performance, therefore, Ni-free anode materials are continuously researched for and developed to overcome these problems. In this work, milled YSZ / MWCNT composites were studied. The effect of attritor milling on structure of 8 mol% yttria-stabilized zirconia (8YSZ) composites with 1wt%, 5 wt% and 10 wt% MWCNTs addition was studied. In all cases, a high dispersivity of the particles with a sharp and irregular shape was found, while the as-received MWCNTs were observed as clusters forming bundles of 2.5μm in length. Raman measurements showed results also supporting structural observations. The apparition of the G and D bands for all the composites at ~1589cm−1 and ~1356cm−1 confirmed the structural integrity of MWCNT after the milling process as well. The next step will be the sintering of milled composites by spark plasma sintering and study effect of MWCNT addition on density and electrical properties.

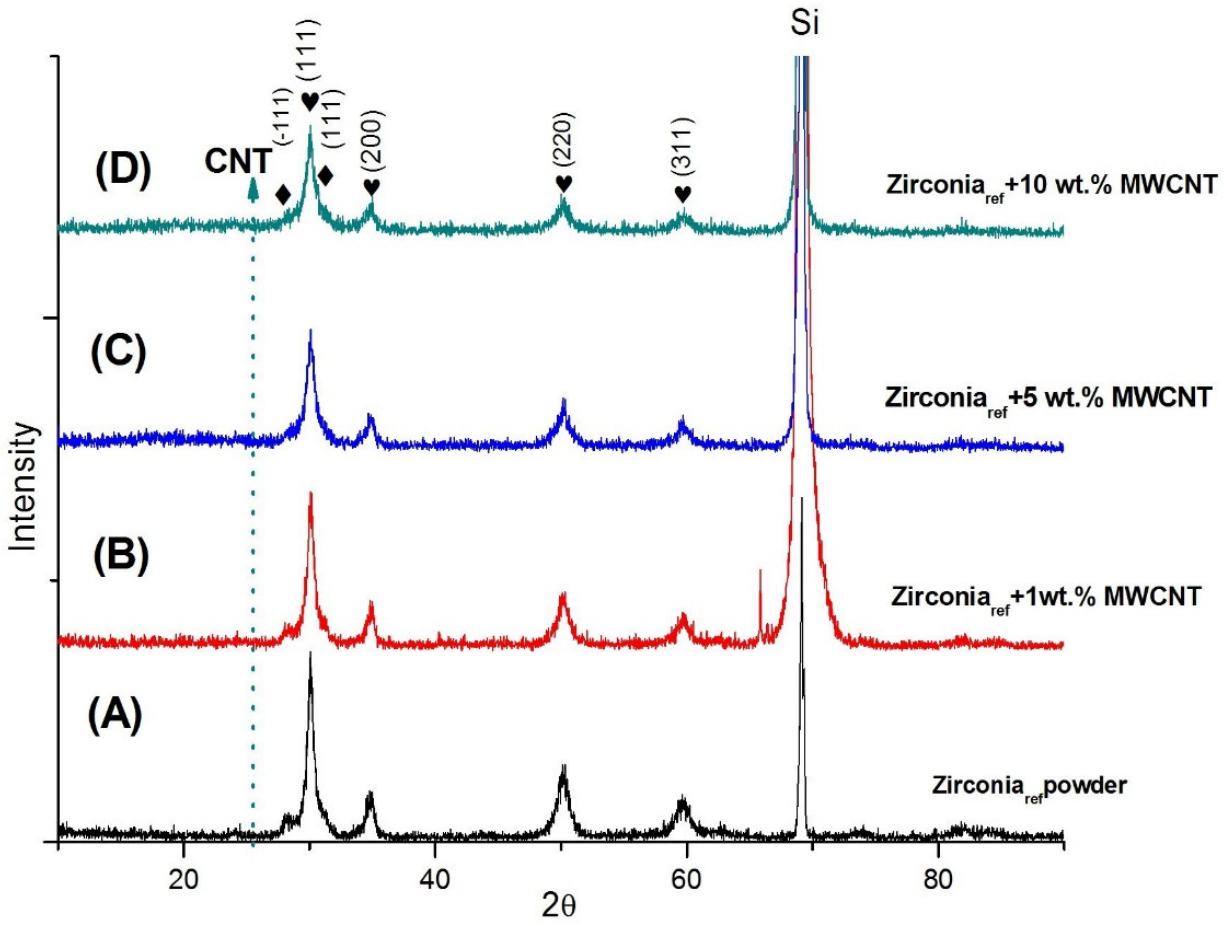

Figure 1: XRD measurements of YSZ/MWCNT composites after 5h intensive attritor milling.

EFFECT OF Si_3N_4 ADDITION ON THE MORPHOLOGICAL AND STRUCTURAL PROPERTIES OF THE 316L STAINLESS STEEL FOR NUCLEAR APPLICATIONS

H. R. Ben Zine, K. Balázsi, and Cs. Balázsi, F. C. Sahin (ITU), Z. E. Horváth, Z. Czigány, and Á. Horváth

316L austenitic stainless steel has attracted attention due to its good mechanical properties at high temperatures, good corrosion resistance and good weldability, which can be an effective solution for several industrial applications. Effect of addition of submicron sized Si_3N_4 on the morphological and structural properties of the ceramic dispersion strengthened (CDS) 316L stainless steel prepared by powder technology was studied. Two composites were prepared; 316L/0.33 wt. % Si_3N_4 and 316L/1 wt. % Si_3N_4. In order to assure a good dispersion of the ceramic particles in the stainless steel powders and a grain size reduction at the same time, highly efficient attrition milling was used. It was found that 5 hours milling in ethanol at 600 rpm and using 3 mm grinding stainless steel balls was sufficient to obtain grains with flake-like shape in case of 316L/0.33wt. % Si_3N_4. Spark plasma sintering (SPS) was used for fast sintering of milled composites.

The samples have been sintered under 50MPa at 900C° for 5 minutes in vacuum. Structural and morphological changes were studied after milling and sintering process. It was found that the amount of Si_3N_4 addition influenced the efficiency of milling process resulting in powder mixtures with different 316L stainless steel grain size and shapes. In the case of 0.33 wt. % Si_3N_4 addition (Fig. 1). The intensive milling assured an optimal coverage of 316L stainless steel grains with submicron sized Si_3N_4 particles in both cases, as demonstrated by EDS and TEM. In this case, the fracture is propagating through both intergranular or transgranular paths as shown in Fig. 2. The slightly damaged globular grains covered with Si_3N_4 particles clearly affected the fracturing behaviour as the SEM images shows a dominance of the intergranular fracturing with the presence of very few transgranular fracturing.

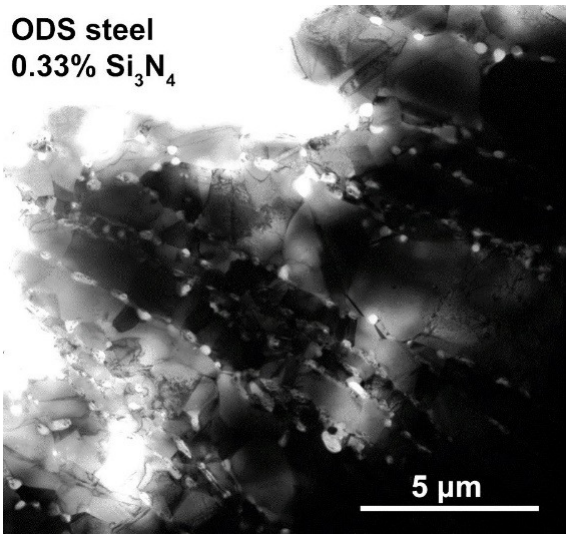

Figure 1: TEM images of sintered samples. a) 316L/0.33wt. % Si_3N_4.

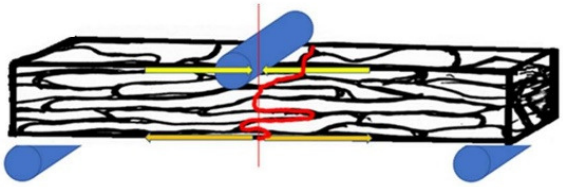

Figure 2: Schematic representation of the dominant fracturing behaviour in the case of the 316L/0.33wt. % Si_3N_4.

ADHESION MODEL OF GRAPHENE ISLANDS ON METAL SUBSTRATES BASED ON MOIRÉ-PATTERNS

M. Szendrő and P. Süle

One problematic aspect of graphene (GR) CVD growth on metal substrates is that GR is capable to create rotational domains, separated by grain boundaries (GBs), sometimes even on a single crystal surface. GBs worsen the electric properties of GR, therefore the nucleation of differently orientated islands is an undesirable phenomenon.

An interesting feature is, that the different existing orientations are very specific to the substrate (e.g. on Cu(111) the most commonly known orientations are: R0°, R7°, but for Ir(111) we have R0°, R14°, R19°, R23°, R26°, R30°). We are not aware of a physical model that can somehow clarify the very basic nature of these orientations. Why only these orientations can appear, and what are circumstances that influence GR to form one or another orientation?

In order to understand these aspects a continuum mathematical model was developed which calculates the adhesion energy of a GR island with a given size and orientation based only on knowledge of the underlying Moiré-pattern which is formed among atomic lattices. This approach agrees surprisingly well with DFT and CMD results. This shows that we have captured some very basic physical insights of the adhesion.

Using our model, Monte-Carlo (MC) simulations can be carried out to perform GR growth simulations on several nuclei to analyse their distribution of orientation (Fig. 1). These MC simulations are several orders of magnitude faster than Kinetic MC methods (Fig. 2).

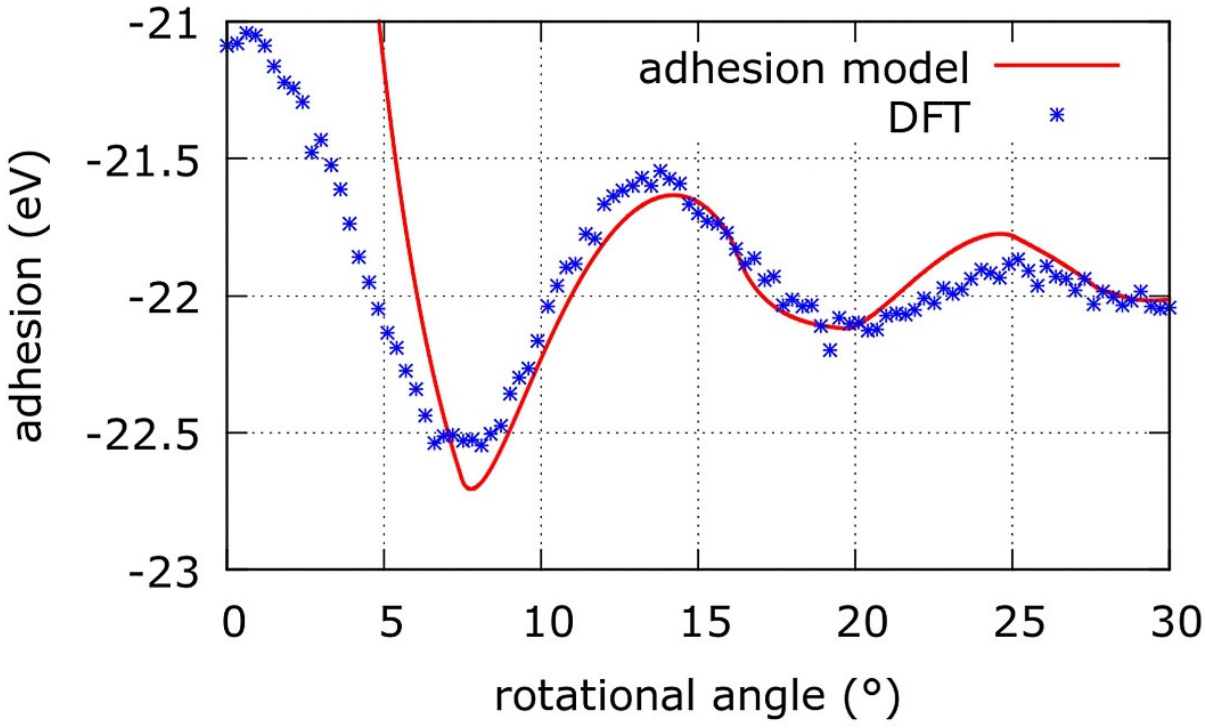

Figure 1: The dependence of the adhesion on the orientation of a GR nanoisland with a diameter of 2.2 nm on Cu(111) surface. Our model (red line) is compared to DFT calculations (blue spots).

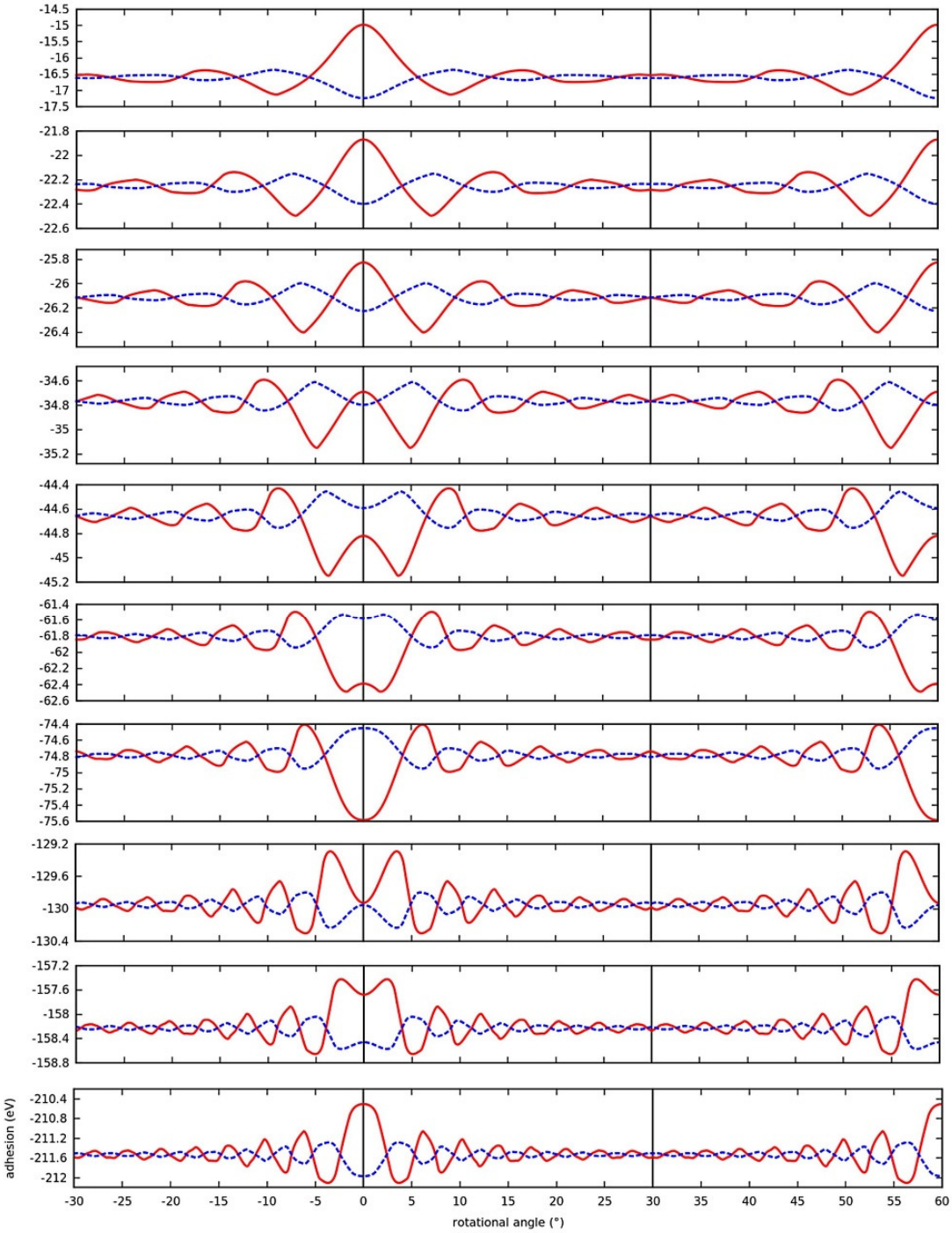

Figure 2: The behaviour of the rotational energy spectrum of a hollow (red line) and a hcp stacking island (blue line) when increasing the size (from top to bottom) according to our model. The spectrums of the two types of islands are almost mirror images of each other. During growth the number of energy minimums increases. The 30° is the source of the minimums: as the island grows new minimums appear at 30°, then they travel towards 0°. When two hollow minimums get close enough to 0° they unite and change the hollow maximum to a minimum and vice versa for the hcp type. This means that 0° is a dynamic minimum.

ONE-SAMPLE COMBINATORY FOR HIGH THROUGHPUT TEM- AND OTHER ANALYTICAL STUDIES OF THIN BINARY LAYER SYSTEMS

G. Sáfrán, T. Lohner, M. Serényi, P. Petrik, B. Kalas, Zs. Zolnai, and J. Gubicza

Our aim was to effectively study the concentration dependent properties of two component thin layer systems. We worked out a high throughput method, so called micro-combinatory, based on the "one-sample concept" i.e., a single gradient sample condenses the whole binary system of components A and B where A_xB_{1-x} (x=0...1) with a geometry that fits the actual analytical measuring technique. The patented method [G. Sáfrán: Hung. Patent, P 15 00500 (2015)] enables a comprehensive study within one specimen within a single measuring session. A specific advantage of μ-combinatory is that the phases of the binary film are formed and investigated side by side, in a single TEM grid that provides superior reproducibility and a straight comparison. The all-in-one feature is very efficient; only one sample is to handle, there is no need for laborious preparations replacement and study of a series of TEM samples. The consistency, and known concentration profile of μ-combinatorial samples are an invitation to high throughput automated TEM. That may be implemented by combining computerized stage positioning, precession electron diffraction and digital image storage and processing.

For a demonstration of the micro-combinatorial method and because of the technological importance Si-Ge binary films were studied by TEM, RBS, and ellipsometry and nanoindentation to reveal the correlation of composition, structure, optical and mechanical properties (Fig. 1).

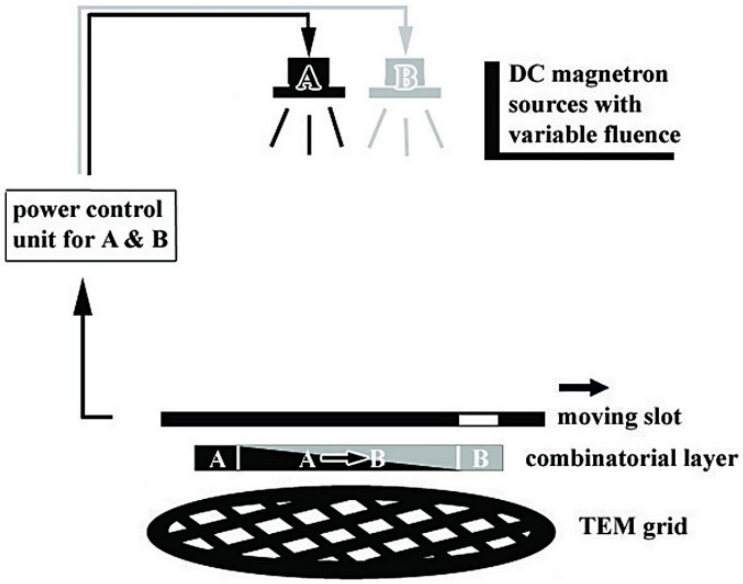

Figure 1: Set-up of micro-combinatorial deposition for TEM samples. For RBS, ellipsometry, nanoindentation, and XRD the sample size is scaled up from 3 mm diameter to 25x10 mm². The combinatorial layer track consists of three sections; sections of components A and B and in between a gradient section of A-to-B.

Research of thin SiGe layers is strongly motivated due to potential of widespread applications, e.g., solar cells, thin film transistors, Schottky diodes, thermal sensors, bolometers. The present study spans the whole cc. range, of the SiGe binary system, while earlier studies cover only the low Ge-content range. Besides, due to enhanced non-linear properties of Ge to Si, layers of higher Ge content are of interest in development of optoelectronic devices for the mid-infrared region [Carletti, et al. Opt. Express, 23 (2015) 32202].

A reveal of the concentration dependent properties of SiGe-on-Si provides the fine tuning of the properties – band gap (Fig. 2 and 3), refractive index – as well, the extension of the range of operation up to 8 μm, the Si absorption wavelength, or to 14 μm, the Ge transparency cut-off (Fig. 4 and 5) [M. Brun, et al. Opt. Express 22, 508 (2014)], [M. Ramirez, et al. Opt. Express 25, 6561-6567 (2017)]. The development of the μ-combinatorial method and device was done in co-operation of MFA and Holocom in a GINOP [Hung. Dev. Innov. Op. Prog. GINOP-2.1.7-15-2016-02073].

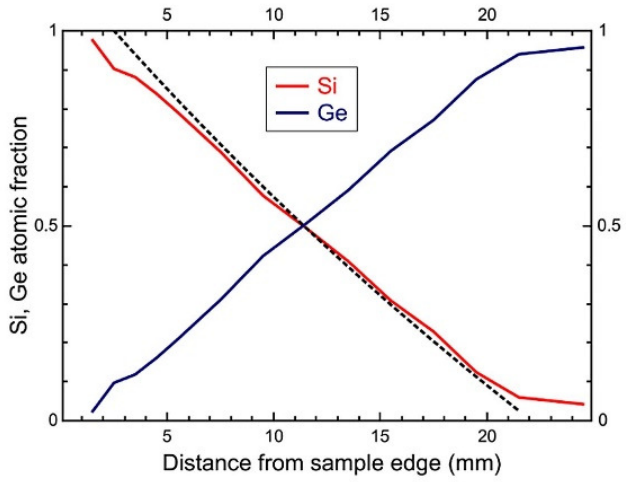

Figure 2: Linear concentration distribution and optical band gap of DC magnetron sputtered Si-Ge obtained by RBS.

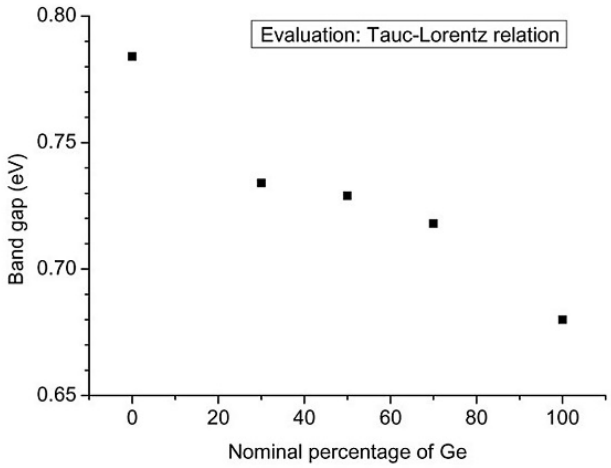

Figure 3: Ellipsometry as a function of Ge-concentration measured in a 25x10 mm² size μ-combinatorial sample.

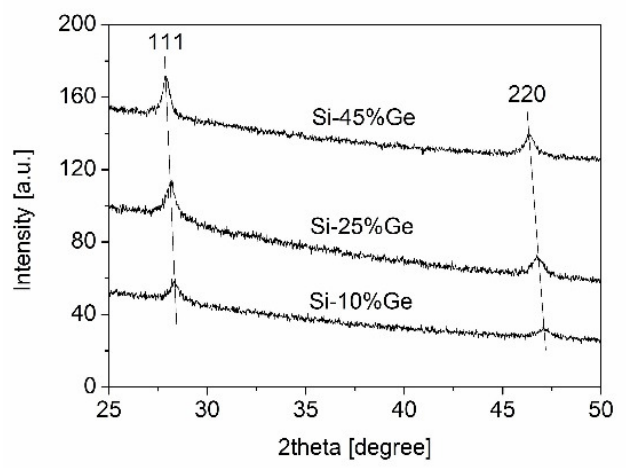

Figure 4: XRD diagrams and the 111 and 220 peak distances of a Si-Ge sample crystallized at 800°C.

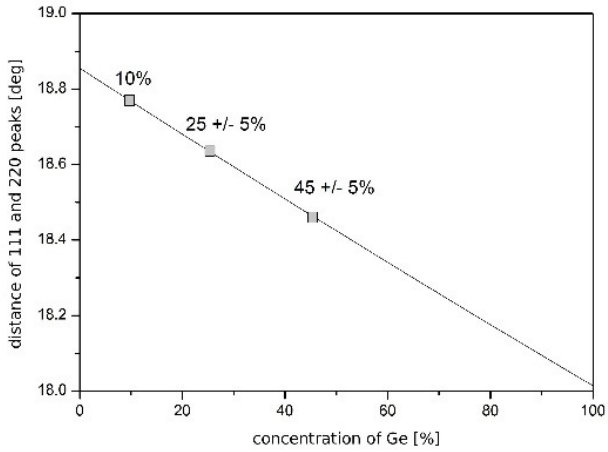

Figure 5: Linear lattice parameter change with Ge concentration.

BIOPHYSICAL CHARACTERISTICS OF PROTEINS AND LIVING CELLS EXPOSED TO THE GREEN TEA POLYPHENOL EPIGALLOCATECIN-3-GALLATE (EGCG): REVIEW OF RECENT ADVANCES FROM MOLECULAR MECHANISMS TO NANOMEDICINE AND CLINICAL TRIALS

(Lendület LP2012-26/2012)

B. Péter, Sz. Bősze (ELTE), and R. Horváth

Traditionally, tea was drunk to eliminate toxins, to improve blood flow and resistance to diseases, so its habitual consumption has long been associated with health benefits. Among natural compounds and traditional Chinese medicines, the green tea polyphenol epigallocatechin gallate (EGCg) is one of the most studied active substance. Tea catechins, especially (-)-EGCg, have been shown to have various health benefits, for example anti-metastasis, anti-cardiovascular, anti-cancer, antiinflammatory and antioxidant effects (Fig. 1).

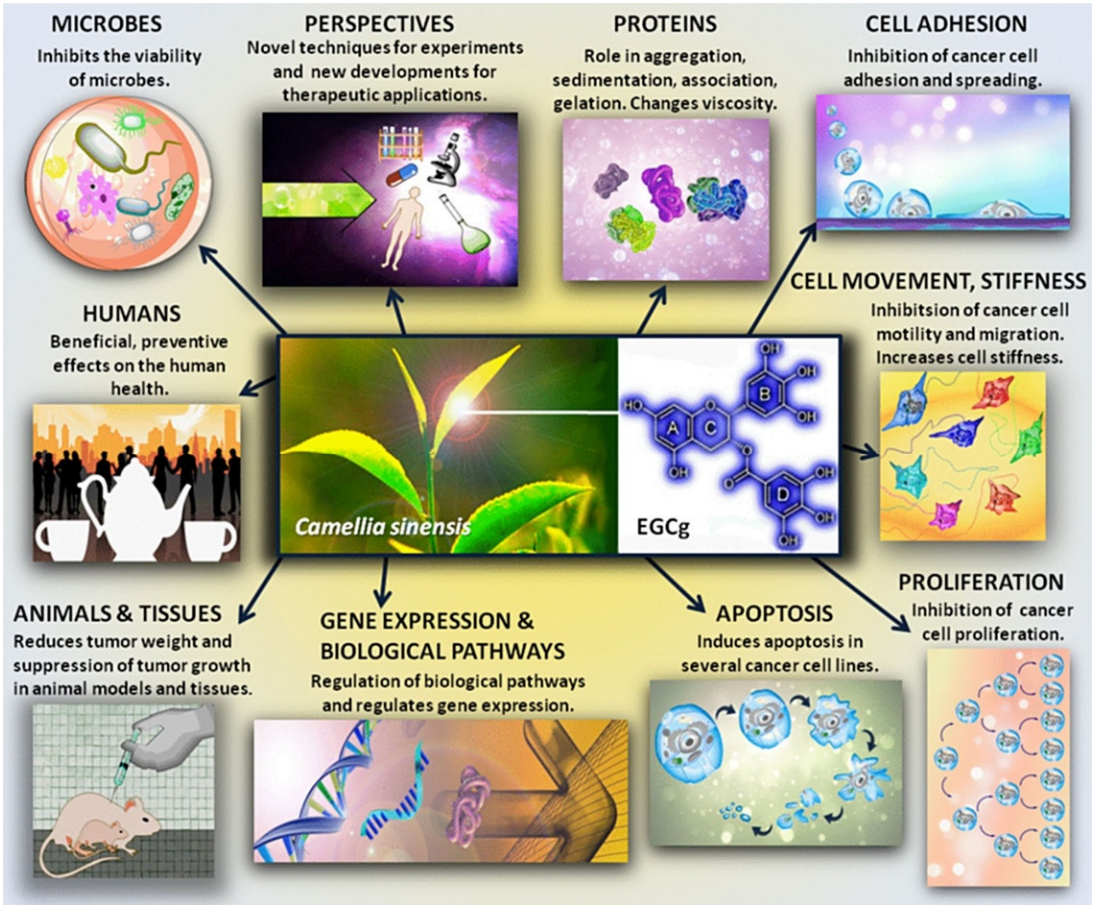

Figure 1: Diversified effects of EGCg

In 2015 we focused on the molecular scale interactions between proteins and EGCg with special focus on its limited stability and antioxidant properties, the observed biophysical effects of EGCg on 112 various cell lines and cultures. The alteration of cell adhesion, motility, migration, stiffness, apoptosis, proliferation, as wells as the different impacts on normal and cancer cells are all summarised in our prospective review article. We also handled the works performed using animal models, microbes and clinical trials. Novel ways to develop its utilization as therapeutic purposes in the future are discussed too, for instance, using nanoparticles and green tea polyphenols together to cure illnesses, and the combination of EGCg and anticancer compounds to intensify their effects. In this review we summarize the experiments and results of the past few years. The limitations of the employed experimental models and the criticisms on the interpretation of the obtained experimental data are summarized as well. We also pointed out some inaccuracies in the literature.

GREEN TEA POLYPHENOL TAILORS CELL ADHESIVITY OF RGD DISPLAYING SURFACES: MULTICOMPONENT MODELS MONITORED OPTICALLY

(Lendület LP2012-26/2012)

B. Péter, E. Farkas, E. Forgács, A. Saftics, B. Kovács, S. Kurunczi, I. Székács, A. Csampai, Sz. Bősze (ELTE), and R. Horváth

A wide range of experimental methods are available to measure cell adhesion and cell–surface interactions, however, most of them have serious disadvantages when a multicomponent model of cell adhesion has to be quantitatively investigated in a reasonable time frame. (For example, labelling techniques use fluorescent markers that may affect normal cell behaviour and the imaging time is often limited by the bleaching of the marker). In contrast, we highlighted the remarkable potentials of high-throughput resonant waveguide gratings in studying multicomponent model systems of cell–surface interactions. The interaction of the anti-adhesive, antifouling coating, PLL-g-PEG and its RGD (Arg-Gly-Asp) functionalized form, PLL-g-PEG-RGD, with the green tea polyphenol, EGCg was in situ monitored. Right after, cellular adhesion on the EGCg exposed coatings was recorded in real-time (Fig.1). The plate based sensor configuration allowed following the above processes with different surface coatings, EGCg states and concentrations in a single run, on the same biosensor plate. Despite the reported excellent antifouling properties of the above polymer coatings, EGCg strongly interacted with them, and affected their cell adhesivity in a concentration dependent manner. The differences between the effects of the freshly prepared and oxidized EGCg solution could be also first demonstrated. The measured interactions were significantly stronger for the oxidized EGCg solution, highlighting the importance of storage conditions of EGCg solutions, often overlooked in present literature. Using a semi empirical quantum chemical method, we showed that EGCg binds to the PEG chains of PLL-g-PEG and PLL-g-PEG-RGD by hydrogen bonds. Moreover, the calculations illuminated the differences in binding affinity between the fresh and oxidized EGCg, well supporting the experimental findings. Our work lead to a new model of polyphenol action on cell adhesion ligand accessibility and matrix rigidity.

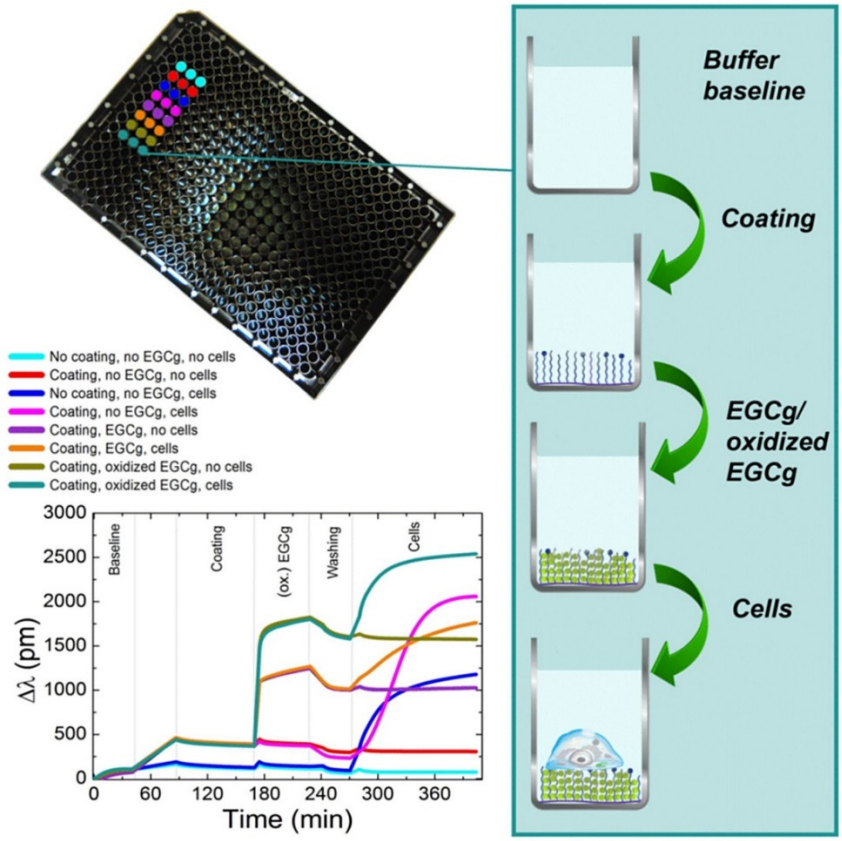

Figure 1: In situ kinetic curves recorded by the Epic BT instrument. A 384-well plate used in the experiment is also shown, together with the manipulation steps in a typical well (right scheme). Typical experimental curves are plotted (bottom left corner) for PP:PPR coating, and 500 µg/ml EGCg concentration. The detailed experimental conditions corresponding to the various kinetic curves are indicated above the graph.

LABEL-FREE OPTICAL BIOSENSOR FOR ON-LINE MONITORING THE INTEGRATED RESPONSE OF HUMAN B CELLS UPON THE ENGAGEMENT OF STIMULATORY AND INHIBITORY IMMUNE RECEPTORS

(Lendület LP2012-26/2012)

I. Kurucz, B. Péter, A. Prosz, I. Székács, R. Horváth, and A. Erdei (ELTE)

The majority of current cell-based assays relies on the measurement of a single event at a predetermined time point in a specifically chosen signalling path-way, let it be second messenger release, reporter-gene production or target translocation. These measurements require the use of labelled compounds, sometimes the modification of cells to express the target in larger amount or to produce a reporter molecule to be able to monitor receptor engagement. The mentioned manipulations can be toxic for the cells and can interfere with normal cellular physiology of the target receptors or their environment and the applied fluorescence and coloured compounds may induce elevated background. Consequently, functional cellular assays which can report from different signalling events in real time without the application of molecular engineering (in providing the suitable cellular partner) and without the use of labelling would be of high value for both theoretical and practical studies even if they are more complex and less specific than cell-based biochemical assays.

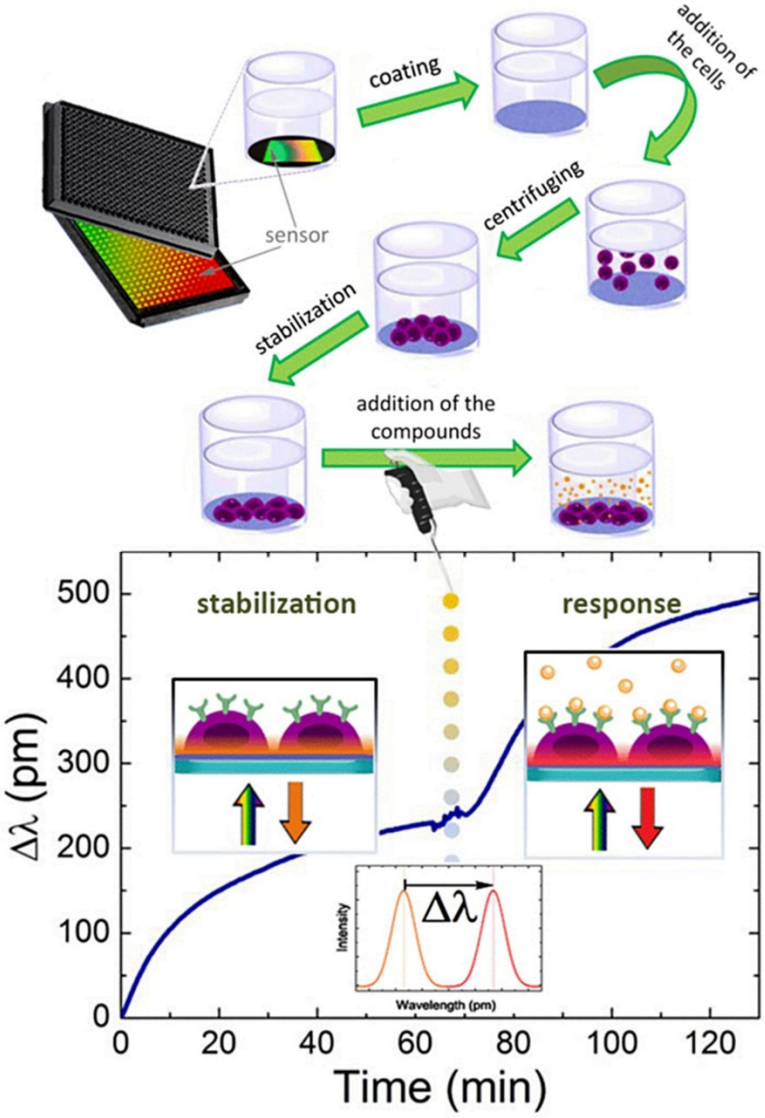

Figure 1: Experimental setup to perform real-time measurement of dynamic mass redistribution (DMR) using B-cell lines (A); and schematic illustration of the principle of DMR detection (B).

To be able to obtain holistic pictures about B cell responses to complex interlocking stimulations Epic BT optical biosensor was applied and set to establishing the method using human B cell lines, derived from Burkitt's lymphomas. We successfully immobilized non-adherent B cells on the surface of the biosensors, without the ligation of any specific receptors or adhesion molecules. This way we were able to demonstrate that engagement of the antigen specific B cell receptors (BCR) induced reproducible dynamic mass redistribution (DMR) inside the cells as a measure of receptor activation (see Fig.1). The initiated DMR response proved to be specific, since only antibodies recognizing the BCR could generate the response; neither the assay-buffer, nor high concentration of indifferent proteins or non-specific antibodies had any effect. The measure of cell activation was sensitive, concentration dependent, and specifically and dose-dependently inhibited by the Syk inhibitor BAY 61-3606. The BCR-triggered DMR response was evoked from three human Epstein-Barr virus (EBV) negative B cell lines, but could not be elicited in two EBV-positive BL cell lines, where the presence of the EBV-derived LMP2A protein desensitizes the cells' response to the BCR-induced signalling.

Therefore, our work opens new avenues to study complex signalling events and to decipher interactions within the signalling network during B cell activation.

FABRICATION AND CHARACTERIZATION OF ULTRATHIN AND SPIN-COATED (THICK) DEXTRAN LAYERS (HYDROGEL FILM FABRICATION FOR BIOSENSING)

(Lendület LP2012-26/2012)

A. Saftics, S. Kurunczi, B. Türk, E. Agócs, B. Kalas, P. Petrik, M. Fried, A. Sulyok, Sz. Bősze (ELTE), and R. Horváth

Fabrication of a stable and reproducible surface with the required chemical functions are one of the major challenge in the development of label-free biosensors. Polysaccharide dextran interface layers are able to improve the sensitivity of biosensors, owing to the anti-fouling property and the high receptor immobilization capacity of the dextran chains.

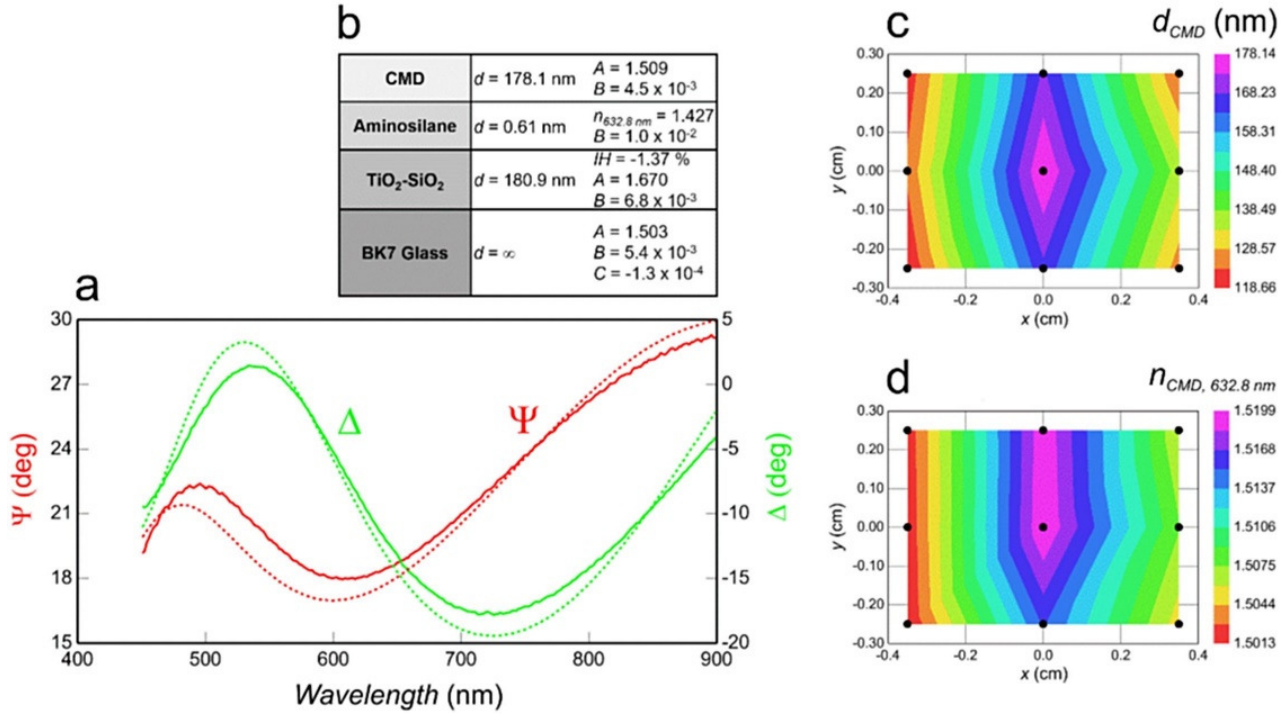

Figure 1: Ψ (—) and Δ (—) spectra measured for the determination of the thickness and refractive index of CMD on the TiO_2-SiO_2 waveguide (a). The solid lines refer to the measured spectra, the dashed lines (- - - and - - -) to the fitted curves (MSE = 20). The spectra were recorded at the centre point (x = 0 cm, y = 0 cm) of the sample fabricated by spin coating of the CMD at 3000 rpm rotational speed. Details about the optical model were also put on the figure (b). Additional figures: thickness (d_{CMD}) (c) and refractive index (n_{CMD}, 632.8 nm) (d) map of the CMD. The refractive index was calculated from the Cauchy equation at the wavelength of 632.8 nm.

Carboxymethyl-dextran (CMD) was synthetized in our laboratory from the native dextran. Grafting methods based on covalent coupling to aminosilane- and epoxysilane-functionalized surfaces were applied to obtain thin CMD layers. The carboxyl moiety of the CMD was coupled to the aminated surface by EDC (Ethyl-3-(3-dimethylaminopropyl)-carbodiimide hydrochloride) and NHS (N-hydroxy-succinimide) reagents, while CMD coupling through epoxysilane molecules was performed without any additional reagents. The surface analysis following the grafting procedures consisted of x-ray photoelectron spectroscopy (XPS), attenuated total reflection infrared spectroscopy (ATR-IR), as well as atomic force microscopy (AFM), which proved the presence and the 1 - 2 nm thickness of the CMD layer, and verified its covalent grafting to the surface. The in situ optical waveguide light mode spectroscopy (OWLS) measurements were suitable to devise the structure of the interfacial dextran layers by the evaluation of the optogeometrical parameters.

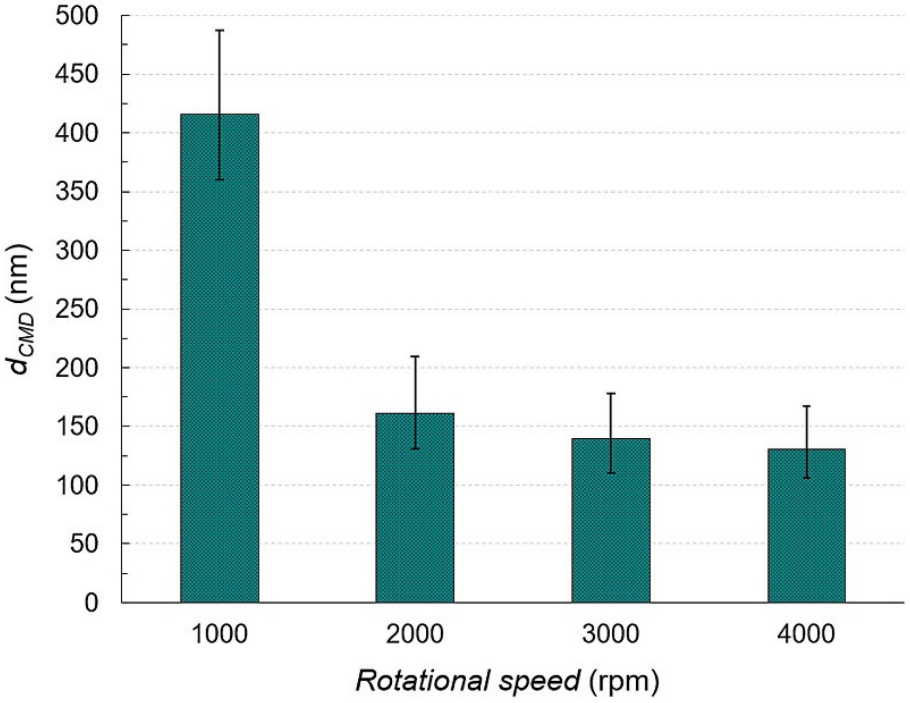

Figure 2: The effect of the rotational speed on the thickness of the spin coated CMD layer (dCMD). The data were collected from the thickness maps of multiple parallel samples. The map values for the individual samples, as well as these data for each parallel sample were averaged. The bars on the columns represent the minimum and maximum values of the measured thicknesses at the corresponding rotational speeds.

Beside the ultrathin films, we also fabricated thicker CMD layers in the thickness range of around 150 - 400 nm using spin-coating technique. The dependence of the layer thickness on the rotational speed as a technical parameter of the fabrication process, was investigated by spectroscopic ellipsometry. Optical model for the evaluation of the ellipsometric data was developed and the refractive index dispersion (Cauchy B parameter) of the CMD layer was determined based on our high sensitivity measurements on gold substrate. The ellipsometric data showed high rotational speed dependence on the CMD layer thickness comparing the thickness values at 1000 and 2000 rpm. However, varying the rotational speeds to 3000 and 4000 rpm did not cause significant difference in the CMD layer thickness. The mapping measurements also provided details about the extent of the inhomogeneity in the thickness and refractive index of the CMD layers.

BACTERIA REPELLENT LAYER MADE OF FLAGELLIN

(Lendület LP2012-26/2012)

B. Kovács, D. Patkó, A. Klein (University of Pannonia), B. Kakasi (University of Pannonia), A. Saftics, S. Kurunczi, F. Vonderviszt (University of Pannonia) and R. Horváth

The development of bacteria repellent surface coatings is critical in various fields ranging from biosensing to health care, biotechnology and food production. In the present study we exploit that the protein flagellin rapidly forms a dense and oriented monolayer on hydrophobic surfaces upon adsorption from aqueous solution. This oriented layer mimics the surface of bacterial flagellar filaments and has excellent E. coli bacteria repellent properties. Quantitative cell adhesion data were obtained by employing fluorescent microscopy and a label-free surface sensitive optical biosensor, OWLS (Optical Waveguide Lightmode Spectroscopy). During the biosensor experiments, injection of the bacterial solution resulted in an almost negligible signal increase on the flagellin covered OWLS chip (Fig. 1). The adhered cells were also visualized by fluorescent microscopy and the formed protein film was characterized by AFM (Atomic Force Microscopy).

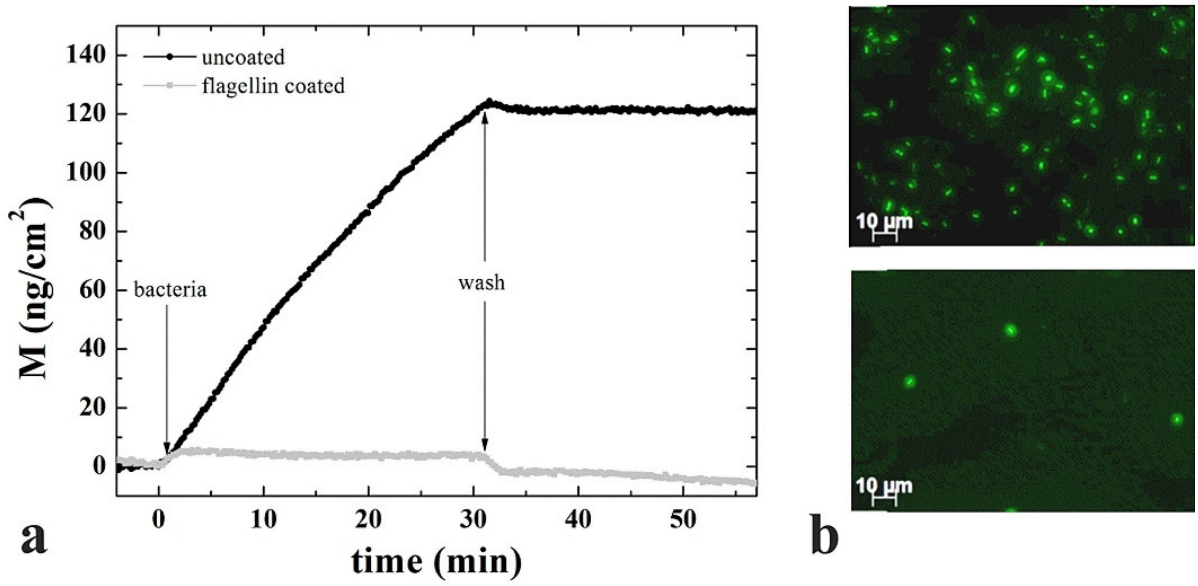

Figure 1: [a] Calculated surface mass densities from the in situ OWLS measurements on the uncoated (black curve) and flagellin coated (grey curve) surfaces in representative experiments. [b] Representative fluorescent microscopic images of adhered bacteria on the uncoated (upper) and flagellin coated (bottom) surfaces. The images were recorded right after the biosensor measurements. (Reference: B. Kovacs, et al., Sensors Actuators B Chem. 257, 839–845 (2018))

In parallel control experiments, the adherence of bacteria was measured on bare hydrophobic surfaces as well. The bacteria adhered irreversibly onto the uncoated surface, but reversibly onto the flagellin coated chip. Both OWLS and microscopy results well confirmed that the flagellin coating drastically reduced the adhesion of E. coli cells. Therefore, a novel type of bacteria repellent layer made of flagellin is demonstrated. The great advantage of the flagellin-based surface coatings is that this protein can be easily produced in large amounts in a cost-effective way. The introduced flagellin-based coatings offer a general toolbox for controlling the surface adhesion of living cells.

RECEPTOR SPECIFIC ADHESION ASSAY FOR THE QUANTIFICATION OF INTEGRIN–LIGAND INTERACTIONS IN INTACT CELLS USING A MICROPLATE BASED, LABEL-FREE OPTICAL BIOSENSOR

(Lendület LP2012-26/2012)

I. Székács, N. Orgován, B. Péter, B. Kovács, and R. Horváth

Integrins are transmembrane heterodimers, a group of plasma membrane receptors that mediate adhesion of cells to the extracellular matrix (ECM). Integrins bind to ECM proteins mainly via the Arg-Gly-Asp (RGD) sequence motif and are crucially involved in many physiological events, including immune responses, cell growth and differentiation, and tissue morphogenesis. In addition, integrins are associated with pathophysiological conditions (e.g., thrombosis, some genetic and autoimmune diseases, and metastatic development), and thus, represent important therapeutic target structures. Disruption of binding to integrin receptors is an important topic in drug discovery, comprising the design, synthesis and biomedical applications of new integrin-targeting drugs. In this proof of principle study, we examine the feasibility of using the resonant waveguide grating technology for analysis of integrin–ligand interactions by measuring the kinetics of cell adhesion. As a model, the smallest known natural disintegrin – echistatin from Echis carinatus – was chosen for inhibition of integrin-mediated cell adhesion. By coating the sensor surfaces with an RGD displaying polymer film, and using different concentrations of echistatin to block the cell adhesion molecules in the cell suspensions transferred onto the sensing surfaces, inhibition of binding was determined using a biosensor assay that uses intact cells, does not require ligand labelling, or isolation of receptors.

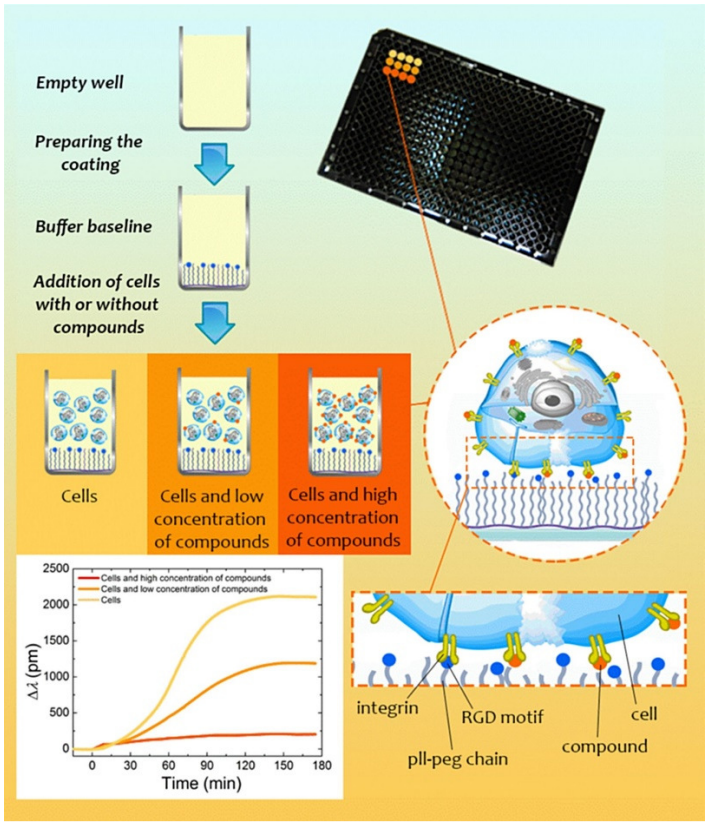

Figure 1: Schematic illustration of the working principle of the measurement of integrin–ligand interactions by detecting cell adhesion with the Epic BT biosensor. Prior to measurement, the bottom of the biosensor wells is covered with a synthetic polymer layer displaying the integrin ligands. Ligand molecules added to the cell suspensions block integrins on the surface of the adhering cells, therefore weaken the cell adhesion on the ligand displaying sensing surfaces. Representative cell spreading curves for low concentration, high concentration, and without any integrin ligands in the employed cell suspension are shown. (Reference: I. Székács, et al., Sensors Actuators B Chem. 256, 729–734 (2018))

Figure 1 illustrates schematically the working principle of the introduced label-free cell adhesion assay. First, surface coating of the Corning Epic sensor microplate was created by incubation with 250 µg/ml PLL-g-PEG-RGD for 30 min at room temperature. After washing out the excess of reagent by rinsing the surface with 20 mM HEPES HBSS (pH 7.0), biosensor plate was placed into the Epic instrument and a baseline was recorded for 1 h in 30 µL 20 mM HEPES HBSS (pH 7.0) per each well. After the stable baselines had been established for all wells, detached HeLa cells were mixed with the inhibitor solutions at varying concentrations of the investigated cell adhesion ligand and then 30 µl (containing 8000 cells) of obtained suspensions were seeded into the wells and biosensor responses were recorded for 2 h. The higher inhibitor concentration was applied, the lower the biosensor response was obtained (see the kinetic curves in Fig. 1).

Using this novel methodology, the half maximal inhibitory concentration (IC_{50}) for echistatin in living cancer cells was determined to be in the range of 20-40 nM, which is in agreement with data in the literature. Although this method detects a combined signal of the number of the adhered cells, it is applicable for rapid, label-free screening of potential pharmaceutical compounds. Moreover, the present methodology uses intact cells so there is no need to isolate or label the integrin receptors involved in binding. In addition, by down-regulating given types of integrins by RNA silencing or by blocking their action with specific antibodies or RGD peptides, the binding assay could be used to study the number of various integrins on the cell surfaces, the integrin-specific affinity of the ligand, as well as processes that are initiated by these integrins. Finally, this methodology has potential application for screening natural, as well as newly developed synthetic molecules that prevent survival mechanisms of tumor cells.

ANTIBIOTIC-INDUCED RELEASE OF SMALL EXTRACELLULAR VESICLES (EXOSOMES) WITH SURFACE-ASSOCIATED DNA

(Lendület LP2012-26/2012)

A. Németh (SE), N. Orgovan, B. W. Sódar (SE), X. Osteikoetxea (SE), K. Pálóczi (SE), K. É. Szabó-Taylor (SE), K. V. Vukman (SE), Á. Kittel (MTA KOKI), L. Turiák (MTA TTK), Z. Wiener (SE), S. Tóth (SE), L. Drahos (MTA TTK), K. Vékey (SE), R. Horvath, and E. I. Buzás (SE)

Recently, biological roles of extracellular vesicles (which include among others exosomes, microvesicles and apoptotic bodies) have attracted substantial attention in various fields of biomedicine. Here we investigated the impact of sustained exposure of cells to the fluoroquinolone antibiotic ciprofloxacin on the released extracellular vesicles. Ciprofloxacin is widely used in humans against bacterial infections as well as in cell cultures against Mycoplasma contamination. However, ciprofloxacin is an inducer of oxidative stress and mitochondrial dysfunction of mammalian cells. Unexpectedly, here we found that ciprofloxacin induced the release of both DNA (mitochondrial and chromosomal sequences) and DNA-binding proteins on the exofacial surfaces of small extracellular vesicles referred to in this paper as exosomes. Furthermore, a label-free optical biosensor analysis revealed DNA-dependent binding of exosomes to fibronectin (Fig.1). DNA release on the surface of exosomes was not affected any further by cellular activation or apoptosis induction. Our results reveal for the first time that prolonged low-dose ciprofloxacin exposure leads to the release of DNA associated with the external surface of exosomes.

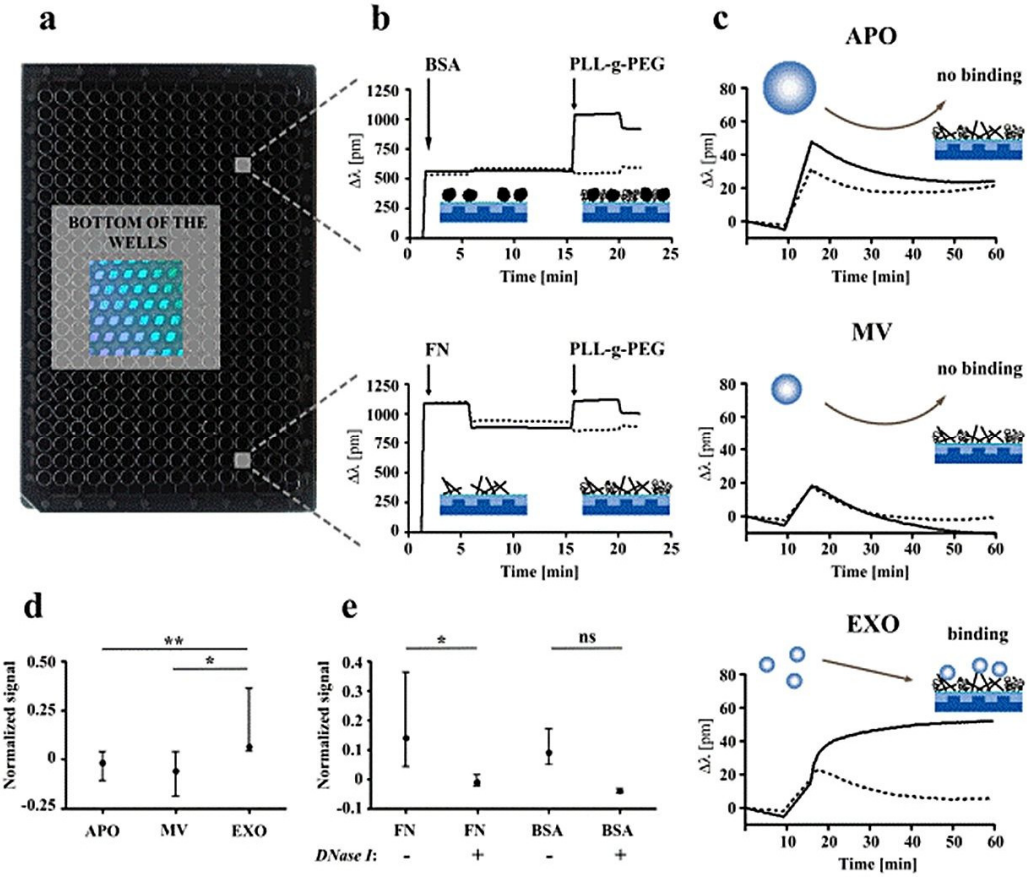

Figure 1: Label-free optical biosensor analysis of surface adhesion of extracellular vesicles (EVs). (a) Photograph of an Epic microplate (384-well) is shown containing biosensors (b) Microplate wells were coated with bovine serum albumin (BSA) as a control protein or with fibronectin (FN) resulting in a shift in the resonant wavelength (Δλ). Microplate wells were equilibrated with PBS, then BSA or FN were added to the wells (indicated by the first arrows). PLL-g-PEG was used in order to block the non-specific binding sites of wells. After 30 min incubation with PLL-g-PEG, Δλ was recorded for another 5 min (starting points are indicated by the second arrows), and finally PLL-g-PEG was changed to PBS. (c) Adsorption of apoptotic bodies (APOs), microvesicles (MVs) and exosomes (EXOs) onto FN+PLL-g-PEG surfaces (continuous lines) or onto surfaces with adsorbed PLL-g-PEG only (dashed lines). (d) The Δλ values of EV adsorption onto PLL-g-PEG were subtracted from adsorption values onto FN+PLL-g-PEG, and were divided by the Δλ value of EV adsorption onto bare surfaces (as a straightforward normalization with the mass concentrations of various samples).

EFFECTS OF HETEROGENEITY IN POWER-GRID NETWORK MODELS

G. Ódor and B. Hartmann

Power-grids are becoming more and more heterogeneous as renewable small (solar, wind, geothermic) suppliers are connected. Therefore, the danger of desynchronization may increase. We have studied the effects of topological and intrinsic (node connection strength) disorder on the second order Kuramoto model with respect to simple homogeneous lattices. Our aim was to provide a description of the desynchronization transition, determine the fluctuations and the heavy tailed failure avalanche distributions, reported in several large blackout events. We have planned to explore possible Griffiths phases and to provide a measure of danger as the function of stochastic elements connected.

We have compared the phase synchronization transition of the second order Kuramoto model, a basic model describing AC electric networks, on 2D lattices and on large synthetic power-grid networks, generated from real data. While admittance matrix of the transmission network is based on a real-life example (the Hungarian power system), matrix of the distribution network is the result of synthetic grid modelling.

Equations of the second order Kuramoto model for the phases Θ_i and the global coupling control parameter K have been analysed numerically, using 4th order Runge-Kutta differential solvers. Here we introduced quenched heterogeneities, via the A_{ij} intrinsic frequencies of the N nodes, connected via the A_{ij} admittance matrix. For the inertia parameter we used α=1,3 and we also considered the of Gaussian as well as exponentially distributed noise terms. We have measured the global phase synchronization order-parameter and determined the static/dynamic phase transition behaviour. We have also determined the distribution of the duration times from fully synchronous (R = 1) to disordered ($R = 1/N^{0.5}$) states, by random sample averaging.

Due to the inertia the transition is of first order type, contrary to the simple Kuramoto model, exhibiting hysteresis at certain global coupling parameter *K* (see Fig. 1). Heterogeneity cannot round the transition to a critical behaviour type, the order parameter fluctuations do not depend on the network size (Fig. 2.). In case of the real power-grid the synchronization is weaker, but breaks down at a smaller *K*, than in case of lattices. The desynchronization duration distributions exhibit scale-free (heavy) tails below the transition without the assumption of self-organized criticality conjectured for power-grids. The control parameter dependent power-laws (Fig. 3.) suggest Griffiths phases, but identification of rare-region effects has not been achieved yet [https://arxiv.org/abs/1801.09492].

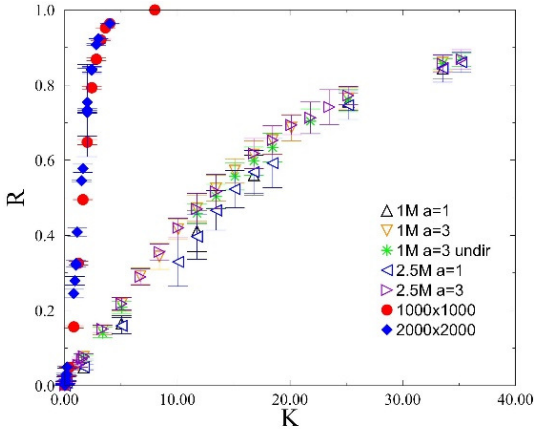

Figure 1: Comparison of the steady-state order parameter for different networks: 1000x1000, 2000x2000 lattices, powergrids 1,4,5 and US high voltage grid.

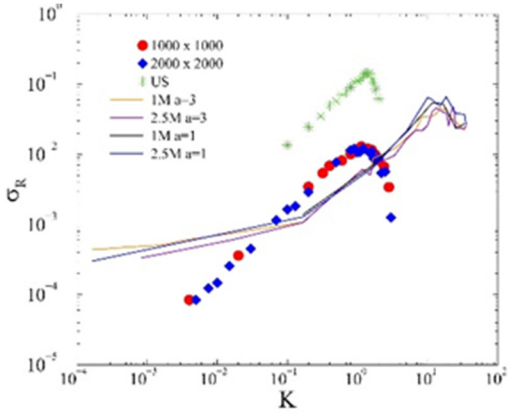

Figure 2: Fluctuation of the steady-state order parameter for different networks.

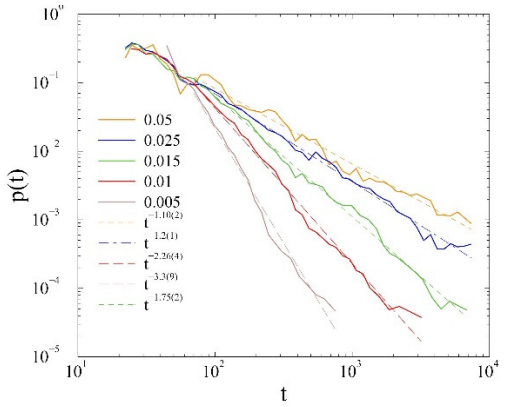

Figure 3: Avalanche duration distribution for power grid 1 at different control parameters. Dashed lines: power-law fits.

SECOND-ORDER FREERIDING ON ANTISOCIAL PUNISHMENT RESTORES THE EFFECTIVENESS OF PROSOCIAL PUNISHMENT

(OTKA K 120785)

A. Szolnoki, and M. Perc

Economic experiments have shown that punishment can increase public goods game contributions. However, the effectiveness of punishment is challenged by second-order free-riding and antisocial punishment. The latter implies that non-cooperators punish cooperators, while the former implies unwillingness to shoulder the cost of punishment. While the threat of punishment has the proven ability to deter would-be defectors, the associated costs challenge its evolutionary stability. Antisocial punishment, the deplorable consequence of which is that non-cooperators punish cooperators, is likewise an important impediment to the viability of punishment. But just as prosocial punishment breeds second-order free-riders -- cooperators who refuse to shoulder the cost of punishment -- so does antisocial punishment. Defectors who do not punish cooperators, and are thus second-order free-riding on antisocial punishment, provide the missing link that enables a successful coevolution of cooperation and punishment, even when antisocial punishment is present.

We extend the theory of cooperation in the spatial public goods game by considering four competing strategies, which are traditional cooperators (C) and defectors (D), as well as cooperators who punish defectors (P_C) and defectors who punish cooperators (P_D). We show that if the synergistic effects are high enough to sustain cooperation based on network reciprocity alone, antisocial punishment does not deter public cooperation. Conversely, if synergistic effects are low and punishment is actively needed to sustain cooperation, antisocial punishment does act detrimental, but only if the cost to fine ratio is low. This behavior is summarized in *Fig. 1*. For relatively large cost cooperation again dominates as a result of spatial pattern formation. Counterintuitively, defectors who do not punish cooperators, and are thus effectively second-order free-riding on antisocial punishment, form an active layer around punishing cooperators, which protects them against defectors that punish cooperators. A representative evolution is illustrated in *Fig. 2*. A stable three-strategy phase that is sustained by an induced cyclic dominance is also possible via the same mechanism. Our results reveal an unlikely evolutionary escape from adverse effects of antisocial punishment, and they provide a rationale for why second-order free-riding is not always an impediment to the evolutionary stability of punishment. All it needs is acknowledging that we live in networks, that is, that interactions among us are not random, but organized [Phys. Rev. X 7, 041027 (2017)].

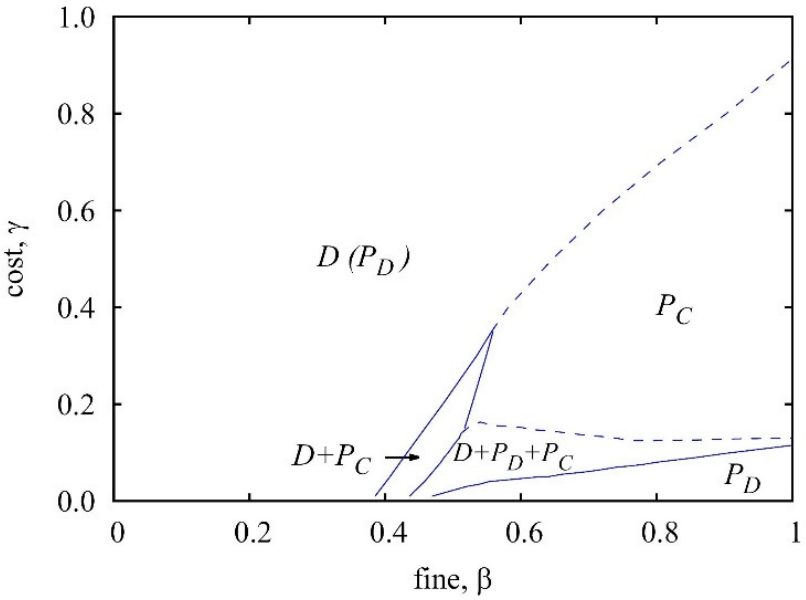

Figure 1: Full fine - cost phase diagram of the spatial public goods game with prosocial and antisocial punishment, as obtained for r = 3.0. Solid lines denote continuous phase transitions while dashed lines denoted discontinuous phase transitions.

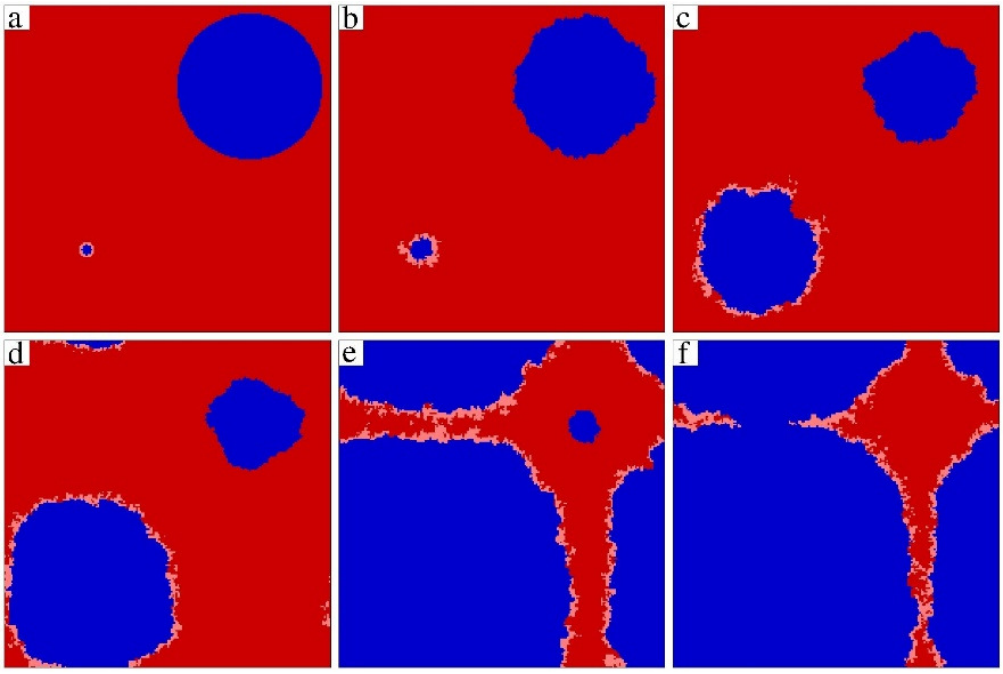

Figure 2: An illustration of how second-order free-riding on antisocial punishment restores the effectiveness of prosocial punishment. A small domain of PC players (dark blue), surrounded by a thin layer of D players (light red) is inserted into the sea of PD players (dark red) in the bottom left corner of the lattice (a). Similarly, a sizable domain of PC players, but without the protective D layer, is inserted into the sea of PD players in upper right corner of the lattice (a). While the large PC domain without the protective layer shrinks over time, the small PC domain with the protective D layer grows (b-f). The absorbing PC phase is reached after 2000 MCS (not shown).

STUDY OF THE EFFECT OF PREHISTORIC HUMAN MIGRATION PROCESSES TO THE RECENT MITOCHONDRIAL AND Y-CHROMOSOMAL HAPLOGROUP DISTRIBUTIONS USING A NEW CORRELATION-BASED SELF-LEARNING ALGORITHM

Z. Juhász and H. Pamjav

We present a new self-learning computational method searching for footprints of early migration processes determining the genetic compositions of recent Human populations. The data being analysed are 26- and 18-dimensional mitochondrial and Y-chromosomal haplogroup distributions representing 50 recent and 34 ancient populations in Eurasia and America. The algorithms search for associations of haplogroups jointly propagating in a significant subset of these populations. Joint propagations of Hgs are detected directly by similar ranking lists of populations derived from Hg frequencies of the 50 Hg distributions. The method provides us the most characteristic associations of mitochondrial and Y-chromosomal haplogroups, and the set of populations where these associations propagate jointly. In addition, the typical ranking lists characterizing these Hg associations show the geographical distribution, the probable place of origin and the paths of their protection. Comparison to ancient data verifies that these recent geographical distributions refer to the most important prehistoric migrations supported by archaeological evidences.

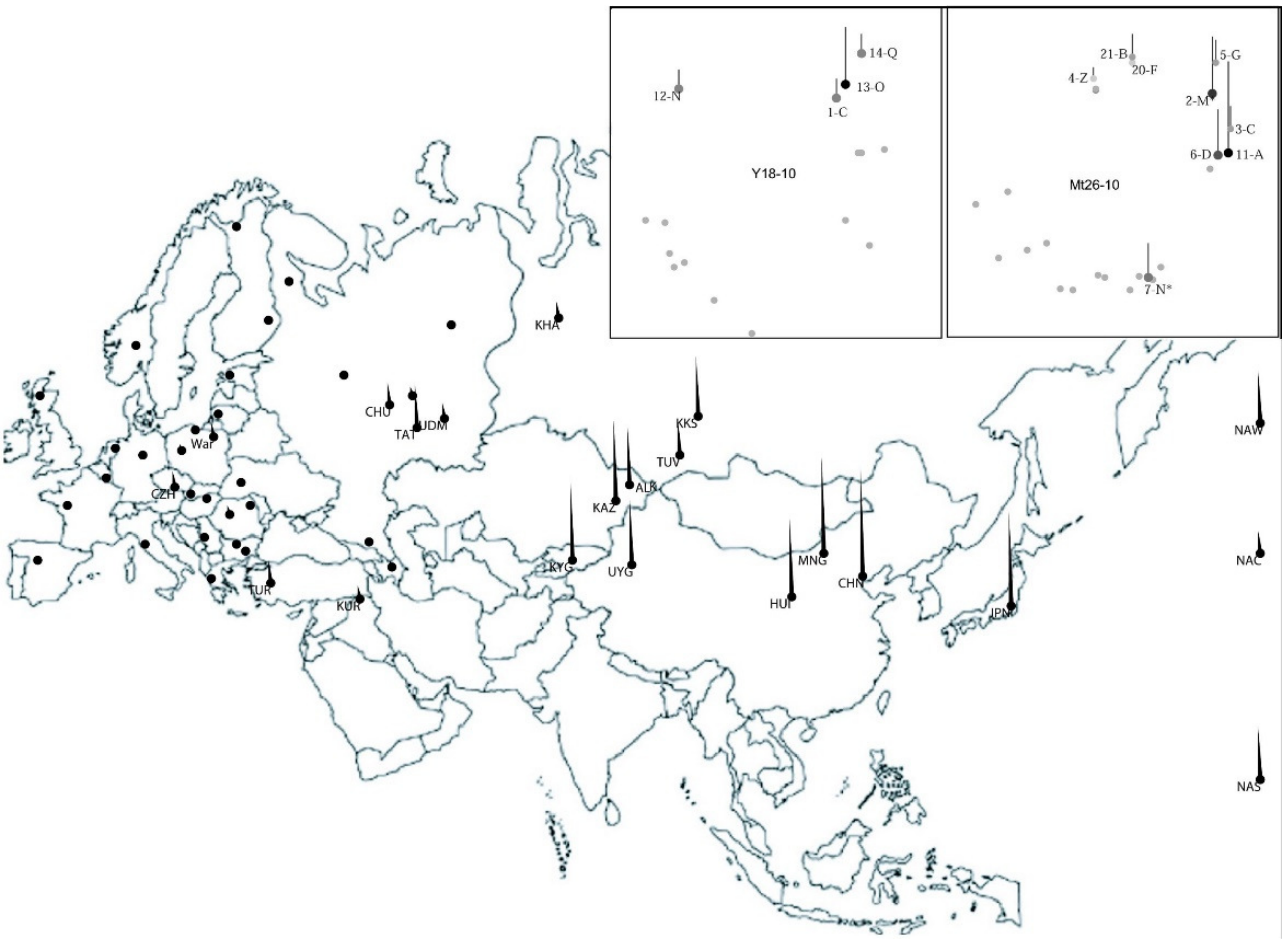

Figure 1: Geographical distribution of the Hg association shown in the right upper part of the figure (Y: Y-chromosomal, Mt: mitochondrial). The Hg association propagates from East- and Inner Asia (CHI, HUI-Chinese, MON-Mongolian, UYG-Uyghur, KAZ-Kazakh, TUV-Tuvan, KHK-Khakass, KYG-Kyrghyz) to Eastern Europe (CHU-Chuvash,TAT-Tatar,UDM-Udmurt) and to the Native Americans (NAS-South, NAC-Central, NAW-North-Western).

ABBREVIATIONS

ABAC	Oxygen Close-packed Stacking
AEKI	Institute for Atomic Energy Research
AER	Atomic Energy Research
AES-1200	VVER-1200 Russian Type Reactor
AES	Auger Electron Spectroscopy
AFM	Atomic Force Microscopy
ALD	Atomic Layer Deposition
ALON	Aluminium Oxynitride Spinel
AMS	Accelerator Mass Spectrometry
AOP	Advanced Oxidation Processes
ARDTM	Automatic Radioactive Material Detection
Asp	Aspartic Acid
ALLEGRO	Experimental Helium Gas Cooled Fast Reactor Developed by the European V4G4
ATHLET	Thermal-hydraulic Computer Code (Analysis of THermal-hydraulics of LEaks and Transients)
ATOMKI	MTA Institute for Nuclear Research
ATR IR	Attenuated Total Reflection Infrared Spectroscopy
ATWS	Anticipated Transient Without Scram
AV	Average Value
BAGIRA	New Irradiation Device at the Budapest Research Reactor
BB	Biomass Burning
BCA	Bicinchoninic Acid
BCC	Body Centred Cubic
BCF	Boda Claystone Formation
BCR	B cell Receptor
BCS	Boron Coated Straw
BDBA	Beyond Design Basis Accident
BNC	Budapest Neutron Centre
BOD	Biological Oxygen Demand
BPM	Bit Patterned Media
BrightnESS	EU Funded Project in Support of the European Spallation Source (ESS)
BRR	Budapest Research Reactor
BZN	Bay Zoltán Nonprofit Ltd. for Applied Research
BWR	Boiling Water Reactor
CATHARE	French Thermohidraulic Code
CAThyMARA	Child and Adult Thyroid Monitoring After Reactor Accident
C-BORD	H-2020 EU Project, effective Container inspection at BORDer control points
CCD	Charge Coupled Device
CDO	Carbon Doped Oxides
CDS	Ceramic Dispersion Strengthened
CERIC	Central European Research Infrastructure Consortium
CERES	Cooling Effectiveness on Reactor External Surface
CERN	Centre Européen pour la Recherche Nucléaire (French name of the European Organization for Nuclear Research)
CETS	Central European Training School
CEMS	Conversion Electron Mössbauer Spectroscopy
CFD	Computational Fluid Dynamics
CGGs	Concentration Gradient Generators
CHANDA	EU Funded Project (CHAllenges in Nuclear Data for the Safety of European Nuclear Facilities)
CHP	Combined Heat and Power

CHF	Critcial Heat Flux
CMD	Classical Molecular Dynamics, Carboxymethyl-dextran
CMOS	Complementary Metal-oxide Semiconductor
CNG	Compressed Natural Gas
COBRA	Thermal-hydraulic Code
COD	Chemical Oxygen Demand
CODEX	Core Degradation Experiment
CONCERT	EU H2020 Project for the Integration of Radiation Protection Research
CONFIDENCE	Consortia of an European Joint Programme (COping with uNcertainties For Improved modelling and DEcision making in Nuclear emergenCiEs)
CPE	Controlled Potential Electrolysis
CPs	Cyclic Peptides
CRP	IAEA Coordinated Research Project
CTM	Constant Temperature Model
CV	Cyclic Voltammetry
CVD	Chemical Vapor Deposition
DBA	Design Basis Accidents
DFT	Density Functional Theory
DGA	Diglycol Amide
DLL	Dynamic Link Library (in the Microsoft Windows Operating System)
DLR	German Aerospace Centre (Deutsches Zentrum für Luft und Raumfahrt)
DMLS	Direct Metal LASER Sintering
DMR	Dynamic Mass Redistribution
DMW	Dissimilar Metal Weld
DNA	Deoxyribonucleic Acid
DNBR	Departure from Nucleate Boiling Ratio
DNC	Delayed Neutron Counting
DPS	Dithiobis(succinimidyl propionate)
DRIE	Deep Reactive Ion Etching
DRIFTS	Diffuse Reflectance Fourier Transform Infrared Spectroscopy
DRM	Dry Reforming
DSA	Deterministic Safety Analysis
DSP	Dithiobis(succinimidyl) Propionate
DSC	Differential Scanning Calorimetry
DTA	Differential Thermal Analysis
EB	Electron Beam
EBV	Epstein-Barr Virus
EC	Elemental Carbon
ECM	Extracellular Matrix
EDC	1-Ethyl-3-(3-dimethylaminopropyl)-carbodiimide
EDS, EDX	Energy-dispersive X-ray Spectroscopy
EEW	Electric Explosion of Wires
EGCg	Epigallocatechin Gallate
EMR	Electron Magnetic Resonance
e-PDF	electronic Pair Distribution Function
EPMA	Electron Probe Micro-analyzer
ELTE	Eötvös Loránd University, Budapest
EPS	Environmental Protection Service
EPR	Electron Paramagnetic Resonance
ESEO	European Student Earth Orbiter
ESI-MS	Electrospray Ionisation Mass Spectrometry
ESIS	European Structural Integrity Society
ESS	European Spallation Source, Lund
ESTEC	European Space Research and Technology Centre, Netherlands

EVA	Extra-vehicular Activity
EWE	Electric Wire Explosion
FAT	Factory Acceptance Tests
FCC	Face Centred Cubic
FEM	Finite Element Method
FF	Flagellar Filament
FFT	Fast Fourier Transform
FIB	Focused Ion Beam
FICI	Fully Implanted Cochlear Implants
FLEXPART	Flexible Particle Dispersion Model
FM	Functional Material
FPE	Fine-grained Pebble Examinations
FRM II	Forschungs-Neutronenquelle Heinz Maier-Leibnitz, Munich
FTIR-ATR	Attenuated Total Reflectance Fourier Transform Infrared Spectroscopy
GIXRF	Grazing Incidence X-ray Fluorescence
GHG	Greenhouse Gas
GR	Graphene
GRAS	Geant4 for Radiation in Space
GREMAN	Laboratory of the University of Tours
GRS	„Gesellschaft für Anlagen- und ReaktorSicherheit"
GTN model	Gurson–Tvergaard–Needleman Material Model
HAADF	High-angle Annular Dark-field Imaging
Hap	Hydroxyapatite
HASYLAB	Hamburger Synchrotronstrahlungslabor (part of DESY)
HEA	High Entropy Alloy
HER	Hydrogen Evolving Half-cell Reaction
Hg	Haplogroup
HIP	Hot Isostatic Pressing
HLW	High-level Radioactive Waste
HMD	Head-mounted Display
HOPG	Growth of MoS2 Single and Few-layer Films on Graphite
HP	Hot Pressing
HPGe	High-purity Germanium
HPLWR	High Performance Light Water Reactor
HREM	High-resolution Electron Microscopy
HRTEM	High Resolution Cross-sectional Transmission Electron Microscopy
HSA	Human Serum Albumin
HTC	High Tech Computer Corporation (a Taiwanese Consumer Electronics Company)
HTO	Tritiated Water
IAEA	International Atomic Energy Agency
IAEA CRP	IAEA Coordinated Research Projects
IBM	Ion-beam Mixing
IBMP	Institute for Biomedical Problems, Moscow
ICIDOSE	Intercomparison on Internal Dose Accessment
ICP-MS	Inductively Coupled Plasma Mass Spectrometry
ICP-OES	Inductively Coupled Plasma Optical Emission Spectrometry
ILL	Institut Laue-Langevin
INAA	Instrumental Neutron Activation Analysis
INSIDER	H-2020 EU Project, Improved Nuclear Site Characterization for Waste Minimization in Decommissioning under Constrained Environment
IPE	International Plant-Analytical Exchange
IPERION CH	EU Funded Project (Integrated Platform for the European Research Infrastructure ON Cultural Heritage)

ISE	International Soil-Analytical Exchange
ISO	International Organization for Standardization
ISS	International Space Station
ITO	Indium-tin-oxide
ITRAP	H-2020 EU Project, Illicit Trafficking Radiation Assessment Program
IVMR	In Vessel Melt Retention
KAERI	Korea Atomic Energy Research Institute
KARATE	Reactor Physical Program Code System
KARATE-1200	Reactor Physical Program Code System for VVER-1200 Reactors
KFKI	Former Name of the Research Centre, Nowadays the Campus Name
Kk	Pin-wise Radial Peaking Factor
KMR	Central Hungarian Region (Hungarian Acronym)
LB	Langmuir-Blodgett
LBNL	Lawrence Berkeley National Laboratory
LDOS	Local Density of States
LET	Linear Energy Transfer
LIBS	Laser Induced Breakdown Spectroscopy
LINTEL	LINear TELescope
LLNL	Lawrence Livermore National Laboratory
LOC	Lab-on-a-Chip
LOCA	Loss of Coolant Accident
LPG	Liquefied Petroleum Gas
LSC	Liquid Scintillation Counting
LTO	Long Term Operation
MAT	Magnetic Adaptive Testing
MATTER	EU FP7 Project (MATerial TEsting and Rules)
MCNP	Monte Carlo N-Particle Transport Code
MELODI	EU Strategic Research Agenda for Low Dose Research
MEMS	Microelectromechanical System
MEST	Mobile Expert Support Team
MFA	Institute of Technical Physics and Materials Science (Hungarian acronym)
MFM	Magnetic Force Microscopy
MILC	Metal Induced Lateral Crystallization
MIS	Minimally Invasive Robotic Surgery
MLG	Multi-layered Graphene
MMS	Microfluidic Magnetic Separation
MOS	Metal-oxide Semiconductor
MOX	Mixed Oxide
MPH	Material property handbook
MS	Mössbauer Spectroscopy
MTA EK	Hungarian Academy of Sciences Centre for Energy Research (Hungarian acronym)
MTR-III	Russian Matroshka-III Experiment
MU	Mock-up
MULTICELL	Reactor Physical Transport Code
MVM	Hungarian Power Companies
MWCNT	Multiwall Carbon Nanotube
NAA	Neutron Activation Analysis
NAL	Nuclear Analysis and Radiography Department, MTA EK
NBD	Nanobeam Diffraction
ND	Neutron Diffraction
NDT	Non-destructive Evaluation Test
NEMS	Nanoelectromechanical Systems
NHS	N-hydroxysuccinimide

NII	Non-Intrusive Inspection
NIR	Near Infrared
NKFIH	National Research, Development and Research Office (Hungarian acronym)
NMI3-II	EU funded project: Neutron Scattering and Muon Spectroscopy Integrated Initiative
NNKP	National Nuclear Research Program
NNFL	National Nuclear Forensics Library
NORM	Naturally-Occurring Radioactive Materials
NP	Nanoparticle
NPI	Nuclear Physics Institute, Acad. of Science of the Czech Republic, Rez Prague
NPP	Nuclear Power Plant
NPs	Nanoparticles
n-TOF	Neutron Time-of-flight
NUBIKI	Nuclear Safety Research Institute
NWP	Numerical Weather Prediction
NW	Nanowire
OAH	Hungarian Atomic Energy Authority (Hungarian acronym)
OC	Organic carbon
OECD	Organisation for Economic Co-operation and Development
OECD NEA	Organisation for Economic Co-operation and Development, Nuclear Energy Agency
OER	Oxygen Evolving Reaction
ORC	Organic Rankine Cycle
OTKA	Hungarian Scientific Research Fund (Hungarian Acronym)
OWLS	Optical Waveguide Light Mode Spectroscopy
Paks NPP	Paks Nuclear Power Plant
PARACELL	Reactor Physical Program Code
PBS	Phosphate Buffered Saline
PCB	Printed Circuit Board
PCMI	Pellet-Cladding Mechanical Interaction
PCT	Peak Cladding Temperature
PDMS	Polydimethylsiloxane
PGAA	Prompt-gamma Neutron Activation Analysis
PGAI	Prompt-gamma Activation Imaging
PHE	Public Health England
PID	Proportional Intergral Device
PIXE	Particle-induced X-ray Emission or Proton-induced X-ray Emission
PKL-4	NEA Primary Coolant Loop Test Facility
PLL-g-PEG	Random Graft Co-polymer with a Poly(L-lysine) Backbone and Poly(ethylene glycol) Side-chains
PM	Particulate Matter
PMF	Positive Matrix Factorization
PRD	Personal Radiation Detector
PSA	Probabilitic Safety Analysis
PSI	Paul Scherrer Institute, Suisse
PSF	Photon Strength Function
PTR-32 HV	Counting Electronics
PXRD	Powder X-ray Diffractometry
pXRF	Portable XRF Spectrometer
PWR	Pressurized Water Reactor
QMS	Quadrupole Mass Spectrometer
RAD	Static/dynamic Thermal-neutron and X-ray Imaging Station at BNC
RADCUBE	A joint Mission Name of the ESA
RadMag	Instrument for Measuring Space Radiation and Magnetic Field Parameters

RBS	Rutherford Backscattering
RE	Renewable Energy
RETINA	REactor Thermohydraulics INterActive simulator
RF	Radio-frequency
RGD	Arg-Gly-Asp (peptide sequence)
RIA	Reactivity Initiated Accident
RIID	Radiation Isotope Identification Device
RIPL	Reference Input Parameter Library
RMC method	Reverse Monte Carlo Method
RNA	Ribonucleic Acid
RPM	Radiation Portal Monitor
RPV	Reactor Pressure Vessel
RTP	Rapid Thermal Process
SAED	Selected Area Electron Diffraction
SAE TP	Sustainable Atomic Energy Technological Platform
SAFEST	EU Funded Project: Severe Accident Facilities for European Safety Targets
SANS	Small Angle Neutron Scattering
SAWCG	Selective Area Wet Chemical Growth
SBF	Simulated Body Fluid
SD	Standard Deviation
SE	Shielding Effectiveness, or Spectroscopic Ellipsometry
SELEX	Systematic Evolution of Ligands by Exponential Enrichment
SEM	Scanning Electron Microscopy
SEM/EDX	Scanning Electron Microscopy Coupled with Energy Dispersive X-ray Spectroscopy
SERS	Surface Enhanced Raman Spectroscopy
SFR	Sodium Cooled Fast Reactor
SGHP	Sol-gel Hydrothermal Process
SI	Structural Integrity
SIMTONIA	SIMulation TOols for Nuclear Industrial Applications
SINE2020	EU Funded Project: Science and Innovation with Neutrons in Europe in 2020
SINAC	Simulator Software for Interactive modelling of environmental consequences of Nuclear ACcidents
SMX	Sulfamethoxazole
SOFC	Solid Oxide Fuel Cells
SOI	Si-on-Insulator
SOP	Standard Operating Procedures
SP	Safeguards Support Programme
SPE	Solar Particle Event
SPENVIS	Space Environment Information System
SPS	Spark Plasma Sintering
SRA	Strategic Research Agenda
SRP	Strategic Research Program
SRPM	Spectroscopic Radiation Portal Monitor
SSD	Solid-state Drive
SSITKA	Steady State Transient Kinetic Analysis
SSNTD	Solid State Nuclear Track Detector
SZIKKTI	Materials Research and Testing Laboratory for Silicate Industry Ltd., Budapest
STEM	Scanning Transmission Electron Microscopy
STM	Scanning Tunnelling Microscopy
STS	Scanning Tunnelling Spectroscopy
STYLE	EU FP7 Project
SWV	Square Wave Voltammetry
TEM	Transmission Electron Microscopy

TLD	Thermoluminescent Dosimeter
TLO	Triple Lorentzian
TMI	Three Mile Island NPP
TNA	Technology Needs Assessment Project
TOC	Total Organic Carbon Content
TOF	Turnover Frequency
TOF-ND	Time of Flight Neutron Diffraction
TPO	Temperature Programed Oxidation
TPR	Temperature Programmed Reduction
TRABCO	Hot Channel Program Code
TRITEL	Three Dimensional Silicon Detector Telescope
ULOF	Unprotected Loss of Flow
UPS	Uninterrupted Power Supply
UTOP	Unprotected Transient of Overpower
UV	Ultraviolet
UV-VIS	Ultraviolet-Visible (Spectroscopy)
VEH	Vibrational Energy Harvesting
VERONA	Reactor Core Monitoring and the Reactivity Measurement System for VVER Type NPPs
VSM	Vibrating Sample Magnetometry
VVER	Water-Cooled Water-Moderated Energetic Reactor, Russian acronym
VVER-SCP	VVER Supercritical Pressure
XPS	X-ray Photoelectron Spectroscopy
XRD	X-ray Diffraction
XRF	X-ray Fluorescence Analysis
YSZ	Yttria-stabilized Zirconia
VSM	Vibrating Sample Magnetometry
WBC	Tungsten Boron Carbide
WEPAL	Wageningen Evaluating Programs for Analytical Laboratories
WG	Work Group
WMDs	Weapons of Mass Destruction
WMO	World Meteorological Organization
WP	Work Package

IMPRINT

Editors

László Redler
Attila R. Imre

Lector

Jesse Weil

Publisher

Ákos Horváth
Tamás Belgya
MTACentre for Energy Research
H-1121, Budapest, Konykoly Thege M. út 29-33.
Hungary

Design

Anikó Jécsai

Picture credits

Centre for Energy Research,
Hungarian Academy of Sciences

Accessibility

http://www.energia.mta.hu/

Contact

Centre for Energy Research, Hungarian Academy of Sciences
Location: *KFKI Campus 29-33 Konkoly-Thege Miklós street 1121 Budapest, Hungary*
Mailing address: *1525 Budapest 114., P.O. Box 49., Hungary*
Phone: *(+36 1) 395 91 59 Fax: (+36 1) 395 92 93*
E-mail adresses: info@energia.mta.hu

Hungarian Academy of Sciences
Centre for Energy Research
Budapest 114, P.O. Box 49, H-1525, Hungary
Phone: +36 1 395 9159, Fax: +36 395 9293
www.energia.mta.hu